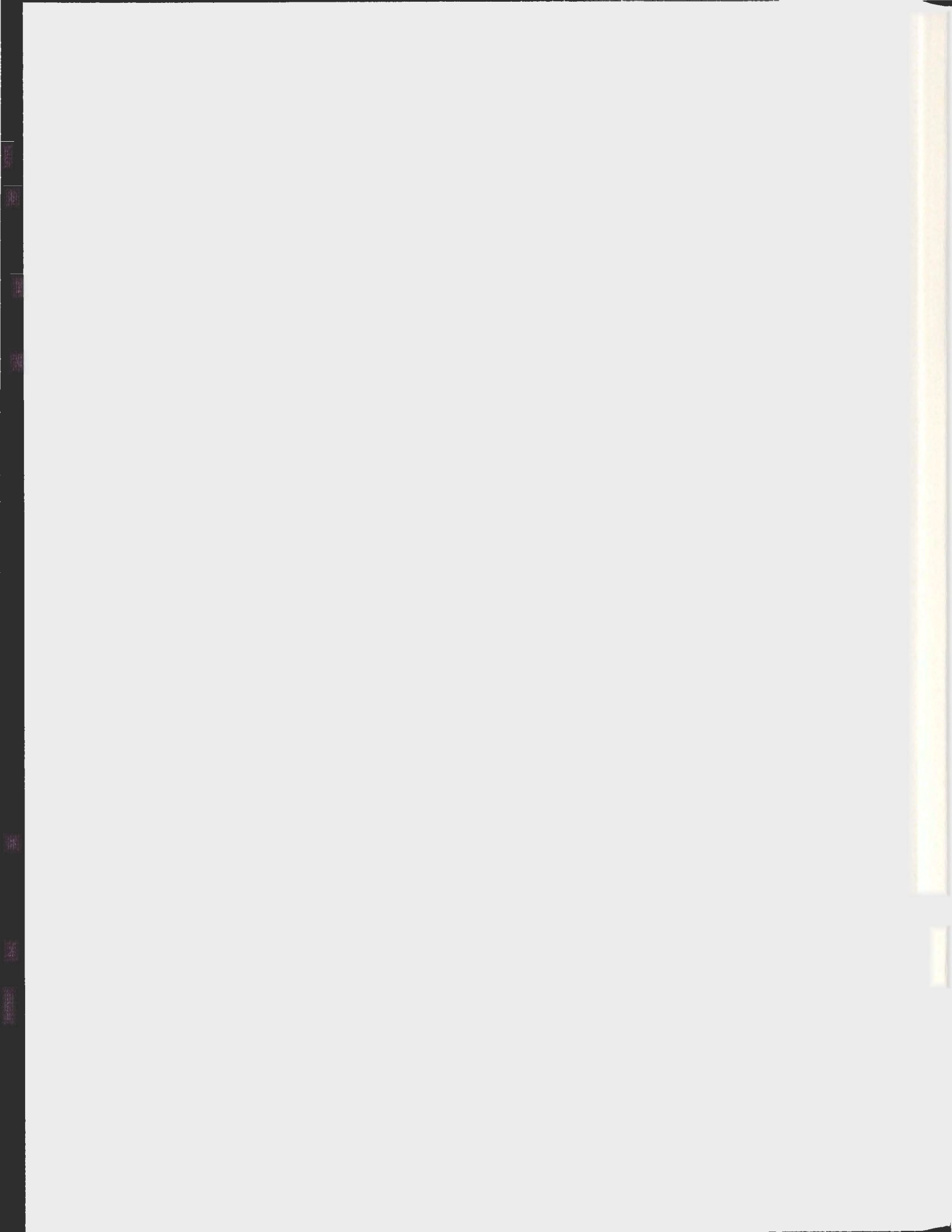


JOINT INVERSION OF GEOLOGICALLY REALISTIC,
SYNTHETIC EARTH MODELS

ANGELA ELIZABETH CARTER-McAUSLAN



**Joint Inversion of Geologically Realistic, Synthetic
Earth Models**

by

© Angela Elizabeth Carter-McAuslan

A Thesis submitted to the

School of Graduate Studies

in partial fulfillment of the requirements for the degree of

Masters of Science

Department of Earth Sciences

Memorial University of Newfoundland

January 2013

St. John's, Newfoundland

Abstract

Inversion modelling problems are ill-posed and non-unique and, as such, they have an infinite number of potential mathematical solutions. By using the joint inversion of two different but complementary geophysical datasets a model can be produced in which there can be a greater degree of confidence. To test the joint inversion methodology a code for the modelling of borehole seismic tomography and gravity data was used to attempt to reproduce geologically-realistic synthetic Earth models. A number of 2D and 3D synthetic Earth models, based on the geology of the Eastern Deeps zone of the Voisey's Bay deposit in Labrador, were constructed. These models consist of unstructured triangular and tetrahedral meshes. The 2D models were based on conceptualized models of the Eastern Deeps and are varied in complexity. The 3D tetrahedral model was built based on Datamine wireframe model of the Eastern Deeps. Single property and joint inversions were carried out to evaluate the ability of the joint inversion methodology to reproduce the models and to determine which inversion parameters were most crucial in generating the best inversion results. Through these tests it has been shown that the joint inversion code was able to locate a buried high contrast target in 2D and 3D cases. During 3D tests it has been concluded that a balance between the noise levels, number of cells in the inversion mesh, seismic acquisition array and gravity measurement locations had to be carefully considered in light of the available memory capacity and computation time in order to attain reasonable joint inversion results.

Acknowledgements

I would like to thank Dr. Peter Lelièvre for providing the software for this project as well as for providing guidance, advice and answering my innumerable questions. I would like to thank my supervisor Dr. Colin Farquharson for his advice and encouragement throughout this project. I would like to thank my committee member Dr. Charles Hurich for his guidance and direction; particularly, on the seismic tomography portions of this project. I would like to thank Vale for providing Datamine and physical property data from the Voisey's Bay deposit as well as providing financial support. I would also like to acknowledge the School of Graduate Studies, the Natural Sciences and Engineering Research Council of Canada and the Atlantic Canada Opportunities Agency for providing funding for this project.

Table of Contents

Abstract.....	ii
Acknowledgments	iii
Table of Contents.....	iv
List of Figures.....	.vii
List of Tables.....	.xxv
Chapter 1: Introduction and Background Information	1
1.1 Geophysical Modelling	1
1.1.1 Forward and Inversion Modelling	2
1.1.2 Joint Inversion Modelling	4
1.2 Wireframe Mesh Models.....	6
1.3 Voisey's Bay Deposit.....	8
1.3.1 The Eastern Deeps Zone	10
1.4 Project Aims.....	12
Chapter 2: Methodology and Code.....	14
2.1 Triangular and Tetrahedral Mesh Generation and Visualization	14
2.2 Forward Modelling and Noise	16
2.3.1 Gravity Forward Modelling.....	16
2.3.2 Seismic Forward Modelling	19
2.3.3 Noise.....	23
2.3 Inversion Modelling	25
2.3.1 Joint Inversion Methodology.....	25
2.3.2 Using VINV	30
Chapter 3: Constructing Models and Forward Modelling in Two Dimensions	33
3.1 The Models	33
3.1.1 Sulphide-Gneiss Model.....	35
3.1.2 Troctolite-Gneiss Model	36
3.1.3 Mixed Model	37
3.2 Gravity Forward Modelling.....	38
3.2.1 Gravity Stations locations.....	38
During forward modelling the relative densities outlined in	39
3.2.2 Gravity Forward Modelling Results	40
Although differences between.....	40
3.3 Seismic Forward Modelling	43
3.4 Adding Noise to Data	48

Chapter 4: Results of 2D Inversion	56
4.1 Overview.....	56
4.1.2 Outline of Results	56
4.1.2 Overview of Results	60
4.1 Sulphide-Gneiss Model Results	61
4.1.1 Seismic –Only Inversion	61
4.1.2 Surface Station Only Inversion Results	68
4.1.3 Borehole Stations Only Inversion Results.....	83
4.1.4 All Gravity Station Inversion Results.....	130
4.2 Mixed Model Results	144
4.2.1 Example 34: Seismic Only Inversion Results.....	144
4.2.2 Surface Gravity Stations Only	147
4.2.3 Borehole A Gravity Stations Only	153
4.2.4 Borehole B Gravity Stations Only	159
4.2.5 Borehole A and B Gravity Stations.....	164
4.2.6 All Station Results	170
4.3 Troctolite-Gneiss Model Inversion Results	175
4.3.1 Low Noise Inversion Results	175
4.3.2 Moderate Noise Inversion	182
4.3.3 High noise Inversions.....	188
4.4 Discussion of 2D Inversion Results	193
4.4.1 Modelling High Contrast Buried Bodies.....	193
4.4.2 Modelling Low Contrast Bodies	198
4.4.3 Modelling Mixed Models.....	202
4.4.4 Discussion of Key Inversion Parameters.....	204
4.5 Conclusions.....	212
 Chapter 5: 3D Tetrahedral Earth Models	 216
5.1 Development of Tetrahedral Meshes.....	216
5.1.1 Developing a Tetrahedral Model from a Surface Wireframe	218
5.2 Developing Simpler Models for 3D Inversion Tests.....	230
5.2.1 The Block Model.....	231
5.2.2 The Sulphide Model.....	231
5.3 Developing Facet Modeller	232
 Chapter 6: 3D Forward Modelling	 234
6.1 Seismic Source and Receiver Layout	234
6.1.1 Panel Arrangement.....	235
6.1.2 Grid-Like Borehole Layout	236
6.1.3 Starburst Layout	237
6.2 Seismic Forward Modelling Results.....	238
6.2.1 Panel Layout	239
6.2.2 Grid-Like Layout.....	242
6.2.3 Starburst I Layout	244
6.2.4 Starburst II Layout	246
6.2.5 Effect of Mesh Coarseness on Seismic Forward Modelling Results	247
6.3 Gravity Forward Modelling.....	251

6.3.1 Gravity Station Layouts and Forward Modelling Results.....	252
Chapter 7: 3D Inversion Results and Discussion	261
7.1 Single Property 3D Inversion Results.....	262
7.1.2 Effects of Grid Coarseness on Seismic Tomography Modelling	267
7.1.3 Adding Receivers: The Starburst II Array.....	276
7.2 Gravity Inversion Results	277
7.2.1 Small Surface Array Inversion Results	278
7.2.2 Large Surface Array Inversion Results	280
7.2.3 Mixed Array Inversion Results	288
7.2.4 Borehole Array Inversion Results	292
7.3 Joint Inversion Results	295
7.3.1 Graduated Mesh Inversion	296
7.3.2 Fine Mesh Inversion	300
Chapter 8: Summary and Conclusions	302
References.....	304
Appendix A: Input Files.....	310
A.1 Gravity_fwd Input File.....	310
A.2 Seismics_fwd Input File.....	311
A.3 VINV Input File.....	313
Appendix B: 2D Inversions.....	317
Appendix C: 3D Inversions.....	326

List of Figures

Fig. 1. 1: Rectilinear-type meshes are an example of the meshes often used for inversion modelling. These meshes are created by overlaying a rectilinear mesh over the base model (left). Each cell is then assigned the physical property of the unit that fills the majority of the cell (right).....	3
Fig. 1. 2: Determination of the statistical relationship between magnetic susceptibility and density derived by Bosch and McGaughey (2001) for the three lithologies in their test model.....	6
Fig. 1. 3: A thin plate model created using the Maxwell forward modelling program for modelling electromagnetic data (figure courtesy of Adam Mercer).....	7
Fig. 1. 4: a) Comparison between a rectilinear and triangular mesh representation of an amorphous body (Jahandari, 2011). b) Comparison between a rectilinear and triangular representation of the letter A (Lelievre, et al., 2012).....	8
Fig. 1. 5: Map of the Voisey's Bay Deposit showing the lateral distribution of the main ore zones and the location of the deposit within Labrador (after Evans-Lamswood et al., 2000).	10
Fig. 1. 6: Cross-section through the Voisey's Bay Deposit showing the location of the Reid Brook, Discovery Hill, Ovoid Extension and Eastern Deeps ore zones with respect to surface (after Li et al., 2000).....	10
Fig. 1. 7: Geological cross-section through the Eastern Deeps intrusion and ore zone (after Evans-Lamswood et al., 2000).....	12
Fig. 2. 1: After a model has been designed (a), an input file for Triangle is created by identifying the vertices in the model (b). The coordinates of each vertex is entered into the input file. Each of the line segments necessary for the model are then identified (c) and two vertices at each end of the line segment are entered into the input file.	16
Fig. 2. 2: Diagram shows the solution front (grey circles) between the downwind nodes shown as black circles, for which the travel-times had been determined, and the upwind nodes shown as white circles, for which the travel times have yet to be determined (after Lelièvre, et al. 2010).	20
Fig. 2. 3: Propagation of a wavefront from source 1 outward through a two dimensional Earth model.....	20

Fig. 3. 1: Cross-section through the Eastern Deeps zone (after Evans-Lamswood et al., 2000), on which the 2D models in this project were based.	34
Fig. 3. 2: The sulphide-gneiss model overlain by a triangular mesh produced from the model.....	36
Fig. 3. 3: The troctolite-gneiss model overlain by a triangular mesh produced from the model.....	37
Fig. 3. 4: The mixed model overlain by a triangular mesh produced from the mixed model.....	38
Fig. 3. 5: The locations of all the gravity measurement locations. Borehole A gravity measurement locations are shown in purple, borehole B measurement locations are shown in blue and surface measurement locations are shown in red. Borehole A measurement locations correspond to the seismic source locations. Borehole B measurement locations correspond to seismic receiver locations. The model has the same dimensions as were shown in Fig. 3. 4.....	39
Fig. 3. 6: Forward-modelled gravity values at all measurement locations for the sulphide-gneiss model. A coloured square at each location indicates the value of gravity. The model has the same dimensions as were shown in Fig. 3. 4.	41
Fig. 3. 7: Forward-modelled gravity values at all measurement locations for the troctolite-gneiss model. A coloured square at each location indicates the value of gravity. This model has the same dimensions as were shown in Fig. 3. 4.	42
Fig. 3. 8: Forward-modelled gravity values at all measurement locations for the mixed model. A coloured square at each location indicates the value of gravity. The model has the same dimensions as were shown in Fig. 3. 4.	43
Fig. 3. 9: Travel-time contours for sources 1 (a), 20 (b), 40 (c), 60 (d), and 79(e) for the mixed model, the sulphide is shown in red, the troctolite in light blue and the gneiss in dark blue. Each contour represents 1/50 of the total travel time range. The models have the same dimensions as was shown in Fig. 3. 4.....	44
Fig. 3. 10: Cartoon depiction of the source-receiver space used to portray the travel time results.	45
Fig. 3. 11: Travel times (a) and anomalous travel times (b) plotted as receiver versus transmitter for the mixed model	47
Fig. 3. 12: Travel times (a) and anomalous travel times (b) plotted for transmitter versus receiver for the sulphide-gneiss model.	47

Fig. 3. 13: Travel times (a) and anomalous travel times (b) plotted for transmitter versus receiver for the troctolite-gneiss model.	47
Fig. 3. 14: Comparison between the gravity response with noise added (a,b,c) for the sulphide-gneiss model at all measurement locations and the noise added (d,e,f) to those data points for low noise (a, d), moderate noise (b,e) and high noise (c,f). The models have the same dimensions as were shown in Fig. 3. 4.....	50
Fig. 3. 15: Comparison between the gravity response with noise added (a,b,c) for the troctolite-gneiss model at all measurement locations and the noise added (d,e,f) to those data points for low noise (a, d), moderate noise (b,e) and high noise (c,f). The models have the same dimensions as were shown in Fig. 3. 4.....	51
Fig. 3. 16: Comparison between the gravity response with noise added (a) for the mixed model at all measurement locations and the noise added (b) for moderate noise levels. The models have the same dimensions as were shown in Fig. 3. 4.....	52
Fig. 3. 17: Mixed model data with noise added: low noise in the top panels, moderate noise in the middle panels and high noise in the bottom panels.	53
Fig. 3. 18: Noisy sulphide-gneiss model synthetic data for low noise (top panels), moderate noise (middle panels) and high noise (bottom panels).....	54
Fig. 3. 19: Noisy troctolite-gneiss model synthetic data with low noise (top panels), moderate noise (middle panels), and high noise (bottom panels).....	55
Fig. 4. 1: a) Predicted travel time data and b) normalized data residual for the seismic-only inversion of moderate noise sulphide-gneiss model synthetic data. The horizontal axis of both plots is the source number and the vertical axis is the receiver number (Fig 3.10).	62
Fig. 4. 2: Resultant slowness model from the seismic-only inversion of moderate noise sulphide-gneiss model synthetic data. The model is 200m across and 400m in depth and the black line outlines the location of the sulphide body in the synthetic models.....	63
fig. 4. 3: Resultant slowness model from the seismic-only inversion of low noise sulphide-gneiss model synthetic data. The model is 200m across and 400m in depth and the black line outlines the location of the sulphide body in the synthetic models.....	65
Fig. 4. 4: Predicted travel time data (a) and normalized data residual (b) for the seismic only inversion of low noise sulphide-gneiss model synthetic data. The horizontal axis of both plots is the source number and the vertical axis is the receiver number (Fig 3.10)...	66
Fig. 4. 5: Resultant slowness model from seismic-only inversion of high noise sulphide-gneiss model synthetic data. The model is 200m across and 400m in depth and the black line outlines the location of the sulphide body in the synthetic models.	67

Fig. 4. 6: Predicted gravity data (a) and normalized data residual (b) for the gravity-only inversion of moderate noise sulphide-gneiss model synthetic data.	69
Fig. 4. 7: Resultant density model from the gravity-only inversion of moderate noise sulphide-gneiss synthetic data. The model is 200m across and 400m in depth and the black line outlines the location of the sulphide body in the synthetic models.	70
Fig. 4. 8: Predicted seismic travel times (a) and associated normalized data residuals (b) for the joint inversion of moderate noise sulphide-gneiss model synthetic data.	72
Fig. 4. 9: Resultant density (a) and slowness (b) models from the joint inversion of moderate noise sulphide-gneiss model synthetic data. The model is 200m across and 400m in depth and the black line outlines the location of the sulphide body in the synthetic models.	73
Fig. 4. 10: Resultant density model from the gravity-only inversion of low noise sulphide-gneiss model synthetic data. The model is 200m across and 400m in depth and the black line outlines the location of the sulphide body in the synthetic models.	75
Fig. 4. 11: Predicted seismic travel times (a) and associated normalized data residuals (b) for the joint inversion of low noise sulphide-gneiss model synthetic data. The horizontal axis of both plots is the source number and the vertical axis is the receiver number (Fig 3.10).	77
Fig. 4. 12: Resultant density (a) and slowness (b) models from the joint inversion of low noise sulphide-gneiss model synthetic data. The model is 200m across and 400m in depth and the black line outlines the location of the sulphide body in the synthetic models.	78
Fig. 4. 13: Resultant density model from the gravity-only inversion of high noise sulphide-gneiss model synthetic data. The model is 200m across and 400m in depth and the black line outlines the location of the sulphide body in the synthetic models.	80
Fig. 4. 14: Resultant density (a) and slowness (b) models from the joint inversion of high noise sulphide-gneiss model synthetic data. The model is 200m across and 400m in depth and the black line outlines the location of the sulphide body in the synthetic models.	82
Fig. 4. 15: Predicted gravity data (a) and associated normalized data residuals (b) for the joint inversion of moderate noise sulphide-gneiss model synthetic data.	84
Fig. 4. 16: Resultant density model from the gravity-only inversion of moderate noise sulphide-gneiss model synthetic data. The model is 200m across and 400m in depth and the black line outlines the location of the sulphide body in the synthetic models.	85
Fig. 4. 17: Predicted gravity data (a) and associated normalized data residuals (b) for the joint inversion of moderate noise sulphide-gneiss model synthetic data.	87

Fig. 4. 18: The resultant density (a) and slowness (b) models from the joint inversion of moderate noise sulphide-gneiss model synthetic data. The model is 200m across and 400m in depth and the black line outlines the location of the sulphide body in the synthetic models.....	88
Fig. 4. 19: Predicted gravity data (a) and associated normalized data residuals (b) for the joint inversion of high noise sulphide-gneiss model synthetic data.....	90
Fig. 4. 20: Resultant density model from the gravity-only inversion of high noise sulphide-gneiss model synthetic data. The model is 200m across and 400m in depth.....	91
Fig. 4. 21: The resultant density (a) and slowness (b) models from the joint inversion of high noise sulphide-gneiss model synthetic data. The model is 200m across and 400m in depth and the black line outlines the location of the sulphide body in the synthetic models.	94
Fig. 4. 22: Predicted gravity data (a) and associated normalized data residuals (b) for the joint inversion of low noise sulphide-gneiss model synthetic data.....	96
Fig. 4. 23: Resultant density model from the gravity-only inversion of low noise sulphide-gneiss model synthetic data. The model is 200m across and 400m in depth and the black line outlines the location of the sulphide body in the synthetic models.	97
Fig. 4. 24: Predicted gravity data (a) and associated normalized data residuals (b) for the joint inversion of low noise sulphide-gneiss model synthetic data.....	99
Fig. 4. 25: The resultant density (a) and slowness (b) models from the joint inversion of low noise sulphide-gneiss model synthetic data. The model is 200m across and 400m in depth and the black line outlines the location of the sulphide body in the synthetic models.	100
Fig. 4. 26: Predicted gravity data (a) and associated normalized data residuals (b) for the joint inversion of moderate noise sulphide-gneiss model synthetic data.....	102
Fig. 4. 27: Resultant density model from the gravity-only inversion of moderate noise sulphide-gneiss model synthetic data. The model is 200m across and 400m in depth and the black line outlines the location of the sulphide body in the synthetic models.....	103
Fig. 4. 28: The resultant density (a) and slowness (b) models from the joint inversion of moderate noise sulphide-gneiss model synthetic data. The model is 200m across and 400m in depth and the black line outlines the location of the sulphide body in the synthetic models.....	105
Fig. 4. 29: Resultant density model from the gravity-only inversion of high noise sulphide-gneiss model synthetic data. The model is 200m across and 400m in depth and the black line outlines the location of the sulphide body in the synthetic models.....	107

Fig. 4. 30: The resultant density (a) and slowness (b) models from the joint inversion of high noise sulphide-gneiss model synthetic data. The model is 200m across and 400m in depth and the black line outlines the location of the sulphide body in the synthetic models. 109

Fig. 4. 31: Predicted gravity data (a) and associated normalized data residuals (b) for the gravity-only inversion of low noise sulphide-gneiss model synthetic data. 111

Fig. 4. 32: Resultant density model from the gravity-only inversion of low noise sulphide-gneiss model synthetic data. The model is 200m across and 400m in depth and the black line outlines the location of the sulphide body in the synthetic models. 112

Fig. 4. 33: The resultant density (a) and slowness (b) models from the joint inversion of low noise sulphide-gneiss model synthetic data. The model is 200m across and 400m in depth and the black line outlines the location of the sulphide body in the synthetic models. 114

Fig. 4. 34: Predicted gravity data (a) and associated normalized data residuals (b) for the joint inversion of moderate noise sulphide-gneiss model synthetic data. 116

Fig. 4. 35: Resultant density model from the gravity-only inversion of moderate noise sulphide-gneiss model synthetic data. The model is 200m across and 400m in depth and the black line outlines the location of the sulphide body in the synthetic models. 117

Fig. 4. 36: Resultant density (a) and slowness (b) models from the joint inversion of moderate noise sulphide-gneiss model synthetic data. The model is 200m across and 400m in depth and the black line outlines the location of the sulphide body in the synthetic models. 119

Fig. 4. 37: Predicted gravity data (a) and associated normalized data residuals (b) for the joint inversion of high noise sulphide-gneiss model synthetic data. 121

Fig. 4. 38: Resultant density model from the gravity-only inversion of high noise sulphide-gneiss model synthetic data. The model is 200m across and 400m in depth and the black line outlines the location of the sulphide body in the synthetic models. 122

Fig. 4. 39: The resultant density (a) and slowness (b) models from the joint inversion of high noise sulphide-gneiss model synthetic data. The model is 200m across and 400m in depth and the black line outlines the location of the sulphide body in the synthetic models. 124

Fig. 4. 40: Resultant density mode from the gravity-only inversion of low noise sulphide-gneiss model synthetic data. The model is 200m across and 400m in depth and the black line outlines the location of the sulphide body in the synthetic models. 126

Fig. 4. 41: Predicted gravity data (a) and associated normalized data residuals (b) for the gravity-only inversion of low noise sulphide-gneiss model synthetic data.	128
Fig. 4. 42: The resultant density (a) and slowness (b) models from the joint inversion of low noise sulphide-gneiss model synthetic data. The model is 200m across and 400m in depth and the black line outlines the location of the sulphide body in the synthetic models.	129
Fig. 4. 43: Predicted gravity data (a) and associated normalized data residuals (b) for the gravity-only inversion of moderate noise sulphide-gneiss model synthetic data.	131
Fig. 4. 44: Resultant density model form the gravity-only inversion of moderate noise sulphide-gneiss model synthetic data collected at all borehole and surface gravity stations. The model is 200m across and 400m in depth and the black line outlines the location of the sulphide body in the synthetic models.	132
Fig. 4. 45: Resultant density (a) and slowness (b) models from the joint inversion of moderate noise sulphide-gneiss model synthetic data. The model is 200m across and 400m in depth and the black line outlines the location of the sulphide body in the synthetic models.	134
Fig. 4. 46: Resultant density model for the gravity-only inversion of low noise sulphide-gneiss model synthetic data. The model is 200m across and 400m in depth and the black line outlines the location of the sulphide body in the synthetic models.	136
fig. 4. 47: Predicted gravity data (a) and associated normalized data residuals (b) for the joint inversion of low noise sulphide-gneiss model synthetic data.	138
Fig. 4. 48: Resultant density (a) and slowness (b) model for the joint inversion of low noise sulphide-gneiss model synthetic data. The model is 200m across and 400m in depth and the black line outlines the location of the sulphide body in the synthetic models. ...	139
Fig. 4. 49: Resultant density model from the gravity-only inversion of high noise sulphide-gneiss model synthetic data. The model is 200m across and 400m in depth and the black line outlines the location of the sulphide body in the synthetic models.	141
Fig. 4. 50: Resultant density (a) and slowness (b) model for the joint inversion of high noise sulphide-gneiss model synthetic data. The model is 200m across and 400m in depth and the black line outlines the location of the sulphide body in the synthetic models. ...	143
Fig. 4. 51: Predicted seismic travel times (a) and associated normalized data residuals (b) for the seismic portion of the joint inversion of Mixed model synthetic data. The horizontal axis of both plots is the source number and the vertical axis is the receiver number (Fig 3.10).	145

Fig. 4. 52: Seismic-Only inversion result from the inversion of mixed model synthetic data. The model is 200m across and 400m in depth. The black line outlines the location of the sulphide and troctolite bodies in the synthetic models. 146

Fig. 4. 53: Predicted gravity data (a) and associated normalized data residuals (b) for the joint inversion of Mixed model synthetic data. 148

Fig. 4. 54 Resultant density model from the gravity-only inversion of Mixed model synthetic data. The model is 200m across and 400m in depth. The black line outlines the location of the sulphide and troctolite bodies in the synthetic models. 149

Fig. 4. 55: Predicted seismic travel times (a) and associated normalized data residuals (b) for the seismic portion of the joint inversion of Mixed model synthetic data. The horizontal axis of both plots is the source number and the vertical axis is the receiver number (Fig 3.10). 151

Fig. 4. 56: Resultant slowness (a) and density (b) model for the joint inversion of Mixed model synthetic data. The models are 200m across and 400m in depth. The black line outlines the location of the sulphide and troctolite bodies in the synthetic models..... 152

Fig. 4. 57: Predicted gravity data (a) and associated normalized data residuals (b) for the joint inversion of moderate noise sulphide-gneiss model synthetic data..... 154

Fig. 4. 58 Resultant density model from the gravity-only inversion of the moderate noise Mixed model synthetic data. The model is 200m across and 400m in depth. The black line outlines the location of the sulphide and troctolite bodies in the synthetic models..... 155

Fig. 4. 59: Resultant slowness (a) and density (b) model for the joint inversion of Mixed model synthetic data. The models are 200m across and 400m in depth. The black line outlines the location of the sulphide and troctolite bodies in the synthetic models..... 158

Fig. 4. 60: Predicted gravity data (a) and associated normalized data residuals (b) for the joint inversion of Mixed model synthetic data. 160

Fig. 4. 61 Resultant density model from the gravity-only inversion of the Mixed model synthetic data. The model is 200m across and 400m in depth. The black line outlines the location of the sulphide and troctolite bodies in the synthetic models. 161

Fig. 4. 62: Resultant density (a) and slowness (b) model for the joint inversion of Mixed model synthetic data. The models are 200m across and 400m in depth. The black line outlines the location of the sulphide and troctolite bodies in the synthetic models..... 163

fig. 4. 63: Predicted gravity data (a) and associated normalized data residuals (b) for the joint inversion of Mixed model synthetic data. 165

Fig. 4. 64 Resultant density model from the gravity-only inversion of the Mixed model synthetic data. The model is 200m across and 400m in depth. The black line outlines the location of the sulphide and troctolite bodies in the synthetic models. 166

Fig. 4. 65: Resultant slowness (a) and density (b) model for the joint inversion of Mixed model synthetic data. The models are 200m across and 400m in depth. The black line outlines the location of the sulphide and troctolite bodies in the synthetic models. 169

Fig. 4. 66: Resultant density model from the gravity-only inversion of the Mixed model synthetic data. The model is 200m across and 400m in depth. The black line outlines the location of the sulphide and troctolite bodies in the synthetic models. 171

Fig. 4. 67: Predicted gravity data (a) and associated normalized data residuals (b) for the gravity-only inversion of Mixed model synthetic data. 173

Fig. 4. 68: The resultant density (a) and slowness (b) models from the joint inversion of Mixed model synthetic data. The models are 200m across and 400m in depth. The black line outlines the location of the sulphide and troctolite bodies in the synthetic models.. 174

Fig. 4. 69: Predicted gravity data (a) and associated normalized data residuals (b) for the joint inversion of low noise sulphide-gneiss model synthetic data. 176

Fig. 4. 70: Resultant model from the gravity only version of low noise troctolite-gneiss model synthetic data. The model is 200m across and 400m in depth. The black line outlines the location of the troctolite body in the synthetic models. 177

Fig. 4. 71: The travel time predicted by this model (a) and the associated normalized data residuals (b) from the seismic-only inversion of low noise troctolite-gneiss model synthetic data. The horizontal axis of both plots is the source number and the vertical axis is the receiver number (Fig 3.10). 178

Fig. 4. 72: Resultant model from the seismic only inversion of low noise troctolite-gneiss model synthetic data. The model is 200m across and 400m in depth. The black line outlines the location of the troctolite body in the synthetic models. 179

Fig. 4. 73: The resultant density (a) and slowness (b) models from the joint inversion of low noise troctolite-gneiss synthetic data. The models are 200m across and 400m in depth. The black line outlines the location of the troctolite body in the synthetic models. 181

Fig. 4. 74: Resultant model from the gravity only inversion of moderately noise troctolite-gneiss model synthetic data. The model is 200m across and 400m in depth. The black line outlines the location of the troctolite body in the synthetic models. 183

Fig. 4. 75: The travel time predicted by this model (a) and the associated normalized data residuals (b) from the seismic-only inversion of moderate noise troctolite-gneiss model

synthetic data. The horizontal axis of both plots is the source number and the vertical axis is the receiver number (Fig 3.10). 184

Fig. 4. 76: Resultant model from the seismic-only inversion of moderately noisy troctolite-gneiss model synthetic data. The model is 200m across and 400m in depth. The black line outlines the location of the troctolite body in the synthetic models. 185

Fig. 4. 77: The resultant density (a) and slowness (b) models from the joint inversion of low noise troctolite-gneiss synthetic data. The models are 200m across and 400m in depth. The black line outlines the location of the troctolite body in the synthetic models. 187

Fig. 4. 78: Predicted gravity data (a) and associated normalized data residuals (b) for the joint inversion of high noise sulphide-gneiss model synthetic data. 189

Fig. 4. 79: Resultant density model from the gravity-only inversion of the high noise Mixed model synthetic data. The model is 200m across and 400m in depth. The black line outlines the location of the troctolite body in the synthetic models. 189

Fig. 4. 80: Resultant slowness model from the gravity-only inversion of the high noise Mixed model synthetic data. The model is 200m across and 400m in depth. The black line outlines the location of the troctolite body in the synthetic models. 190

Fig. 4. 81: Resultant density (a) and slowness (b) model for the joint inversion of high noise sulphide-gneiss model synthetic data. The models are 200m across and 400m in depth. The black line outlines the location of the troctolite body in the synthetic models. 192

Fig. 4. 82: The slowness models resultant from the seismic-only inversion of low (a), moderate (b) and high noise (c) sulphide-gneiss model synthetic data. Slowness is given in s/km. 194

Fig. 4. 83: Typical results from moderate noise gravity-only inversions for a) all gravity stations, b) borehole A and B gravity stations, and c) borehole A gravity stations. Density values are given a g/cm^3 195

Fig. 4. 84: Gravity-only inversion for (a) surface stations data and (b) borehole B station data results showing the density in g/cm^3 196

Fig. 4. 85: Example of various patterns seen in normalized data residuals from gravity inversions: a) contact affect; b) density estimation affect. 197

Fig. 4. 86: Comparison between the physical property models resultant from a) gravity-only inversion b) joint inversion c) seismic-only inversion of the same high noise data sets. 198

Fig. 4. 87: Single property inversion results for the troctolite-gneiss model: a) seismic-only low noise; b) gravity-only low noise; c) seismic-only moderate noise; d) gravity-only moderate noise; e) seismic-only high noise; f) gravity-only high noise.	200
Fig. 4. 88: Joint inversion results from the troctolite-gneiss model tests: a) low noise results; b) moderate noise results; c) high noise results.	201
Fig. 4. 89: Contrasting the resultant density and slowness model from the moderate noise joint inversion of seismic and all station gravity data for the troctolite-gneiss model (a) and mixed model (b).	203
Fig. 4. 90: Black and white scaled version of the resultant density(a) and slowness(b) models from the joint inversion of moderate noise mixed model seismic and all station gravity data. The areas enclosed the red ovals indicate areas	204
Fig. 4. 91: Comparison between two joint inversions of high noise sulphide-gneiss model data with gravity from surface stations only: a) a low similarity parameter used ($\rho_{hoe}=0.01$) b) high similarity parameter ($\rho_{hoe}=1.0$)	206
Fig. 4. 92: Normalized data residual for seismic only inversion of low noise sulphide-gneiss model data (a), moderate noise sulphide-gneiss model data (b), and high noise sulphide-gneiss model data (c).....	208
Fig. 4. 93: Density models from gravity-only borehole A inversion results: a) low noise; b) moderate noise; c) high noise.	210
Fig. 4. 94: A demonstration of the effect of sensitivity weighting on gravity inversion result when borehole only data was employed. a) 2.0, b) 1.0, c) 0.5, d)0.0	212
Fig. 5. 1: Datamine model of the eastern portion of the Voisey's Bay deposit looking towards the north. The orange body is the Eastern Deep's zone. The portion of the Voisey's Bay deposit model used is centred around 57000m East, 47500m North. It has an east-west extent of 2600m, and north-south extent of 1200m and a depth of 1210m.	217
Fig. 5. 2: A Data mine cross-section at large scale showing as much possible detail of the ore body (orange/red) as possible.	218
Fig. 5. 3: A small scale Datamine cross-section showing the full troctolite pluton.	219
Fig. 5. 4: Node selections and facet selection on the southern-most Datamine cross-section. The yellow line is the actual intersection between the ore and troctolite and black numbered dots represent the nodes selected along this contact.	221
Fig. 5. 5: Node selection and facet formations for the second cross-section. The x-axis of the project is the easting and the z-axis is the elevation the red nodes are those transcribed from the first cross-section. The black nodes are those chosen for the second cross-	

section. The green numbers within the enclosed shapes are the facets defined for this cross-section. Facet 19 is the temporary facet which is removed after the completion of the testing of this model.223

Fig. 5. 6: An example of a hole in a poly file.224

Fig. 5. 7: A “geological” map showing the surface exposure of the troctolite pluton within the footwall gneiss. The blue area indicates the surface exposure of the troctolite body, the red area is a projection to surface of the sulphide body, and the red dots are nodes on the edge of the upper surface of the troctolite (the black dots show the location of a hypothetical set of the boreholes).228

Fig. 5. 8: The upper surface of the 3D earth model showing out lines of the facets in blue.228

Fig. 5. 9: Figure showing a version of the final model where meshing has been done using a maximum cell size of $100\ 000\text{m}^3$. The outer block indicates the maximum extent of the model, the pink mesh is the troctolite body depicted by the facets on the contact surface between the troctolite and the gneiss, and the blue mesh is the sulphide body depicted by the facets on the contact surface between the sulphide and troctolite.230

Fig. 5. 10: A combination of the block model and the sulphide model; showing a rectangular prism (in light blue) approximating the sulphide body (in purple) from Fig. 5. 9. The grey enclosing block shows the limits of the models which are smaller than the full model of the Eastern Deeps zone (Fig. 5. 9).232

Fig. 5. 11: Screenshot showing both 2D and 3D visualization panels for Facet_Modeller.233

Fig. 5. 12: Screenshot of FacetModeller in use to create of complete model of the Voisey’s Bay deposit with a correct topographic surface (picture courtesy of Cassandra Tycholiz).234

Fig. 6. 1: Visualization of the three borehole panels. The box containing the boreholes is 2600m long, 1300m wide and 1210m in depth.235

Fig. 6. 2: Side (a) and top (b) views of the straight paths from sources to receivers from the grid-like borehole layout. The surrounding block is the same as is seen in Fig. 6. 1.236

Fig. 6. 3: Straight ray paths for the Starburst I layout of sources and receivers a) side view b) top view. The box containing this array is 2000m across, 900m wide and 1210m deep.238

Fig. 6. 4: Straight ray paths for the Starburst II layout of sources and receivers.238

Fig. 6. 5: Resultant travel time data from the forward modelling of the block model using the panel source-receiver layout.	240
Fig. 6. 6: Anomalous travel-times from the forward modelling of the block model using the panel source-receiver layout.	241
Fig. 6. 7: A zoom into the four central panels in Fig. 6. 6.	241
Fig. 6. 8: This figure illustrates the effect of the position of the area of anomalous slowness (red body to left) on the pattern seen in a plot (right side of figure). The thick black lines on the diagram (left) represent two boreholes with the green dots representing source locations and the yellow dots representing receiver locations. The thin black lines represent the wavefront path between sources and receivers. The pink squares on the plot (right) represent anomalous travel times and the blue squares on the same plot represent travel times consistent with the background slowness value.	242
Fig. 6. 9: Resultant travel time data from the forward modelling of the block model using the grid-like array.	243
Fig. 6. 10: Resultant anomalous travel times from the forward modelling of the block model using the grid-like array. The area in the black box is shown in more detail below.	243
Fig. 6. 11: Zoom into the area surrounded by the black box in Fig. 6. 10.	244
Fig. 6. 12: Resultant travel time data from the forward modelling of the block model.	245
Fig. 6. 13: Resultant anomalous travel time data from the forward modelling of the block model.	245
Fig. 6. 14: Resultant travel time data from the forward modelling of the block model.	246
Fig. 6. 15: Resultant anomalous travel time data from the forward modelling of the block model.	247
Fig. 6. 16: The block model (see Section 5. 2. 1) meshed with different maximum cell sizes: a) 1000m ³ maximum cell size and 4 084 686 cells, b) 10 000m ³ maximum cell size and 411 300 cells, c) 50 000m ³ maximum cell size and 82 369 cells, d)100 000m ³ maximum cell size ad 41 792 cells, e) 250 000m ³ maximum cell size and 17 076 cells.	248
Fig. 6. 17: Small surface array.	254
Fig. 6. 18: The anomalous gravity data shown with a surface projection of the sulphide body in the sulphide-gneiss model.	254
Fig. 6. 19: Birds-eye view of the extended array.	255

Fig. 6. 20: Results from gravity forward modelling of the sulphide model at surface stations for an extended surface grid.....	256
Fig. 6. 21: Mixed gravity measurement location array shown with the sulphide body from the Eastern Deeps model shown in blue. The axis going into the page is the northing and ranges from 40 000m north to 44 000m north	257
Fig. 6. 22: Gravity data for the mixed array shown in Fig. 6. 21. The axis going into the page is the northing and it ranges from 40 000m north to 44 000m north	257
Fig. 6. 23: Results from gravity forward modelling of the sulphide model at borehole stations.	258
Fig. 7. 1: Result of a seismic only inversion of the Eastern Deeps model using the panel array of seismic sources and receivers. The red have slowness values between 0.164 s/km and 0.17 s/km, the blue cells have slowness values between 0.1625 s/km and 0.164 s/km, and the cells not shown have slowness values less than 0.1625 s/km. The transparent orange body is the sulphide body from the Eastern Deeps model. The axis going into the page is the northing and extends from 41900m to 43100m.....	265
Fig. 7. 2: Results of a seismic only inversion using the grid-like source and receiver array. The purple cells have slownesses between 0.166 s/km and 0.174 s/km, the blue cells have between 0.164 s/km and 0.166 s/km, and all cells not shown have slownesses of less than 0.164 s/km. The axis going into the page is the northing and it extends from 42100m to 42900m.	266
Fig. 7. 3: The slowness model for the seismic-only inversion of starburst array block model synthetic data inverted on a very coarse mesh. The dipping block shown by an outline is the sulphide block from the block model (see Section 5.2.1). The red cells have slowness values between 0.185 s/km and 0.237 s/km. The purple cells have slowness values between 0.167 s/km and 0.185 s/km. All cells not shown have slowness values less than 0.167 s/km. Those cells not shown have slowness values less than 0.165ms. The axis going in to the page is the northing and extends from 42000m to 42900m.....	269
Fig. 7. 4: a) The predicted travel times and b) normalized data residuals in ms calculated for the slowness distribution seen in Fig. 7. 3.....	270
Fig. 7. 5: The slowness model for the seismic-only inversion of starburst array block model synthetic data inverted on a coarse mesh. The dipping block shown by an outline is the sulphide block from the block model (see Section 5.2.1).The red cells have slowness values between 0.19 s/km and 0.226 s/km. The purple cells have slowness values of 0.168 s/km and 0.19 s/km. All of the cells not shown have slowness values of less than 0.168 s/km. Those cells not shown have slowness values less than 0.165ms. The axis going in to the page is the northing and extends from 42000m to 42900m	271

Fig. 7. 6: a) The predicted travel times and b) normalized data residuals in ms calculated from the slowness model in Fig. 7. 5. 272

Fig. 7. 7: The slowness model from the seismic-only inversion of starburst array block model synthetic data inverted on a medium mesh. The dipping block shown by an outline is the sulphide block from the block model (see Section 5.2.1). The red cells have slowness values of 0.173 s/km to 0.1911 s/km. The purple cells have slowness values from 0.168 s/km to 0.173 s/km. The blue cells have slowness values between 0.164s/km and 0.167s/km. Those cells not shown have slowness values below 0.164 s/km. Those cells not shown have slowness values less than 0.165ms. The axis going in to the page is the northing and extends from 42000m to 42900m 273

Fig. 7. 8: a)The predicted travel times and b) normalized data residuals in ms calculated from the slowness model in Fig. 7. 7. 273

Fig. 7. 9: The slowness model for the seismic-only inversion of starburst array block model synthetic data inverted on a fine mesh. The dipping block shown by an outline is the sulphide block from the block model (see Section 5.2.1). Red cells have slowness values between 0.17s/km and 0.1745s/km. The purple cells have slowness values between 0.1675s/km to 0.17s/km. The blue cells have slowness values between 0.165s/km to 0.1675s/km. Those cells not shown have slowness values less than 0.165ms. The axis going in to the page is the northing and extends from 42000m to 42900m..... 274

Fig. 7. 10: The predicted travel times (a) and normalized data residuals (b) calculated from the density distribution seen in Fig. 7. 9. 275

Fig. 7. 11: Graph showing the linear relationship between the number of cells in an inversion mesh and the computation time for the seismic inversion run using that mesh and the Starburst I array. 276

Fig. 7. 12: Resultant slowness model from the seismic-only inversion of block model synthetic data. . The dipping block shown by an outline is the sulphide block from the block model (see Section 5.2.1). The red cells have slowness values between 0.2 s/km and 0.24 s/km, the purple cells have slowness values between 0.18 s/km and 0.2 s/km, the blue cells have slowness values between 0.17 s/km to 0.18 s/km, and cells that are not shown have slowness values less than 0.17 s/km. 277

Fig. 7. 13: a) Predicted gravity anomaly and b) associated normalized data residuals for the small surface array data inversion on the fine inversion mesh. 279

Fig. 7. 14: Resultant density distributions from the small surface array gravity inversion on the fine inversion mesh. The red cells had relative densities between 0.035 g/cm³ to 0.0433 g/cm³, the purple cells have relative densities between 0.035 g/cm³ and 0.035 g/cm³, the blue cells have densities between 0.015 g/cm³ and 0.025 g/cm³ and all other cells have densities less than 0.015 g/cm³. The sulphide body is shown in black and has a

relative density of 1.652 g/cm³ and the axis going in to the page is the northing and extends from 42000m to 42900m. 280

Fig. 7. 15: A depiction of the graduated block model showing the three prisms. 281

Fig. 7. 16: a) Predicted gravity anomaly and b) associated normalized data residuals for the default sens_norm inversion on the large surface gravity array. 283

Fig. 7. 17: Resultant density distributions from the default sensitivity large surface array gravity inversion. The red cells had relative densities between 0.045 g/cm³ to 0.0625 g/cm³, the purple cells have relative densities between 0.03 g/cm³ and 0.045 g/cm³, the blue cells have densities between 0.015 g/cm³ and 0.03 g/cm³ and all other cells have densities less than 0.015 g/cm³. The sulphide body is shown in black and has a relative density of 1.652 g/cm³ and the axis going in to the page is the northing and extends from 42000m to 42900m. 283

Fig. 7. 18: Resultant density distributions from the moderate sensitivity large surface array gravity inversion. The red cells had relative densities between 0.035 g/cm³ to 0.0444 g/cm³, the purple cells have relative densities between 0.025 g/cm³ and 0.035 g/cm³, the blue cells have densities between 0.015 g/cm³ and 0.025 g/cm³ and all other cells have densities less than 0.015 g/cm³. The sulphide body is shown in black and has a relative density of 1.652 g/cm³ and the axis going in to the page is the northing and extends from 42000m to 42900m. 284

Fig. 7. 19: Resultant density distributions from the low sensitivity large surface array gravity inversion. The red cells had relative densities between 0.03 g/cm³ to 0.036 g/cm³, the purple cells have relative densities between 0.025 g/cm³ and 0.035 g/cm³, the blue cells have densities between 0.015 g/cm³ and 0.025 g/cm³ and all other cells have densities less than 0.015 g/cm³. The sulphide body is shown in black and has a relative density of 1.652 g/cm³ and the axis going in to the page is the northing and extends from 42000m to 42900m. 285

Fig. 7. 20: Resultant density distributions from the large surface array gravity inversion with no sensitivity weighting. The red cells had relative densities between 0.03 g/cm³ to 0.039 g/cm³, the purple cells have relative densities between 0.025 g/cm³ and 0.035 g/cm³, the blue cells have densities between 0.015 g/cm³ and 0.025 g/cm³ and all other cells have densities less than 0.015 g/cm³. The sulphide body is shown in black and has a relative density of 1.652 g/cm³ and the axis going in to the page is the northing and extends from 42000m to 42900m. 286

Fig. 7. 21: Resultant density distributions from the large surface array gravity inversion on the fine inversion mesh. The red cells had relative densities between 0.045 g/cm³ to 0.06273 g/cm³, the purple cells have relative densities between 0.03 g/cm³ and 0.045 g/cm³, the blue cells have relative densities between 0.015 g/cm³ and 0.03 g/cm³ and all other cells have densities less than 0.015 g/cm³. The sulphide body is shown in grey and

has a relative density of 1.652 g/cm^3 and the axis going in to the page is the northing and extends from 42000m to 287

Fig. 7. 22: Predicted relative gravity measurements predicted by the inversion of mixed gravity array data for a) borehole measurements and b) surface measurements on the graduated inversion mesh. 289

Fig. 7. 23: Normalized data residuals calculated for the results of the inversion of the mixed array a) for borehole measurements and b) surface locations on the graduated inversion mesh. 290

Fig. 7. 24: Resultant density distributions from the inversion of mixed array data on the graduated inversion mesh. The pink cells in the centre of the model have relative densities between 0.8 g/cm^3 to 1.451 g/cm^3 , the turquoise cells have relative densities between 0.25 g/cm^3 and 0.8 g/cm^3 , the light blue cells have densities between 0.10 g/cm^3 and 0.25 g/cm^3 and all other cells have densities less than 0.010 g/cm^3 . The sulphide body is shown in black and has a relative density of 1.652 g/cm^3 and the axis going in to the page is the northing and extends from 42000m to 42900m. The grey dots are gravity measurement locations. 290

Fig. 7. 25: Resultant density distributions from the large surface array gravity inversion on the fine inversion mesh. The red cells had relative densities between 0.9 g/cm^3 to 2.1833 g/cm^3 , the purple cells have relative densities between 0.3 g/cm^3 and 0.9 g/cm^3 and all other cells have densities less than 0.015 g/cm^3 . The sulphide body is shown in grey and has a relative density of 1.652 g/cm^3 and the axis going in to the page is the northing and extends from 42000m to 42900m..... 292

Fig. 7. 26: Predicted relative gravity measurements predicted by the inversion of borehole-only gravity array data on the graduated inversion mesh. 293

Fig. 7. 27: Normalized data residuals calculated for the results of the inversion of borehole-only gravity array data on the graduated inversion mesh. 293

Fig. 7. 28: Resultant density distributions from the inversion on the graduated inversion mesh. The red cells had relative densities between 0.9 g/cm^3 to 2.0 g/cm^3 , the purple cells have relative densities between 0.3 g/cm^3 and 0.9 g/cm^3 and all other cells have densities less than 0.3 g/cm^3 . The sulphide body is shown in grey and has a relative density of 1.652 g/cm^3 and the axis going in to the page is the northing and extends from 42000m to 42900m. 294

Fig. 7. 29: Resultant density distributions from the inversion on the fine inversion mesh. The red cells had relative densities between 0.9 g/cm^3 to 2.0 g/cm^3 , the purple cells have relative densities between 0.3 g/cm^3 and 0.9 g/cm^3 and all other cells have densities less than 0.3 g/cm^3 . The sulphide body is shown in grey and has a relative density of 1.652 g/cm^3 and the axis going in to the page is the northing and extends from 402000m to 42900m. 295

Fig. 7. 30: a) Gravity data and b) associated normalized data residuals for the gravity half of the joint inversion on the graduated inversion mesh. 297

Fig. 7. 31: a) Travel time data and b) associated normalized data residuals for the gravity half of the joint inversion on the graduated inversion mesh. 298

Fig. 7. 32: Resultant density distributions from the joint inversion on the graduated inversion mesh. The red cells had relative densities between 1 g/cm^3 to 2.0 g/cm^3 , the purple cells have relative densities between 0.3 g/cm^3 and 1.0 g/cm^3 and all other cells have densities less than 0.3 g/cm^3 . The sulphide body is shown in grey and has a relative density of 1.652 g/cm^3 and the axis going in to the page is the northing and extends from 42000m to 42900m. 299

Fig. 7. 33: Slowness distributions from joint inversion on the graduated inversion mesh. The red cells had slowness values between 0.166 s/km to 0.169 s/km , the purple cells have slowness values between 0.164 s/km and 0.163 s/km and all other cells have slowness values less than 0.163 s/km . The sulphide body is shown in grey and has a slowness of 0.2218 s/km and the axis going in to the page is the northing and extends from 42000m to 42900m. 299

Fig. 7. 34: a) Gravity data and b) associated normalized data residuals for the gravity half of the joint inversion on the fine inversion mesh. 301

Fig. 7. 35: a) Travel time data and b) associated normalized data residuals for the gravity half of the joint inversion on the graduated inversion mesh. 301

Fig. 7. 36: The sulphide body is shown in grey in both a) and b) has a relative density of 1.1652 g/cm^3 and a slowness 0.2218 s/km and the axis going in to the page is the northing and extends from 42000m to 42900m. a) Resultant density distributions from the joint inversion on the graduated inversion mesh. The red cells had relative densities between 1 g/cm^3 to 2.0 g/cm^3 , the purple cells have relative densities between 0.3 g/cm^3 and 1.0 g/cm^3 and all other cells have densities less than 0.3 g/cm^3 . b) Slowness distributions from joint inversion on the graduated inversion mesh. The red cells had slowness values between 0.175 s/km to 0.186 s/km , the purple cells have slowness values between 0.175 s/km and 0.170 s/km and all other cells have slowness values less than 0.170 s/km 303

List of Tables

Table 3. 1: Physical properties for lithologies of interest	35
Table 3. 2: Summary of <i>add_noise</i> inputs of all datasets.	48
Table 4. 1: A summary of the examples presented in this chapter. Model indicates the synthetic model used to create the data inverted in the example. Inv_Type indicates whether the example is a single property or joint inversion. Data_Type specifies which datasets were being inverted: travel-time, gravity, or both. Noise indicates how much noise was added to the data (see Sections 2.3.3, and 3.4). ρ_e specifies the value of the similarity parameter used in the inversion. Page indicates the page in this chapter where the inversion can be found.	57
Table 4. 2: Summary of important input values for example 1.	61
Table 4. 3: Summary of important input values for example 2.	63
Table 4. 4: Summary of important input values for example 3.	65
Table 4. 5: Summary of important input values for example 4.	68
Table 4. 6: Summary of important input values for example 5.	71
Table 4. 7: Summary of important input values for example 6.	74
Table 4. 8: Summary of important input values for example 7.	76
Table 4. 9: Summary of important input values for example 8.	79
Table 4. 10: Summary of important input values for example 9.	81
Table 4. 11: Summary of important input values for example 10.	83
Table 4. 12: Summary of important input values for example 11.	86
Table 4. 13: Summary of important input values for example 12.	89
Table 4. 14: Summary of important input values for example 13.	92
Table 4. 15: Summary of important input values for example 14.	95
Table 4. 16: Summary of important input values for example 15.	98
Table 4. 17: Summary of important input values for example 16.	101
Table 4. 18: Summary of important input values for example 16.	104
Table 4. 19: Summary of important input values for example 18.	106
Table 4. 20: Summary of important input values for example 19.	108
Table 4. 21: Summary of important input values for example 20.	110
Table 4. 22: Summary of important input values for example 21.	113
Table 4. 23: Summary of important input values for example 22.	115
Table 4. 24: Summary of important input values for example 23.	118
Table 4. 25: Summary of important input values for example 24.	120

Table 4. 26: Summary of important input values for example 25.	123
Table 4. 27: Summary of important input values for example 27.	125
Table 4. 28: Summary of important input values for example 27.	127
Table 4. 29: Summary of important input values for example 28.	130
Table 4. 30: Summary of important input values for example 29.	133
Table 4. 31: Summary of important input values for example 30.	135
Table 4. 32: Summary of important input values for example 31.	137
Table 4. 33: Summary of important input values for example 32.	140
Table 4. 34: Summary of important input values for example 33.	142
Table 4. 35: Summary of important input values for example 34.	144
Table 4. 36: Summary of important input values for example 35.	147
Table 4. 37: Summary of important input values for example 36.	150
Table 4. 38: Summary of important input values for example 37.	153
Table 4. 39: Summary of important input values for example 38.	156
Table 4. 40: Summary of important input values for example 39.	159
Table 4. 41: Summary of important input values for example 40.	162
Table 4. 42: Summary of important input values for example 41.	164
Table 4. 43: Summary of important input values for example 42.	167
Table 4. 44: Summary of important input values for example 43.	170
Table 4. 45: Summary of important input values for example 44.	172
Table 4. 46: Summary of important input values for example 45.	175
Table 4. 47: Summary of important input values for example 46.	178
Table 4. 48: Summary of important input values for example 47.	180
Table 4. 49: Summary of important input values for example 48.	182
Table 4. 50: Summary of important input values for example 50.	184
Table 4. 51: Summary of important input values for example 50.	186
Table 4. 52: Summary of important input values for example 51.	188
Table 4. 53: Summary of important input values for example 52.	189
Table 4. 54: Summary of important input values for example 53.	191
Table 5. 1: Tabulation of the maximum cell sizes used in mesh generation.	229
Table 6. 1: Summary of the largest travel time differences between the finest mesh and other meshes.	249

Table 6. 2: Summary of the maximum change to the finest mesh travel time data with different levels of noise. 250

Table 7. 1: Mesh specification for the inversion meshes used during the coarseness tests. 268

Chapter 1: Introduction and Background Information

In this project a new approach to geophysical modelling was tested. In this chapter the background information on the modelling method and model types used in this project are presented in order to provide context to the rest of the thesis.

1.1 Geophysical Modelling

The use of modelling techniques to determine the subsurface physical property structure of the Earth is a frequently used technique for interpreting geophysical data. It is a useful tool for gaining further insight into the Earth's subsurface physical property structure. The development of modelling techniques that can see deeper into the Earth and produce increasingly faithful representations of the subsurface physical property structures is necessary to further the utility of geophysical datasets (Vozoff and Jupp, 1975). In this section a summary of the geophysical modelling techniques will be presented in order to provide context to the methods used in this project.

Geophysical modelling has developed from simple calculations on paper, where curves calculated for simple geometric shapes were compared to geophysical data (Nettleton, 1942), to complex computer algorithms. This progression stems, in greater part, from the immense increase in computing power over the past fifty years. Two different approaches to modelling geophysical data have been developed: forward modelling and inversion modelling.

1.1.1 Forward and Inversion Modelling

Forward modelling involves the calculation of the geophysical response of a synthetic model. The geophysical response that this model produces is compared to field measurements. The investigator can adjust the model to achieve an acceptable fit between the calculated response and the measured data.

Forward modelling has the benefits of being a well-posed and mathematically unique problem. A physical property distribution produces only one correct geophysical response. This type of modelling allows the investigator direct control of the changes made to the model; as such, the changes made should make geological sense, as well as being mathematically correct. The disadvantage of forward modelling is the time required to make many tedious modifications to a model and to recalculate the expected geophysical response.

Inversion modelling is an automated process, during which a computer makes changes to an Earth model. As inversion modelling is an automated process it requires less human time to create a final model than forward modelling (Vozoff and Jupp, 1975). However, it is a non-unique ill-posed problem (Oldenburg, et al., 1996); as such, unlike forward modelling there are an infinite set of potentially correct solutions to an inversion problem.

Inversion modelling is a two part problem: the first part is solving the forward problem and the second part is the minimization of a model objective function (Oldenburg, et al., 1996). The objective functions used in inversion modelling techniques generally include a measure of data misfit and some parameters regulating

the physical property distribution of the resultant model. Often a minimum structure term is used to regularize physical property distribution (Oldenburg, et al., 1996). Due to the non-unique nature of inversion modelling care must be taken when determining the weighting of the structure and misfit terms in order to produce models that are geologically reasonable.

Earth models used in inversion modelling generally consist of fixed mesh models. These meshes are frequently rectilinear (2D) as is seen in Fig. 1. 1 or consist of cubes (3D) (Oldenburg, et al., 1996). However, in this project triangular (2D) or tetrahedral (3D) meshes were used and are discussed in more detail below. Each cell in the mesh is assigned a physical property value (Bosch and McGaughey, 2001). Although each cell is homogeneous the Earth model can be heterogeneous as the physical property value can vary between cells. Although other methods exist, in standard inversions the physical property values of the cells are changed but the mesh boundaries remain unchanged.

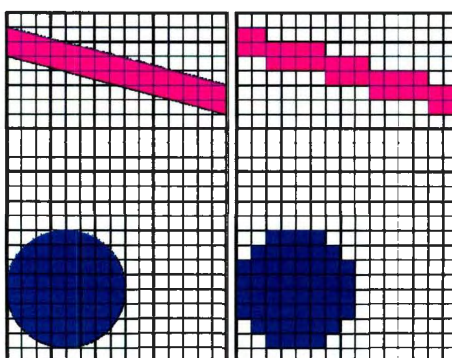


Fig. 1. 1: Rectilinear-type meshes are an example of the meshes often used for inversion modelling. These meshes are created by overlaying a rectilinear mesh over the base model (left). Each cell is then assigned the physical property of the unit that fills the majority of the cell (right).

1.1.2 Joint Inversion Modelling

Joint inversion is the simultaneous inversion of two geophysical data sets to produce a single Earth model (Bosch and McGaughey, 2001, Fregoso and Gallardo, 2009, Lelievre, et al., 2012). The premise is that an Earth model which can replicate two different sets of geophysical data is more likely to have replicated the subsurface physical property structure than if the model only holds true for a single data type (Manglik and Verma, 1998, Nishiyama, et al., 2012, Shamsipour, et al., 2012). The concept of joint inversion has been around for more than thirty years (Vozoff and Jupp, 1975). Yet it has yet to become a commonly used technique. There are examples in the literature of joint inversion being used to invert a number of different combinations of data types: seismic travel time and gravity (Afnimar, et al., 2002, Vernant, et al., 2002, Villasenor, et al., 2012); between gravity and magnetics (Fregoso and Gallardo, 2009, Pilkington, 2006, Gallardo and Thebaud, 2012, Shamsipour, et al., 2012); DC resistivity and ultra-low frequency electromagnetic data (Vernant, et al., 2002, Lelievre, et al., 2012); seismic travel time and magnetotelluric data (Manglik and Verma, 1998, Manglik, et al., 2011); and gravity and radiographic data (Nishiyama, et al., 2012).

There are two approaches to joint inversion: the first is to carry out two separate inversions where the result of the inversion of the first data set is used to inform the inversion of the second dataset (Lines, et al., 1988, Vernant, et al., 2002); the second approach is to simultaneously invert the two data sets by including terms in the objective function which link the two physical properties (Gallardo and Thebaud, 2012, Lelievre, et al., 2012). In this project the second method is employed.

There are two different methods for linking the physical property distributions in the simultaneous joint inversion approach.

The first method is a structural approach (Haber and Oldenburg, 1997, Colombo and De Stefano, 2007, Fregoso and Gallardo, 2009, Hu, et al., 2009, Gallardo and Thebaud, 2012, Villasenor, et al., 2012) where the joint inversion uses a measure of the structural difference between the distributions of the two physical properties being used in the inversion.

The second method is a lithological approach (Bosch and McGaughey, 2001). The lithological approach involves the development of a mathematical relationship between the two physical properties. This relationship can be an empirical relationship or it can be a statistical relationship (Fig. 1. 2). The relationship developed between different physical properties tends to depend on the geology of the area and the number of rock units with unique physical property character. The relationship used in the lithological approach is dependant on the rock types in the local geology; as such, a relationship that works in one area will not necessarily work in another (Bosch and McGaughey, 2001). This lithological approach plays a large role in the joint inversion approach studied in this thesis.

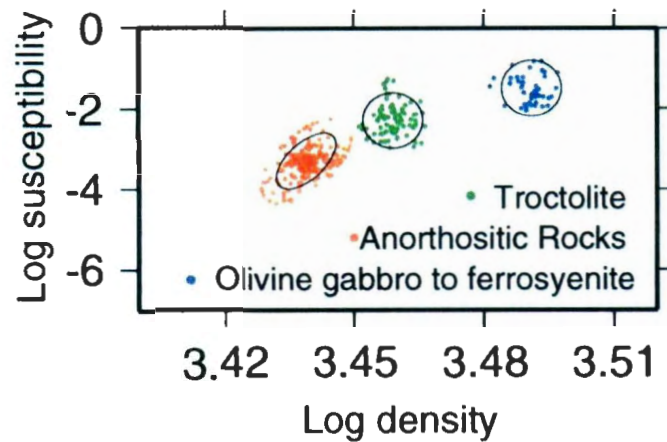


Fig. 1. 2: Determination of the statistical relationship between magnetic susceptibility and density derived by Bosch and McGaughey (2001) for the three lithologies in their test model.

1.2 Wireframe Mesh Models

Geological models of ore deposits are commonly created during delineation drilling and the accuracy of these models is crucial to determining if a deposit is economically viable. The models generally consist of wireframe meshes enclosing different geological units. Triangular wireframe meshes are used because they are an efficient way to model complex surfaces. Geophysical models, in comparison, generally come in one of two different forms: rectilinear-type meshes (Haber and Oldenburg, 1997, Hu, et al., 2009, Shamsipour, et al., 2012), which consist of horizontal and vertical lines, and objects and anomalous body modelled by a geometrical simple shape, such as plates (Fig. 1. 3) and spheres. Rectilinear-type meshes (Fig. 1. 1) are most often used for inversion modelling whereas simple volumes are more often used in forward modelling.

The choice of model type is made mostly to simplify the mathematics necessary to calculate the expected geophysical response of an Earth model both in forward modelling and in the forward modelling half of the inversion problem. Due to the inherent differences between geophysical and geological models they are often difficult to compare. This impedes communication between geologists and geophysicists. The development of geophysical modelling algorithms which use triangular (2D) and tetrahedral (3D) meshes, which can fit seamlessly with geological wireframe models, rather than thin plates or rectilinear meshes will improve the communication between geophysicists and geologists, potentially aiding in the production of more accurate ore deposit models (Fig. 1. 4). In this project unstructured triangular (2D) and tetrahedral (3D) meshes will be used to define the models in this project.

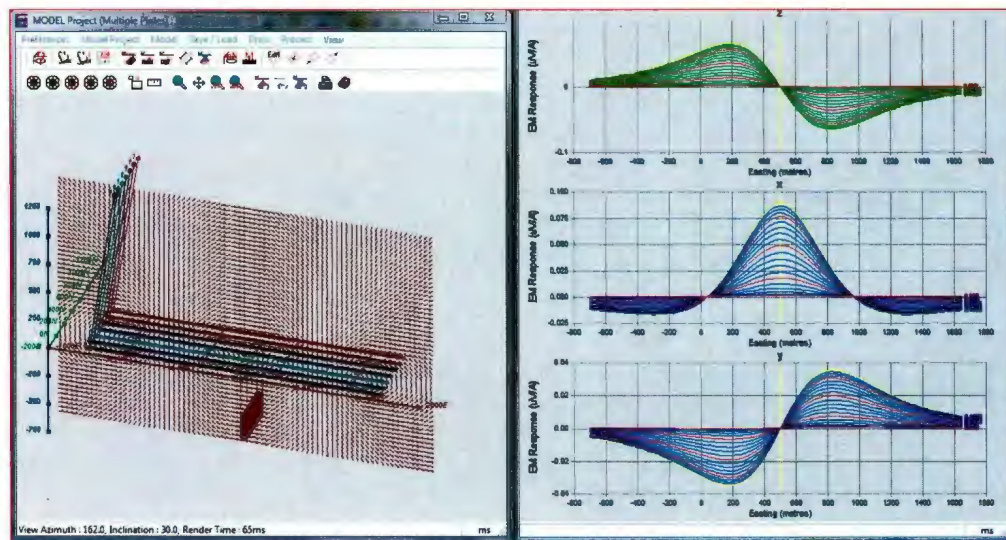


Fig. 1. 3: A thin plate model created using the Maxwell forward modelling program for modelling electromagnetic data (figure courtesy of Adam Mercer).

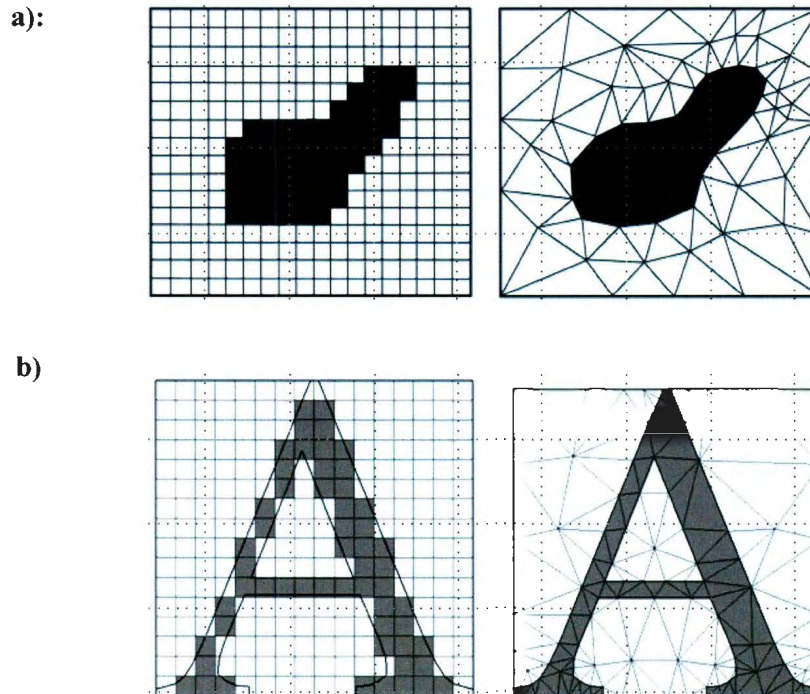


Fig. 1. 4: a) Comparison between a rectilinear and triangular mesh representation of an amorphous body (Jahandari, 2011). b) Comparison between a rectilinear and triangular representation of the letter A (Lelievre, et al., 2012).

1.3 Voisey's Bay Deposit

The Voisey's Bay deposit is a magmatic nickel-copper-cobalt massive sulphide deposit in northern Labrador (Huminicki, et al., 2008; Naldrett, et al., 2000) named for its location near Voisey's Bay on the Labrador Sea (Fig. 1. 5). The deposit was discovered in 1993 by Diamond Fields Resources, when a gossanous outcropping at Discovery Hill was recognized (Evans-Lamswood, et al., 2000). Subsequently a number of mineralized zones trending roughly east-west for a distance of 6km have been discovered (Fig. 1. 6). Open pit mining of the Ovoid Zone commenced in 2005 (Weldon, 2005).

The Voisey's Bay deposit consists of massive sulphide lenses hosted in the 1.34 Ga Voisey's Bay troctolite and gabbro intrusions (Huminiki et al., 2008). The Voisey's Bay intrusions are part of the Nain Plutonic Suite, which were intruded as stitching plutons along 1.85 Ga fault between the Archean Nain Province and the Paleoproterozoic Churchill province (Kerr and Ryan, 2000). The footwall of the Voisey's bay intrusions are the Nain province gneisses (Evans-Lamswood et al., 2000).

Voisey's Bay mineralization consists predominantly of pyrrhotite, pentlandite and chalcopyrite. A database of physical property data measured from drill core was compiled by Vale (Duff, 2007). By calculating the mean for the slowness and density of the different rock types it was determined that the massive sulphide lenses are significantly denser ($\sim 4.47 \text{ g/cm}^3$) and slower ($\sim 2.22 \times 10^{-4} \text{ s/m}$) than the troctolite ($\sim 2.91 \text{ g/cm}^3, \sim 1.66 \times 10^{-4} \text{ s/m}$) host rock. The troctolite, in turn, is denser and slightly slower than the gneissic wall rock ($\sim 2.82 \text{ g/cm}^3, \sim 1.62 \times 10^{-4} \text{ s/m}$). The felsic sills and dykes have similar physical properties as the gneissic wall rock.

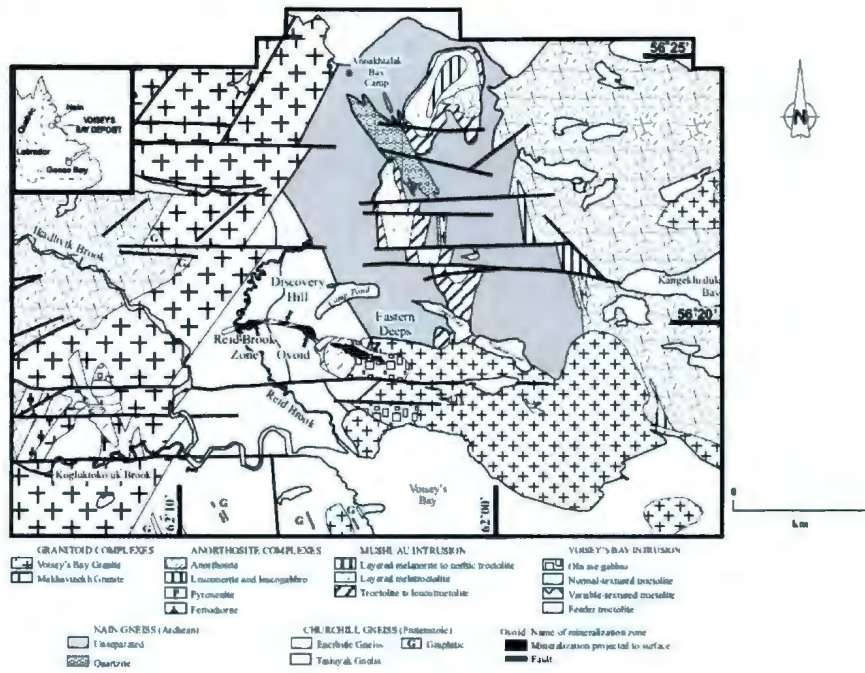


Fig. 1. 5: Map of the Voisey's Bay Deposit showing the lateral distribution of the main ore zones and the location of the deposit within Labrador (after Evans-Lamswood et al., 2000).

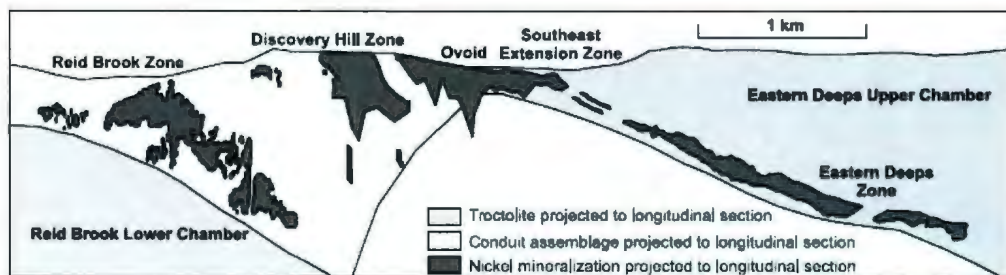


Fig. 1. 6: Cross-section through the Voisey's Bay Deposit showing the location of the Reid Brook, Discovery Hill, Ovoid Extension and Eastern Deeps ore zones with respect to surface (after Li et al., 2000).

1.3.1 The Eastern Deeps Zone

The Eastern Deeps zone of the Voisey's Bay deposits consists of a troctolite and olivine gabbro pluton and feeder system emplaced into Archean gneisses (Evans-Lamswood et al., 2000). The massive sulphide lenses are located in the basal breccia

sequence at the bottom of the intrusion and extend part way into the feeder pipe. The basal breccia is overlain by varied and normal textured troctolite. The uppermost part of the intrusion consists of olivine gabbro. The pluton is cross-cut by granitic to syenitic dykes and sills (Fig. 1. 7).

As a magmatic sulphide deposit Voisey's Bay shows relatively little evidence of major hydrothermal alteration. The absence of extensive hydrothermal alteration and the limited variety of rock types present in the deposit as well as the relatively sharp contacts between the different lithologies (Naldrett et al., 2000) all make this deposit well suited for geophysical modelling.

Investigating the response of synthetic models based on the Eastern Deeps will allow for a better understanding of how well seismic tomography and gravity joint inversion can delineate a buried sulphide lens. Also, by incorporating the presence of the troctolite intrusion, it will be possible to determine if joint inversion will allow for the resolution of a body with small physical properties contrast in the presence of a body with high physical properties is contrasts.

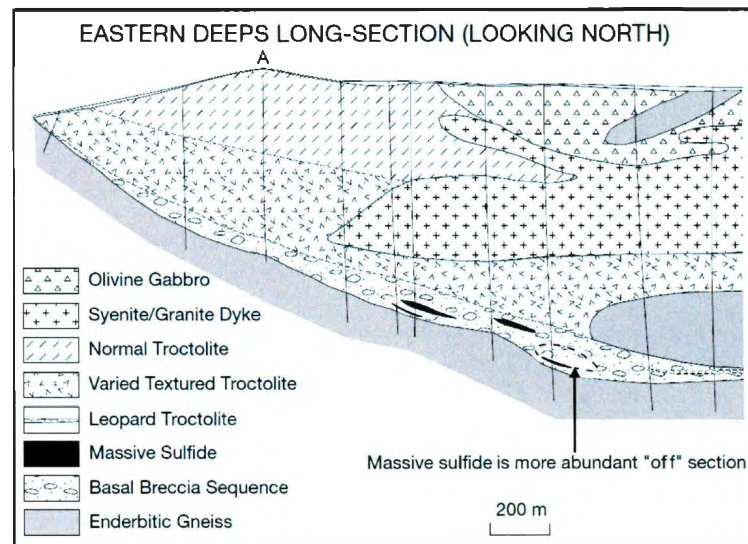


Fig. 1. 7: Geological cross-section through the Eastern Deeps intrusion and ore zone (after Evans-Lamswood et al., 2000).

1.4 Project Aims

The goal of this project is to determine the viability of joint borehole seismic tomography and gravity inversion method, developed by Dr. Peter Lelièvre, a post-doctoral fellow at Memorial University of Newfoundland, for the delineation of geologically realistic scenarios. This was attained through a series of tests using 2D and 3D synthetic unstructured mesh models based on the geology of the Eastern Deeps zone of the Voisey's Bay Deposit in Labrador, Canada. An attempt is made to answer a number of questions during the course of this investigation, including the following: Does joint inversion lead to better models than single property inversion? Are travel-time and gravity data complementary in such a way that their joint inversion is useful? Is 3D joint inversion even computationally feasible and if not really, what are the limits? How does survey design affect the applicability of joint

inversion? Most importantly, is it worth investing the time and effort to perform, or are the results not really worth it?

In Chapter 2 a detailed explanation of the methodologies used in this thesis is presented. In Chapter 3 the construction of two dimensional (2D) models and production of synthetic datasets through forward modelling is discussed. In Chapter 4 the results for 2D inversion tests are presented and discussed. In Chapter 5 the construction of three dimensional (3D) models is presented. In Chapter 6 the production of the synthetic datasets through forward modelling from the 3D models is presented. In Chapter 7 the results of 3D inversion tests are presented and discussed. In Chapter 8 a summary of the findings of this thesis are presented.

Chapter 2: Methodology and Code

The computer programs used in this project come from two sources: the results of the work of Dr. Lelièvre, and publicly available open source software.

2.1 Triangular and Tetrahedral Mesh Generation and Visualization

All of the models used during this project consisted of triangular or tetrahedral meshes. These meshes were generated using third party open source software packages: Triangle was used to generate the 2D triangular meshes (Shewchuk, 1996; Shewchuk, 2002) and Tetgen was used to generate the 3D tetrahedral meshes (Si and Gartner, 2004; Si and Gartner, 2005). These programs create meshes based on an input file provided by the user. The input file specifies the location of the nodes in the mesh and defines edges (2D) or surfaces (3D) between nodes which must be present in the model. Triangle and Tetgen also allow for the assignment of attributes to user defined regions. In this project a unique unit identification number was assigned to each of the regions (Fig. 2. 1). More detail on 2D and 3D mesh generation is provided in sections 3.1.1 and 6.1 respectively.

Physical properties were assigned to the models based on unit identification numbers using a program called *rockunits2ele* written by Dr. P. Lelièvre. During this project, two different physical properties, relative density and relative seismic slowness, were assigned to each region in the models. The gravity forward modelling used in this project required that each triangle or tetrahedron must be assigned a uniform relative density given as:

$$\rho_{rel} = \rho_{unit} - \rho_{background} \quad 2.1$$

where ρ_{unit} and ρ_{rel} are the density and relative density of the rock unit respectively and $\rho_{background}$ is the density of the background. Likewise the seismic travel time forward modelling required that all of the triangles (2D) or tetrahedrons (3D) in the model must be assigned constant relative slowness values given as:

$$S_{rel} = S_{unit} - S_{background} \quad 2.2$$

Where S_{rel} is the relative slowness, S_{unit} is the slowness of the unit in question and $S_{background}$ is the slowness of the background. In this project the background was always assigned the density and slowness of the felsic gneiss.

To visualize the models produced by Triangle and Tetgen, as well as the data produced during forward and inversion modelling, Paraview, an open source mesh visualization program, was used. The output files produced by the mesh generation and modelling programs are not in the format required by Paraview. As such, Dr. Lelièvre has developed a number of small programs for converting the output files of the mesh generation, forward modelling and inversion modelling programs to the .vtu files required by Paraview. These include: *mesh2vtu*, *nodes2vtu*, *ele2vtu*, and *poly2vtu*.

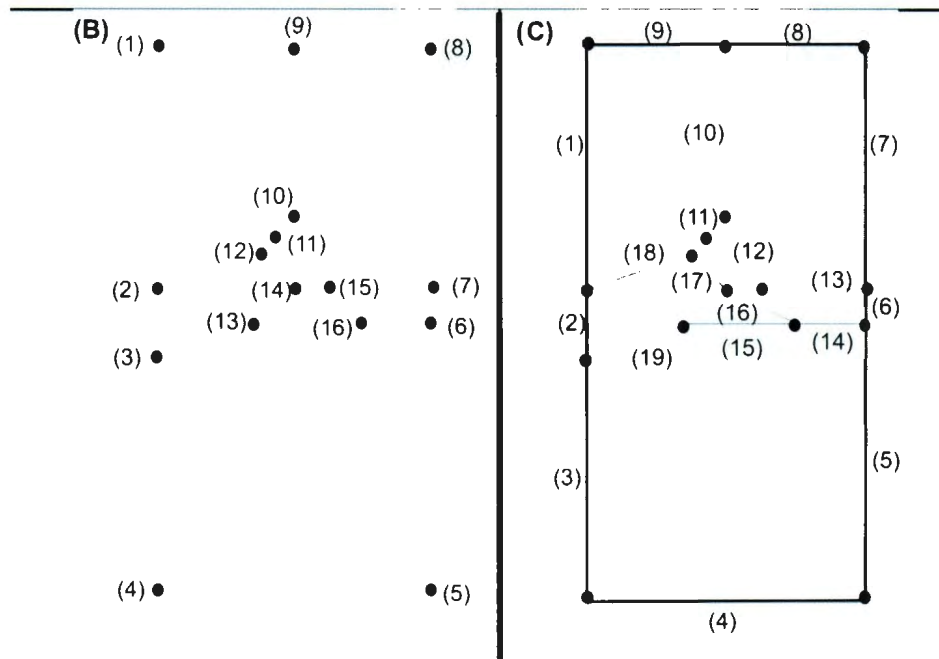
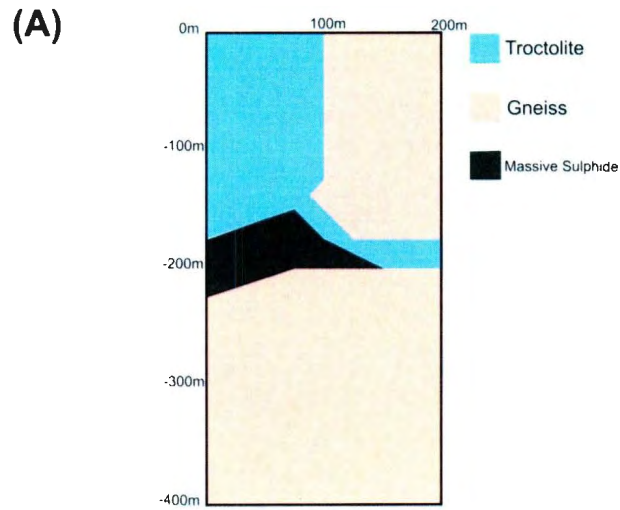


Fig. 2. 1: After a model has been designed (a), an input file for Triangle is created by identifying the vertices in the model (b). The coordinates of each vertex is entered into the input file. Each of the line segments necessary for the model are then identified (c) and two vertices at each end of the line segment are entered into the input file.

2.2 Forward Modelling and Noise

Dr. Lelièvre has developed two forward modelling programs: *gravity_fwd* and *seismics_fwd*, which are used here.

2.3.1 Gravity Forward Modelling

2.3.1.1 Overview of *Gravity_fwd*

Gravity_fwd was used to calculate the gravity response of a model for a specified set of data collection stations. There are formulae derived for calculating the gravity response of a tetrahedral cell given the location of that tetrahedron relative to a gravity station (Okabe, 1979), which have been modified to apply to two dimension situations with triangular cells (Jahandari, 2011; Lelièvre, et al., 2012). The gravity of each cell is calculated separately and the principle of superposition is used to calculate the overall gravity response of all the cells.

2.3.1.2 Using *gravity_fwd*

Gravity forward modelling was accomplished using the program *gravity_fwd* (see Section 2.3.1). In order to operate *gravity_fwd* an input file defining the parameters must be provided. All potential inputs for *gravity_fwd* are presented in the documentation written by Dr. Lelièvre (see Appendix A). The following is the subset of inputs used during this project. The values presented here are the default values for each input parameters. For the gravity forward modeling conducted in this project the following inputs were kept in the input file:

```

ismag 'f' ! set to true if you want to perform magnetic modelling instead of gravity
istensor 'f' ! specifies the type of gravity data
zdir 1 ! specifies the coordinate system
gridtype 'unstructured' ! the type of grid (the other option is 'rectilinear')
meshfile ! file containing mesh information
modelfile ! file containing model information
split 0 ! how to convert from rectilinear to unstructured grid
obsfile " ! file containing the observation locations
ai 1 ! attribute index to use as the model
gmul 1.0 ! multiplicative scalar to convert model to density
gadd 0.0 ! additive scalar to convert model to density
approx 'f' ! perform approximate modelling or not
move 'f' ! allows you to copy the data to the x or z coordinate
comps ttttt ! specify which tensor components to use

```

For most inputs the defaults were used. However, some inputs were changed regularly:

- Meshfile: defines the mesh in this case a .node file produced by *triangle* was used in the case of 2D models or *tetgen* in the case of 3D models (see Section 2.1)
- Modelfile: contains the model information, such as the physical property values of the various cells; in the case of this project a .ele file produced through the use of *tetgen* (3D) or *triangle* (2D) to which the physical property information had been added using *rockunits2ele* (see Section 2.1)

- `obsfile`: contains the locations for which *gravity_fwd* needs to calculate the gravity response
- `ai`: the attribute index. This indicates which column in the `.ele` file contains the density values for each cell
- `gmul` and `gadd`: used to scale the densities if necessary such that $gmul * (\text{physical property given in .ele}) + gadd = \text{actual density of cell}$

After an input file has been created *gravity_fwd* is executed using the following statement from the command line “`./gravity_fwd input_file`”.

2.3.2 Seismic Forward Modelling

2.3.2.1 Overview of *Seismics_fwd*

Seismics_fwd was used during this project to generate the first-arrival times at a user defined set of receivers locations based on a user defined set of source locations for tetrahedral and triangular models. The seismic forward modelling algorithm generates the first arrival times at the receivers by propagating wave fronts from the sources outward through the model. The wave fronts are propagated using the fast marching method (FMM) (Lelièvre, et al., 2010).

The fast marching method involves the propagation of a solution front through the model. This is accomplished by choosing a starting node within the solution front and calculating the travel-times between that node and its nearest upwind neighbours. The neighbour with the shortest travel time is then added to the solution front and the node from which the travel times were calculated becomes a downwind node with a fixed travel time value. Once the solution front has been propagated all the way through a model the first arrival

times at the receivers are determined (Fig. 2. 2). As each node is assigned a travel time it is possible to display the forward modelled data as travel-time contours (Fig. 2. 3).

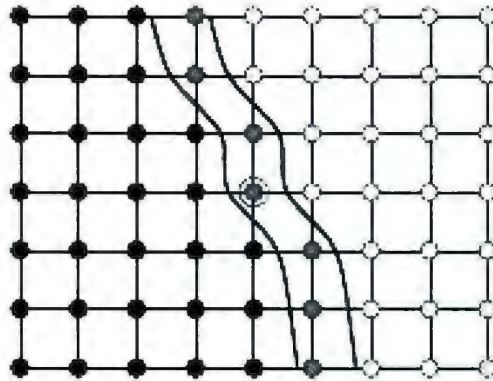


Fig. 2. 2: Diagram shows the solution front (grey circles) between the downwind nodes shown as black circles, for which the travel-times had been determined, and the upwind nodes shown as white circles, for which the travel times have yet to be determined (after Lelièvre, et al. 2010).

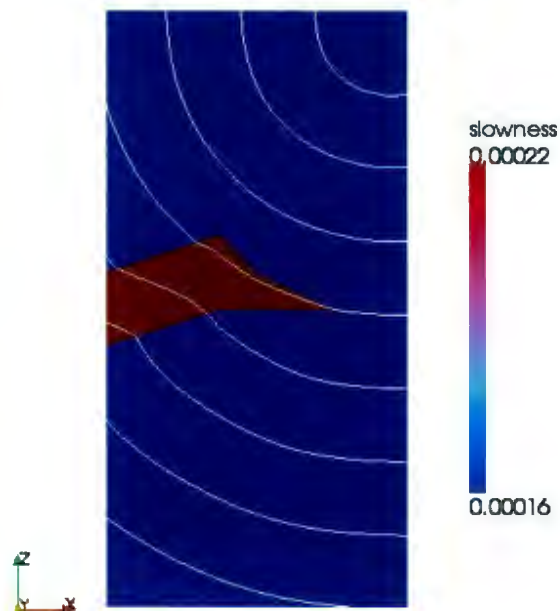


Fig. 2. 3: Propagation of a wavefront from source 1 outward through a two dimensional Earth model.

2.3.2.2 Using *Seismics_fwd*

As with *gravity_fwd* (see Section 2.3.1.2) in order to run *seismics_fwd* it is necessary to create an input file containing the necessary information to create the desired dataset.

There is a large set of parameters that can be included in an input file in the *seismics_fwd*.

All the parameters are listed in the documentation written by Dr. Lelièvre (see Appendix A). The following is a subset that was included in the input files created for this project:

default values for each input parameters. For the seismic forward modeling conducted in this project the following inputs were kept in the input file.

```
zdir      1  ! specifies the coordinate system
gridtype 'unstructured' ! the type of grid (the other option is 'rectilinear')
meshfile   ! file containing mesh information
modelfile  ! file containing model information
neighfile  ! another file containing mesh information (unstructured grids only)
split     0  ! how to convert from rectilinear to unstructured grid
sourcesfile " ! node file specifying the source locations
receiversfile " ! node file specifying the receiver locations
combosfile 'null' ! ele file specifying the source-receiver combinations
ai        1  ! attribute index to use as the model
tmul     1.0 ! multiplicative scalar to convert model to slowness
tadd     0.0 ! additiative scalar to convert model to slowness
trend    0.0      ! background slowness depth trend
```

```

recip      'f'      ! set to true ('t') to perform reciprocal modelling
radius    10.0      ! the initialization radius in the fast marching
tracemode 'none'    ! specifies the type of tracing to perform (if any)
gradflag  't'      ! how to interpolate travel times at the receiver locations
senflag   'f'      ! set to true ('t') to calculate the sensitivity matrix
senfullflag 'f'    ! set to true ('t') to use a full sensitivity matrix instead of sparse
bruteflag 'f' ! set to true ('t') to perform a brute-force finite-difference sensitivity
calculation
writetimes 't' ! if true ('t') then the travel times are written to the output unstructured grid
files
writetypes 'f' ! if true ('t') then the travel types are written to the output unstructured
grid files
writesen   'f' ! if true ('t') then the sensitivity matrix is written to the output
unstructured grid files
sloray    0.0 ! homogeneous slowness value to remove when calculating travel times
along ray paths

```

The values of the inputs shown are the default values they would be assigned if they did not appear in the input file. Of these only a few parameters were used regularly.

- meshfile, modelfile, ai, tmul and tadd: as were defined for the gravity input file in Section 2.3.1.2

- `neighfile`: indicates which cells are neighbours. It is produced through the employment of the `-n` flag when the models were meshed in triangle (2D) or tetgen (3D)
- `sourcesfile`: a `.node` file which defines the seismic source locations
- `receiversfile`: a `.node` file which defines the seismic receiver locations
- `combosfile`: defines which source-receiver combinations travel-times need to be calculated for. In 2D this was not required as all sources were paired with all receivers; however, this was not the case in 3D where each source was paired with a potential different subset of the receivers
- `radius`: determines the search radius for the forward marching method, for a full explanation see Lelièvre, et al., 2011.
- `Tracemode`: indicates how the seismic rays are traced through the model. This was generally kept as none unless `sloray` was being used.
- `Sloray`: `sloray` is a function that allows `seismic_fwd` to produce anomalous travel-times by subtracting the travel times for a given slowness along the same path as those calculated using the model.

After an input file has been created `seismics_fwd` is executed using the following statement from the command line “`./seismics_fwd input_file`”.

2.3.3 Noise

When geophysical data is collected in the field there will always be some amount of noise. The noise level of the data can strongly impact the quality of modelling results. In order to

create synthetic data which mimics field data, therefore, it is necessary to add noise to it. In this project Gaussian random noise was added to the data after forward modelling using a program written by Dr. Lelièvre called *add_noise*.

There are three different parameters for which values must be given in order for *add_noise* to calculate the noise for a given data set. The first parameter is the relative percentage noise which is a set percentage multiplied by the value of the datum for which the noise is being calculated. In cases where the value of the datum is close to zero it is necessary to have a second relative noise level, this is seen in the second parameter, as a percentage of the total data range. The final parameter is an absolute noise floor below which the data is indistinguishable from the noise. These noise types are combined as follows:

$$\sigma_i = (per)|d_i| + (floper)[data_{range}] + flo \quad 2.3$$

where σ_i is the noise value for the *i*th datum, d_i is the value of the *i*th datum, *per* is the relative percentage noise of the datum, *floper* is the relative percentage of the data range, and *flo* is the absolute noise floor.

In this project only the percentage noise and noise floor terms are employed. For the seismic travel-times data only the percentage term is crucial as the data is never close to zero. For the gravity data it is necessary to use both the percentage noise parameter and the noise floor parameter. This is crucial as borehole gravity data can show cross-overs from positive to negative values. As this leads to measurements close to zero which, if only a percentage error is added, will have very small error bars. Due to the formulation of the

misfit calculations used in the inversion modelling methodology (section 2.3: eq. 2.5) these data points would have a higher weighting and be considered more accurate than they would otherwise have been.

2.3 Inversion Modelling

2.3.1 Joint Inversion Methodology

Inversion modelling was accomplished using Dr. Lelièvre's Versatile Inversion program, VINV (formerly "*First Arrival Times and Gravity Inversion*"). VINV has been designed to handle the inversion of multiple and single datasets from a variety of data types including: seismic travel-time, gravity, gravity gradiometry, and magnetic data. VINV follows the method presented by Lelièvre et al. (2012) and uses a deterministic approach, typical of minimum structure inversion, in which an objective function is minimized by a descent optimization method. This objective function is formulated such that its minimization produces a reasonable model.

When a single dataset is being inverted there are two terms in the objective function,

$$\phi = \phi_d + \beta\phi_m \tag{2.4}$$

the data misfit term ϕ_d and the regularization term ϕ_m . The trade-off parameter β determines the relative importance of the two terms. The data misfit term,

$$\phi_d = \sum_{i=1}^N \left(\frac{F[\mathbf{m}]_i - d_i}{\sigma_i} \right)^2 \tag{2.5}$$

where $F[\mathbf{m}]_i$ is the calculated geophysical response at the i th position, d_i is the actual geophysical response at the i th position and N is the total number of data; determines how well the inversion has matched data provided to the inversion.

The regularization term is given as,

$$\phi_m = \alpha_s \|\mathbf{W}_s(\mathbf{m} - \mathbf{m}_{ref})\|_p^p + \alpha_m \|\mathbf{W}_m \mathbf{m}\|_p^p \quad 2.6$$

where $\|\mathbf{W}_s(\mathbf{m} - \mathbf{m}_{ref})\|_p^p$ is the measure of similarity between the model \mathbf{m} and a reference model \mathbf{m}_{ref} , α_s and α_m are parameters allowing of the adjustment of the relative importance of the two terms, \mathbf{W}_s contains information about the cell volumes and \mathbf{W}_m determines the difference between the physical properties of adjacent cells.

In the case of joint inversion the objective function is expanded to included terms for both datasets (Lelièvre, et al., 2010; Lelièvre, et al., 2012),

$$\phi(\mathbf{m}_1, \mathbf{m}_2) = \lambda_1 \phi_{d1}(\mathbf{m}_1) + \lambda_2 \phi_{d2}(\mathbf{m}_2) + \alpha_1 \phi_{m1}(\mathbf{m}_1) + \alpha_2 \phi_{m2}(\mathbf{m}_2) + \phi_j(\mathbf{m}_1, \mathbf{m}_2) \quad 2.7$$

where ϕ_{d1} and ϕ_{d2} are measures of the data misfit for the two datasets, ϕ_{m1} and ϕ_{m2} are the measures of structural complexity for the two physical property distributions, λ_1 , λ_2 , α_1 , and α_2 are parameters determining the relative importance of the associated terms and ϕ_j determines the coupling of the two models.

The coupling term,

$$\phi_j = \sum_i \rho_i \Psi_i(m_1, m_2) \quad 2.8$$

where ϕ_j is the coupling term, ρ_i is a multiplier related to the similarity parameter which will be discussed later, and $\Psi_i(m_1, m_2)$ is the joint coupling function which determines how the two models will be coupled.

There are five potential coupling methods that can be used in VINV. Four involve lithological coupling and the fifth is a structural coupling method.

If there is a linear relationship between the slowness and density this relationship is used:

$$\Psi_1(\vec{r}, \vec{s}) = \sum_{M=1}^i (a r_i + b s_i + c)^2 \quad 2.9$$

Where $\vec{r} = [r_1, r_2, \dots, r_M]^T$ is the set of density values for the cells in the model, $\vec{s} = [s_1, s_2, \dots, s_M]^T$ is the set of slowness values for the cells in the model, and a,b,c are constants which define the linear relationship. These constants are determined by the inversion code which attempts to fit the physical properties to a line rather than being provided by the modeller. Although, this is a mathematically simple means of lithological coupling it is not a good approximation of geological reality for models of more than two geological units as the physical properties will rarely present a linear relationship.

In the instance where there is not a strict linear relationship between the physical properties a statistical relationship between the two physical properties can be used:

$$\Psi_2(\vec{r}, \vec{s}) = \frac{\sum_{i=1}^M (r_i - \mu_r)(s_i - \mu_s)}{M\sigma_r\sigma_s} \quad 2.10$$

where r_i is the density of the i th cell, s_i is the slowness of the i th cell, σ_r , and σ_s are the standard deviation, μ_r , and μ_s are the means of the physical property distributions, M is the number of cells in the model.

As the physical properties of a rock unit can demonstrate significant variability within a single outcrop it is not uncommon for the different rock types to plot as clusters in physical property space as is seen in Fig 1.3. In such cases the use of a fuzzy c-mean to develop a statistical relationship between physical properties may be appropriate (Lelièvre et al, 2010):

$$\Psi_3(\vec{r}, \vec{s}) = \sum_{i=1}^C \sum_{k=1}^M (w_{ik}^f)(z_{ik}^2) \quad 2.11$$

where $w_{ik} = z_{ik}^{-2/(f-1)} \sigma_k^{-1}$, $z_{ik}^2 = (r_k - \mu_i)^2 + (s_k - v_i)^2$, $\sigma_k = \sum_{j=1}^C z_{jk}^{-2/(f-1)}$, C is the number of clusters (Figure 2), f is the “fuzzification factor” defining the amount of overlap between clusters (Paasche et al., 2006).

If a simple differentiable function, $P_i(\mathbf{r}, \mathbf{s})$ can be used to describe the relationship between the two physical properties this function can be used to define the coupling measure,

$$\Psi_4(\mathbf{r}, \mathbf{s}) = \sum_i P_i(\mathbf{r}, \mathbf{s}) \quad 2.12$$

To measure the structural difference between two physical property models the cross-gradient measure is used. A cross gradient measure of the similarity of the direction of the spatial gradient of the physical property values is frequently used (Hu, et al., 2009). The cross gradient is expressed in 2D as a function of the x and z components of the gradient of the physical property values s and r as given by:

$$\Psi_5(\mathbf{r}, \mathbf{s}) = \|(\mathbf{G}_x \mathbf{r}) \cdot (\mathbf{G}_z \mathbf{s}) - (\mathbf{G}_z \mathbf{r}) \cdot (\mathbf{G}_x \mathbf{s})\|^2 \quad 2.13$$

where \mathbf{G}_x and \mathbf{G}_z are the x and z components of the spatial gradient for the physical property distribution s and r (Lelièvre, et al., 2012).

The Gauss-Newton descent search method is used to minimize the objective function.

Within this method the calculation of the jacobian matrix,

$$\mathbf{J} = \frac{dF[\mathbf{m}]}{d\mathbf{m}} \quad 2.14$$

where $F[\mathbf{m}]$ is the response calculated for the model \mathbf{m} , is required. The jacobian includes sensitivity information including depth and distance weightings for each cell. In the case of gravity this calculation is a linear problem; however, the calculation of the jacobian and sensitivities for the seismic travel times is a non-linear problem as is explained Lelièvre et al. (2011).

Weights are assigned based on a sensitivity matrix given by,

$$w_j = \left(\sum_{i=1}^N G_{ij}^2 \right)^{\beta/4} \quad 2.15$$

where w_j is the weighting for cell j , where $j=1, \dots, m$ where m is the number of cell, N is the number of data points, G_{ij} represents the elements of the sensitivity matrix and β is the weighting factor which can vary between 0.5 and 1.5.

2.3.2 Using VINV

In order to use VINV two different types of input files must be provided: a forward input file and an inversion input file. The forward input file contains information specific to each data set and if a joint inversion is being performed a forward input file must be provided for each dataset. The inversion input file contains information necessary to specify the different inversion parameters. Only one inversion input file needs to be provided for an inversion as it contains information applied to all datasets.

The forward input files needed for the inversions are similar to those outlined in Sections 2.3.1.2 (gravity) and 2.3.2.2. (seismic). These input files have some minor changes. An input parameter “datafile” was added to the seismic forward input file. Datafile indicates the name of the file containing the data that will be inverted. The following are the input parameters added to the gravity forward input file:

- datafile: specifies the name of the file containing gravity data to be inverted
- wmode: specifies the type of weighting to be used
- wpower, wzero, wnorm, and wbeta: specify the weighting parameters (see Section 2.3.1 eq. 2.7)

A complete list of the possible input parameter exists in the documentation for VINV written by Dr. Lelièvre and can be seen in Appendix A. The following is a list of the inputs which were changed regularly during this project; any inputs not included were maintained at the default values.

- `zdir`: defines the co-ordinate system of the model. In the case of this project all 2D models were defined with positive z direction being down, however, the 3D models the positive z direction was up.
- `meshfile`, `modelfile`, `neighfile`: a `.node`, `.ele` and `.neigh` file respectively produced by triangle (2D) or tetgen (3D) to define the mesh used to produce the inversion model
- `ndatasets`: indicates the number of datasets to be inverted. In the case of a single-property inversion this was set to 1, for joint inversion it was set to 2.
- `usebounds`: indicates whether bounds will be set on the potential physical property values
- `betainit`: sets the initial beta value.
- `rhoe`: set the similarity parameter. This parameter is a multiplier of the parameter ρ_i in eq. 2.8
- `maxbetasteps`: sets the number of beta steps that the inversion can go through.
- `totitprefix`: indicates whether an image (`.vtu` file) of the model should be produced at the end of each iteration with a different name

The following inputs must be used once for each data set being inverted. A number after the input name indicates which dataset that it refers to.

- `datatype`: indicated which data type was being used. In this project this was set to `gz` (vertical gravity) or `fat` (first arrival time).
- `datainp`: provides the name of the forward input file a dataset
- `chifact`: is the target misfit divided by the number of data . By setting this parameter the target misfit is selected
- `chitol`: sets the tolerance on `chifact` which indicates how close the target misfit the inversion has to get before it stops
- `initfile`: provides the name of an `.ele` file containing the initial model information. This is only used if the inversion is to start from a specific model.
- `initindex`: indicates which attribute in the `.ele` file contains the correct information for the physical property in question.
- `lowervalue`: lowest possible value for a given physical property.
- `uppervalue`: highest possible value for a given physical property.

Although most parameters will affect the final model there are some that affect the time it takes for the inversion to converge. After a input file has been created, `vinv` is executed using the following statement from the command line “`./vinv input_file`”.

Chapter 3: Constructing Models and Forward Modelling in Two Dimensions

3.1 The Models

When a geophysical survey is conducted there can be different goals based on what aspects of the geology one wishes to investigate. When trying to find exploration targets, for example, often the target is small but has large physical property contrasts with the surrounding rocks. On the other hand if the survey is being run to try to delineate the geology the rock units may be much larger but the physical property contrasts between rock units can be quite small. In this project three different two dimensional (2D) models were developed. Each model was developed to test a specific aspect of the abilities of the method to accurately reproduce different aspects of the geology. The models were based on the geology of the Eastern Deeps zone of the Voisey's Bay deposit, discussed in section 1.2, as presented by Evans-Lamswood et al. (2000) (Fig. 3. 1).

Simplifications were made to the geology depicted in Fig. 3. 1 during the construction of the 2D models. The general shape of the sulphide lens was maintained, however, the depth to the sulphide lens was decreased to 200m and its composition changed from a mix of massive and disseminated sulphide to purely massive sulphide. These changes were made to decrease complexity and to ensure that the body would be detectable by gravity measured at the surface.

In this project travel times from synthetic cross-borehole seismic tomography surveys (see Section 3.3) and gravity measurements from borehole and surface locations (see Section 3.2) were used. As seismic waves would be attenuated as they travel through the ground there is a maximum distance between a source and receiver before the signal will be below the background levels. In order to ensure that the synthetic setup could be replicated in an actual survey a separation of less than 180m between the source and receiver boreholes was used. The 2D models were 200m across with a total depth of 400m.

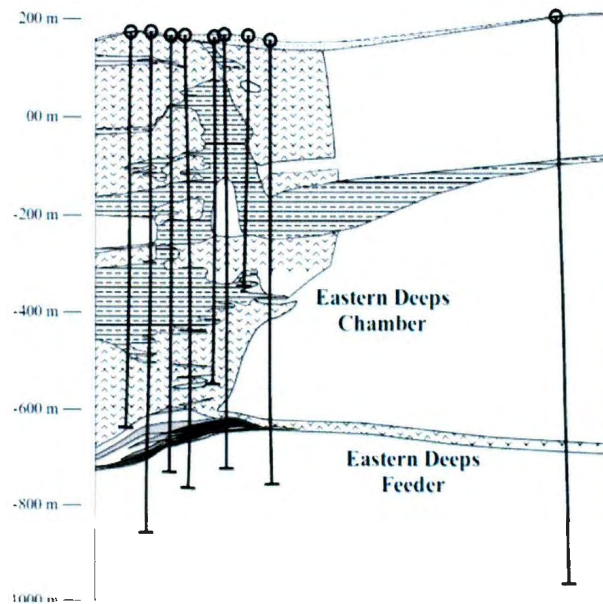


Fig. 3. 1: Cross-section through the Eastern Deeps zone (after Evans-Lamswood et al., 2000), on which the 2D models in this project were based.

Three 2D models were considered in this project. The physical property values assigned to units in the models were determined by calculating averages for troctolite, gneiss and sulphide from Voisey's Bay density and seismic velocity data (Table 3.1). The density and

seismic data was collected from drill core samples from Voisey's Bay (Ash, 2007; Duff, 2007). The relative density and slowness given in the table are the difference between the physical properties of a given unit and those of the gneiss. The relative physical property values are necessary to run the modelling codes. However, the results produced by the codes are given as the actual physical property values.

Table 3. 1: Physical properties for lithologies of interest

Lithology	Slowness (s/km)	Relative Slowness (s/km)	Density (g/cm ³)	Relative Density (g/cm ³)
Troctolite	0.1655	0.0032	2.908	0.091
Massive Sulphide	0.2218	0.0595	4.469	1.652
Gneiss	0.1623	0.0	2.817	0.0

3.1.1 Sulphide-Gneiss Model

The sulphide-gneiss model (Fig. 3. 2) is the simplest of the 2D models as it consists only of two rock types which have high physical property contrasts for both slowness and density. This model consists of a roughly wedge shaped sulphide lens in a uniform background of gneiss. The sulphide lens is buried about 200m below the surface and is about 150m long. The model was developed to test the ability of the code to reproduce a small body with relatively high physical property contrasts. In Fig. 3. 2 both the model and triangular mesh constructed by the method described in Section 2.1 are shown.

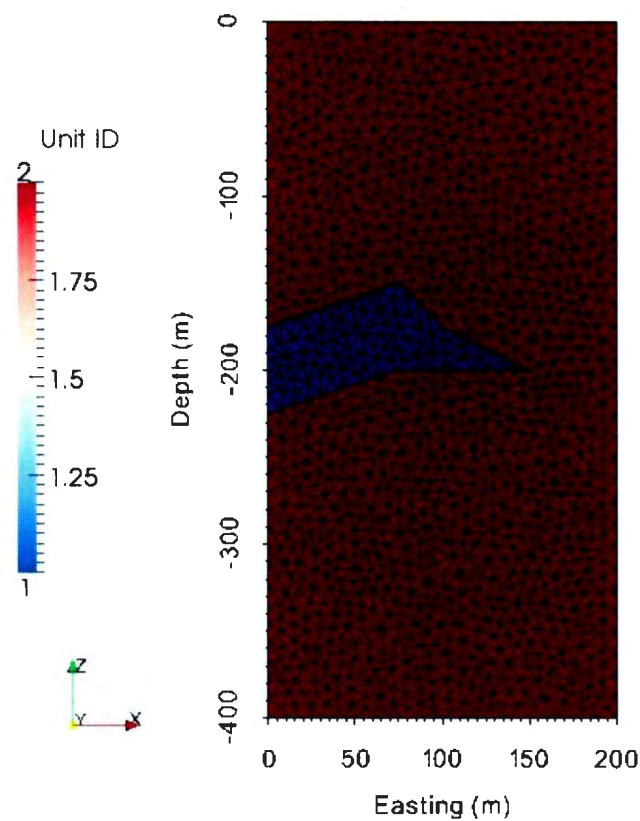


Fig. 3. 2: The sulphide-gneiss model overlain by a triangular mesh produced from the model.

3.1.2 Troctolite-Gneiss Model

The troctolite-gneiss model (Fig. 3. 3) was designed to test the ability of the inversion code to resolve two units with relatively small physical properties contrast. The troctolite-gneiss model is based on the Eastern Deeps zone pluton and feeder pipe (Fig. 3. 1). The model consists of a troctolite pluton extending from surface to a depth of about 200m. The intrusion extends about 100m laterally with a thin feeder pipe about 10m in width extending across the rest of the model. The troctolite is in a uniform gneiss background.

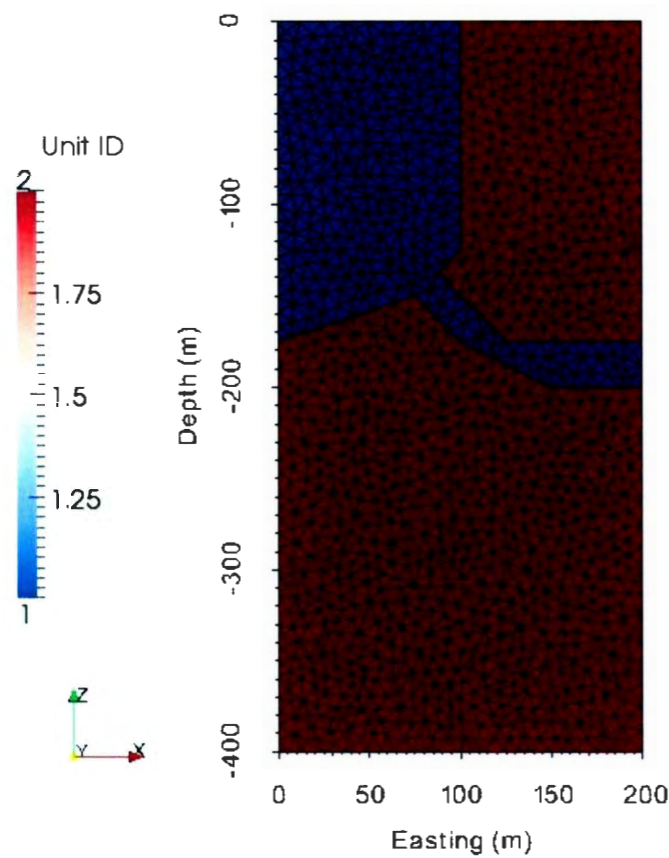


Fig. 3. 3: The troctolite-gneiss model overlain by a triangular mesh produced from the model.

3.1.3 Mixed Model

The mixed model (Fig. 3. 4) is a combination of the sulphide-gneiss model and the troctolite-gneiss model. The model consists of the troctolite pluton and feeder pipe with a sulphide lens at the base of the intrusion and extending partway into the feeder pipe. The background as before is uniform gneiss. This model was developed to test several scenarios: first, to determine if the method could reproduce a small high contrast buried body in a non-uniform background; second, to determine if a large shallow low contrast

body could be reproduced in the presence of a smaller high contrast body; third to determine if the small low-contrast feeder pipe could be detected.

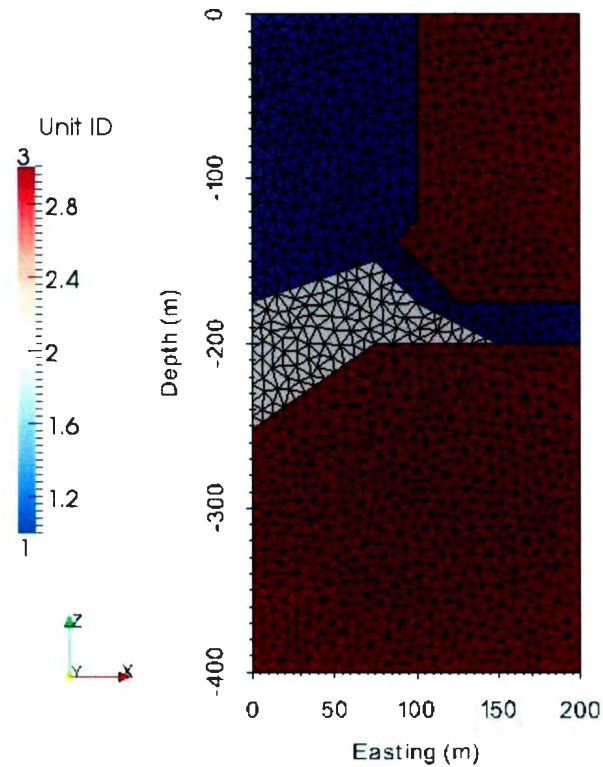


Fig. 3. 4: The mixed model overlain by a triangular mesh produced from the mixed model.

3.2 Gravity Forward Modelling

3.2.1 Gravity Stations locations

Five different gravity station configurations were investigated: surface stations, borehole A stations, borehole B stations, borehole A and B stations and all stations (Fig. 3. 5). A total of 21 gravity stations are spread along the top of the model with a spacing of 10m between the stations. Borehole A was the hole in which the seismic sources were deployed and

contained 79 borehole gravity stations. Borehole B was the hole in which the seismic receivers were deployed and contained 79 borehole gravity stations.

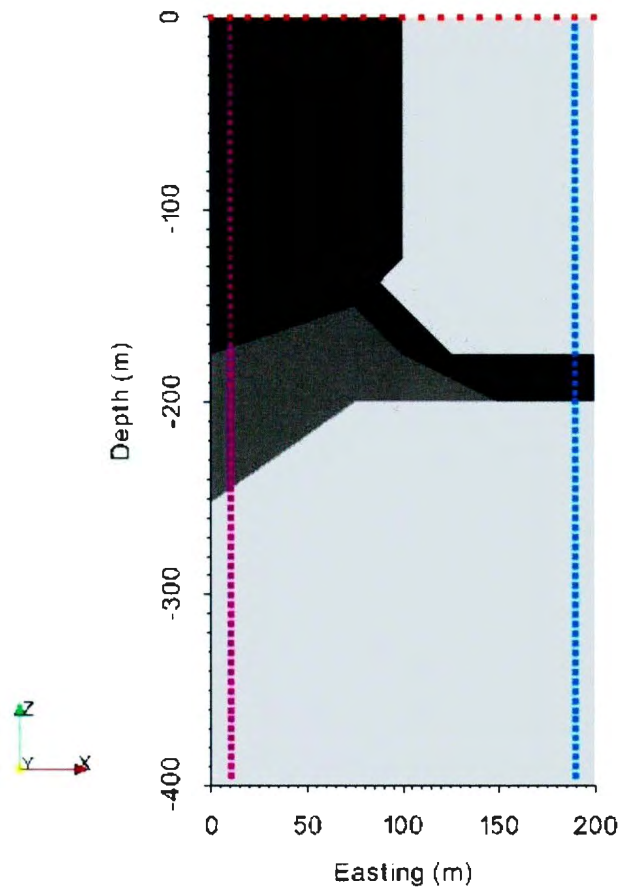


Fig. 3. 5: The locations of all the gravity measurement locations. Borehole A gravity measurement locations are shown in purple, borehole B measurement locations are shown in blue and surface measurement locations are shown in red. Borehole A measurement locations correspond to the seismic source locations. Borehole B measurement locations correspond to seismic receiver locations. The model has the same dimensions as were shown in Fig. 3. 4.

During forward modelling the relative densities outlined in Table 3. 1, where all the densities are considered relative to the density of the gneiss was used. Forward modelling was conducted using *gravity_fwd*, a gravity forward modelling program as seen in Chapter 2.3.1 (Jahandari, 2011, Lelièvre, et al., 2012).

3.2.2 Gravity Forward Modelling Results

Although differences between the gravity values for the different models exist there are some similarities seen for all the models. The surface gravity measurements show a broad positive gravity anomaly. The borehole gravity variation is a cross-over from positive to negative for both boreholes A and B; however, the curve produced from the data in borehole B is much smoother than that in borehole A. This is not surprising as borehole B is further from the anomalous bodies.

The sulphide-gneiss model produced strong distinct gravity anomalies; the surface anomaly is about 50mGal (Fig. 3. 6). This suggests that although the body is buried that it should be able to be reproduced during modelling. The troctolite-gneiss model has a very weak gravity response (Fig. 3. 7). The surface gravity stations show only a 1-2mGal response which would be below the noise level of most gravimeters. This is not surprising due to the very low physical properties contrasts. The gravity response produced by the mixed model (Fig. 3. 8) is very similar to the response seen for the sulphide-gneiss model (Fig. 3. 6). Small variations from the sulphide-gneiss model response are related to the presence of the troctolite body.

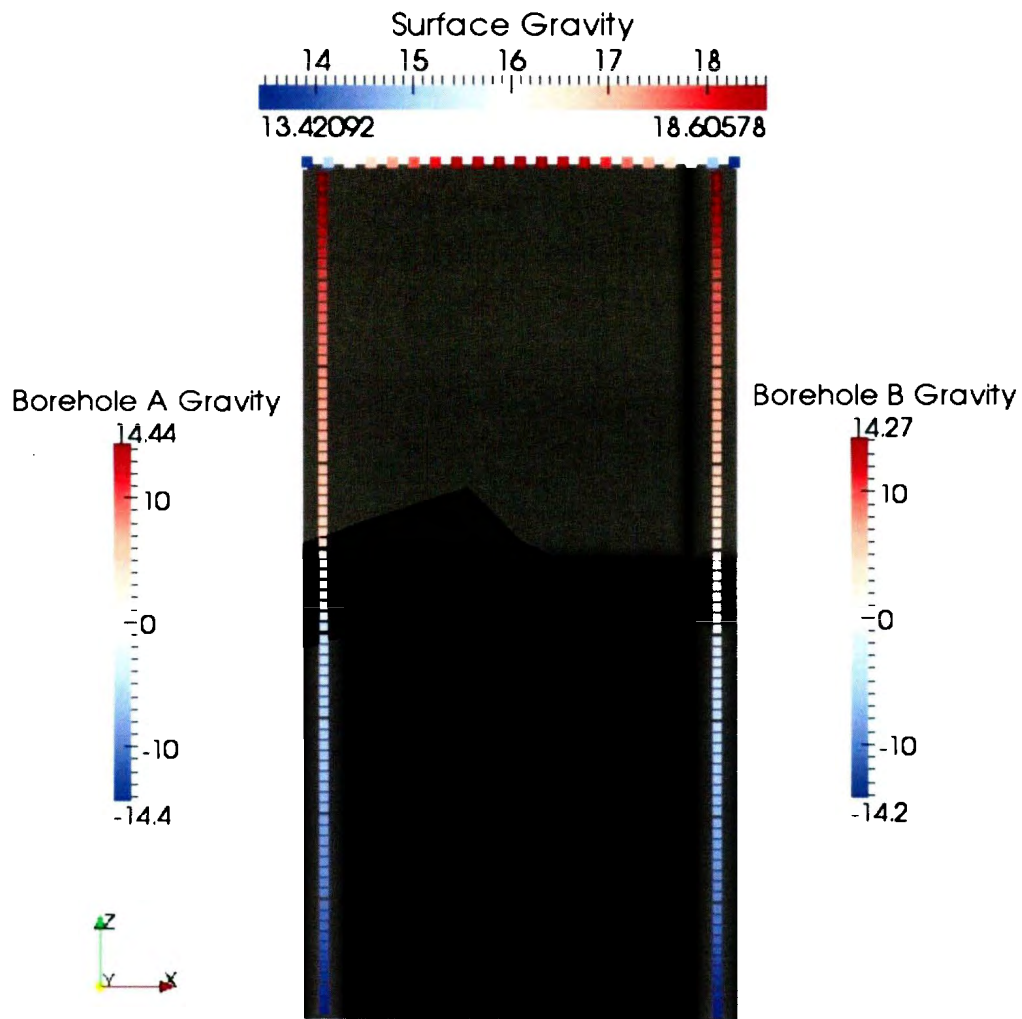


Fig. 3. 6: Forward-modelled gravity values at all measurement locations for the sulphide-gneiss model. A coloured square at each location indicates the value of gravity. The model has the same dimensions as were shown in Fig. 3. 4.

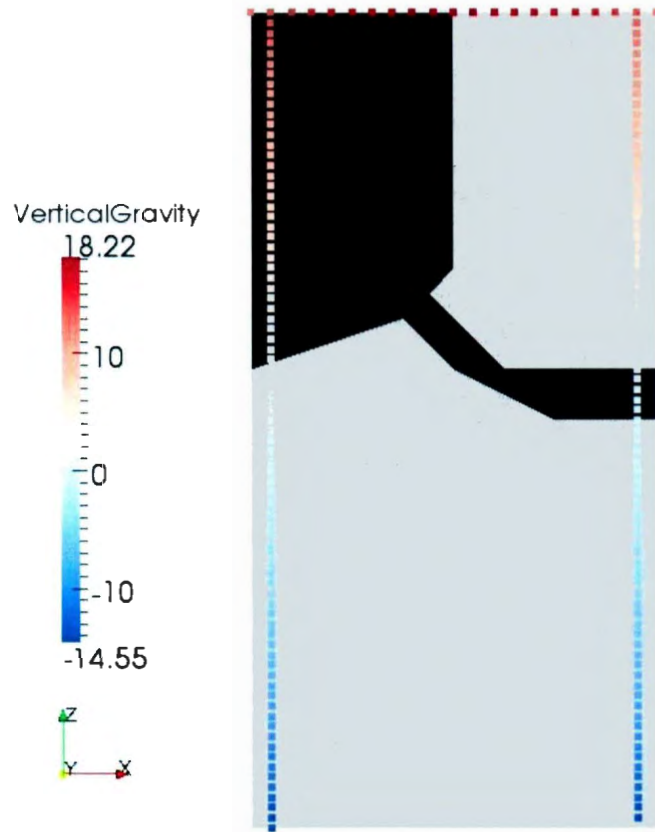


Fig. 3. 7: Forward-modelled gravity values at all measurement locations for the troctolite-gneiss model. A coloured square at each location indicates the value of gravity. This model has the same dimensions as were shown in Fig. 3. 4.

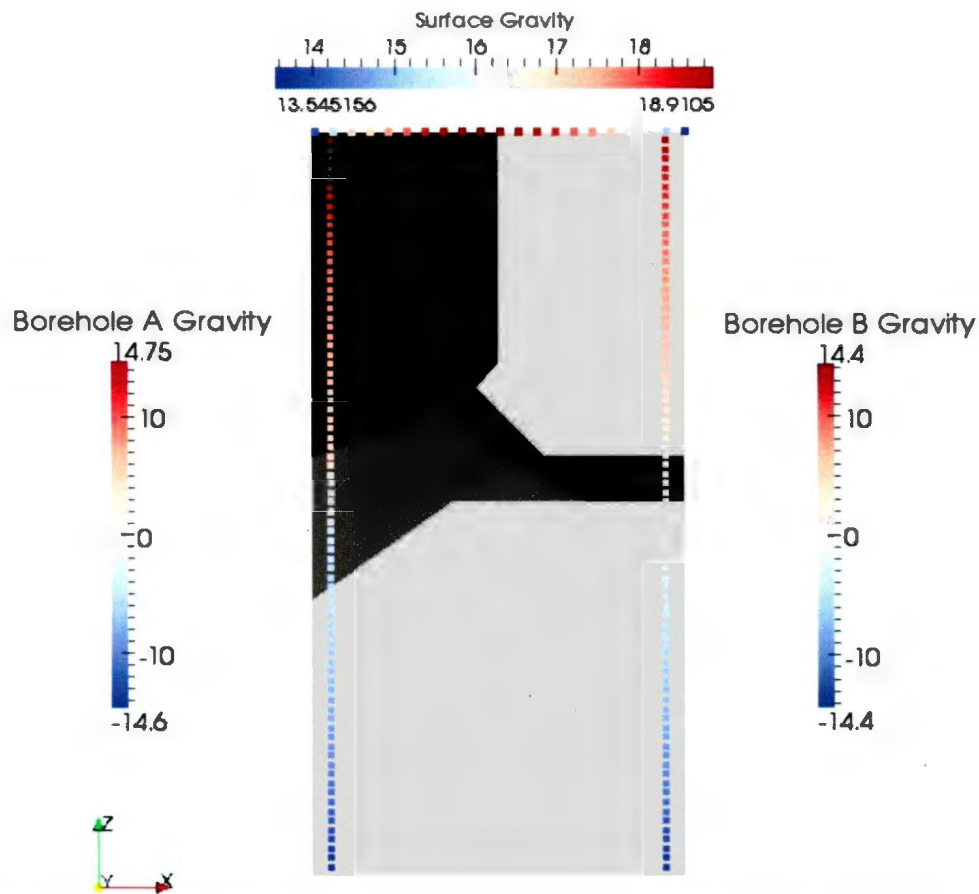


Fig. 3. 8: Forward-modelled gravity values at all measurement locations for the mixed model. A coloured square at each location indicates the value of gravity. The model has the same dimensions as were shown in Fig. 3. 4.

3.3 Seismic Forward Modelling

Seismic travel time data was generated for all three models using *seismics_fwd*, a forward modelling software which derives the seismic first-arrival travel times using the fast marching method (Lelièvre, et al., 2011). Seismic travel-times were determined for all combinations of the 79 sources in borehole A and the 79 receivers in borehole B (Fig. 3. 5).

The results of the seismic forward modelling can be displayed in two ways: as travel-time contours and as a plot of the first-arrival times at each of the source-receiver combinations.

Each travel-time contour indicates how far the wave fronts have propagated in a given period of time. The travel-time contours can be plotted for any of the sources. In Fig. 3. 9 the contours for five different sources are shown. The closer spacing of the wave fronts in the slower sulphide body is clearly evident. This compression to the wave front is also seen as a distortion at the contacts of the sulphide body and the other two units.

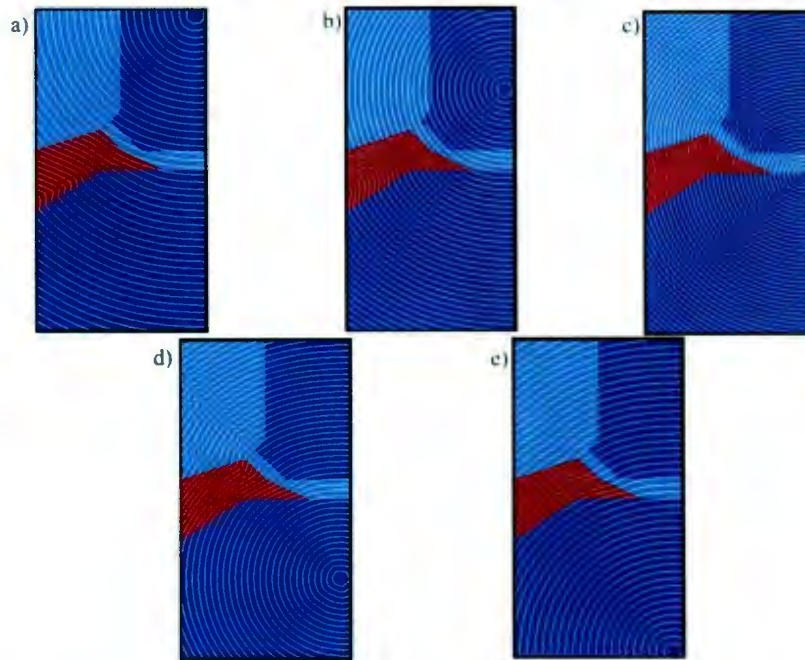


Fig. 3. 9: Travel-time contours for sources 1 (a), 20 (b), 40 (c), 60 (d), and 79(e) for the mixed model, the sulphide is shown in red, the troctolite in light blue and the gneiss in dark blue. Each contour represents 1/50 of the total travel time range. The models have the same dimensions as was shown in Fig. 3. 4.

The travel time data and associated normalized data residuals can also be plotted in source-receiver space, where the source number is along the bottom edge and the receiver number is along the side and each coloured pixel represents a given source receiver pair (Fig. 3. 10). A colour scale is used to indicate the travel-time or normalized data residual for each of the source-receiver combinations. In this configuration the travel-time information is dominated by the distance between the sources and receivers; however, using *seismics_fwd* this effect can be removed leaving only the anomalous travel times.

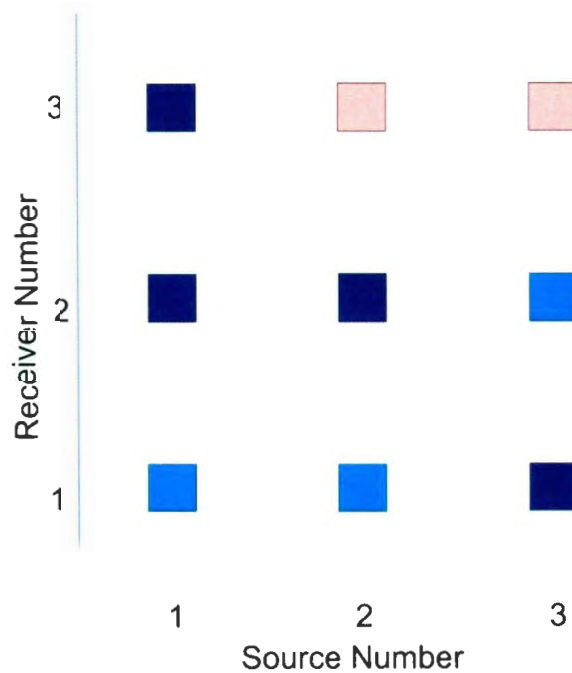


Fig. 3. 10: Cartoon depiction of the source-receiver space used to portray the travel time results.

The travel times for the mixed model (Fig. 3. 11a) and the sulphide-gneiss model (Fig. 3. 12a) show a distinct disturbance of the distance dominated pattern around the middle of the forward modelling results. This shows the effect of the anomalous sulphide body. The

higher slowness of the sulphide slows down waves travelling through the body. The anomalous travel times were calculated using the sloray parameter in *seismics_fwd*. This parameter provides the forward modelling process with a background slowness value. When sloray is used the code calculates two travel times for each of the source-receiver pairs. The first travel time is the travel time based on the slownesses of the cells in the model the second travel time assumes that all the cells have the slowness provided by the sloray parameter for the same path length as was calculated during the calculation of the true travel times. The difference between the true travel times and those calculated using the sloray slowness is taken and this is the anomalous travel time. The anomalous travel times from the mixed model (Fig. 3. 11b) and sulphide-gneiss model (Fig. 3. 12b) show that there is a visible effect of the troctolite body which is present in the mixed model but absent in the sulphide-gneiss model.

The results of seismic forward modelling for the troctolite-gneiss model (Fig. 3. 13a) does not show the very obvious anomaly that is seen in the forward modelling results from the other models. This is to be expected due to the very small slowness contrasts between the troctolite and the gneiss the effect on the travel times is entirely masked by the distance effect. However, the anomalous travel times (Fig. 3. 13b) show that there is a small effect from the troctolite intrusion; resulting in a deviation from the expected result of a homogenous half space.

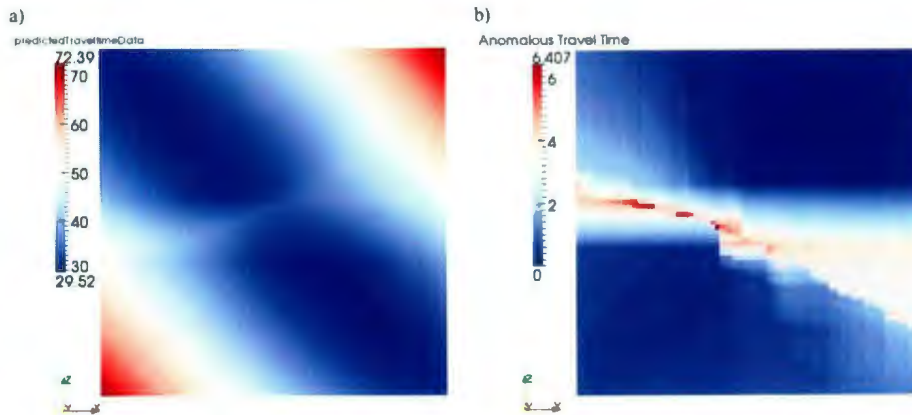


Fig. 3. 11: Travel times (a) and anomalous travel times (b) plotted as receiver versus transmitter for the mixed model .

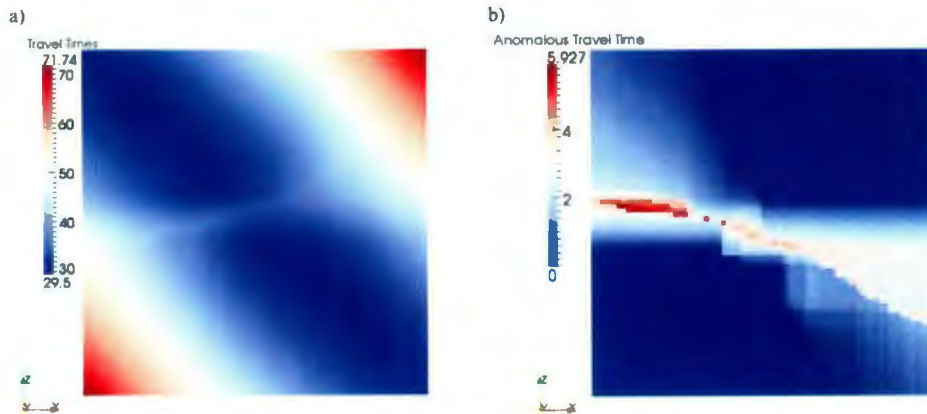


Fig. 3. 12: Travel times (a) and anomalous travel times (b) plotted for transmitter versus receiver for the sulphide-gneiss model.

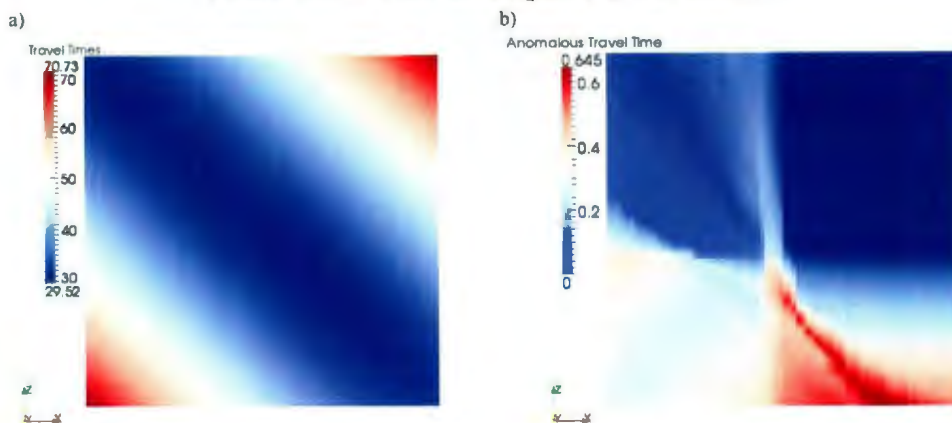


Fig. 3. 13: Travel times (a) and anomalous travel times (b) plotted for transmitter versus receiver for the troctolite-gneiss model.

3.4 Adding Noise to Data

To prepare both gravity and seismic travel-time data produced in forward modelling for inversion noise was added. This is done to mimic the noise which would have occurred naturally in data collected in the field. Hence, the addition of noise to the synthetic data makes the inversion trials more realistic.

Three levels of noise were added to the data produced from the forward modelling. The low noise data had only 0.1% noise, moderate noise data had 1% noise added to it and the high noise data had 10% noise added. Noise was added using a program called *add_noise*. As was presented in Section 2.3.3 this program can add three different types of noise to the data. In the case of this project, only the ‘per’ which is a percentage of the datum value to which the noise is being added and ‘flo’ which is an absolute noise floor are used. The inputs for *add_noise* used in this project are tabulated (Table 3.2).

Table 3. 2: Summary of *add_noise* inputs of all datasets.

Dataset	Per	Flo	Floper
Low Noise Gravity	0.1%	0.01 mGal	0.0%
Moderate Noise Gravity	1.0%	0.1 mGal	0.0%
High Noise Gravity	10.0%	1.0 mGal	0.0%
Low Noise Travel-time	0.1%	0.10 ms	0.0%
Moderate Noise Travel-Time	1.0%	1.0 ms	0.0%
High Noise Travel-Time	10.0%	5.0 ms	0.0%

It is barely possible to detect the difference between the low noise gravity data (Fig. 3.13) from the clean forward modelling results. This is true for each of the three models. The moderate noise gravity data (Fig 3.14) deviates from the noiseless data significantly; however, the shape of the original anomalies can still be clearly seen. The high noise gravity data (Fig 3.15) deviates greatly from the noiseless data; however, the data still gives a vague impression of the overall shape of the anomaly.

Noise was also added to the full range of the travel-time data not simply to the anomalous travel times. This was done in the same manner as it was added to the gravity data. The resultant noisy data are show in Fig. 3.16, Fig. 3.17 and Fig. 3.18. The effect of the noise on the travel time patterns is less obvious than for the gravity data. However, in essence the addition of noise had the same affect with increasing amounts of noise added to the data leading to greater distortion of the data.

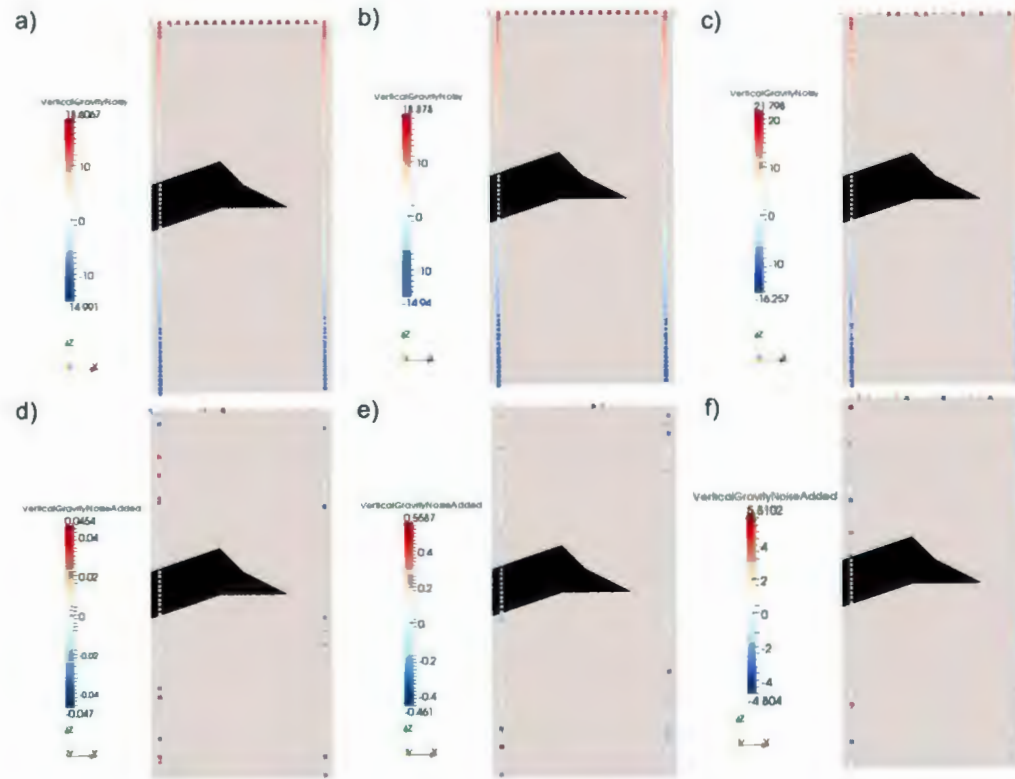


Fig. 3. 14: Comparison between the gravity response with noise added (a,b,c) for the sulphide-gneiss model at all measurement locations and the noise added (d,e,f) to those data points for low noise (a, d), moderate noise (b,e) and high noise (c,f). The models have the same dimensions as were shown in Fig. 3. 4.

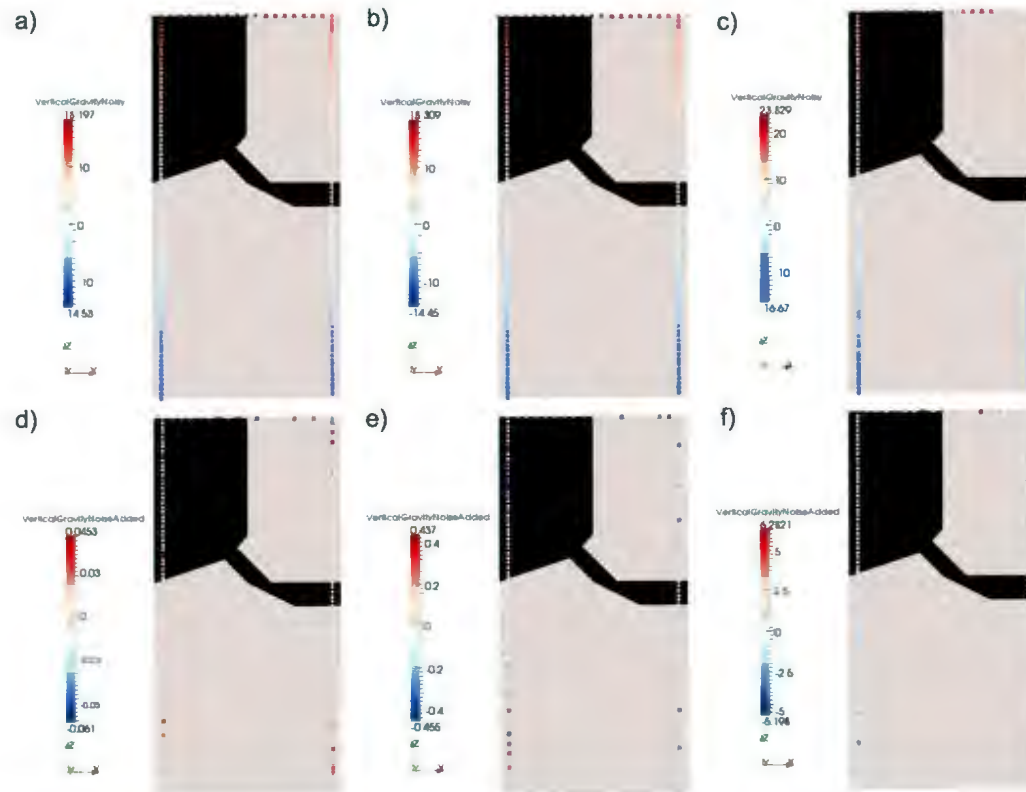


Fig. 3.15: Comparison between the gravity response with noise added (a,b,c) for the troctolite-gneiss model at all measurement locations and the noise added (d,e,f) to those data points for low noise (a, d), moderate noise (b,e) and high noise (c,f). The models have the same dimensions as were shown in Fig. 3.4.

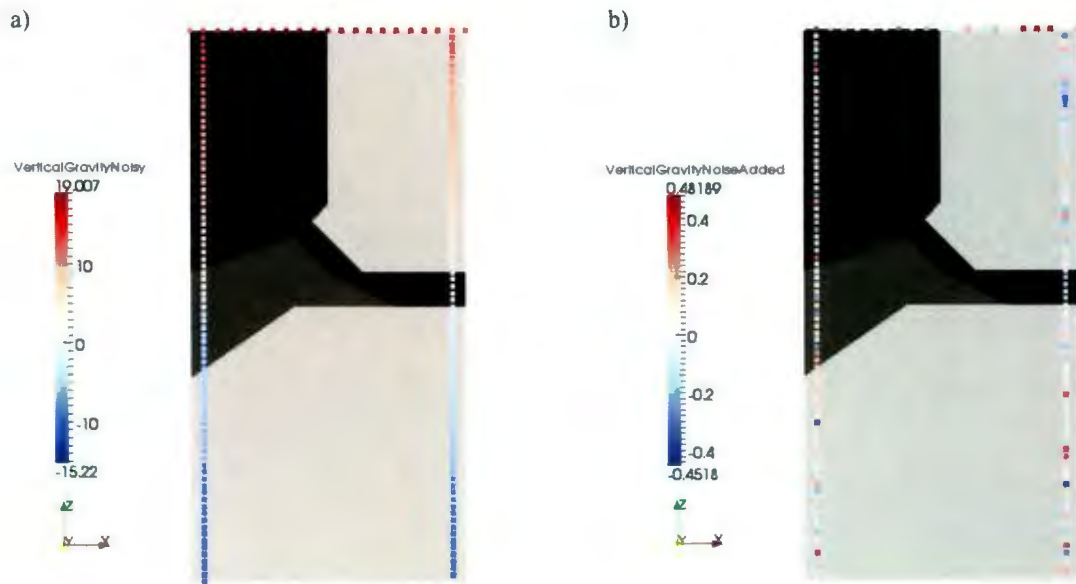


Fig. 3. 16: Comparison between the gravity response with noise added (a) for the mixed model at all measurement locations and the noise added (b) for moderate noise levels. The models have the same dimensions as were shown in Fig. 3. 4.

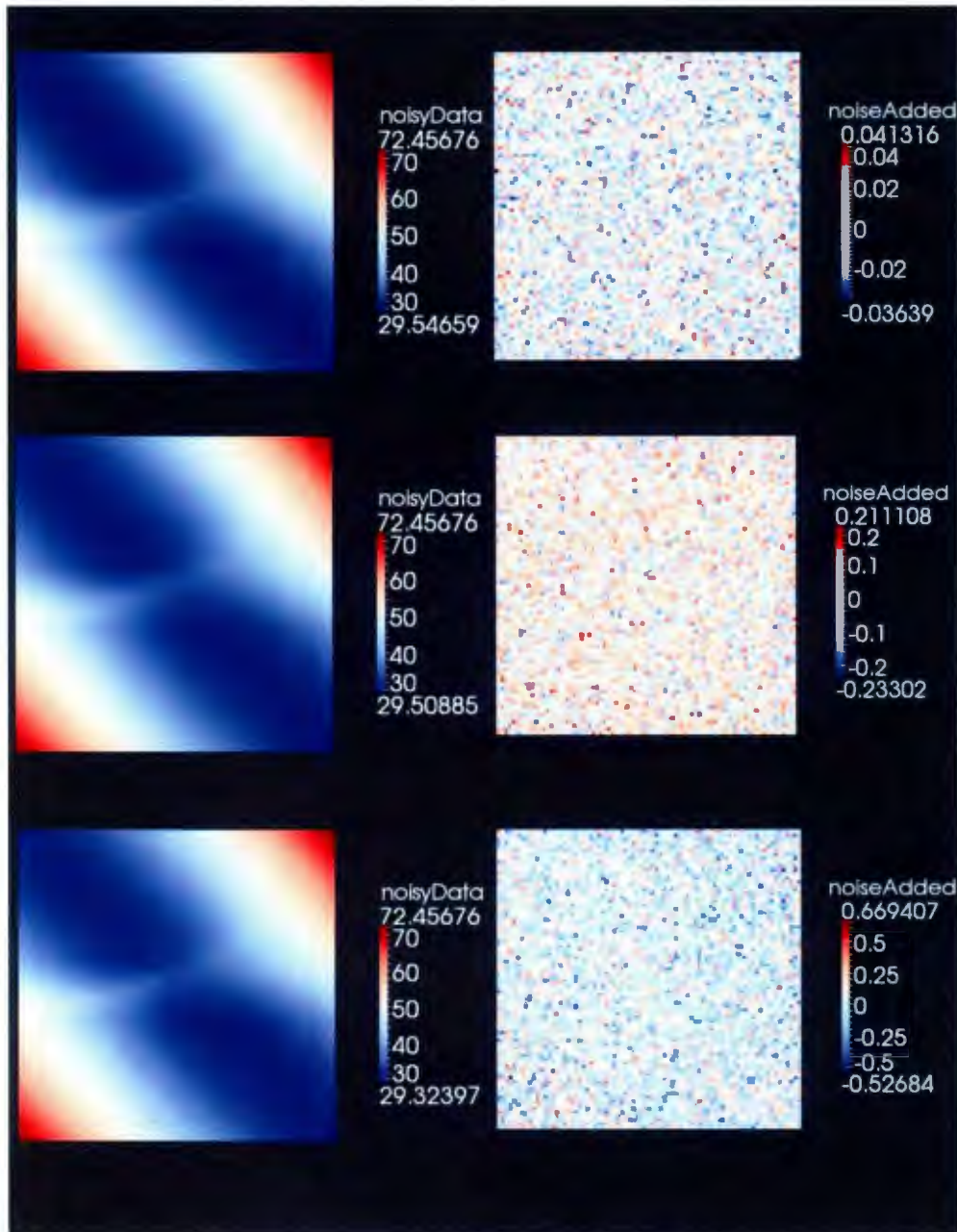


Fig. 3. 17: Mixed model data with noise added: low noise in the top panels, moderate noise in the middle panels and high noise in the bottom panels.

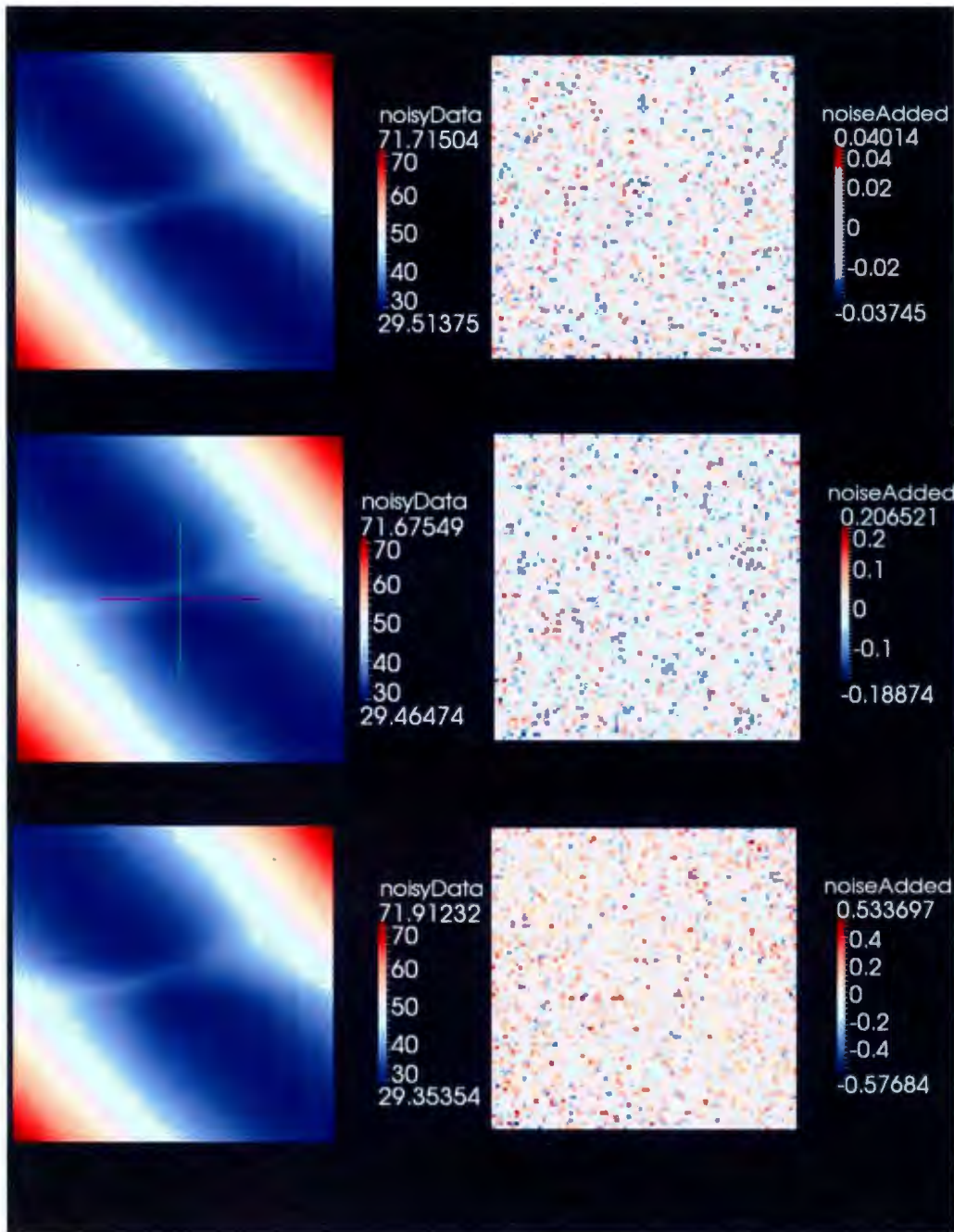


Fig. 3. 18: Noisy sulphide-gneiss model synthetic data for low noise (top panels), moderate noise (middle panels) and high noise (bottom panels).

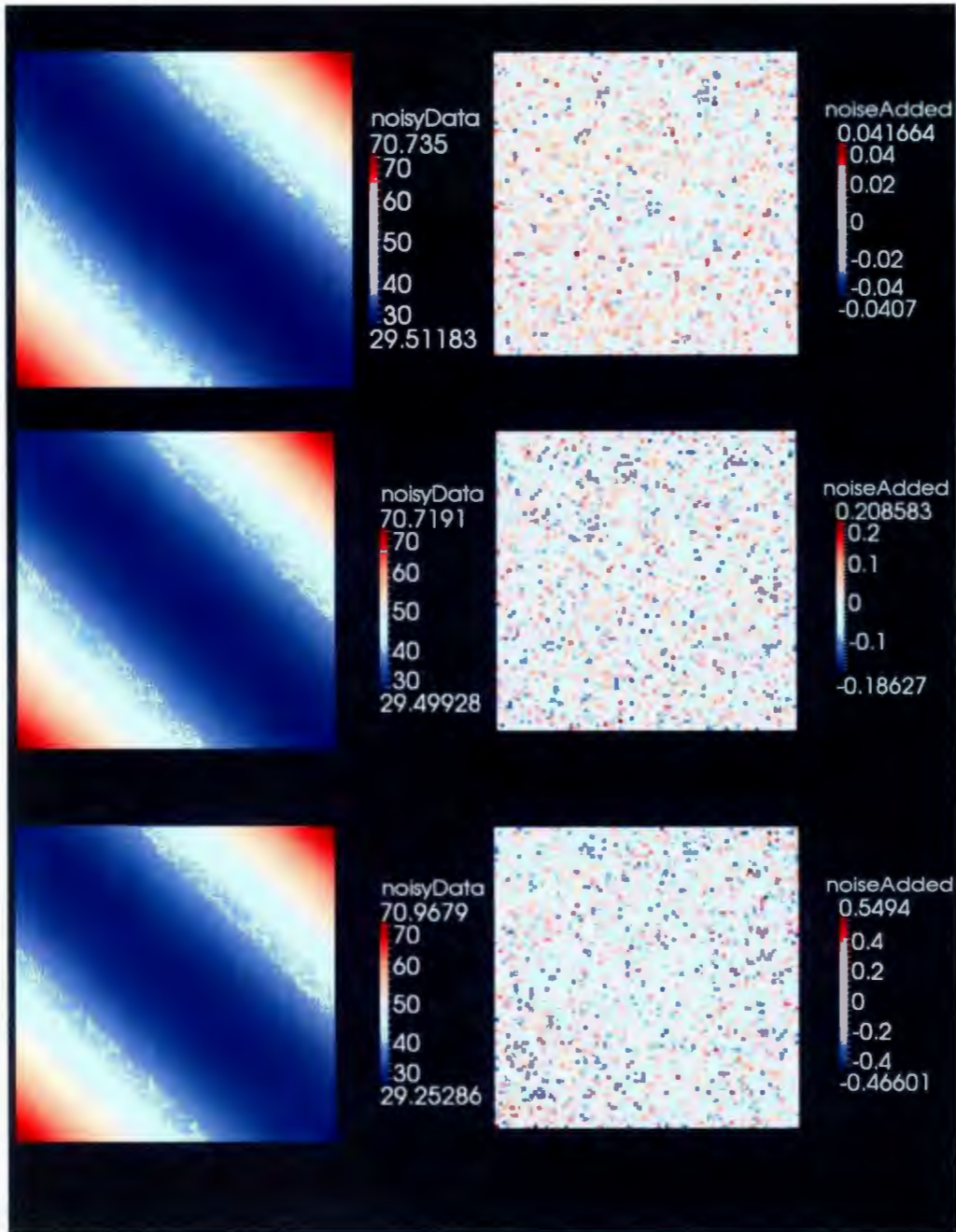


Fig. 3. 19: Noisy troctolite-gneiss model synthetic data with low noise (top panels), moderate noise (middle panels), and high noise (bottom panels).

Chapter 4: Results of 2D Inversion

4.1 Overview

4.1.2 Outline of Results

Inversions of the 2D model synthetic data were designed to test the joint inversion methodology and the effect of the different inversion parameters. This exercise involved many small changes of the inversion parameters. As such there were hundreds of different inversions run. In this chapter a sample of the inversion results obtained during this project will be presented; for a complete compilation of all 2D inversion results see Appendix B.

The inversion results are presented below as a combination of the physical property model(s) produced by the inversion, and plots of the predicted geophysical response and normalized data residuals for those models. The normalized data residuals have been calculated by (eq.4.1):

$$data\ residuals = \frac{d_i^{pred} - d_i^{synth}}{\sigma_i} \quad eq. 4.1$$

where d_i^{pred} is the i th datum predicted by the physical property distribution of the model constructed by the inversion, d_i^{synth} is the i th datum from the synthetic dataset that was provided by the inversion, and σ_i is the uncertainty on the i th datum.

Results from the moderate noise inversions are presented first as this is the most realistic noise level used. By comparison, the low noise and high noise data would be considered unusual during field operations. The results of single property inversions are presented before the joint inversion results for the same data sets. This is done to facilitate comparison between the two.

Table 4. 1: A summary of the examples presented in this chapter. Model indicates the synthetic model used to create the data inverted in the example. Inv_Type indicates whether the example is a single property or joint inversion. Data_Type specifies which datasets were being inverted: travel-time, gravity, or both. Noise indicates how much noise was added to the data (see Sections 2.3.3, and 3.4). ρ_e specifies the value of the similarity parameter used in the inversion. Page indicates the page in this chapter where the inversion can be found.

Example	Model	Inv_Type	Data Type	Noise	ρ_e	page
1	Sulphide-Gneiss	Single	Travel-Time	Moderate	—	61
2	Sulphide-Gneiss	Single	Travel-Time	Low	—	63
3	Sulphide-Gneiss	Single	Travel-Time	High	—	65
4	Sulphide-Gneiss	Single	Surface Gravity	Moderate	—	68
5	Sulphide-Gneiss	Joint	Surface Gravity, Travel-Time	Moderate	1.0	71
6	Sulphide-Gneiss	Single	Surface Gravity	Low	—	74
7	Sulphide-Gneiss	Joint	Surface Gravity, Travel-Time	Low	1.0	76
8	Sulphide-Gneiss	Single	Surface Gravity	High	—	79
9	Sulphide-Gneiss	Joint	Surface Gravity, Travel-Time	High	10^{-2}	81
10	Sulphide-Gneiss	Single	BH A Gravity	Moderate	—	83
11	Sulphide-Gneiss	Joint	BHA Gravity,	Moderate	0.0	86

Travel-Time						
12	Sulphide-Gneiss	Single	BHA Gravity	High	—	89
13	Sulphide-Gneiss	Joint	BHA Gravity, Travel-Time	High	10 ⁻¹⁰	92
14	Sulphide-Gneiss	Single	BHA Gravity	Low	—	95
15	Sulphide-Gneiss	Joint	BHA Gravity, Travel-Time	Low	10 ⁻⁴	98
16	Sulphide-Gneiss	Single	BHB Gravity	Moderate	—	101
17	Sulphide-Gneiss	Joint	BHB Gravity, Travel-Time	Moderate	1.0	104
18	Sulphide-Gneiss	Single	BHB Gravity	High	—	106
19	Sulphide-Gneiss	Joint	BHB Gravity, Travel-Time	High	10 ⁻¹⁰	108
20	Sulphide-Gneiss	Single	BHB Gravity	Low	—	110
21	Sulphide-Gneiss	Joint	BHB Gravity, Travel-Time	Low	10 ⁻⁴	113
22	Sulphide-Gneiss	Single	BHAB Gravity	Moderate	—	115
23	Sulphide-Gneiss	Joint	BHAB Gravity, Travel-Time	Moderate	1.0	118
24	Sulphide-Gneiss	Single	BHAB Gravity	High	—	120
25	Sulphide-Gneiss	Joint	BHAB Gravity, Travel-Time	High	1.0	122
26	Sulphide-Gneiss	Single	BHAB Gravity	Low	—	125
27	Sulphide-Gneiss	Joint	BHAB Gravity, Travel-Time	Low	1.0	127
28	Sulphide-Gneiss	Single	All Station Gravity	Moderate	—	130
29	Sulphide-Gneiss	Joint	All Station Gravity, Travel-	Moderate	1.0	133

Time						
30	Sulphide-Gneiss	Single	All Station Gravity	High	—	135
31	Sulphide-Gneiss	Joint	All Station Gravity, Travel-Time	High	1.0	136
32	Sulphide-Gneiss	Single	All Station Gravity	Low	—	140
33	Sulphide-Gneiss	Joint	All Station Gravity, Travel-Time	Low	1.0	142
34	Mixed	Single	Travel-Time	Moderate	—	144
35	Mixed	Single	Surface Gravity	Moderate	—	147
36	Mixed	Joint	Surface Gravity, Travel-Time	Moderate	1.0	150
37	Mixed	Single	BHA Gravity	Moderate	—	153
38	Mixed	Joint	BHA Gravity, Travel-Time	Moderate	1.0	156
39	Mixed	Single	BHB Gravity	Moderate	—	159
40	Mixed	Joint	BHB Gravity, Travel-Time	Moderate	1.0	162
41	Mixed	Single	BHAB Gravity	Moderate	—	164
42	Mixed	Joint	BHAB Gravity, Travel-Time	Moderate	1.0	167
43	Mixed	Single	Surface and BH Gravity	Moderate	—	170
44	Mixed	Joint	Surface and BH Gravity, Travel-Time	Moderate	10 ⁻⁴	172

45	Troctolite-Gneiss	Single	Surface and BH Gravity	Low	—	175
46	Troctolite-Gneiss	Single	Travel-Time	Low	—	178
47	Troctolite-Gneiss	Joint	Surface and BH Gravity, Travel-Time	Low	10^{-4}	180
48	Troctolite-Gneiss	Single	Surface and BH Gravity	Moderate	—	182
49	Troctolite-Gneiss	Single	Travel-Time	Moderate	—	184
50	Troctolite-Gneiss	Joint	Surface and BH Gravity, Travel-Time	Moderate	1.0	186
51	Troctolite-Gneiss	Single	Surface and BH Gravity	High	—	188
52	Troctolite-Gneiss	Single	Travel-Time	High	—	189
53	Troctolite-Gneiss	Joint	Surface and BH Gravity, Travel-Time	High	10^{-10}	191

4.1.2 Overview of Results

The results from the sulphide-gneiss and full Mixed models were quite similar, and will be discussed first; however, the troctolite-gneiss results were significantly different and will be discussed separately below. Both single property and joint inversions using a linear coupling term (see Section 2.3.1) were run for five different gravity sensor configurations, and with three different amounts of added noise. Attempts were made to attain the best possible inversion results through the modification of different inversion

parameters. This exercise allows for the determination of which parameters produce the best inversion results.

4.1 Sulphide-Gneiss Model Results

The seismic inversions reproduced the model quite well throughout the sulphide-gneiss model tests irrespective of the noise level or whether a single property or joint inversion was being performed. The results attained for the single property inversions of the sulphide-gneiss model synthetic data for each of the noise levels is very similar to the results attained in most of the joint inversions at the same noise levels. By contrast there was a great deal of variability in the quality of the gravity inversions between different noise levels

4.1.1 Seismic –Only Inversion

Example 1: Moderate Noise Results

Table 4. 2: Summary of important input values for example 1.

Target Misfits	Chifact	1.0
	Chitol	0.1
Bounds	Upper	100.1623 s/km
	Lower	0.0 s/km

The travel times predicted by this inversion are acceptably close to the inverted data (Fig. 4. 1a). The normalized data residual is acceptably small. The highest normalized data

residuals occur in the centre of the model. This is not concerning as most of the anomalous travel times also occur in this region.

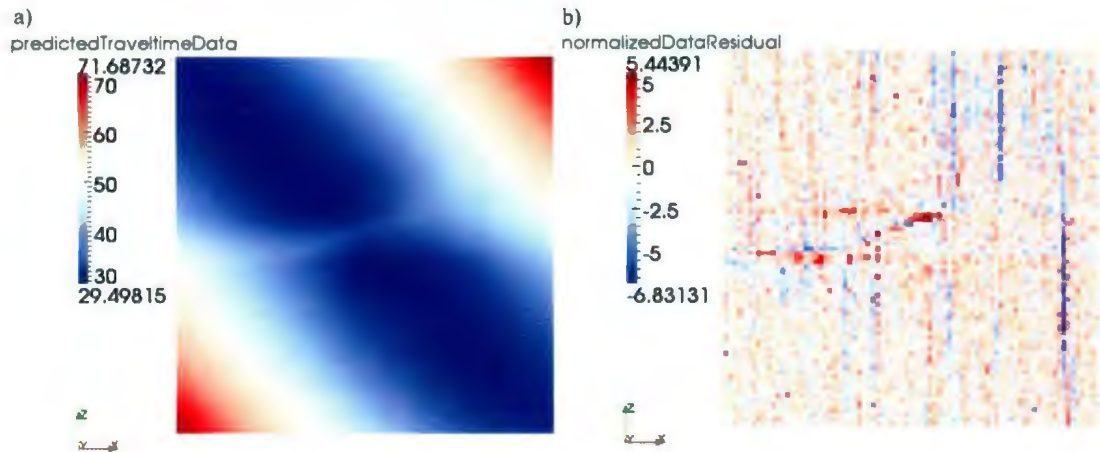


Fig. 4. 1: a) Predicted travel time data and b) normalized data residual for the seismic-only inversion of moderate noise sulphide-gneiss model synthetic data. The horizontal axis of both plots is the source number and the vertical axis is the receiver number (Fig 3.10).

The slowness model produced by this inversion located the sulphide body nearly perfectly. The slowness values estimated by the inversion are acceptably close to the true values (Table 3.1). There is some noise in the background, particularly along the right edges of the model, this is a common feature in many of the slowness distributions produced during both joint and single property inversions. These artefacts are related to the location of the seismic receivers. If the code was having trouble matching all the travel times for a given receiver it tends to change the cells near the receivers leading to the presence of artefacts along the right edge of the models.

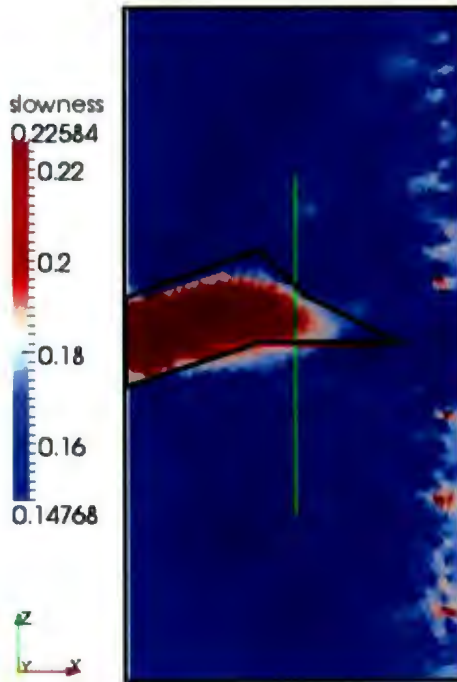


Fig. 4. 2: Resultant slowness model from the seismic-only inversion of moderate noise sulphide-gneiss model synthetic data. The model is 200m across and 400m in depth and the black line outlines the location of the sulphide body in the synthetic models.

Example 2: Low Noise Results

Table 4. 3: Summary of important input values for example 2.

Target Misfits	Chifact	2.1
	Chitol	0.1
Bounds	Upper	100.1623 s/km
	Lower	0.0 s/km

The slowness model produced by this inversion has located and determined the size and shape of the sulphide body. However, the model is somewhat fuzzy and there is a good amount of noise in the background. There are also a significant number of seismic receiver artefacts.

The travel times predicted by the inversion are quite close to those used in the inversion (Fig. 4. 4a). The normalized data residual, however, are very large, ~50% of the travel time range (Fig. 4. 4b). This is not unusual for low noise inversion and appears to be an effect of dividing the data differences between low uncertainty values, as such these high values are not necessarily identifying an inability to match the given dataset in these situations.

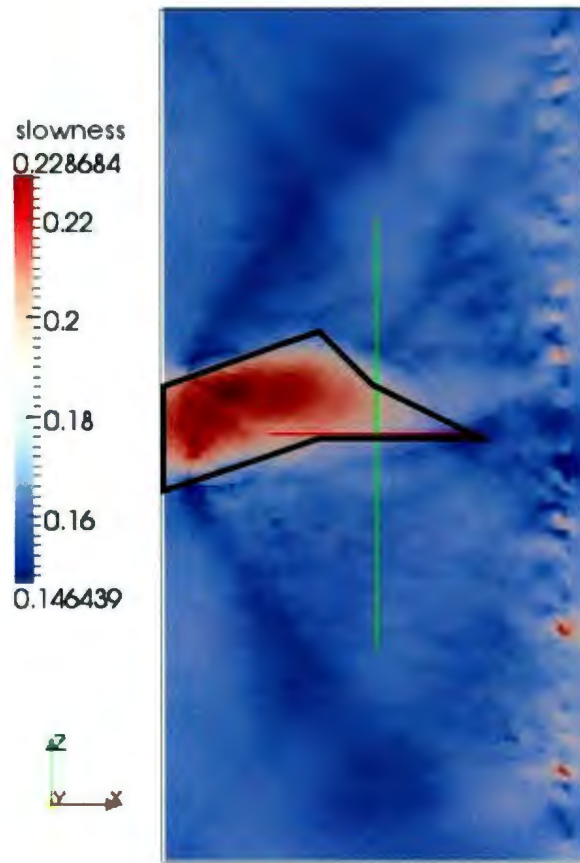


fig. 4. 3: Resultant slowness model from the seismic-only inversion of low noise sulphide-gneiss model synthetic data. The model is 200m across and 400m in depth and the black line outlines the location of the sulphide body in the synthetic models.

Example 3: High Noise Results

Table 4. 4: Summary of important input values for example 3.

Target Misfits	Chifact	1.0
	Chitol	0.1
Bounds	Upper	100.1623 s/km

	Lower	0.0 s/km
--	-------	----------

The seismic travel times predicted by this inversion and the associated normalized data residual are very similar to those seen in Fig. 4.3. The range of the normalized data residuals from this example is -5.95 to 5.06.

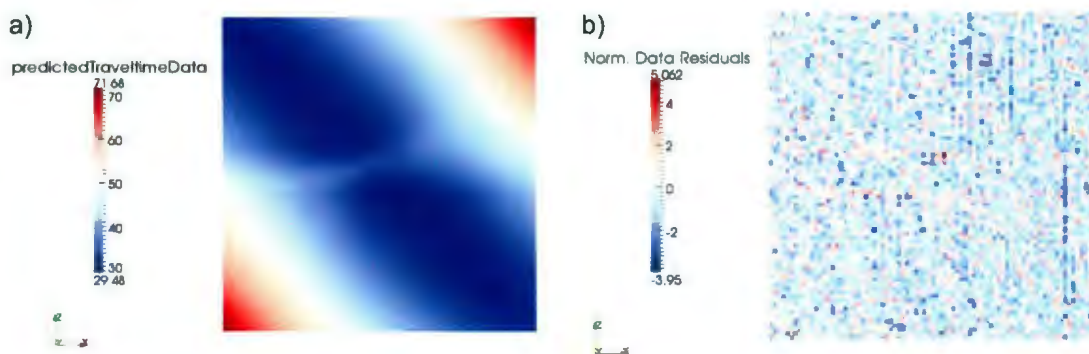


Fig. 4. 4: Predicted travel time data (a) and normalized data residual (b) for the seismic only inversion of low noise sulphide-gneiss model synthetic data. The horizontal axis of both plots is the source number and the vertical axis is the receiver number (Fig 3.10).

The results from the seismic only inversion of very noisy data produced surprisingly good results (Fig. 4. 5). The sulphide lens is well located and the slowness of the sulphides has been fairly well determined. The uniform background to the sulphide lens has not been as well modelled. The significant amount of chatter in the background could be evidence that the inversion was trying to model the noise in the data.

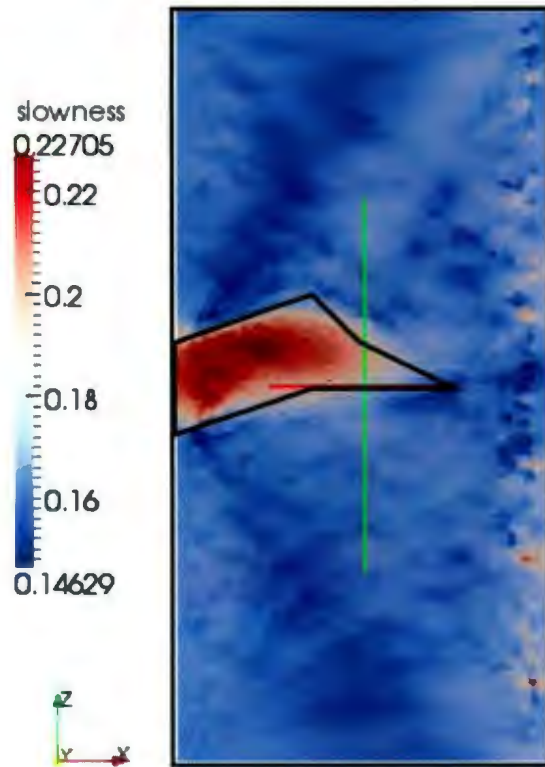


Fig. 4. 5: Resultant slowness model from seismic-only inversion of high noise sulphide-gneiss model synthetic data. The model is 200m across and 400m in depth and the black line outlines the location of the sulphide body in the synthetic models.

4.1.2 Surface Station Only Inversion Results

4.1.2.1 Moderate Noise Results

Example 4: Density-Only Inversion:

Table 4. 5: Summary of important input values for example 4.

Weighting	Type	Sensitivity
	Wpower	2.5
	Wzero	-1.0
	Wnorm	1.5
Target Misfits	Chifact	0.35
	Chitol	0.1
Bounds	Upper	5.817g/cm ³
	Lower	2.817 g/cm ³

The gravity response predicted by this inversion is similar in range and topology to the synthetic data produced during forward modelling of the sulphide-gneiss model (Fig. 4. 6a). The normalized data residuals calculated from the predicted and noisy synthetic data are quite low and show no particular spatial pattern (Fig. 4. 6b). This suggests that the inversion was able to match the synthetic data quite well.

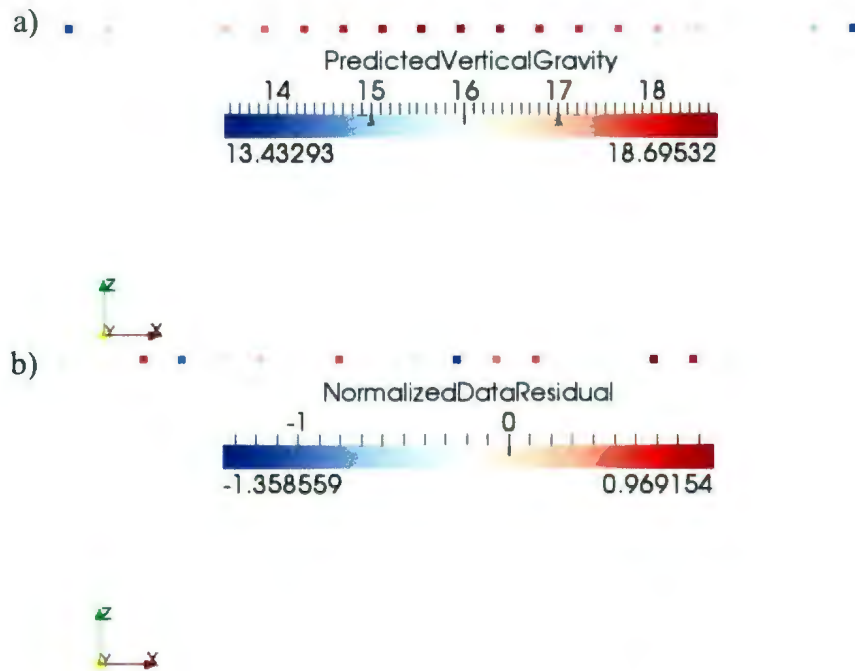


Fig. 4. 6: Predicted gravity data (a) and normalized data residual (b) for the gravity-only inversion of moderate noise sulphide-gneiss model synthetic data.

The density model produced by this inversion has not been able to locate the sulphide body, although it has been able to determine that there is dense material on the left side of the model (Fig. 4. 7). The presence of the high density artefact in the lower right hand corner as well as the under estimation of the density of the model can be attributed to the inaccuracy with which the model determined the depth of the sulphide body.

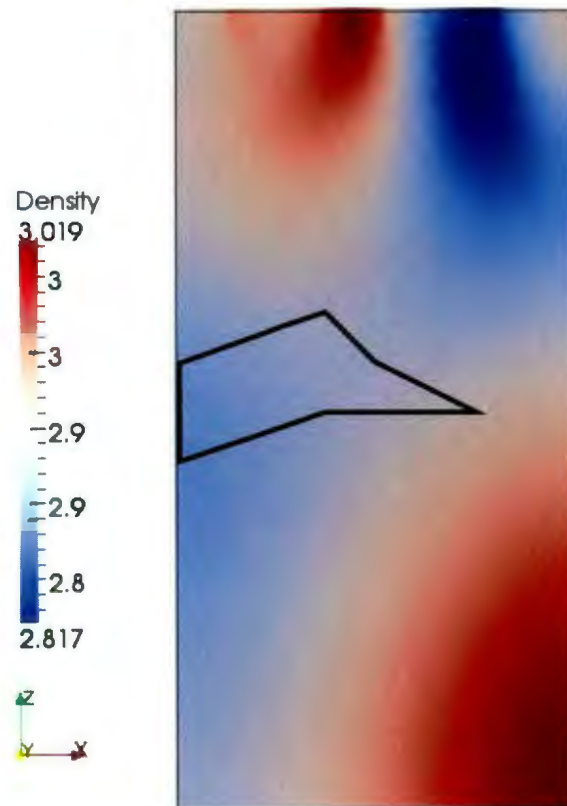


Fig. 4. 7: Resultant density model from the gravity-only inversion of moderate noise sulphide-gneiss synthetic data. The model is 200m across and 400m in depth and the black line outlines the location of the sulphide body in the synthetic models.

Example 5: Joint Inversion:

Table 4. 6: Summary of important input values for example 5.

Weighting	Gravity	Type	Sensitivity
		Wpower	2.5
		Wzero	-1.0
	Wnorm	1.5	
	Seismic	Type	None
Target Misfits	Gravity chifact		0.35
	Gravity chitol		0.1
	Travel-Time chifact		1.0
	Travel-Time chifact		0.1
Bounds	Density	Upper	5.817g/cm ³
		Lower	2.817 g/cm ³
	Slowness	Upper	1.1623 s/km
		Lower	0.1623 s/km
Similarity	Rhoe		1.0

The seismic travel times predicted by this inversion as well as the associated normalized data residuals are similar to those seen in Fig. 4. 1. The seismic normalized data residuals for this example range from -3.82 to 5.28.

The gravity response predicted by this inversion has a similar range and topology to the clean synthetic data created during forward modelling of the sulphide-gneiss model (Fig. 4. 8a). The normalized data residuals calculated from the moderately noisy synthetic and predicted data are fairly low and show no particular spatial distribution (Fig. 4. 8b). This suggests that the inversion was able to match the given data set well.

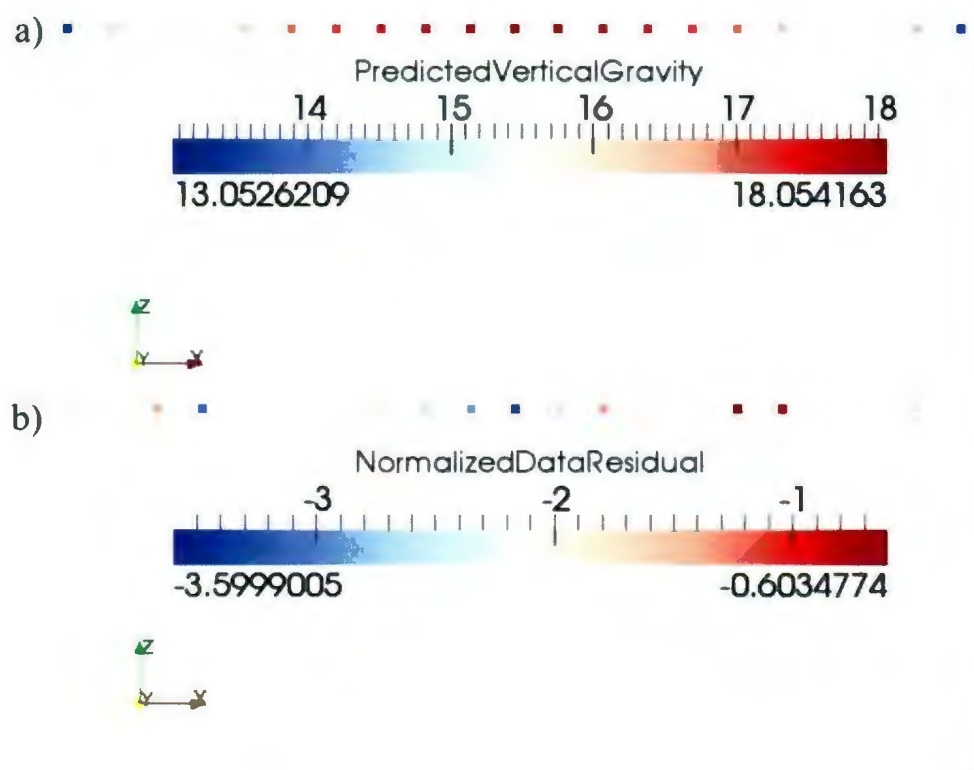


Fig. 4. 8: Predicted seismic travel times (a) and associated normalized data residuals (b) for the joint inversion of moderate noise sulphide-gneiss model synthetic data.

The density model produced by this inversion has located and reproduced the shape and size of the sulphide body (Fig. 4. 9a). The inversion has underestimated the density of the

sulphide body, although it has been able to determine the density of the background correctly. There are a number of artefacts along the right edge of the model.

The slowness model produced by this inversion has located the sulphide body and determined the size and shape of the body (Fig. 4. 9b). The inversion has overestimated the slowness of the body slightly, however, only a very few cells have extremely large slowness values.

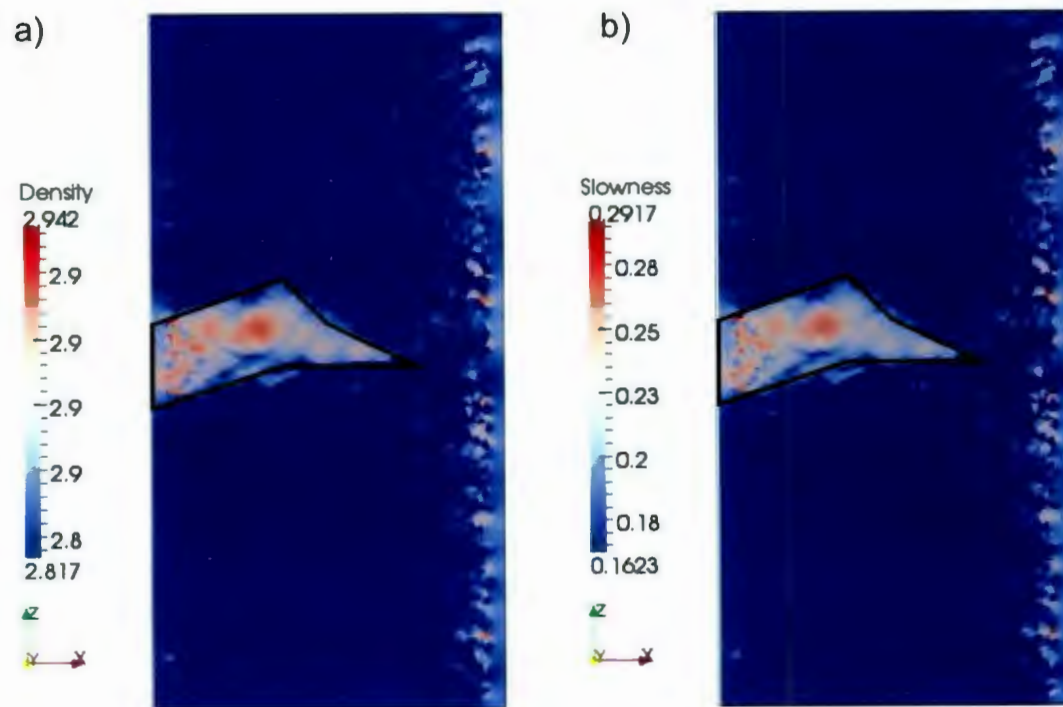


Fig. 4. 9: Resultant density (a) and slowness (b) models from the joint inversion of moderate noise sulphide-gneiss model synthetic data. The model is 200m across and 400m in depth and the black line outlines the location of the sulphide body in the synthetic models.

4.1.2.2 Low Noise Results

Example 6: Gravity – Only Inversion:

Table 4. 7: Summary of important input values for example 6.

Weighting	Type	Sensitivity
	wbeta	1.0
	wnorm	2.0
Target Misfits	Chifact	0.5
	Chitol	0.1
Bounds	Upper	5.817 g/cm ³
	Lower	2.817 g/cm ³

The gravity response predicted by this inversion and the associated normalized data residuals are similar to those seen in Fig. 4. 8. The normalized data residuals from this example range from -1.1 to 1.71.

The density model attained from the gravity-only inversion of low noise data from surface stations. The inversion has determined that the dense body is located to the left of the model and has roughly located the top of the body. The inversion has not, however, been able to resolve the shape or dimensions of the body. Nor has the inversion been able to resolve the bottom edge of the body (Fig. 4. 10). The density of the body has been underestimated by the inversion.

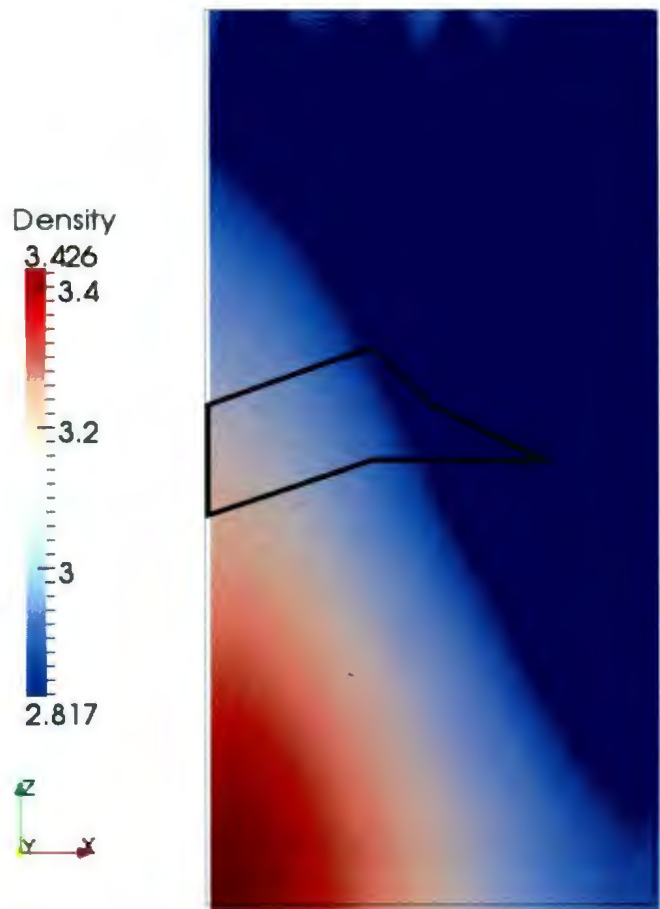


Fig. 4. 10: Resultant density model from the gravity-only inversion of low noise sulphide-gneiss model synthetic data. The model is 200m across and 400m in depth and the black line outlines the location of the sulphide body in the synthetic models.

Example 7: Joint Inversion:

Table 4. 8: Summary of important input values for example 7.

Weighting	Type		Sensitivity
		wbeta	
	wnorm		2.0
Target Misfits	Gravity chifact		1.0
	Gravity chitol		0.2
	Travel-Time chifact		1.0
	Travel-Time chifact		0.2
Bounds	Density	Upper	5.817g/cm ³
		Lower	2.817g/cm ³
	Slowness	Upper	1.1623 s/km
		Lower	0.1623 s/km
Similarity	Rhoe		1.0

The seismic travel times predicted by this inversion (Fig. 4. 11a) are similar in range and topology to the clean synthetic data calculated from the forward modelling of the sulphide-gneiss model. The normalized data residuals calculated from the predicted and low noise synthetic data are quite high (Fig. 4. 11b). As the body was well modelled and the predicted travel times appear reasonable it is likely that these large data residuals are due to the low noise levels in the synthetic data.

The gravity response predicted by this inversion and the associated normalized data residuals are similar to those seen in Fig. 4. 9. The normalized data residuals from this example range from -1.57 to 1.86.

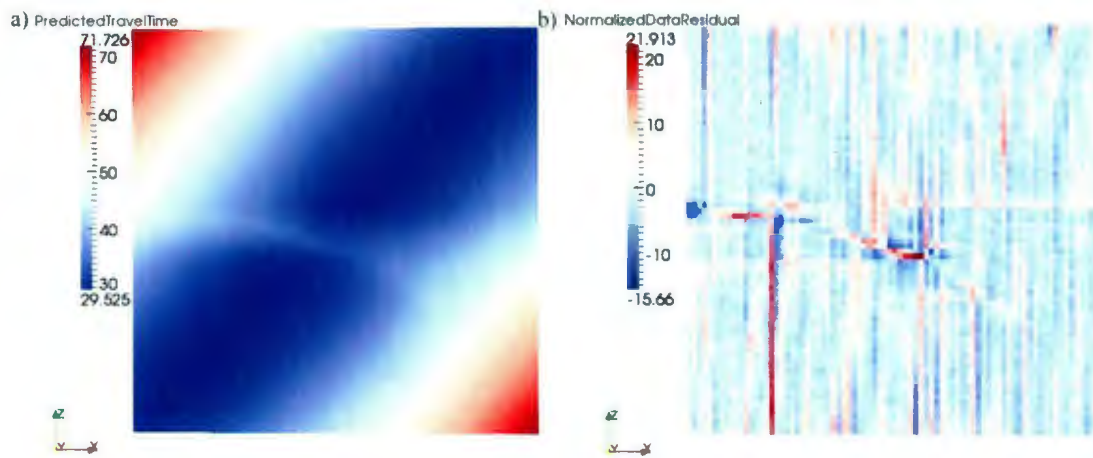


Fig. 4. 11: Predicted seismic travel times (a) and associated normalized data residuals (b) for the joint inversion of low noise sulphide-gneiss model synthetic data. The horizontal axis of both plots is the source number and the vertical axis is the receiver number (Fig 3.10).

The density model produced by this inversion has not been able to locate the sulphide body, although it has determined that there is more dense material to the left side of the model (Fig. 4. 12a). The slowness model produced by this inversion has located and has roughly determined the size and shape of the sulphide body (Fig. 4. 12b). The slowness of the sulphide body has been overestimated and there are a significant amount of seismic receiver artefacts along the right edge of the model.

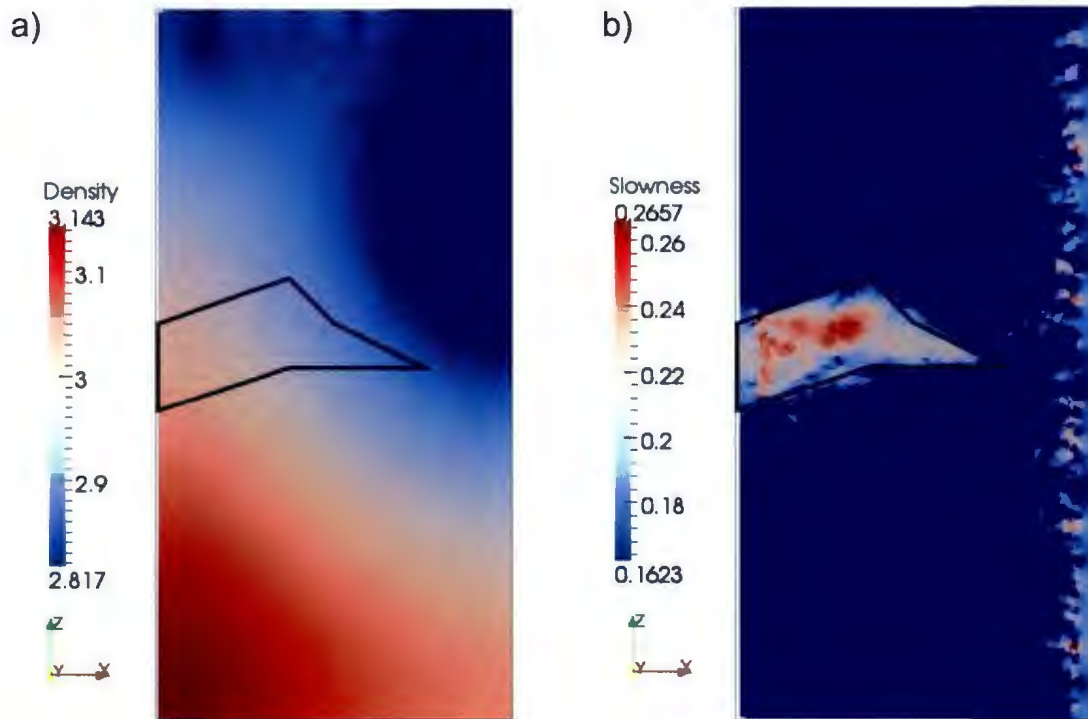


Fig. 4. 12: Resultant density (a) and slowness (b) models from the joint inversion of low noise sulphide-gneiss model synthetic data. The model is 200m across and 400m in depth and the black line outlines the location of the sulphide body in the synthetic models.

4.1.2.3 High Noise Results

Example 8: Gravity-Only Inversion:

Table 4. 9: Summary of important input values for example 8.

Weighting	Type	Sensitivity
	Wpower	2.5
	Wbeta	1.0
	Wnorm	2.0
Target Misfits	Chifact	0.75
	Chitol	0.1
Bounds	Upper	5.817 g/cm ³
	Lower	2.817 g/cm ³

The gravity response predicted by this inversion and the associated normalized data residuals are similar to those seen in Fig. 4. 10. The normalized data residuals for this example range from -1.63 to 1.81.

The gravity-only inversion of high noise sulphide-gneiss model data from surface only stations has been able to determine that a dense body exists along the left edge of the body. The inversion has not, however, been able to determine the exact vertical location of the body or been able to resolve the shape of the sulphide body (Fig. 4. 13). The inversion has underestimated the density of the sulphide body.

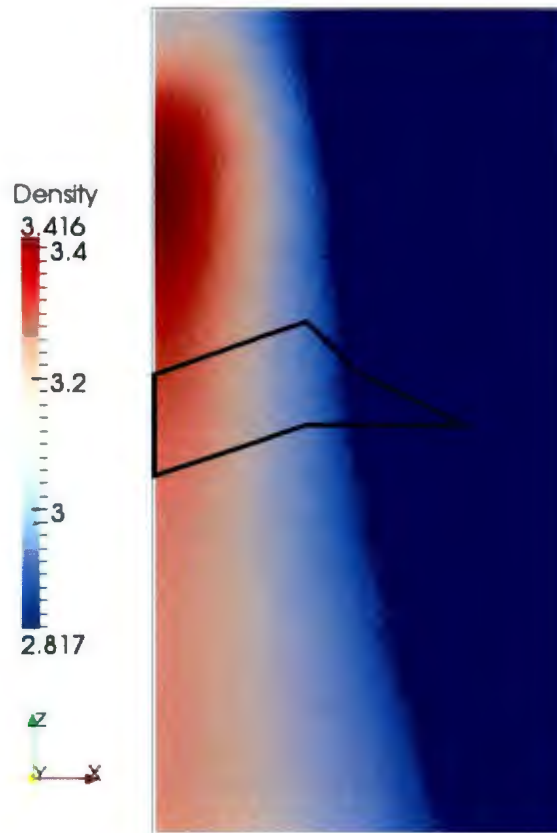


Fig. 4. 13: Resultant density model from the gravity-only inversion of high noise sulphide-gneiss model synthetic data. The model is 200m across and 400m in depth and the black line outlines the location of the sulphide body in the synthetic models.

Example 9: Joint Inversion:

Table 4. 10: Summary of important input values for example 9.

Weighting	Type		Sensitivity
	wbeta		1.0
	wnorm		2.0
Target Misfits	Gravity	chifact	1.0
		Chitol	0.2
	Travel-Time	Chifact	1.0
		Chifact	0.2
	Joint inversion	Alphaj	1.0
		jchitol	0.05
Bounds	Density	Upper	5.817 g/cm ³
		Lower	2.817 g/cm ³
	Slowness	Upper	0.1623 s/km
		Lower	1.1623 s/km
Similarity	Rhoe		1.0

The seismic travel times predicted by this inversion and the associated normalized data residuals are similar to those seen in Fig. 4. 1. The normalized data residuals for this example range from -4.02 to 5.04.

The gravity response predicted by this inversion and associated normalized data residuals are similar to those seen in Fig. 4. 6. The normalized data residuals for this example range from -2.09 to 1.58.

The density and slowness models produced by the joint inversion of high noise sulphide gneiss model data have been able to model the sulphide body well. Both models have been able to replicate the size and shape of the body. The density of the body has been significantly underestimated (Fig. 4. 14a), however the slowness of the body has been well estimated by the inversion (Fig. 4. 14b).

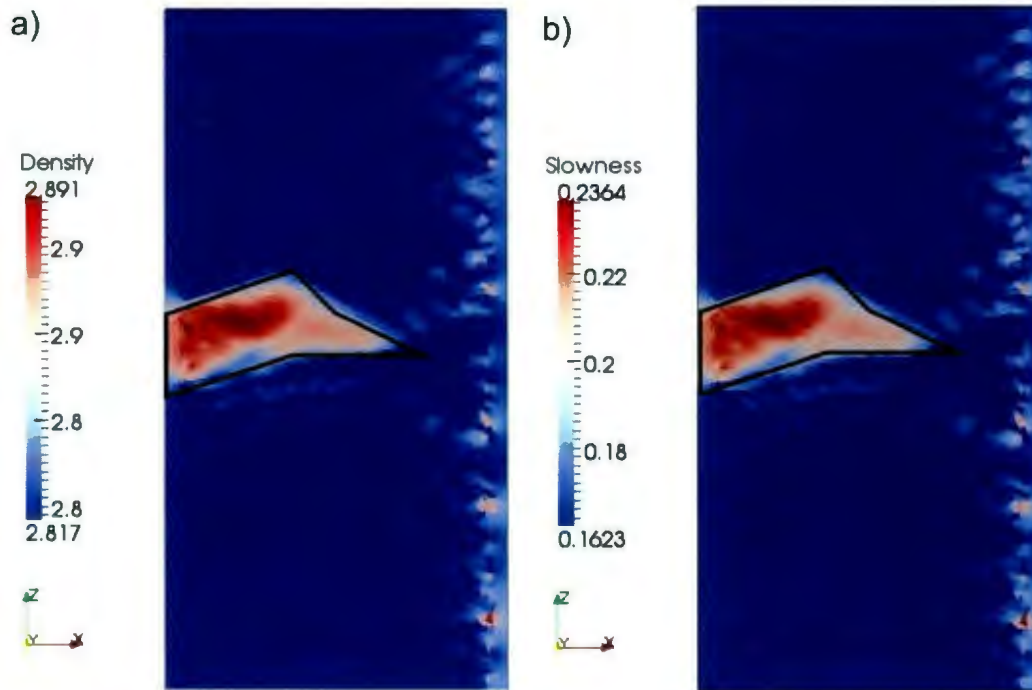


Fig. 4. 14: Resultant density (a) and slowness (b) models from the joint inversion of high noise sulphide-gneiss model synthetic data. The model is 200m across and 400m in depth and the black line outlines the location of the sulphide body in the synthetic models.

4.1.3 Borehole Stations Only Inversion Results

4.1.3.1 Moderate Noise Data from Borehole A Stations

Example 10: Gravity-Only Inversion:

Table 4. 11: Summary of important input values for example 10.

Weighting	Type	Sensitivity
	Wbeta	1.0
	Wnorm	2.0
Target Misfits	Chifact	1.0
	Chitol	0.2
Bounds	Upper	5.817 g/cm ³
	Lower	2.817 g/cm ³

The gravity response predicted by this inversion has replicated the topology and range of values seen in the synthetic data (Fig. 4. 15a). The normalized data residuals calculated from the synthetic and predicted data from this inversion are relatively low (Fig. 4. 15b). This suggests that the inversion was able to match the synthetic data quite well.

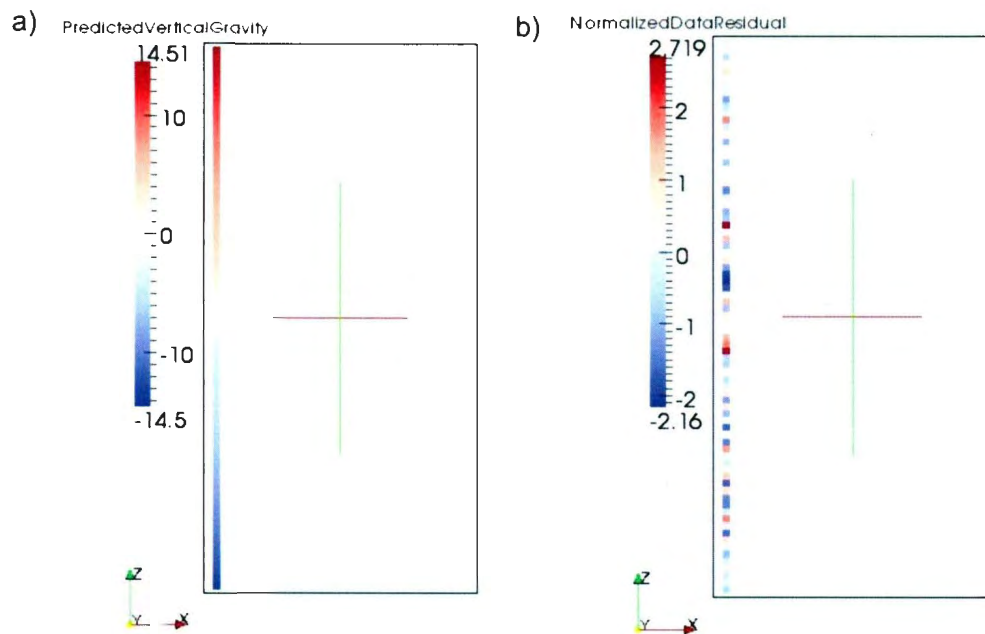


Fig. 4.15: Predicted gravity data (a) and associated normalized data residuals (b) for the joint inversion of moderate noise sulphide-gneiss model synthetic data.

The density model produced by the gravity-only inversion of moderate noise synthetic data from stations in borehole A has modelled the sulphide body well (Fig. 4.16). The inversion has accurately located the body and the vertical extent of the body has been well determined. However, the shape of the anomaly is that of a slightly defuse blob and does not accurately determine the full lateral extent of the body. The density of the sulphide has been accurately estimated on the whole, although there is some overestimation at the centre of the body and some underestimation at its edges. The density of the gneissic background has been estimated well.

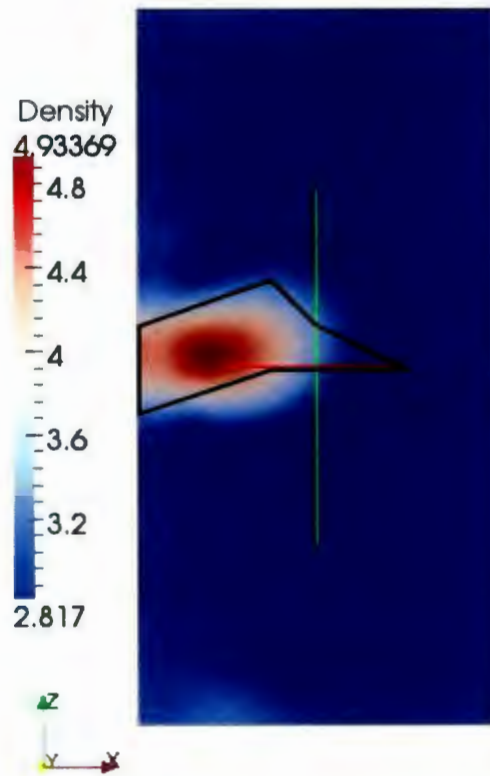


Fig. 4. 16: Resultant density model from the gravity-only inversion of moderate noise sulphide-gneiss model synthetic data. The model is 200m across and 400m in depth and the black line outlines the location of the sulphide body in the synthetic models.

Example 11: Joint Inversion:

Table 4. 12: Summary of important input values for example 11.

Weighting	Type		Sensitivity
	wbeta		1.0
	wnorm		2.0
Target Misfits	Gravity	chifact	1.0
		chitol	0.2
	Travel-Time	chifact	1.0
		chitol	0.2
	Joint Inversion	Alphaj	1.0
		Jchitol	0.05
Bounds	Density	Upper	5.817 g/cm ³
		Lower	2.817 g/cm ³
	Slowness	Upper	1.1623 s/km
		Lower	0.1623 s/km
Similarity	Rhoe		0.0

The seismic travel times predicted by this inversion and the associated normalized data residuals are similar to those seen in Fig. 4. 1. The normalized data residuals from this example range from -4.1 to 5.28.

The gravity response predicted by this inversion shows a similar topology and range of values to the synthetic data provided to the inversion (Fig. 4. 17). The normalized data residuals calculated from the synthetic and predicted gravity response are relatively low (Fig. 4. 17b). This suggests that the inversion was able to match the synthetic gravity data moderately well. The concentration of large normalized data residuals near the upper and lower sulphide contacts suggests that these areas had the most trouble matching the synthetic data.

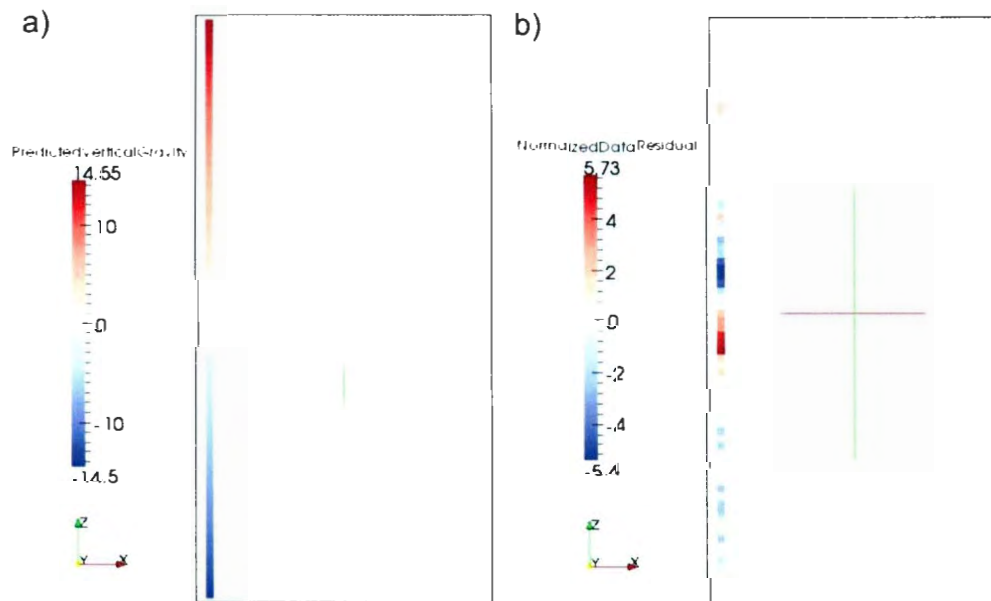


Fig. 4. 17: Predicted gravity data (a) and associated normalized data residuals (b) for the joint inversion of moderate noise sulphide-gneiss model synthetic data.

The density (Fig. 4. 18a) and slowness (Fig. 4. 18b) models produced by the joint inversion of moderate noise synthetic data from stations in borehole A has modelled the sulphide body well. The density model has placed the body correctly and has accurately predicted its vertical and lateral extent. The shape of the anomaly has more resemblance

to the initial model than was produced from the gravity-only inversion of the same gravity data (Fig. 4. 16). The density of the sulphide body has been estimated very well as has the density of the gneissic background. The slowness model shows that the sulphide body was modelled quite well in the seismic half of the inversion. It has accurately positioned the body and replicated its shape. The slowness of the body has been overestimated in small parts of the model, however, as a whole the slowness of both the sulphide and gneissic background have been estimated well by the inversion. There is some noise seen in the background of the slowness model, particularly around the location of the seismic receivers.

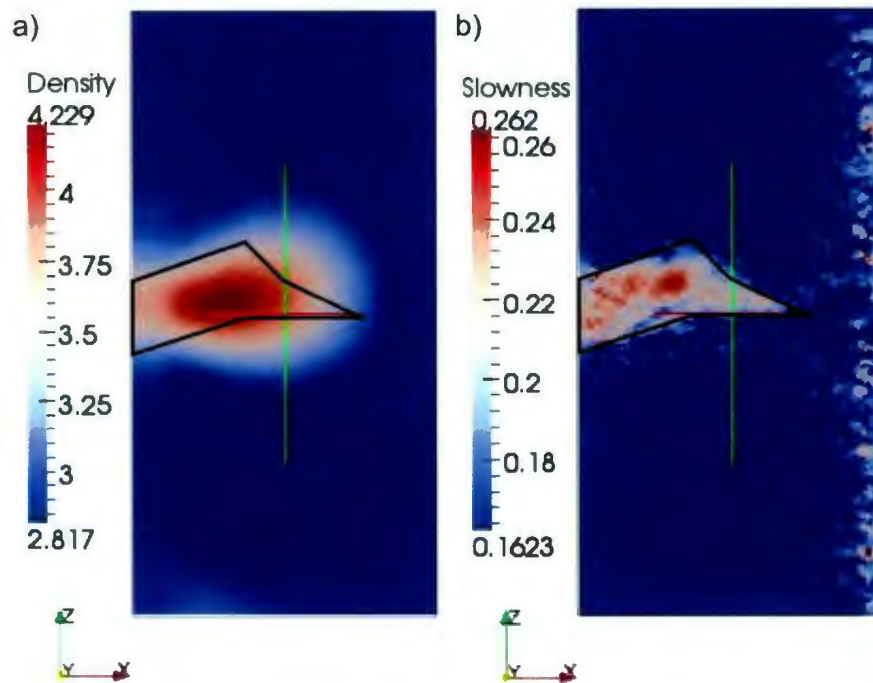


Fig. 4. 18: The resultant density (a) and slowness (b) models from the joint inversion of moderate noise sulphide-gneiss model synthetic data. The model is 200m across and 400m in depth and the black line outlines the location of the sulphide body in the synthetic models.

4.1.3.2 High Noise Data from Borehole A Stations

Example e 12: Gravity-Only Inversion

Table 4. 13: Summary of important input values for example 12.

Weighting	Type	Sensitivity
	Wbeta	1.0
	Wnorm	2.0
Target Misfits	Chifact	0.5
	Chitol	0.1
Bounds	Upper	5.817 g/cm ³
	Lower	2.817 g/cm ³

The gravity response predicted by this inversion has a similar topology to the synthetic data, and the range of the gravity response is within that of the high noise synthetic data (Fig. 4. 19a). The range is, however, quite different from the clean synthetic data, this in conjunction with the small normalized data residuals calculated for this inversion (Fig. 4. 19b) which indicates that the synthetic data was very well matched, suggests that the inversion may have been matching noise in the data.

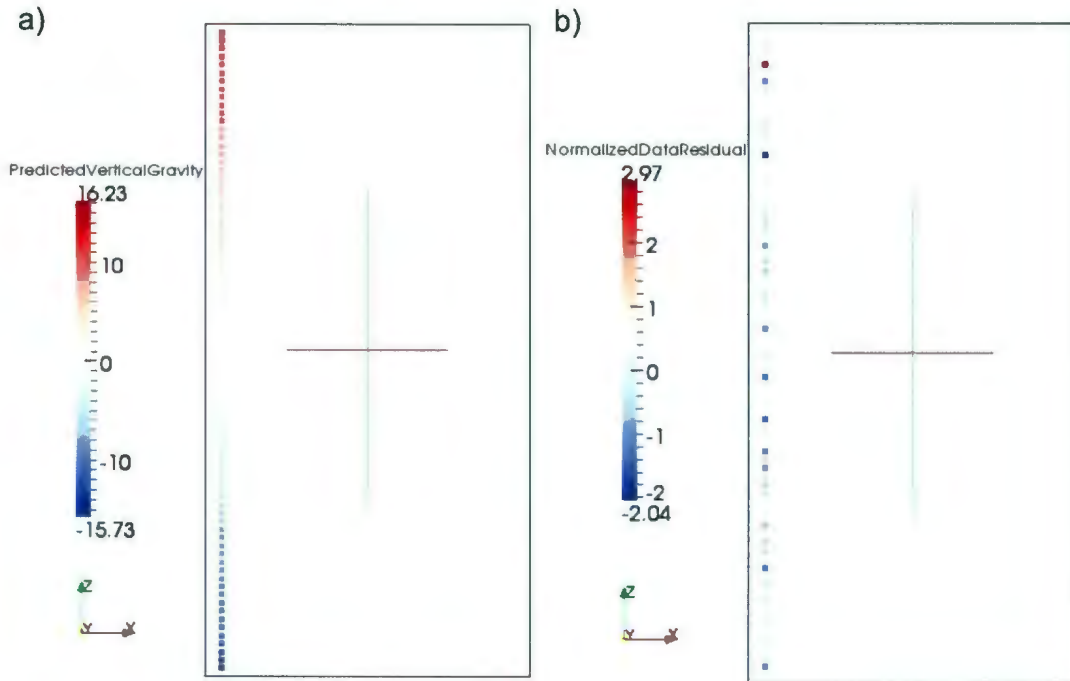


Fig. 4. 19: Predicted gravity data (a) and associated normalized data residuals (b) for the joint inversion of high noise sulphide-gneiss model synthetic data.

The density model produced by the gravity-only inversion of high noise sulphide-gneiss model synthetic data from gravity stations in borehole A only has not modelled the sulphide body very well. The inversion has located the high density body correctly; however, the inversion has not accurately determined the dimensions or the shape of the sulphide body. The inversion has also identified many extraneous high density bodies (Fig. 4. 20). The density of the sulphide body has been overestimated by the inversion; however, the density of the gneissic background has been well estimated.

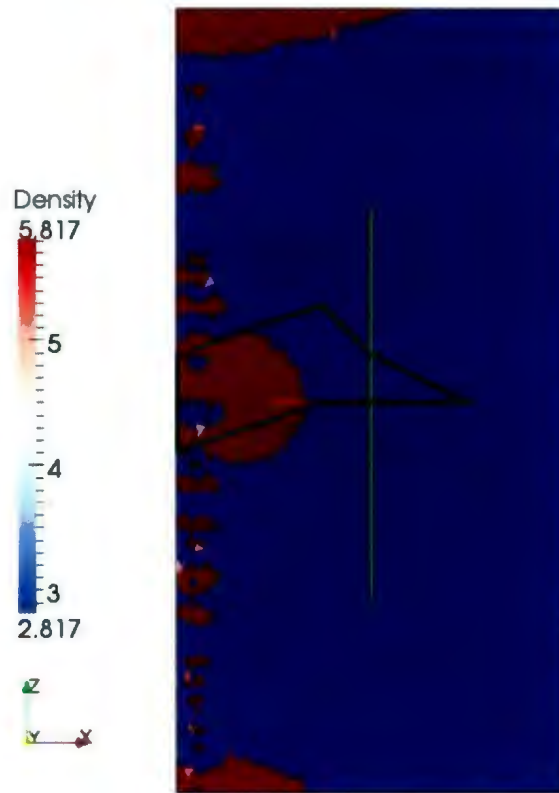


Fig. 4. 20: Resultant density model from the gravity-only inversion of high noise sulphide-gneiss model synthetic data. The model is 200m across and 400m in depth.

Example 13: Joint Inversion

Table 4. 14: Summary of important input values for example 13.

Weighting	Type		Sensitivity
		wbeta	1.0
		wnorm	2.0
Target Misfits	Gravity	chifact	0.5
		chitol	0.1
	Travel-Time	chifact	1.0
		chifact	0.2
		alphaj	1.0
		jchitol	0.05
Bounds	Density	Upper	5.817 g/cm ³
		Lower	2.817 g/cm ³
	Slowness	Upper	1.1623 s/km
		Lower	0.1623 s/km
Similarity	Rhoe	10 ⁻¹⁰	

The seismic travel times predicted by this inversions and the associated normalized data residuals are similar to those seen in Fig. 4. 1. The normalized data residuals from this example range from -4.16 to 3.99. The gravity response and associated normalized data

residuals are similar to those seen in Fig. 4. 15. The normalized data residuals for this example range from -2.28 to 3.35.

The density model produced by this inversion (Fig. 4. 21a) has located the sulphide body and roughly determined its size. Although, it has not been able to determine the shape of the sulphide body. The density of the sulphide has been underestimated and the inversion has introduced a number of artefacts, including paired positive and negative artefacts near the location of the gravity stations.

The slowness model produced by this inversion (Fig. 4. 21b) has located and determined the approximate shape and size of the sulphide body. The slowness of the sulphide body has been overestimated, however, there are only a few very high slowness cells. There are a high number of artefacts in this model including a large concentration near the locations of the seismic receivers.

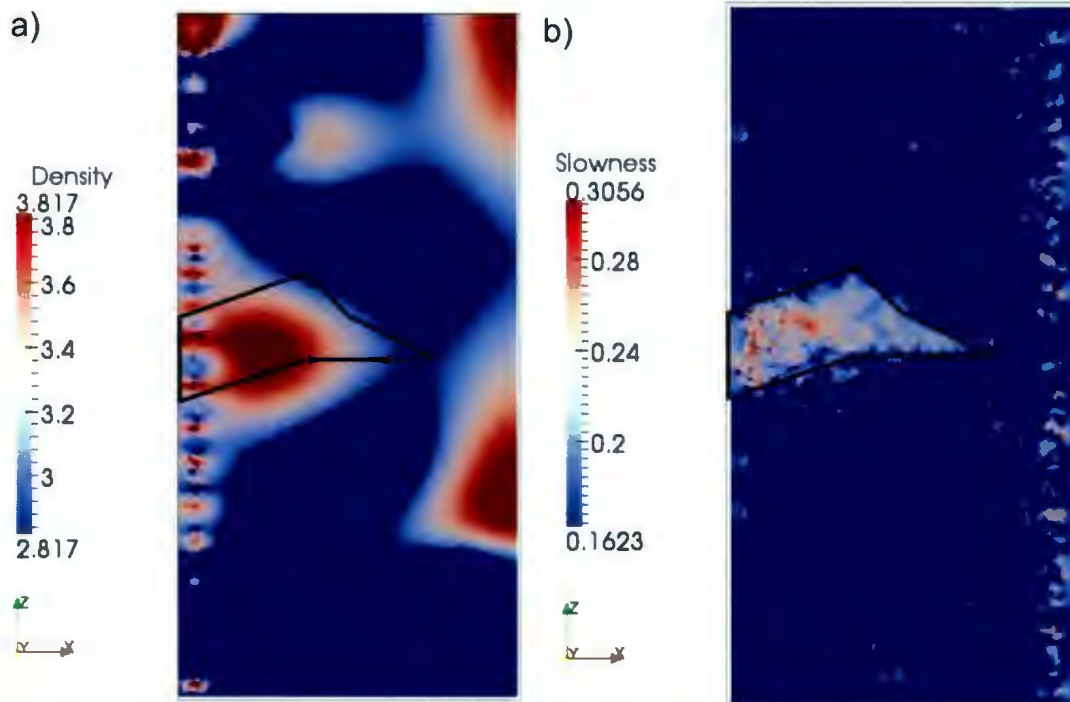


Fig. 4. 21: The resultant density (a) and slowness (b) models from the joint inversion of high noise sulphide-gneiss model synthetic data. The model is 200m across and 400m in depth and the black line outlines the location of the sulphide body in the synthetic models.

4.1.3.3 Low Noise Data from Borehole A Stations

Example 14: Gravity-Only Inversion:

Table 4. 15: Summary of important input values for example 14.

Weighting	Type	Sensitivity
	Wbeta	1.0
	Wnorm	2.0
Target Misfits	Chifact	1.0
	Chitol	0.2
Bounds	Upper	5.817 g/cm ³
	Lower	2.817 g/cm ³

The gravity response predicted by this inversion is similar in topology and range of data to the synthetic gravity data provided to the inversion. (Fig. 4. 22a). The normalized data residuals calculated from the predicted and synthetic gravity data are very low (Fig. 4. 22b). This suggests that the inversion matched the synthetic data very well. The cells with the highest normalized data residuals appear near the surface and the lowest at the bottom of the borehole.

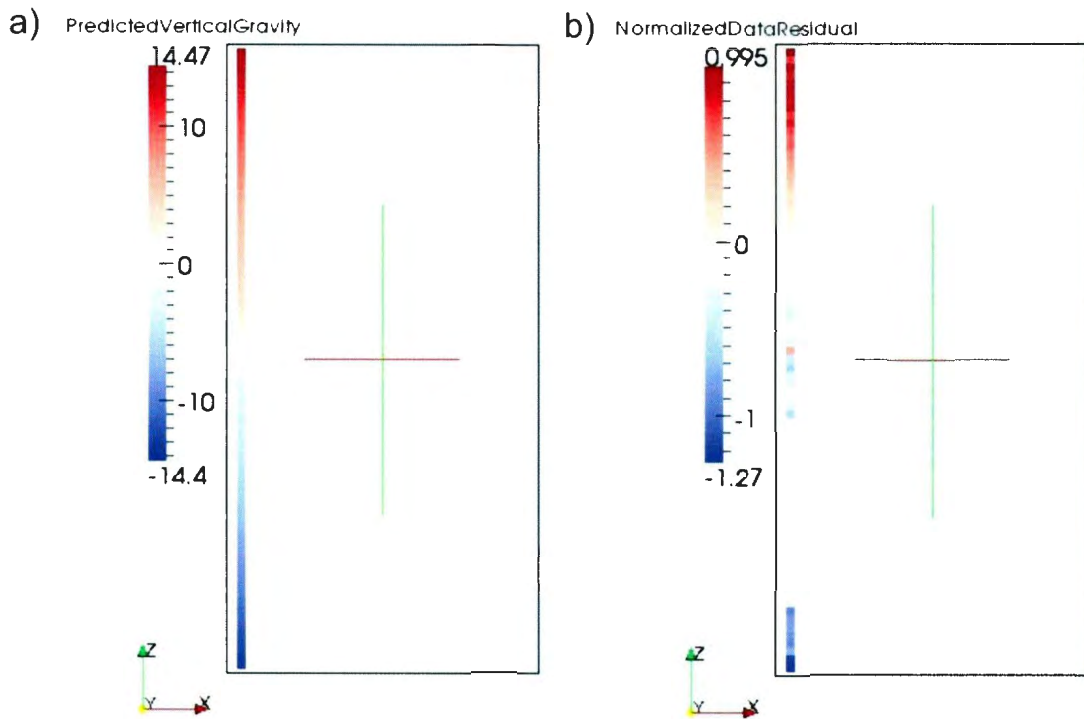


Fig. 4. 22: Predicted gravity data (a) and associated normalized data residuals (b) for the joint inversion of low noise sulphide-gneiss model synthetic data.

The density model produced by the gravity-only inversion of low noise synthetic data has reproduced the sulphide body moderately well. The body has been correctly positioned and the vertical extent of the body has been correctly determined by the inversion.

However, the lateral extent has been slightly underestimated (Fig. 4. 23). The density of the sulphide body has been significantly overestimated at its centre and underestimated at its edges. The density of the gneissic background, however, has been well estimated.

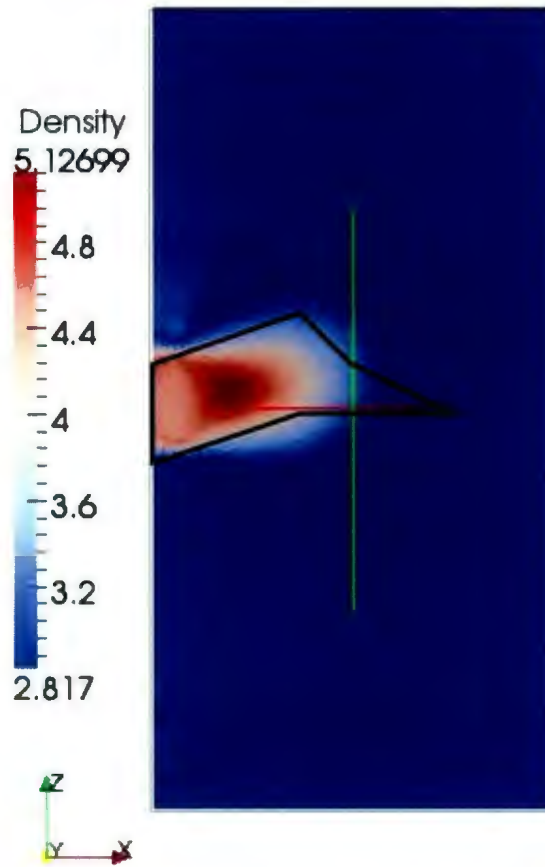


Fig. 4. 23: Resultant density model from the gravity-only inversion of low noise sulphide-gneiss model synthetic data. The model is 200m across and 400m in depth and the black line outlines the location of the sulphide body in the synthetic models.

Example 15: Joint Inversion:

Table 4. 16: Summary of important input values for example 15.

Weighting	Type		Sensitivity
		wbeta	
	wnorm		2.0
Target Misfits	Gravity chifact		1.0
	Gravity chitol		0.2
	Travel-Time chifact		1.0
	Travel-Time chifact		0.2
Bounds	Density	Upper	5.817 g/cm ³
		Lower	2.817 g/cm ³
	Slowness	Upper	1.1623 s/km
		Lower	0.1623 s/km
Similarity	Rhoe		10 ⁻⁴

The seismic travel times predicted by this inversion and their associated normalized data residuals are similar to those seen in Fig. 4. 11. The normalized data residuals from this example range from -16 to 20.7.

The gravity response predicted by this inversion (Fig. 4. 24a) is similar in range and topology to the clean synthetic data produced from forward modelling the sulphide-gneiss model. The normalized data residuals calculated from the low noise synthetic and

predicted data are high (Fig. 4. 24b), however, there are only a few very high values and these are located near the contacts between the sulphide and the troctolite. In light of the low noise in the synthetic data and the low values of most of the normalized data residuals it can be said that the inversion was able to match the given data set.

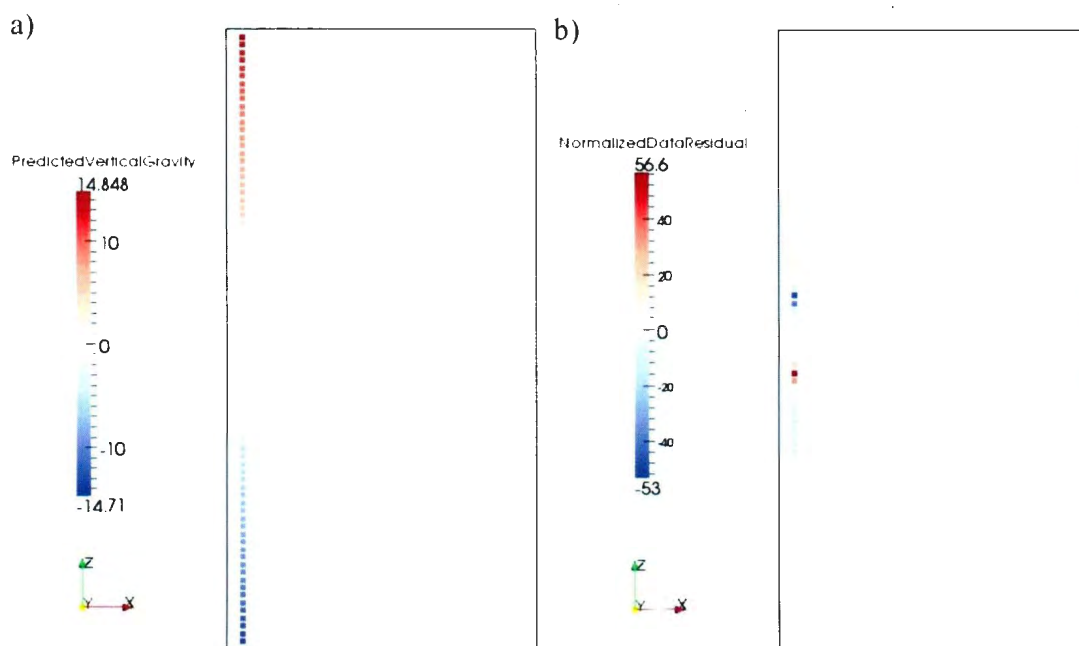


Fig. 4. 24: Predicted gravity data (a) and associated normalized data residuals (b) for the joint inversion of low noise sulphide-gneiss model synthetic data.

The density model produced by this inversion has been able to locate and determine the size of the sulphide body (Fig. 4. 25a). The density has been estimated well for both the sulphide and the background gneiss. The slowness model produced by this inversion has

been able to locate and determined the size and shape of the sulphide body (Fig. 4. 25b). The slowness of the sulphide body has been overestimated while the slowness of the background has been well estimated with exception of a significant number of seismic receiver artefacts.

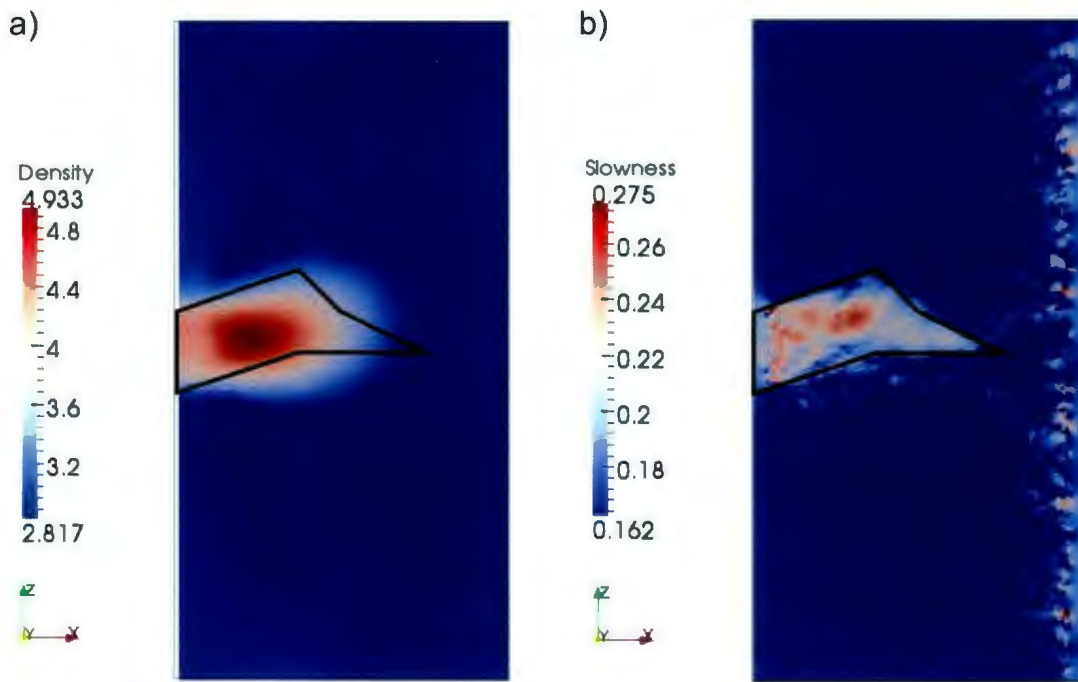


Fig. 4. 25: The resultant density (a) and slowness (b) models from the joint inversion of low noise sulphide-gneiss model synthetic data. The model is 200m across and 400m in depth and the black line outlines the location of the sulphide body in the synthetic models.

4.1.3.4 Moderate Noise Data from Borehole B Stations

Example 16: Gravity-Only Inversion:

Table 4. 17: Summary of important input values for example 16.

Weighting	Type	Sensitivity
	Wbeta	1.0
	Wnorm	2.0
Target Misfits	Chifact	1.0
	Chitol	0.2
Bounds	Upper	5.817 g/cm ³
	Lower	2.817 g/cm ³

The gravity response predicted by this inversion has a similar topology and range of values to the synthetic gravity data provided to the inversion (Fig. 4. 26a). The normalized data residuals calculated from the predicted and synthetic gravity data are fairly low (Fig. 4. 26b). This suggests that the inversion was able to match the synthetic data fairly well. Many of the normalized data residuals are larger than zero; this suggests that the inversion was consistently getting larger gravity measurements than those seen in the synthetic data.

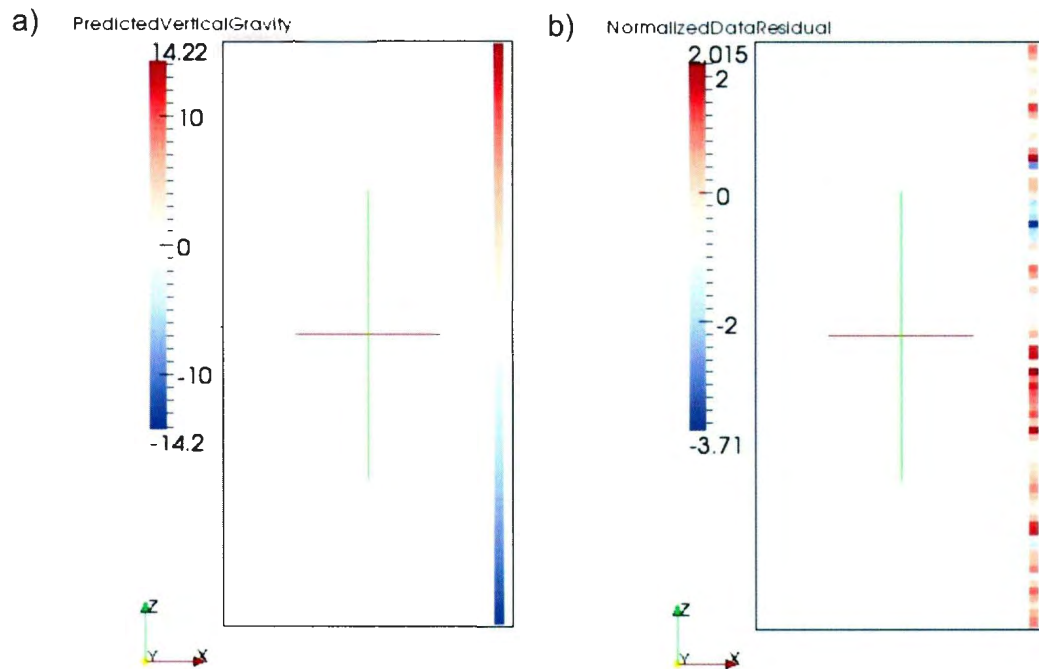


Fig. 4. 26: Predicted gravity data (a) and associated normalized data residuals (b) for the joint inversion of moderate noise sulphide-gneiss model synthetic data.

The density model produced by the gravity-only inversion of moderately noisy synthetic data from stations in borehole B has correctly positioned the sulphide body. However, the lateral and vertical extent as well as the shape of the body has not been well determined (Fig. 4. 27). The density of the sulphide body has been significantly underestimated by the inversion; however the gneissic background has been correctly estimated.

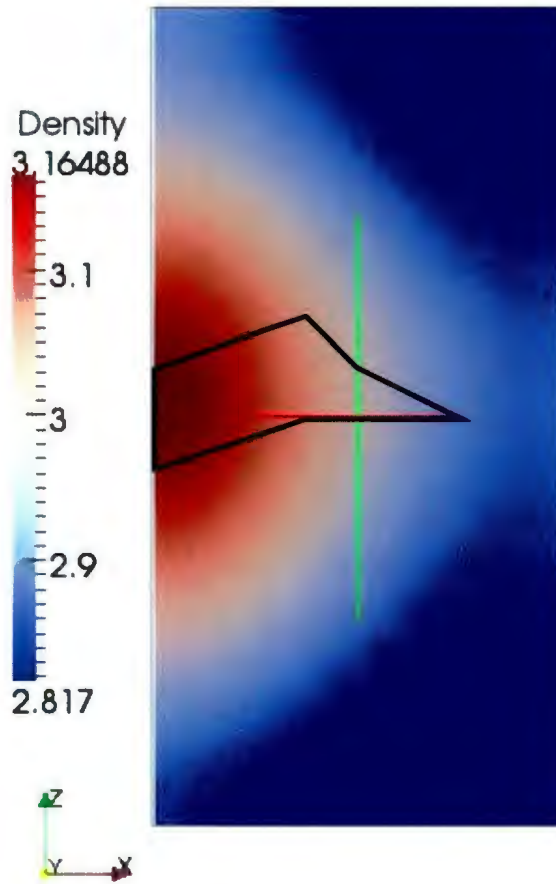


Fig. 4. 27: Resultant density model from the gravity-only inversion of moderate noise sulphide-gneiss model synthetic data. The model is 200m across and 400m in depth and the black line outlines the location of the sulphide body in the synthetic models.

Example 17: Joint Inversion

Table 4. 18: Summary of important input values for example 16.

Weighting	Type		Sensitivity
	wbeta		1.0
	wnorm		2.0
Target Misfits	Gravity	chifact	1.0
		chitol	0.2
	Travel-Time	chifact	0.5
		chifact	0.1
	Joint inversion	alphaj	1.0
		jchitol	0.05
Bounds	Density	Upper	5.817 g/cm ³
		Lower	2.817 g/cm ³
	Slowness	Upper	1.1623 s/km
		Lower	0.1623 s/km
Similarity	Rhoe		1.0

The gravity response predicted by this inversion, as well as the associated normalized data residuals are similar to those seen in Fig. 4. 26. The normalized data residuals for this example range from -1.68 to 2.37. The seismic travel times predicted by this inversion

and the associated normalized data residuals are similar to those seen Fig. 4. 1. The normalized data residuals for this example range from -3.65 to 5.27.

The density model produced by this inversion has located the sulphide body, although it has not been able to determine its size or shape (Fig. 4. 28a). The inversion has also underestimated the density of the sulphide body. The slowness model produced by this inversion has located and determined the size and shape of the sulphide body. The slowness of the body has been slightly over estimated. There are a moderate number of seismic receiver artefacts along the right edge of the model (Fig. 4. 28b).

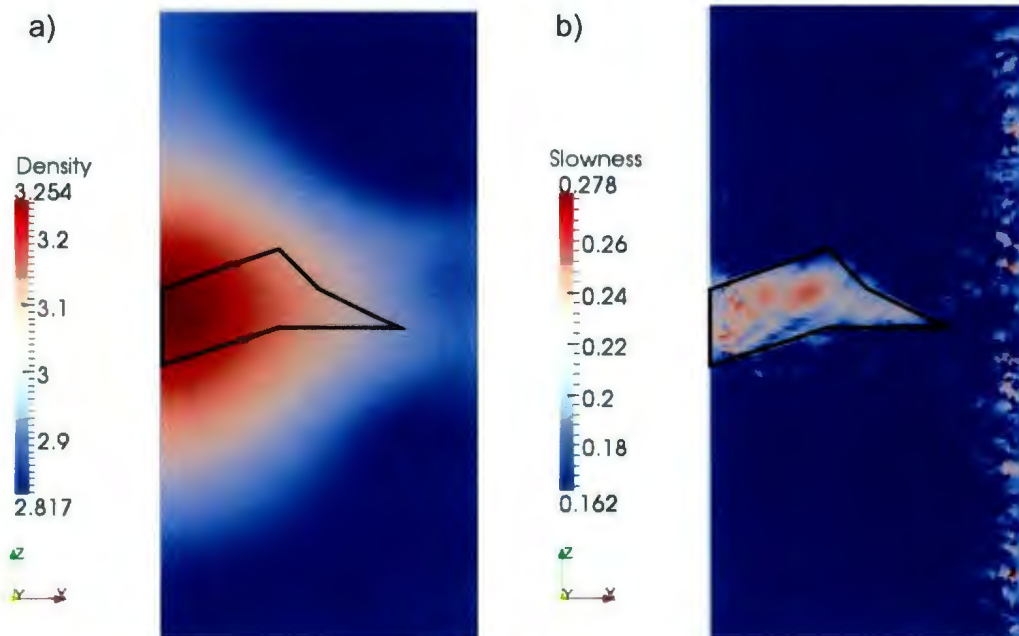


Fig. 4. 28: The resultant density (a) and slowness (b) models from the joint inversion of moderate noise sulphide-gneiss model synthetic data. The model is 200m across and 400m in depth and the black line outlines the location of the sulphide body in the synthetic models.

4.1.3.5 High Noise Data from Borehole B Stations

Inversion 18: Gravity-Only Inversion

Table 4. 19: Summary of important input values for example 18.

Weighting	Type	Sensitivity
	Wbeta	1.0
	Wnorm	2.0
Target Misfits	Chifact	0.5
	Chitol	0.1
Bounds	Upper	5.817 g/cm ³
	Lower	2.817 g/cm ³

The gravity response predicated by this inversion and the associated normalized data residuals are similar to those seen in Fig. 4. 26. The normalized data residuals for this example range from -2.34 to 2.53. The density model produced by the gravity-only inversion of high noise sulphide-gneiss model synthetic data from stations only in borehole B has not replicated the sulphide body at all. The inversion has been able to determine that some high density material exist, however, it has been unable to locate this material correctly (Fig. 4. 29). Although, the density of the gneissic background has been correctly estimated, the inversion has overestimated the density of the anomalous material.

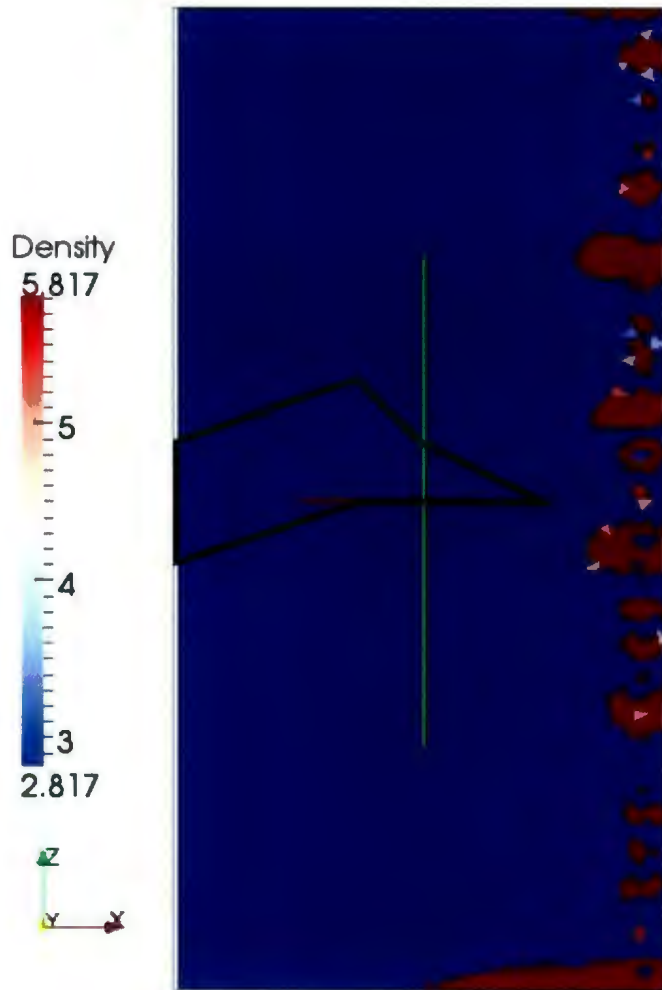


Fig. 4. 29: Resultant density model from the gravity-only inversion of high noise sulphide-gneiss model synthetic data. The model is 200m across and 400m in depth and the black line outlines the location of the sulphide body in the synthetic models.

Inversion 19: Joint Inversion

Table 4. 20: Summary of important input values for example 19.

Weighting	Type		Sensitivity
	wbeta		1.0
	wnorm		2.0
Target Misfits	Gravity	chifact	0.5
		chitol	0.1
	Travel-Time	chifact	1.0
		chitol	0.2
	Joint inversion	alphaj	1.0
		jchitol	0.05
Bounds	Density	Upper	5.817 g/cm ³
		Lower	2.817 g/cm ³
	Slowness	Upper	1.1623 s/km
		Lower	0.1623 s/km
Similarity	Rhoe		10 ⁻¹⁰

The gravity response predicted by this inversion and the associated normalized data residuals are similar to those seen in Fig. 4. 26. The normalized data residuals from this example range from -3.29 to 2.89. The seismic travel times predicted by this inversion and the associated normalized data residuals are similar to those seen in Fig. 4. 1. The normalized data residuals for this example range from -3.75 to 4.83.

The density model produced by this inversion has located the sulphide body but has been unable to determine its size and shape (Fig. 4. 30a). The density of the sulphide has been seriously underestimated. The slowness model produced by this inversion has located and determined the size and shape of the sulphide body (Fig. 4. 30b). The inversion has overestimated the slowness of the sulphide; however, there are only a few extremely high slowness cells. There are a moderate number of seismic receiver artefacts.

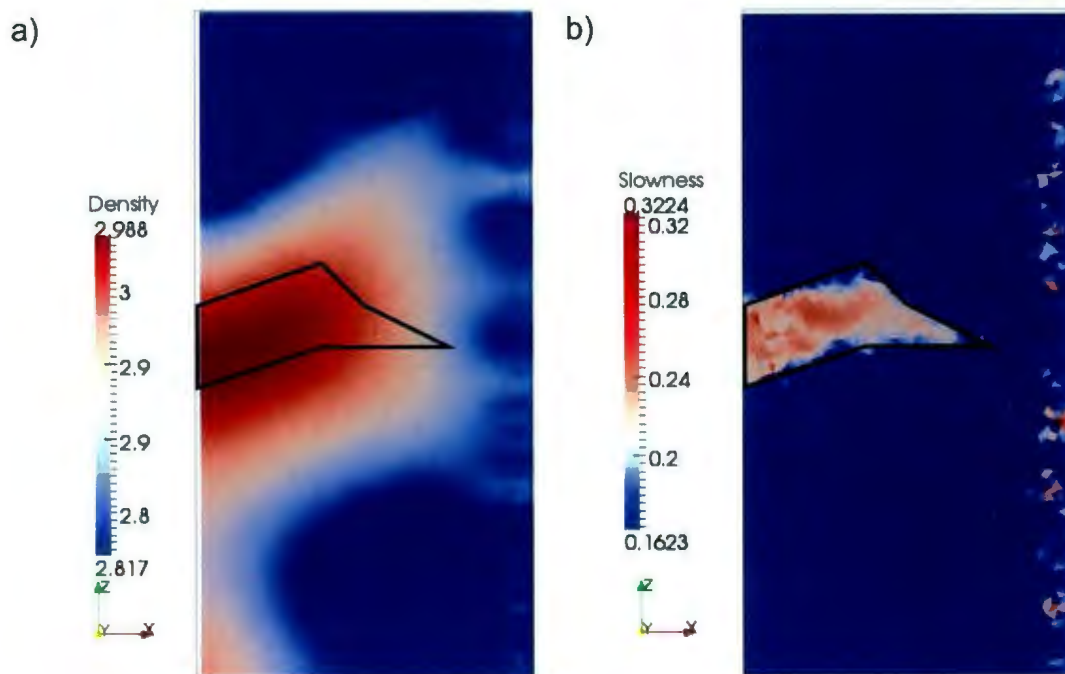


Fig. 4. 30: The resultant density (a) and slowness (b) models from the joint inversion of high noise sulphide-gneiss model synthetic data. The model is 200m across and 400m in depth and the black line outlines the location of the sulphide body in the synthetic models.

4.1.3.6 Low Noise Data from Borehole B Stations

Example 20: Gravity-Only Inversion

Table 4. 21: Summary of important input values for example 20.

Weighting	Type	Sensitivity
	Wbeta	1.0
	Wnorm	2.0
Target Misfits	Chifact	1.0
	Chitol	0.2
Bounds	Upper	5.817 g/cm ³
	Lower	2.817 g/cm ³

The gravity response predicted by this inversion has a similar topology and range of values as the synthetic gravity data provided to this inversion (Fig. 4. 31a). The normalized data residuals calculated from the synthetic and predicted data are fairly low (Fig. 4. 31b). This suggests that the inversion has been able to match the synthetic data fairly well. Many of the higher normalized data residuals are located towards the centre of the model near the depth of the sulphide body.

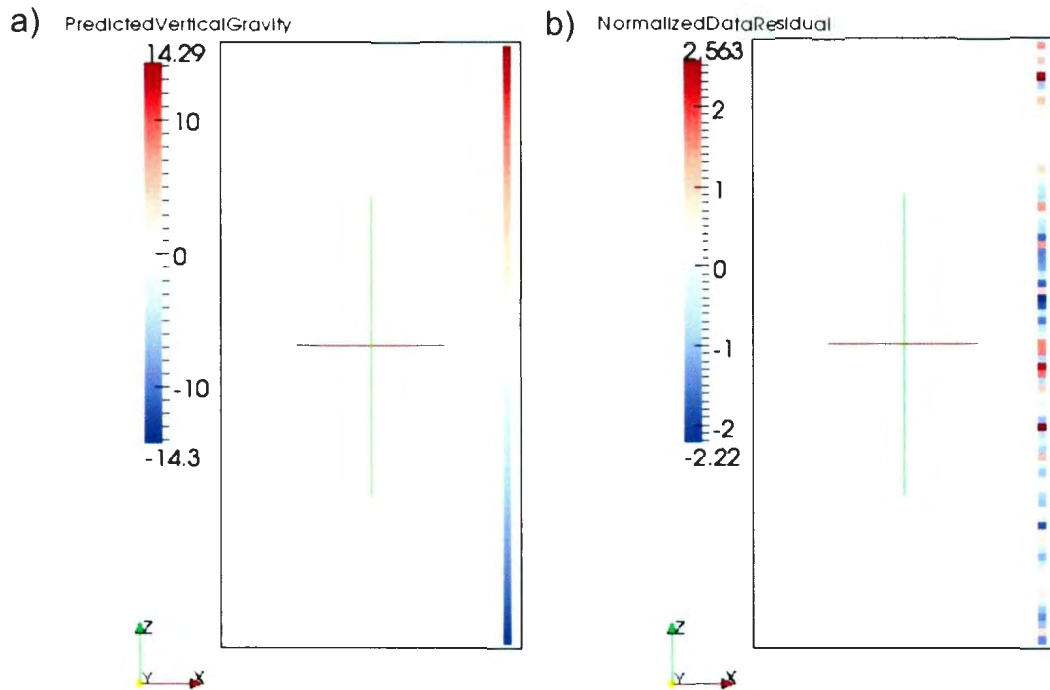


Fig. 4. 31: Predicted gravity data (a) and associated normalized data residuals (b) for the gravity-only inversion of low noise sulphide-gneiss model synthetic data.

The density model produced by the gravity-only inversion of data collected only in borehole B is large anomalous body. The inversion has located centre of the body well vertically and has estimated the lateral extent of the body well. The vertical extent of the body has not been well resolved (Fig. 4. 32). The density estimated for the body by the inversion has been significantly underestimated.

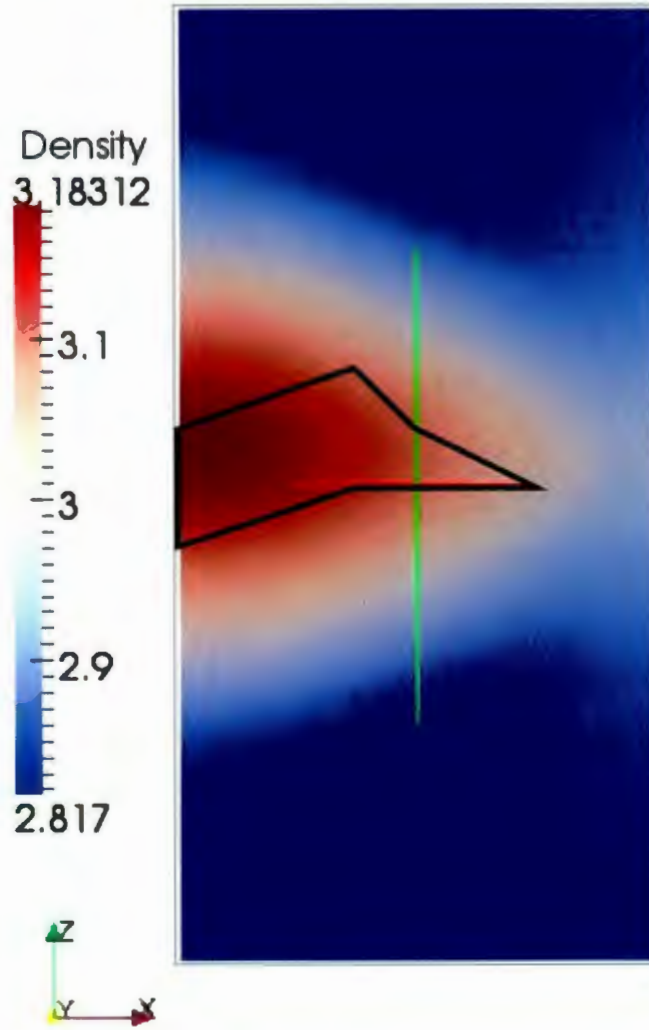


Fig. 4. 32: Resultant density model from the gravity-only inversion of low noise sulphide-gneiss model synthetic data. The model is 200m across and 400m in depth and the black line outlines the location of the sulphide body in the synthetic models.

Example 21: Joint Inversion

Table 4. 22: Summary of important input values for example 21.

Weighting	Type		Sensitivity
	wbeta		1.0
	wnorm		2.0
Target Misfits	Gravity	chifact	1.0
		chitol	0.2
	Travel-Time	chifact	1.0
		chitol	0.2
	Join inversion	alphaj	1.0
		jchitol	0.05
Bounds	Density	Upper	5.817 g/cm ³
		Lower	2.817 g/cm ³
	Slowness	Upper	1.1623 s/km
		Lower	0.1623 s/km
Similarity	Rhoe		10 ⁻⁴

The gravity response predicted by this inversion and the associated normalized data residuals are similar to those seen in Fig. 4. 31. The normalized data residual for this example range from -1.7 to 2.37. The seismic travel times predicted by this inversion and the associated normalised data residuals are similar to those seen in Fig. 4. 11. The normalized data residuals for this example range from -1 to 21.1.

The gravity model produced by this inversion has been able to located the sulphide body. However, it has not been able to determine the size and shape of the body and the density has been significantly underestimated. The slowness model produced by this inversion has been able to determine the location, size and shape of the sulphide body (Fig. 4. 33b). The inversion has slightly overestimated the slowness of the sulphide body and there are a moderate number of seismic receiver artefacts along the right edge of the model.

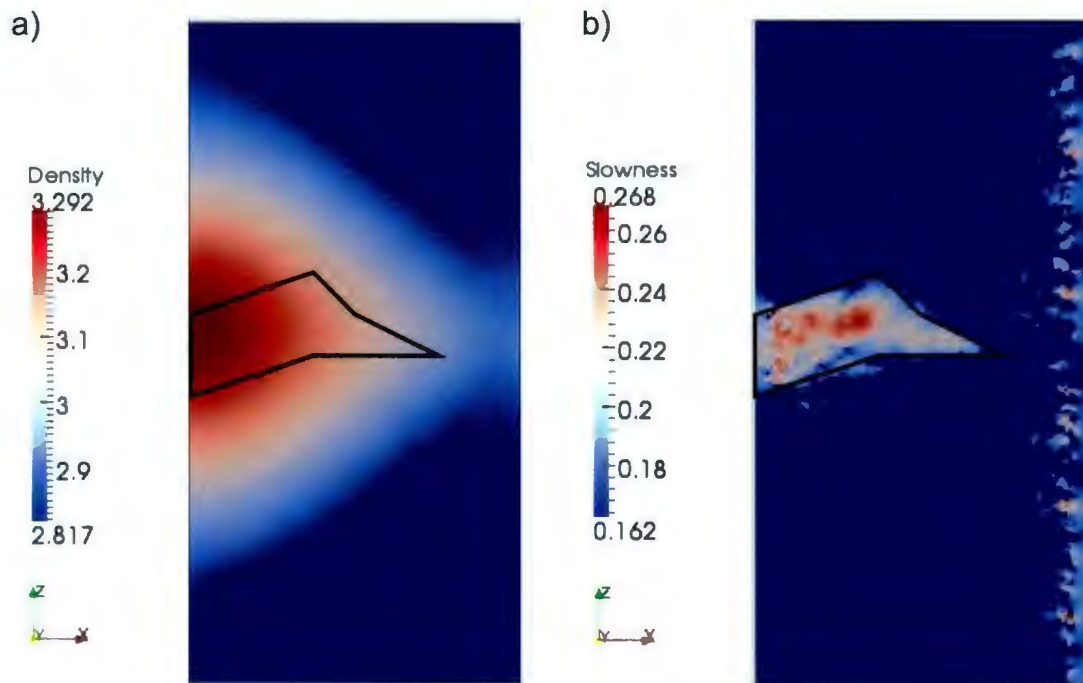


Fig. 4. 33: The resultant density (a) and slowness (b) models from the joint inversion of low noise sulphide-gneiss model synthetic data. The model is 200m across and 400m in depth and the black line outlines the location of the sulphide body in the synthetic models.

4.1.3.7 Moderate Noise Data from Stations in Boreholes A and B

Example 22: Gravity-Only Inversion

Table 4. 23: Summary of important input values for example 22.

Weighting	Type	Sensitivity
	Wbeta	1.0
	Wnorm	2.0
Target Misfits	Chifact	1.0
	Chitol	0.2
Bounds	Upper	5.817 g/cm ³
	Lower	2.817 g/cm ³

The gravity response predicted by this inversion is similar in range of values and topology to the synthetic gravity data provided to the inversion (Fig. 4. 34a). The normalized data residuals calculated from the synthetic and predicted data are relatively low (Fig. 4. 34b). This indicates that the inversion was able to match the synthetic data fairly well.

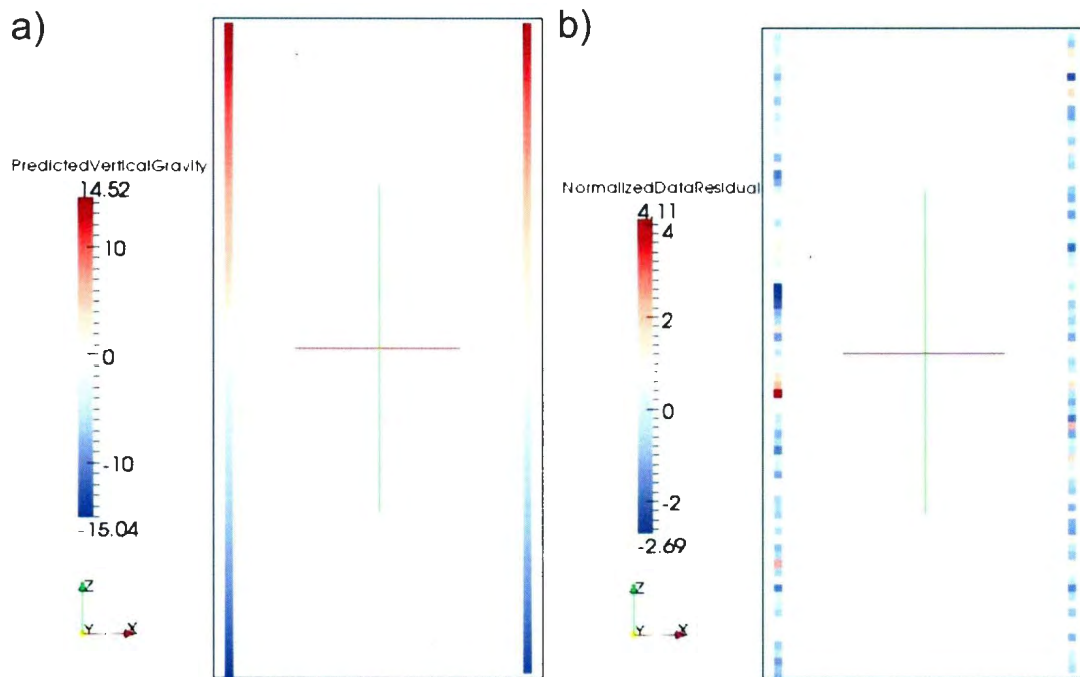


Fig. 4.34: Predicted gravity data (a) and associated normalized data residuals (b) for the joint inversion of moderate noise sulphide-gneiss model synthetic data.

The density model produced by the gravity-only inversion of moderate noise synthetic data from stations in boreholes A and B has determined the position and vertical extent of the sulphide body quite well (Fig. 4.35). The lateral extent, however, has not been resolved as well and the body has taken the shape of a slightly diffuse blob rather than the shape of the actual body. The inversion has overestimated the density at the centre of the sulphide body and underestimated its density at the edges; however, as a whole the estimation of density was fairly good. The inversion has correctly estimated the density of the gneissic background.

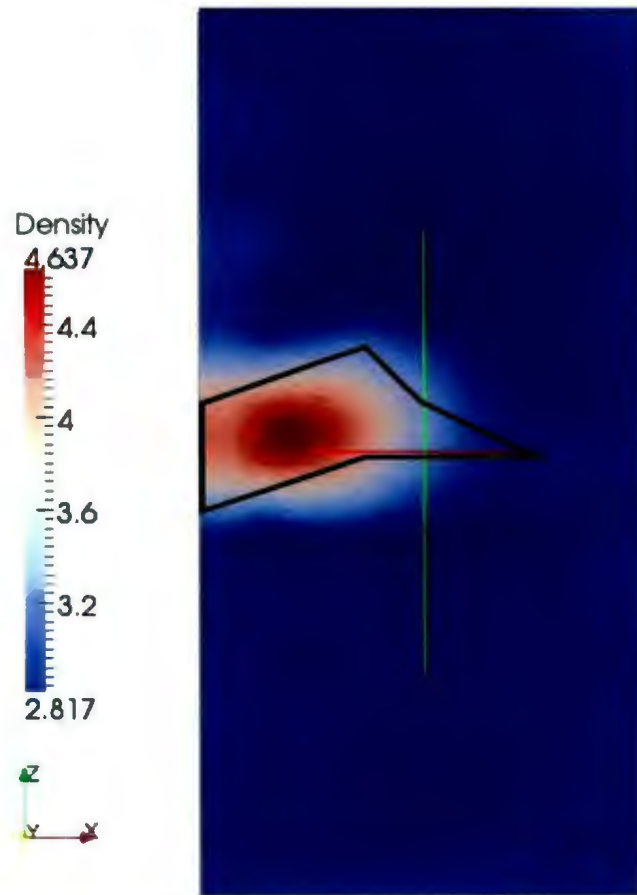


Fig. 4. 35: Resultant density model from the gravity-only inversion of moderate noise sulphide-gneiss model synthetic data. The model is 200m across and 400m in depth and the black line outlines the location of the sulphide body in the synthetic models.

Example 23: Joint Inversion

Table 4. 24: Summary of important input values for example 23.

Weighting	Type		Sensitivity
	wbeta		1.0
	wnorm		2.0
Target Misfits	Gravity	chifact	1.0
		chitol	0.2
	Travel-Time	chifact	1.0
		Chitol	0.2
	Joint inversion	Alphaj	1.0
		Jchitol	0.05
Bounds	Density	Upper	5.817 g/cm ³
		Lower	2.817 g/cm ³
	Slowness	Upper	1.1623 s/km
		Lower	0.1623 s/km
Similarity	Rhoe		1.0

The seismic travel times predicted by this inversion and the associated normalized data residuals are similar to those seen in Fig. 4. 1. The normalized data residuals for this inversion range from -3.9 to 5.39. The gravity data and associated normalized data

residuals are similar to those seen in Fig. 4. 34. The normalized data residuals for this example range from -4.2 to 5.55.

The joint inversion of moderate noise seismic travel time data and moderate noise gravity data collected only in the two boreholes reproduced the anomalous body well in the seismic half of the inversion (Fig. 4. 36a), however, although the inversion was able to locate the depth of the sulphide body fairly accurately it had difficulty positioning the dense body laterally in the gravity half of the inversion (Fig. 4. 36b).

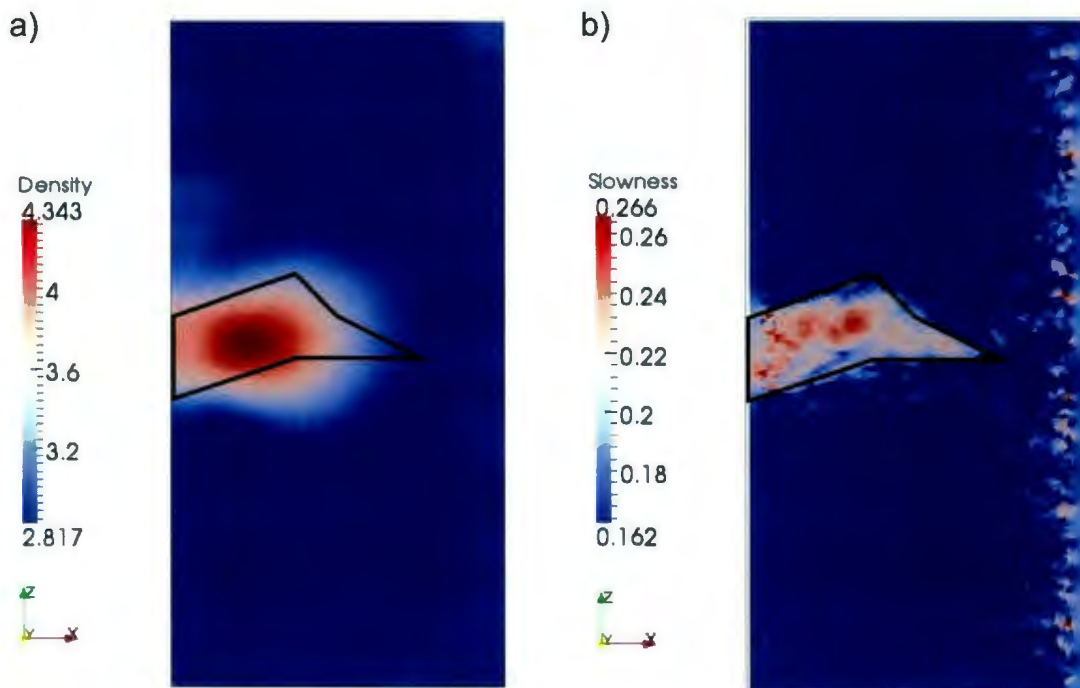


Fig. 4. 36: Resultant density (a) and slowness (b) models from the joint inversion of moderate noise sulphide-gneiss model synthetic data. The model is 200m across and 400m in depth and the black line outlines the location of the sulphide body in the synthetic models.

4.1.3.8 High Noise Data from Stations in Boreholes A and B

Example 24: Gravity-Only Inversion

Table 4. 25: Summary of important input values for example 24.

Weighting	Type	Sensitivity
	Wbeta	1.0
	Wnorm	2.0
Target Misfits	Chifact	0.5
	Chitol	0.1
Bounds	Upper	5.817 g/cm ³
	Lower	2.817 g/cm ³

The topology of the gravity response calculated for this inversion is similar to the synthetic data provided to the inversion. The range of the gravity response differ somewhat, however (Fig. 4. 37a). The low normalized data residuals calculated from the synthetic and predicted data indicate that the synthetic data has been adequately matched by the inversion (Fig. 4. 37b).

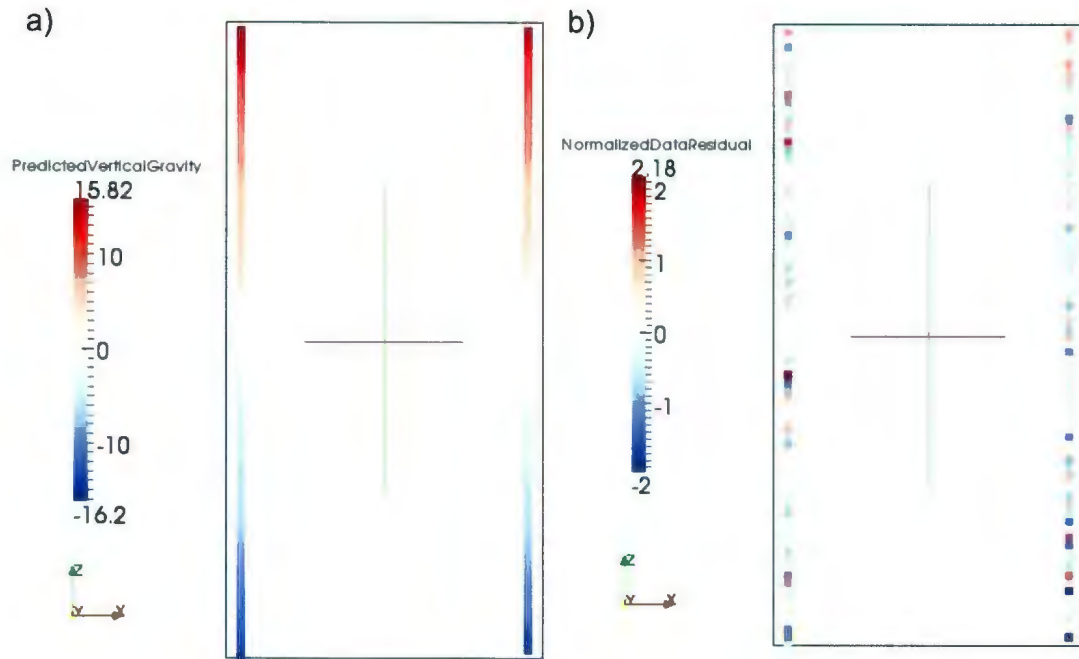


Fig. 4. 37: Predicted gravity data (a) and associated normalized data residuals (b) for the joint inversion of high noise sulphide-gneiss model synthetic data.

The density model produced by the gravity-only inversion of high noise sulphide-gneiss model data from gravity station in boreholes A and B has poorly modelled the sulphide body. The inversion has located the sulphide body vertically; however, the inversion has been unable to determine the size and shape of the sulphide body (Fig. 4. 38). There are many extraneous high density bodies erroneously produced by the inversion. The density of the sulphide body has been overestimated by the inversion, although, the density of the gneissic-background has been correctly estimated.

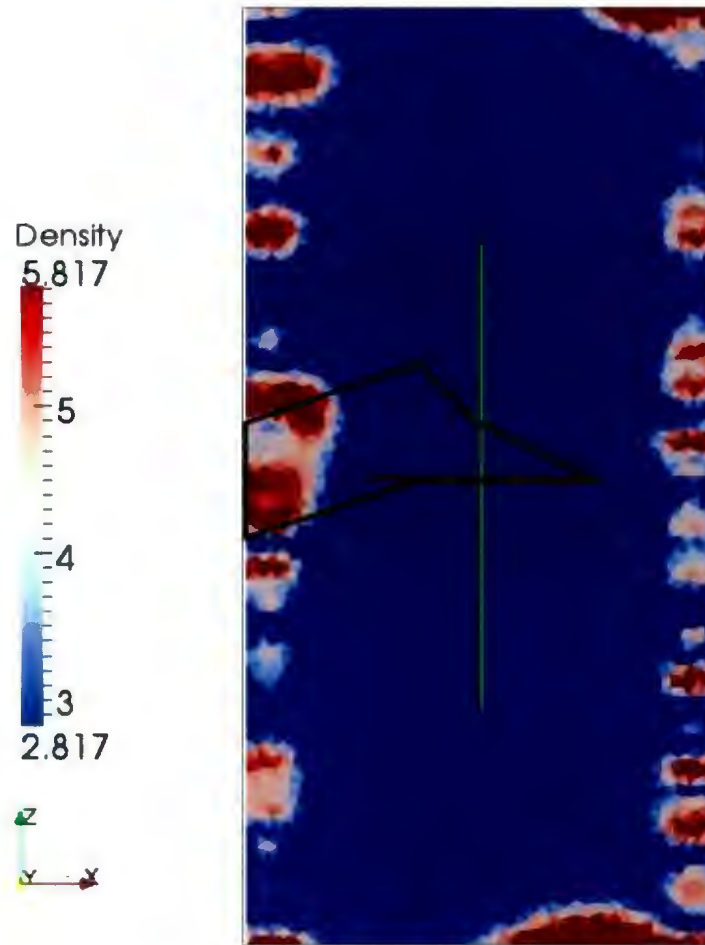


Fig. 4. 38: Resultant density model from the gravity-only inversion of high noise sulphide-gneiss model synthetic data. The model is 200m across and 400m in depth and the black line outlines the location of the sulphide body in the synthetic models.

Example 25: Joint Inversion

Table 4. 26: Summary of important input values for example 25.

Weighting	Type		Sensitivity
	wbeta		1.0
	wnorm		2.0
Target Misfits	Gravity	chifact	0.5
		chitol	0.1
	Travel-Time	chifact	1.0
		chitol	0.2
	Joint inversion	Alphaj	1.0
		jchitol	0.05
Bounds	Density	Upper	5.817 g/cm ³
		Lower	2.817 g/cm ³
	Slowness	Upper	1.1623 s/km
		Lower	0.1623 s/km
Similarity	Rhoe		1.0

The gravity response predicated by this inversion and the associated normalized data residuals are similar to those seen in Fig. 4. 34. The normalized data residuals for this example range from -2.2 to 3.35. The seismic travel time data predicted by this inversion and the associated normalized data residuals are similar to those seen in Fig. 4. 1. The normalized data residuals for this example range from -3.6 to 4.83.

The density model produced by this inversion has located and roughly approximated the size of the sulphide body (Fig. 4. 39a). The inversion has under estimated the density of the sulphide body. The slowness model produced by this inversion has located and determined the size and shaped of the sulphide body (Fig. 4. 39b). The slowness has been somewhat overestimated but there are very few extremely high slowness cells.

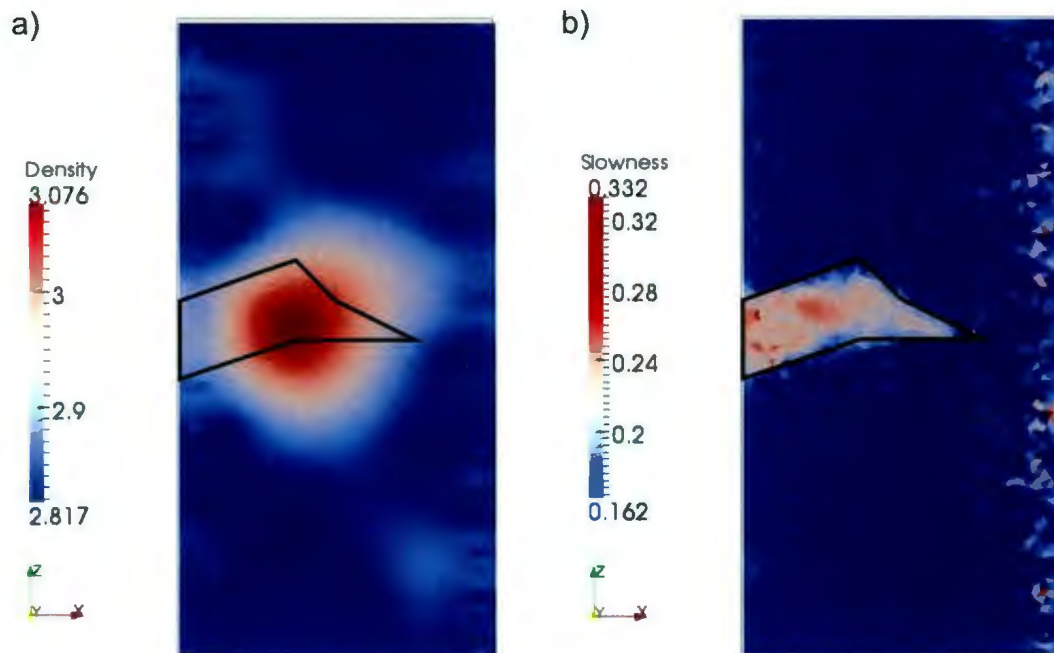


Fig. 4. 39: The resultant density (a) and slowness (b) models from the joint inversion of high noise sulphide-gneiss model synthetic data. The model is 200m across and 400m in depth and the black line outlines the location of the sulphide body in the synthetic models.

4.1.3.9 Low Noise Data from Stations in Boreholes A and B

These inversions look at the results acquired when gravity data was collected along a borehole which penetrates the sulphide body.

Example 26: Gravity Only Inversion:

In this example the results of a gravity-only inversion of low noise gravity data from borehole A and B gravity stations are presented.

Table 4. 27: Summary of important input values for example 27.

Weighting	Type	Sensitivity
	Wbeta	1.0
	Wnorm	2.0
Target Misfits	Chifact	1.0
	Chitol	0.2
Bounds	Upper	5.817 g/cm ³
	Lower	2.817 g/cm ³

The gravity response predicted by this inversion as well as the associated normalized data residual is similar to those seen in Fig. 4. 34. The normalized data residuals for this example range from -5.56 to 5.95.

The gravity model produced by this inversion has located the sulphide body and approaches the correct size; however it has not determined the shape of the body (Fig. 4. 40). The inversion has significantly overestimated the density at the centre of the body; however, the density at the edges is underestimated.

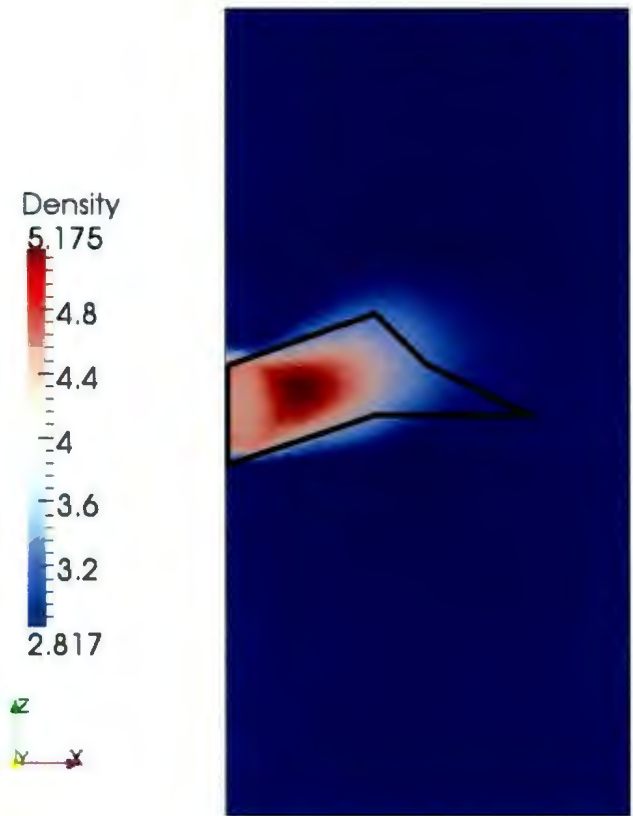


Fig. 4. 40: Resultant density mode from the gravity-only inversion of low noise sulphide-gneiss model synthetic data. The model is 200m across and 400m in depth and the black line outlines the location of the sulphide body in the synthetic models.

Example 27: Joint Inversion

In this example the results of a joint inversion of low noise seismic and borehole A and B gravity data are presented.

Table 4. 28: Summary of important input values for example 27.

Weighting	Type		Sensitivity
	wbeta		1.0
	wnorm		2.0
Target Misfits	Gravity	chifact	1.0
		chitol	0.2
	Travel-Time	chifact	1.0
		chitol	0.2
	Joint Inversion	Alphaj	1.0
		jchitol	0.05
Bounds	Density	Upper	5.817 g/cm ³
		Lower	2.817 g/cm ³
	Slowness	Upper	1.1623 s/km
		Lower	0.1623 s/km
Similarity	Rhoe		1.0

The gravity response predicted by this inversion is similar in topology and range to the clean synthetic data produced during the forward modelling of the sulphide-gneiss model

(Fig. 4. 41a). The normalized data residuals calculated from the predicted and low noise synthetic data are for the most part acceptably low, with the exception of a few very high values near the contacts between the sulphide and troctolite (Fig. 4. 41b). The slowness of the sulphide body has been estimated fairly well, although there are a few cells with overestimated slowness values. There are also a significant number of seismic receiver artefacts. The seismic travel times estimated for this inversion and the associated normalized data residuals are similar to those seen in Fig. 4. 11. The normalized data residuals for this example range from -16.25 to 20.18.

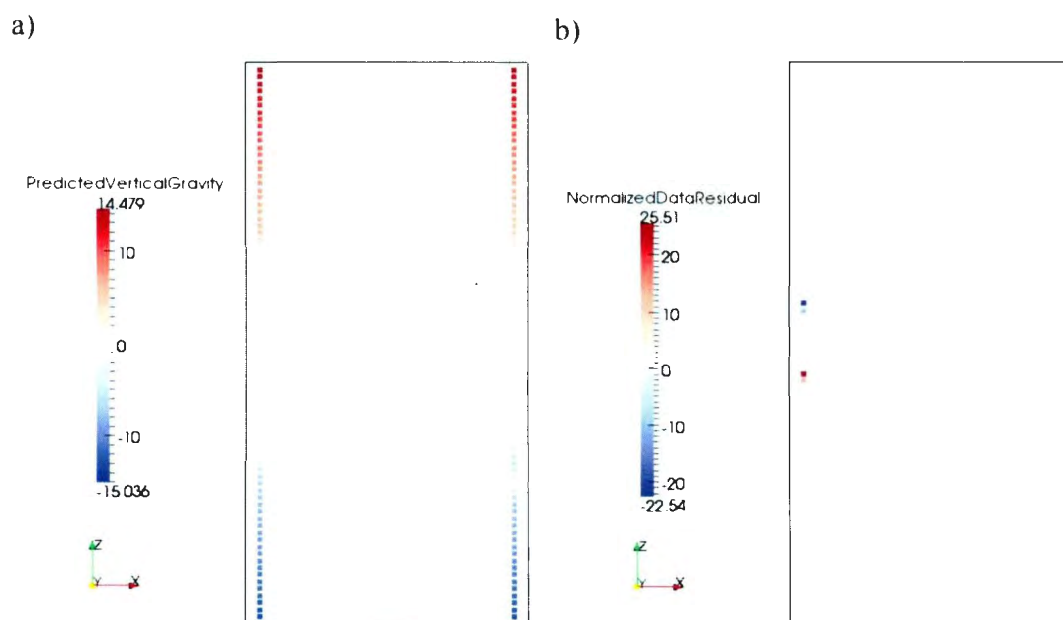


Fig. 4.41: Predicted gravity data (a) and associated normalized data residuals (b) for the gravity-only inversion of low noise sulphide-gneiss model synthetic data.

The density model produced by this inversion has located the sulphide body and correctly determined its approximate size (Fig. 4. 42a). The inversion was not able to determine the shape of the high density body and overestimated its density. The slowness models produced by this inversion have been able to locate and determine the size and shape of the sulphide body (Fig. 4. 42b).

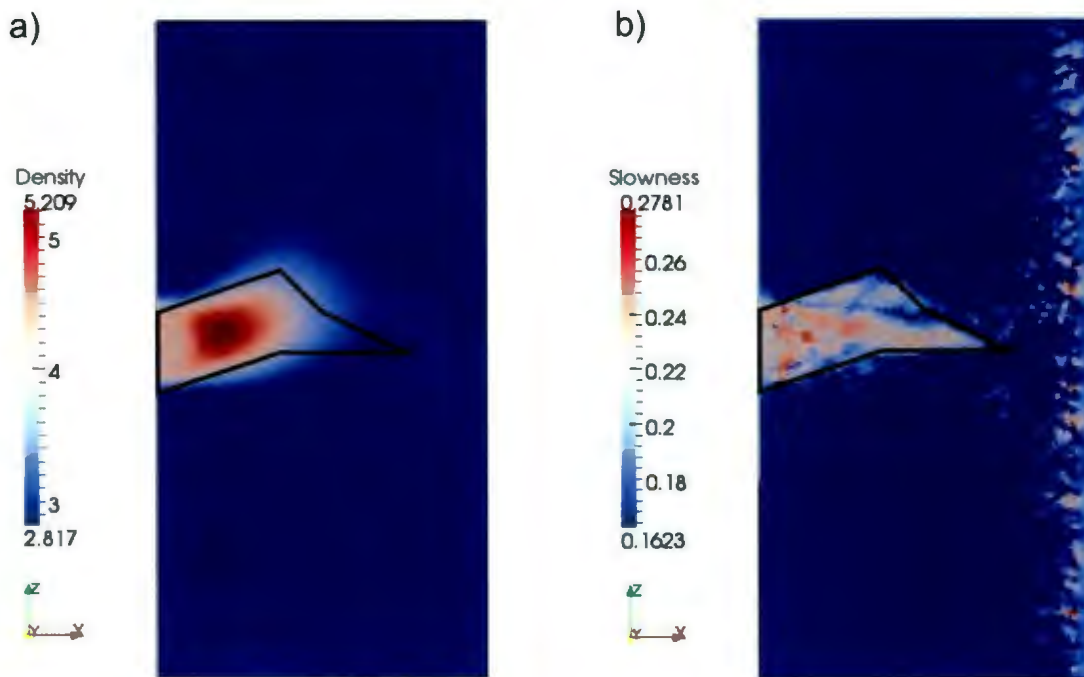


Fig. 4. 42: The resultant density (a) and slowness (b) models from the joint inversion of low noise sulphide-gneiss model synthetic data. The model is 200m across and 400m in depth and the black line outlines the location of the sulphide body in the synthetic models.

4.1.4 All Gravity Station Inversion Results

4.1.4.1 Moderate Noise Results

Example 28: Gravity Only Inversion

Table 4. 29: Summary of important input values for example 28.

Weighting	Type	Sensitivity
	Wbeta	1.0
	Wnorm	2.0
Target Misfits	Chifact	1.0
	Chitol	0.2
Bounds	Upper	5.817 g/cm ³
	Lower	2.817 g/cm ³

The gravity response predicted by this inversion is similar in range and topology to the clean synthetic data (Fig. 4. 43a). The normalized data residuals are relatively low with the most extreme values near the sulphide-troctolite contacts (Fig. 4. 43b). This suggests that the synthetic gravity data provided to the inversion was well matched.

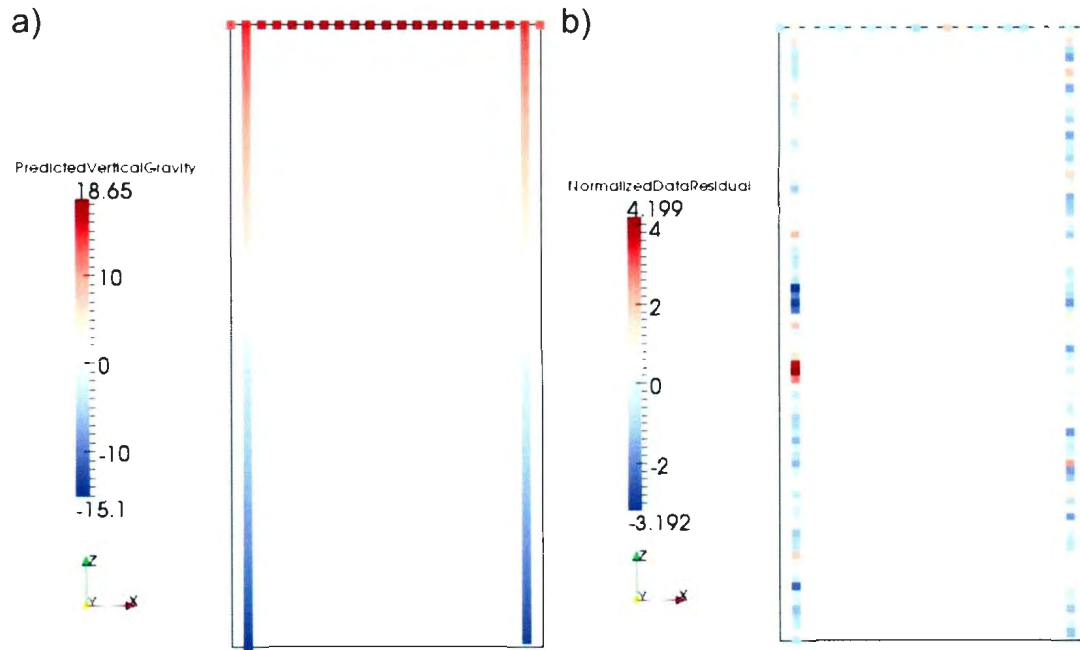


Fig. 4.43: Predicted gravity data (a) and associated normalized data residuals (b) for the gravity-only inversion of moderate noise sulphide-gneiss model synthetic data.

The density model produced from this inversion of gravity data has located and determined the size of the sulphide body (Fig. 4.44). It has not, however, determined the shape of the body and the density of the sulphide has been slightly over estimated at the centre and underestimated at the edges.

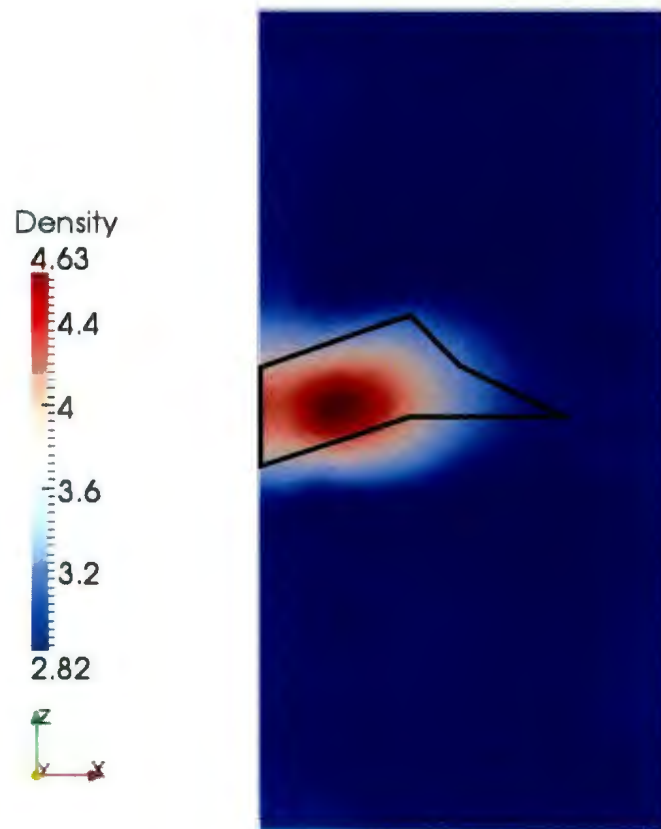


Fig. 4. 44: Resultant density model form the gravity-only inversion of moderate noise sulphide-gneiss model synthetic data collected at all borehole and surface gravity stations. The model is 200m across and 400m in depth and the black line outlines the location of the sulphide body in the synthetic models.

Example 29: Joint Inversion

Table 4. 30: Summary of important input values for example 29.

Weighting	Type		Sensitivity
	wbeta		1.0
	wnorm		2.0
Target Misfits	Gravity	chifact	1.0
		chitol	0.2
	Travel-Time	chifact	1.0
		chitol	0.2
	Joint Inversion	Alphaj	1.0
		Jchitol	0.05
Bounds	Density	Upper	5.817 g/cm ³
		Lower	2.817 g/cm ³
	Slowness	Upper	1.1623 s/km
		Lower	0.1623 s/km
Similarity	Rhoe		1.0

The seismic travel times predicted by this inversion and the associated normalized data residuals are similar to those seen in Fig. 4. 1. The seismic normalized data residuals for this example range from -4.3 to 5.8. The gravity response predicted by this inversion and its associated normalized data residuals are similar to those seen in Fig. The normalized data residuals in this example range from -3.55 to 2.47.

The joint inversion has located the slow, dense body well. As has been seen in previous examples the seismic half of the inversion has modelled the body very well in body shape, and location, although it has overestimated the slowness of the body (Fig. 4. 45a). The gravity half of the joint inversion has located the dense body well, however the inversion is quite diffuse and the shape of the body has not been well defined (Fig. 4. 45b). The density of the body has been underestimated by the inversion, whereas the background has been over estimated.

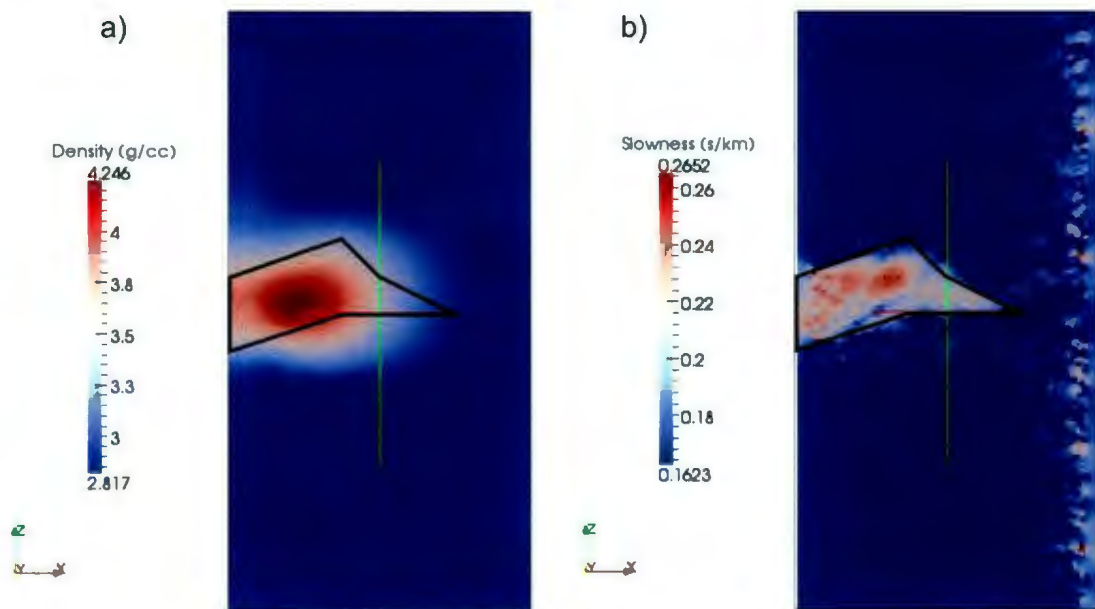


Fig. 4. 45: Resultant density (a) and slowness (b) models from the joint inversion of moderate noise sulphide-gneiss model synthetic data. The model is 200m across and 400m in depth and the black line outlines the location of the sulphide body in the synthetic models.

4.1.4.2 Low Noise Results

Example 30: Density Only

Table 4. 31: Summary of important input values for example 30.

Weighting	Type	Sensitivity
	Wbeta	1.0
	Wnorm	2.0
Target Misfits	Chifact	0.5
	Chitol	0.1
Bounds	Upper	5.817 g/cm ³
	Lower	2.817 g/cm ³

The gravity response predicted by this inversion and the associated normalized data residuals are similar to those seen in Fig. 4. 43. The normalized data residuals in this example range from -3.29 to 3.31.

The density model resultant from the gravity-only inversion of low noise sulphide-gneiss model synthetic data has correctly located the sulphide body. The body has been modelled with the correct vertical extent, however, the horizontal extend and shape of the model has not been accurately modelled. The density of the centre of the sulphide body has been overestimated; however, as a whole the density of the body has been estimated well. The density of the gneissic background has been estimated well.

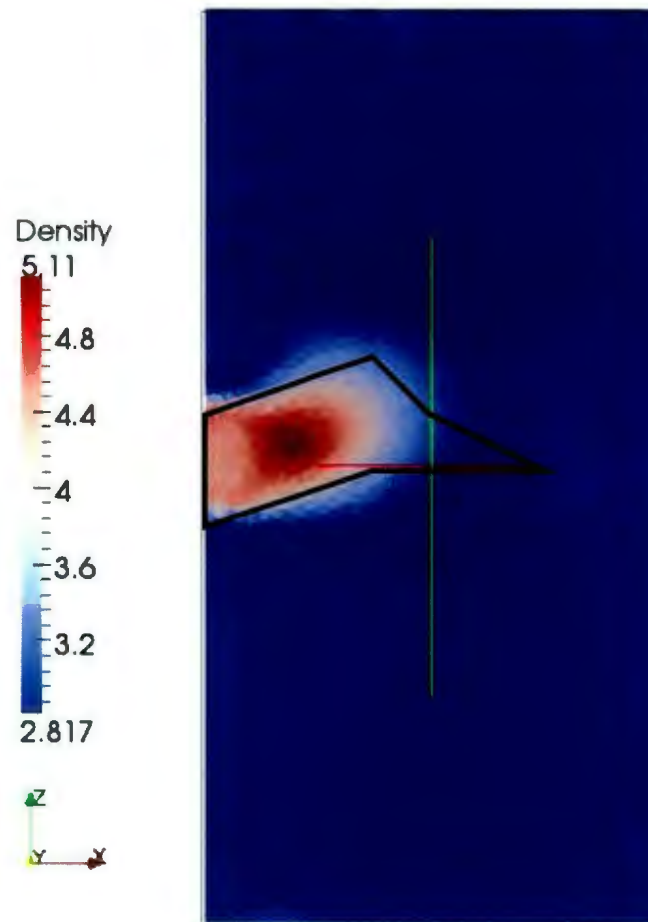


Fig. 4. 46: Resultant density model for the gravity-only inversion of low noise sulphide-gneiss model synthetic data. The model is 200m across and 400m in depth and the black line outlines the location of the sulphide body in the synthetic models.

Example 31: Joint Inversion

Table 4. 32: Summary of important input values for example 31.

Weighting	Type		Sensitivity
	wbeta		1.0
	wnorm		2.0
Target Misfits	Gravity	chifact	0.5
		chitol	0.1
	Travel-Time	chifact	1.0
		chitol	0.2
	Joint Inversion	Alphaj	1.0
		Chitol	0.05
Bounds	Density	Upper	5.817 g/cm ³
		Lower	2.817 g/cm ³
	Slowness	Upper	1.1623 s/km
		Lower	0.1623 s/km
Similarity	Rhoe		1.0

The seismic travel times predicted by this inversion and the associated normalized data residuals are similar to those seen in Fig. 4. 4. The seismic normalized data residuals for this example range from -23.52 to 36.01. The gravity response predicted by this inversion is similar in range and topology to the clean synthetic data produced from the sulphide-gneiss model. The normalized data residuals from this example have a large range with

some very high normalized data residuals which are concerning. However, as the very high values are spatially associated with the contacts between the sulphide body and the troctolite and as the rest of the normalized data residuals are quite low as such the inversion was probably able to match the synthetic data quite well.

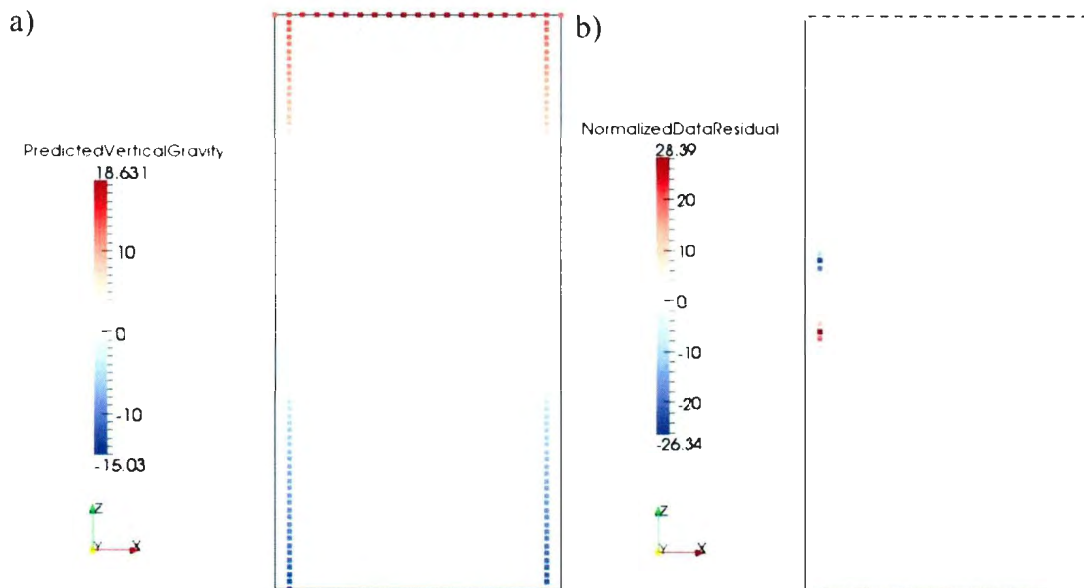


fig. 4. 47: Predicted gravity data (a) and associated normalized data residuals (b) for the joint inversion of low noise sulphide-gneiss model synthetic data.

The density model produced from this inversion has located and determined the size of the sulphide body (Fig. 4. 48a). The density of the sulphide has be overestimated at the centre and underestimated at the edges and the inversion has not been able to determine the shape of the sulphide body. The slowness model produced by this inversion has

located and determined the shape and size of the sulphide body (Fig. 4. 48b). The inversion has overestimated the density of the sulphide and produced a moderate number of seismic receiver artefacts.

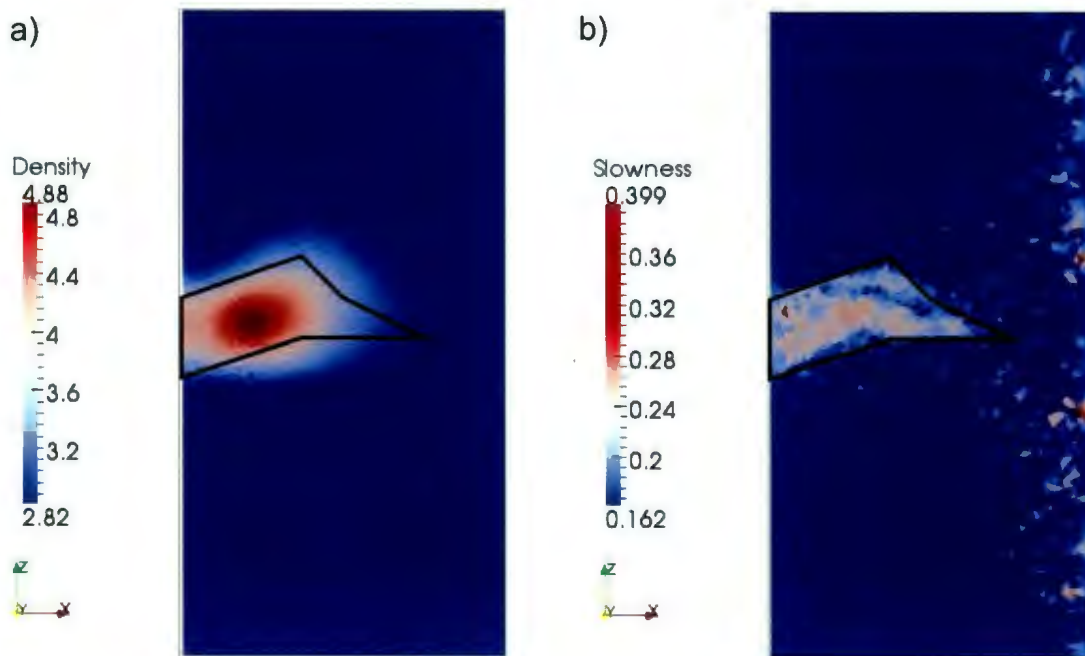


Fig. 4. 48: Resultant density (a) and slowness (b) model for the joint inversion of low noise sulphide-gneiss model synthetic data. The model is 200m across and 400m in depth and the black line outlines the location of the sulphide body in the synthetic models.

4.1.4.3 High Noise Results

Example 32: Gravity-Only Inversion

Table 4. 33: Summary of important input values for example 32.

Weighting	Type	Sensitivity
	Wbeta	1.0
	Wnorm	2.0
Target Misfits	Chifact	1.0
	Chitol	0.2
Bounds	Upper	5.817 g/cm ³
	Lower	2.817 g/cm ³

The gravity response predicted by this inversion and the associated normalized data residuals are similar to those Fig. 4. 43. The normalized data residuals for this example vary from -3.42 to 2.4.

The density model produced by the gravity-only inversion of high noise synthetic data has located and estimated the vertical and lateral extent of the sulphide body well. The shape of the body, however, has not been well modelled (Fig. 4. 49). The density of the sulphide body has been underestimated by the inversion, although the density of the gneissic background has been estimated well.

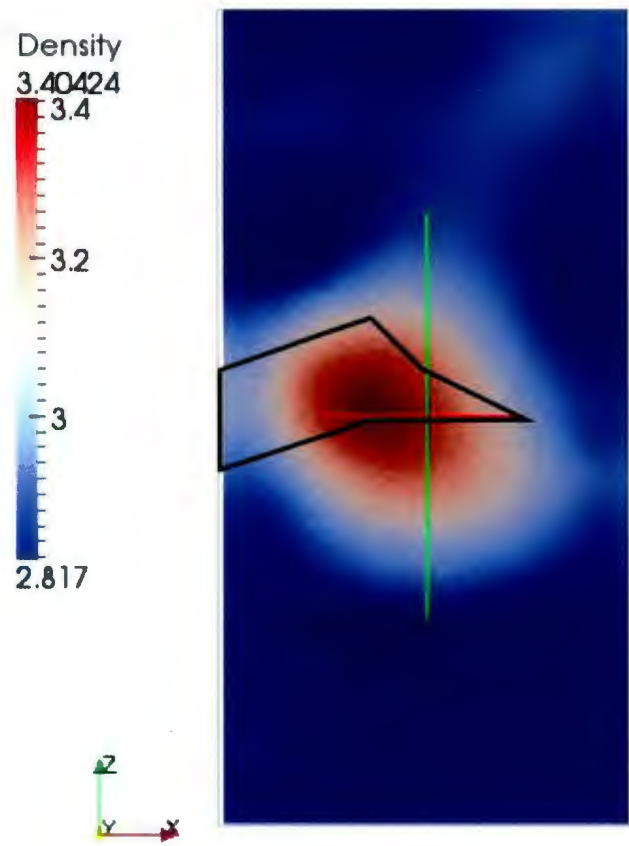


Fig. 4. 49: Resultant density model from the gravity-only inversion of high noise sulphide-gneiss model synthetic data. The model is 200m across and 400m in depth and the black line outlines the location of the sulphide body in the synthetic models.

Example 33: Joint Inversion

Table 4. 34: Summary of important input values for example 33.

Weighting	Type		Sensitivity
	wbeta		1.0
	wnorm		2.0
Target Misfits	Gravity	chifact	1.0
		chitol	0.2
	Travel-Time	chifact	1.0
		chitol	0.2
	Joint Inversion	Alphaj	1.0
		jchitol	0.05
Bounds	Density	Upper	5.817
		Lower	2.817
	Slowness	Upper	1.1623 s/km
		Lower	0.1623 s/km
Similarity	Rhoe		1.0

The gravity response predicted by this inversion and associated normalized data residuals are similar to those seen in Fig. 4. 43. The normalized data residuals for this example range from -3.76 to 2.64.

The density model achieved by this inversion has located and determined the size and shape of the sulphide body (Fig. 4. 50a). The density of the sulphide body has been significantly underestimated. The slowness model produced by this inversion has been able to locate and determine size and shape of the sulphide body (Fig. 4. 50b). The inversion has overestimated the slowness of some cells; however, for the most part the slowness of the sulphide has been well determined. The background slowness has been well estimated, however, there are a large number of seismic receiver artefacts.

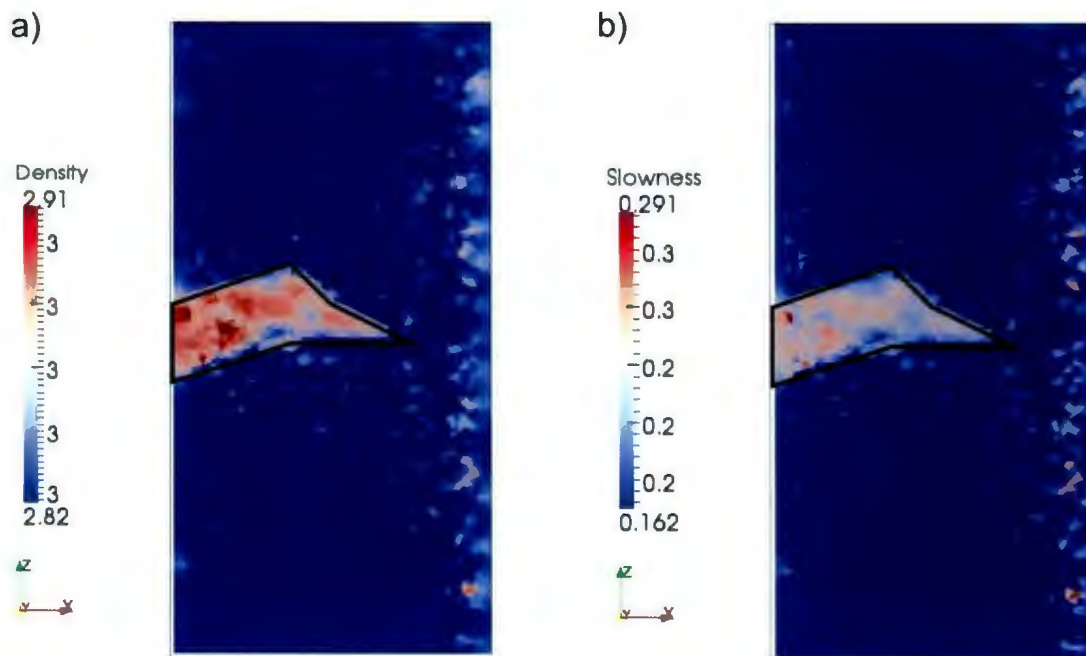


Fig. 4. 50: Resultant density (a) and slowness (b) model for the joint inversion of high noise sulphide-gneiss model synthetic data. The model is 200m across and 400m in depth and the black line outlines the location of the sulphide body in the synthetic models.

4.2 Mixed Model Results

The mixed model inversion is a test of the code's ability to model more than 2 geological units. The initial plan for the mixed model tests was to run the same battery of tests as were carried out for the sulphide-gneiss model. However, based on the results from the sulphide-gneiss inversion only moderate noise data was used for the mixed model tests. This decision was made based on observation of the relationship between the noise in the data, the model quality, and the code's ability to reach convergence.

4.2.1 Example 34: Seismic Only Inversion Results

Table 4. 35: Summary of important input values for example 34.

Target Misfits	Chifact	1.0
	Chitol	0.2
Bounds	Upper	1.1623 s/km
	Lower	0.1623 s/km

The seismic travel times predicted by this inversion (Fig. 4. 51a) are similar in range and topology to the clean synthetic data calculated for the mixed model (fig. 3.10a). The normalized data residuals calculated from the predicted and moderate noise synthetic data are relatively small (Fig. 4. 51b). Most of the normalized data residuals are close to or greater than zero. The large negative normalized data residuals seem to be associated with specific sources as they form vertical blue stripes.

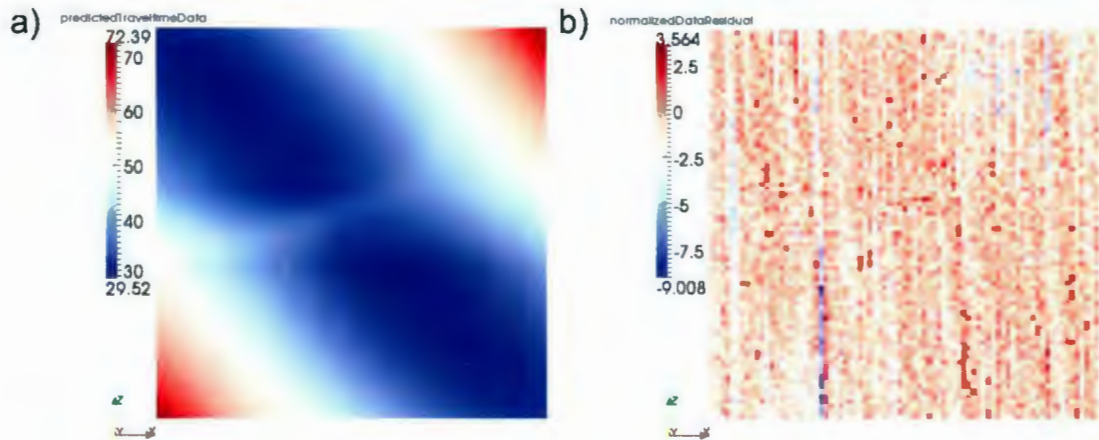


Fig. 4. 51: Predicted seismic travel times (a) and associated normalized data residuals (b) for the seismic portion of the joint inversion of Mixed model synthetic data. The horizontal axis of both plots is the source number and the vertical axis is the receiver number (Fig 3.10).

The slowness model produced by this inversion (Fig. 4. 52) shows that the sulphide body has been located and the size and shape of the body has been fairly well determined. However, the slowness of the sulphide has been moderately overestimated by the inversion. There is no clear evidence from the slowness model that the inversion has been able to image the troctolite body. The background of the model shows an increase in noise when compared to the moderate noise sulphide-gneiss model results (Fig. 4. 2). This may be a consequence of the inversion attempting to match the weak troctolite signal.

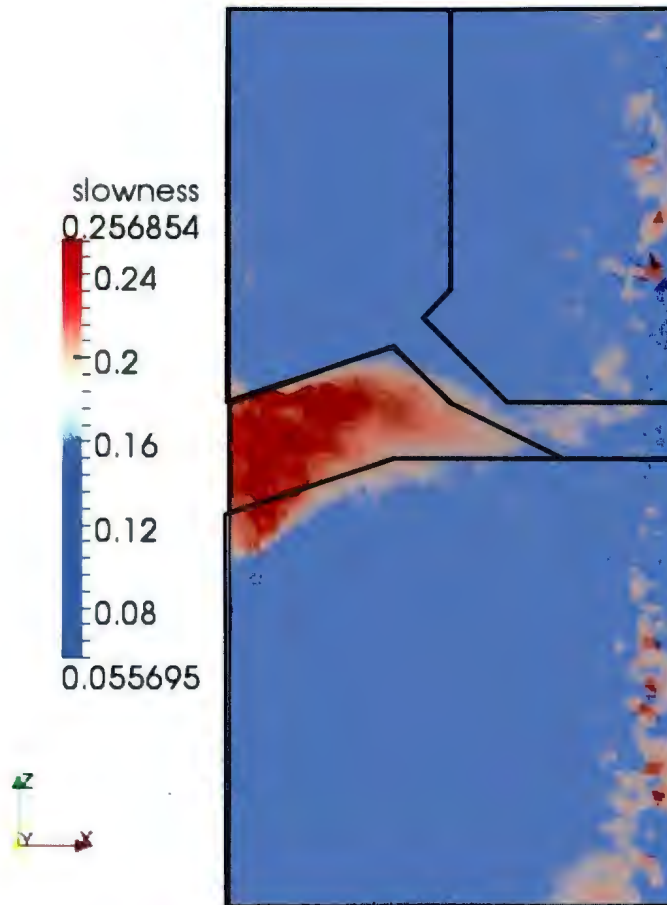


Fig. 4. 52: Seismic-Only inversion result from the inversion of mixed model synthetic data. The model is 200m across and 400m in depth. The black line outlines the location of the sulphide and troctolite bodies in the synthetic models.

4.2.2 Surface Gravity Stations Only

Example 35: Gravity-Only Inversions

Table 4. 36: Summary of important input values for example 35.

Weighting	Type	Sensitivity
	Wbeta	1.0
	Wnorm	2.0
Target Misfits	Chifact	1.0
	Chitol	0.2
Bounds	Upper	5.817 g/cm ³
	Lower	2.817 g/cm ³

The gravity response predicted by this inversion (Fig. 4. 53a) is similar in range and topology to the clean synthetic data produced during forward modelling of the mixed model (Fig. 3.8). The normalized data residuals (Fig. 4.53b) calculated from the predicted data and the moderate noise synthetic data are quite low. Most of the normalized data residuals greater than zero occur at gravity stations to the right and most to the left are below zero.

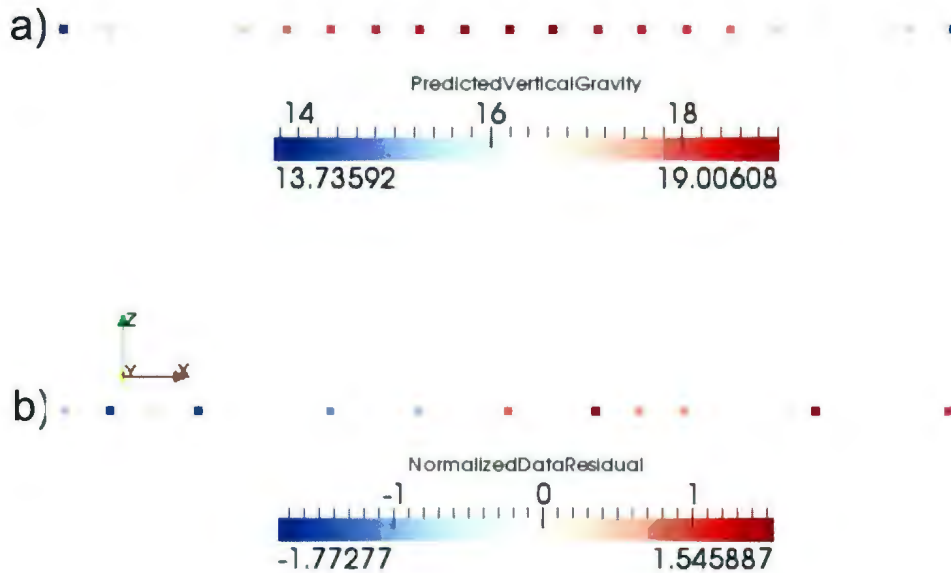


Fig. 4. 53: Predicted gravity data (a) and associated normalized data residuals (b) for the joint inversion of Mixed model synthetic data.

The density model produced by this inversion has not located the sulphide or troctolite bodies (Fig. 4. 54). The distribution of dense material indicates a determination that the anomalous material is located to the left side of the model and that the less dense anomalous material is closer to surface.

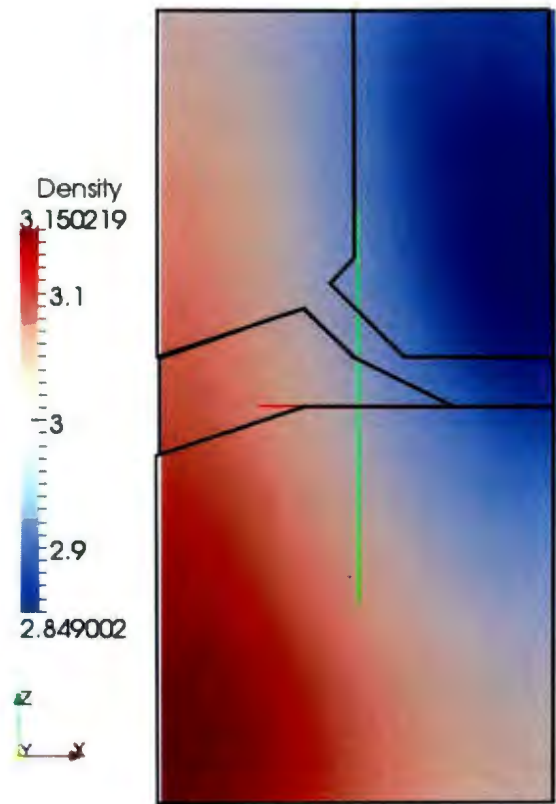


Fig. 4. 54 Resultant density model from the gravity-only inversion of Mixed model synthetic data. The model is 200m across and 400m in depth. The black line outlines the location of the sulphide and troctolite bodies in the synthetic models.

Example 36: Joint Inversion:

Table 4. 37: Summary of important input values for example 36.

Weighting	Type		Sensitivity
	wbeta		1.0
	wnorm		1.0
Target Misfits	Gravity	chifact	0.5
		chitol	0.1
	Travel-Time	chifact	1.0
		chitol	0.2
	Joint Inversion	alphaj	1.0
		Jchitol	0.05
Bounds	Density	Upper	5.817 g/cm ³
		Lower	2.817 g/cm ³
	Slowness	Upper	1.1623 s/km
		Lower	0.1623 s/km
Similarity	Rhoe		1.0

The gravity response predicted by this inversion and the associated normalized data residuals are similar to those seen in Fig. 4. 53. The normalized data residuals for this example range from -1.43 to 1.34. The seismic travel times predicted by this inversion (Fig. 4. a) are similar in range and topology to the clean synthetic data produced from forward modelling of the mixed model (Fig. 3.10a). The normalized data residuals

calculated from the predicted and moderate noise synthetic data are relatively low (Fig. 4. b) and show no particular spatial distribution.

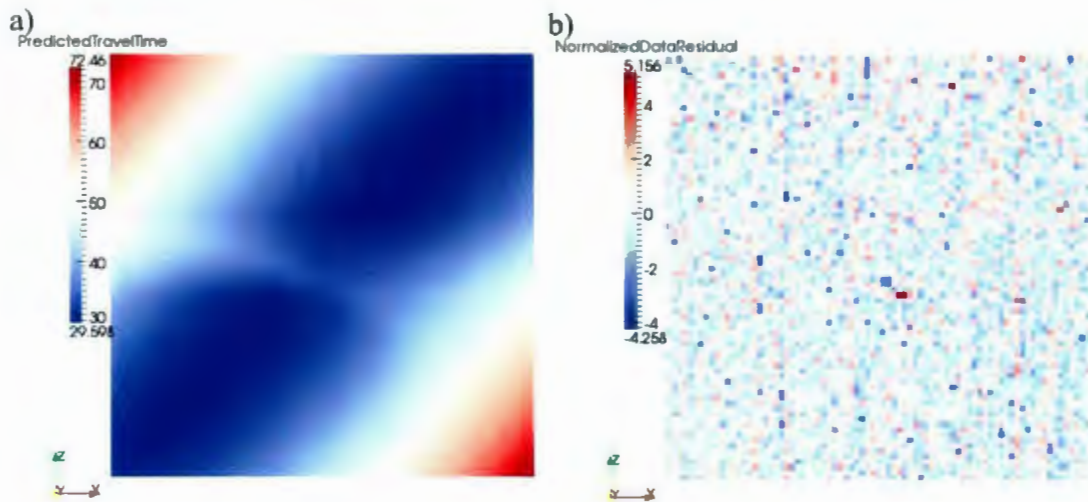


Fig. 4. 55: Predicted seismic travel times (a) and associated normalized data residuals (b) for the seismic portion of the joint inversion of Mixed model synthetic data. The horizontal axis of both plots is the source number and the vertical axis is the receiver number (Fig 3.10).

The gravity model produced by this inversion (Fig. 4. 56a) has located the dense material on the correct side of the model and the width of the anomaly is consistent with the width of the troctolite body. However, it has not been able to determine the location, size or shape of the sulphide body nor has it modelled the troctolite feeder pipe. The slowness model produced by this inversion (Fig. 4. 56b) has located and roughly determined the size and shape of the sulphide body, although it has not determined the location of the lower edge of the body as well as it has the upper edge. There is some indication that the inversion has begun to image the troctolite feeder pipe and the left edge of the troctolite

body; however, such conclusions would be difficult to draw had the correct model not been known.

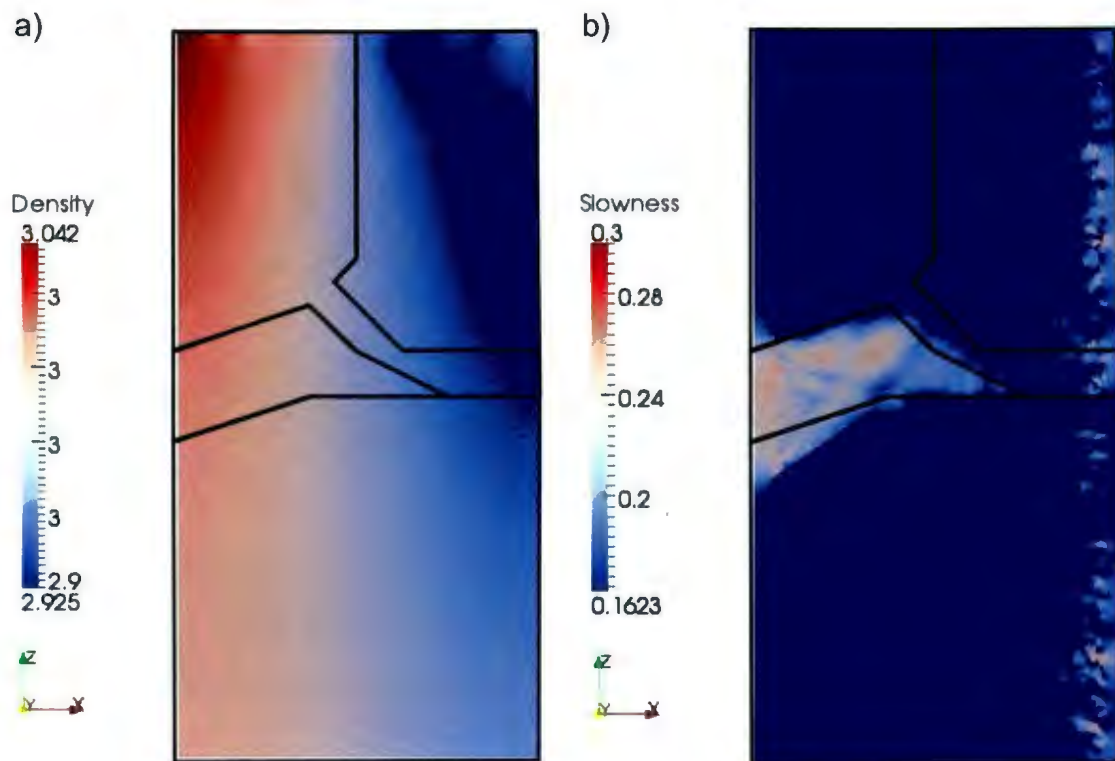


Fig. 4. 56: Resultant slowness (a) and density (b) model for the joint inversion of Mixed model synthetic data. The models are 200m across and 400m in depth. The black line outlines the location of the sulphide and troctolite bodies in the synthetic models.

4.2.3 Borehole A Gravity Stations Only

Example 37: Gravity-Only Inversions

Table 4. 38: Summary of important input values for example 37.

Weighting	Type	Sensitivity
	Wbeta	1.0
	Wnorm	2.0
Target Misfits	Chifact	1.0
	Chitol	0.2
Bounds	Upper	5.817 g/cm ³
	Lower	2.817 g/cm ³

The gravity response predicted by this inversion (Fig. 4. 57a) is similar in range and topology to the clean synthetic data produced from forward modelling of the mixed model (Fig. 4. 6). The normalized data residuals calculated from the predicted and moderate noise synthetic data (Fig. 4. 57b) are reasonably low and don't show any particular spatial orientation.

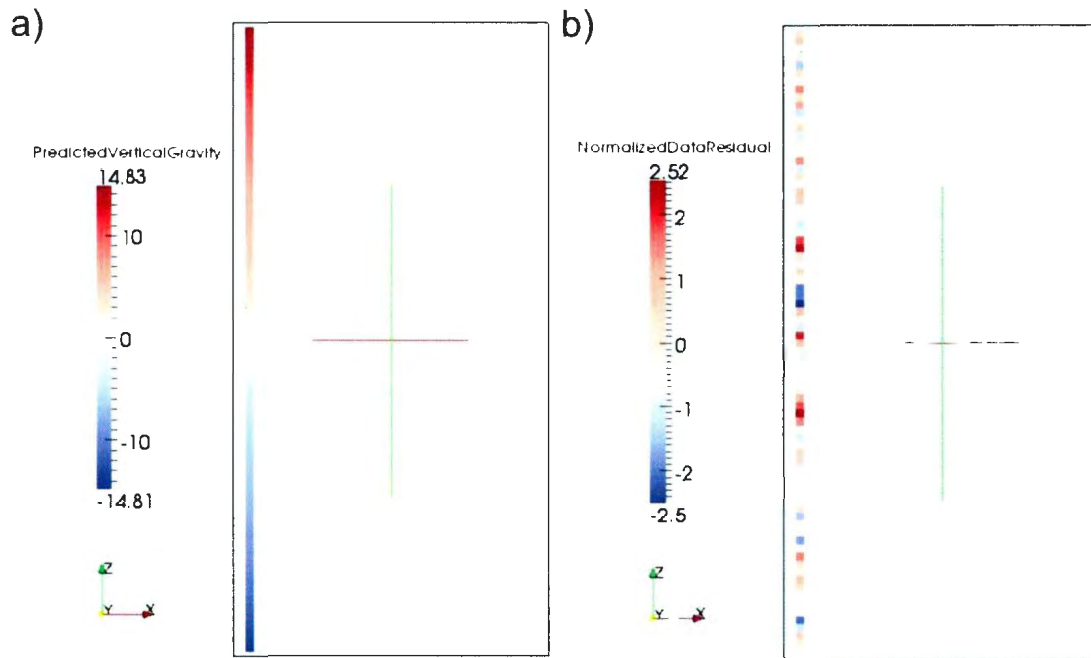


Fig. 4. 57: Predicted gravity data (a) and associated normalized data residuals (b) for the joint inversion of moderate noise sulphide-gneiss model synthetic data.

The density model produced by this inversion (Fig. 4. 58) has located and approximately determined the size of the sulphide body. The shape of the sulphide has not been determined, however. The presence of a small amount of material with slightly higher than background density at the surface and along the left side of the model is evidence that the inversion was attempting to match the weak troctolite signal. The density of the sulphide was on average well determined; however, the density of the cells at the top of the model is slightly higher than that of the troctolite.

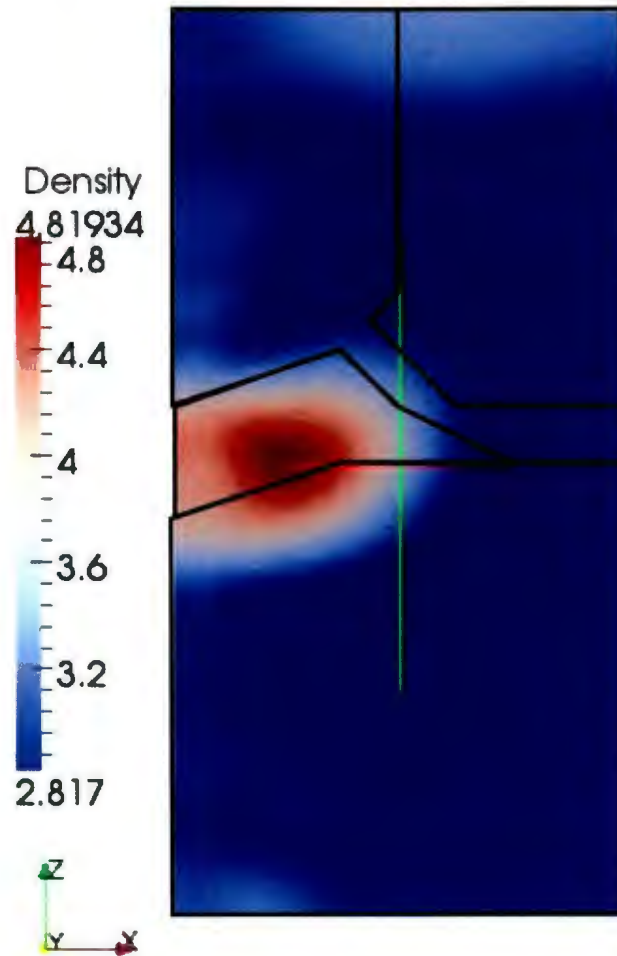


Fig. 4. 58 Resultant density model from the gravity-only inversion of the moderate noise Mixed model synthetic data. The model is 200m across and 400m in depth. The black line outlines the location of the sulphide and troctolite bodies in the synthetic models.

Example 38: Joint Inversion

Table 4. 39: Summary of important input values for example 38.

Weighting	Type		Sensitivity
	wbeta		1.0
	wnorm		2.0
Target Misfits	Gravity	chifact	1.0
		chitol	0.2
	Travel-Time	chifact	1.0
		chitol	0.2
	Joint Inversion	alphaj	1.0
		jchitol	0.05
Bounds	Density	Upper	5.817 g/cm ³
		Lower	2.817 g/cm ³
	Slowness	Upper	1.1623 s/km
		Lower	0.1623 s/km
Similarity	Rhoe		1.0

The gravity response predicted by this inversion and the associated normalized data residuals are similar to those seen in Fig. 4. 58. The normalized data residuals for this example range from -5.31 to 5.18. The seismic travel times predicted by this inversion and the associated normalized data residuals are similar to those in Fig. 4. 56. The normalized data residuals for this example range from -4.52 to 5.44.

The density model produced by this inversion (Fig. 4. 59a) has located the sulphide body fairly well. It has slightly overestimated the density of the body and although the upper edge of the body has been well modelled the lower edge has not. The dragged out nature of the right edge may be evidence that the inversion was trying to model part of the troctolite. There is also some anomalous material of much lower density than the troctolite near surface. However, it is not near the location of the troctolite.

The slowness model produce by this inversion (Fig. 4. 59b) has located and determined the approximated size and shape of the sulphide body. The location of the lower edge of the body is not as well determined as the upper edge. There is some evidence that the feeder pipe has been located. Although there are some higher slowness cells above the sulphide body it is a very tenuous modelling of the troctolite and if the experimenter didn't know the true model it is unlikely they would have made such an interpretation, particularly in light of their proximity to the seismic sources. The slowness of the sulphide has been well estimated by this inversion.

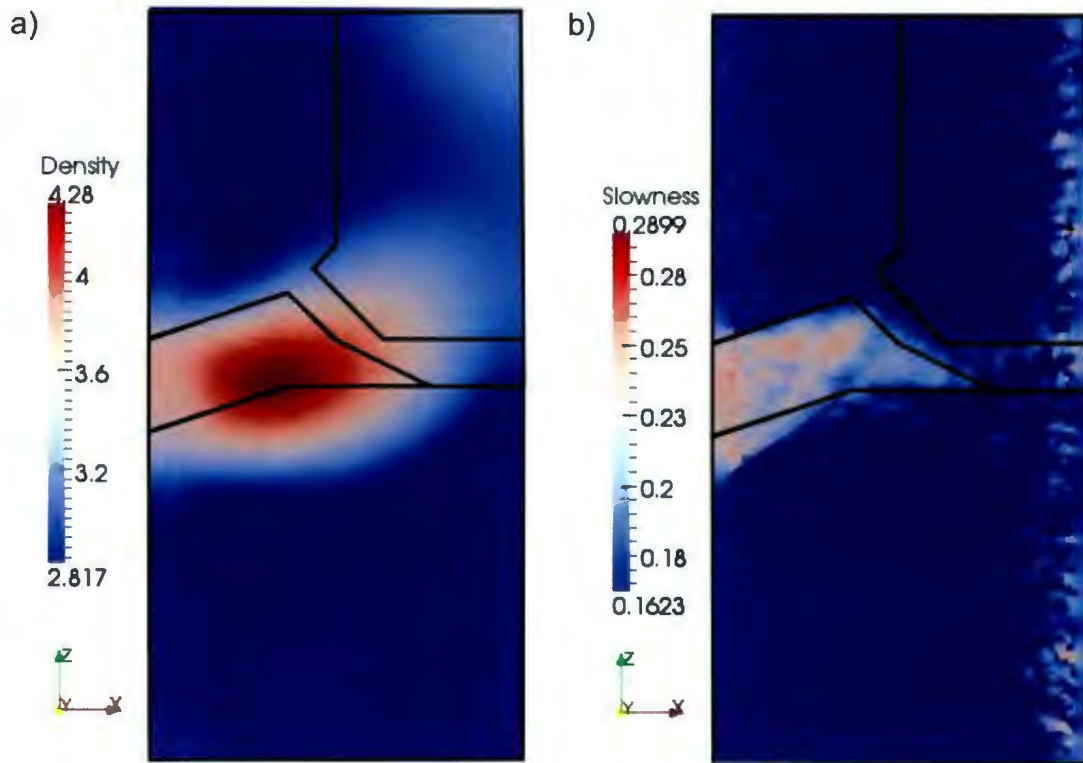


Fig. 4. 59: Resultant slowness (a) and density (b) model for the joint inversion of Mixed model synthetic data. The models are 200m across and 400m in depth. The black line outlines the location of the sulphide and troctolite bodies in the synthetic models.

4.2.4 Borehole B Gravity Stations Only

Example 39: Gravity-Only Inversions

Table 4. 40: Summary of important input values for example 39.

Weighting	Type	Sensitivity
	Wbeta	1.0
	Wnorm	2.0
Target Misfits	Chifact	1.0
	Chitol	0.2
Bounds	Upper	5.817 g/cm ³
	Lower	2.817 g/cm ³

The topology and range of the gravity response predicated by this inversion (Fig. 4. 60a) are similar to the clean synthetic data produced during forward modelling of the mixed model (fig.3.8). The normalized data residuals from the predicted and moderate noise synthetic data are relatively low (Fig. 4. 60b). There is no apparent pattern to the spatial distribution of normalized data residual values.

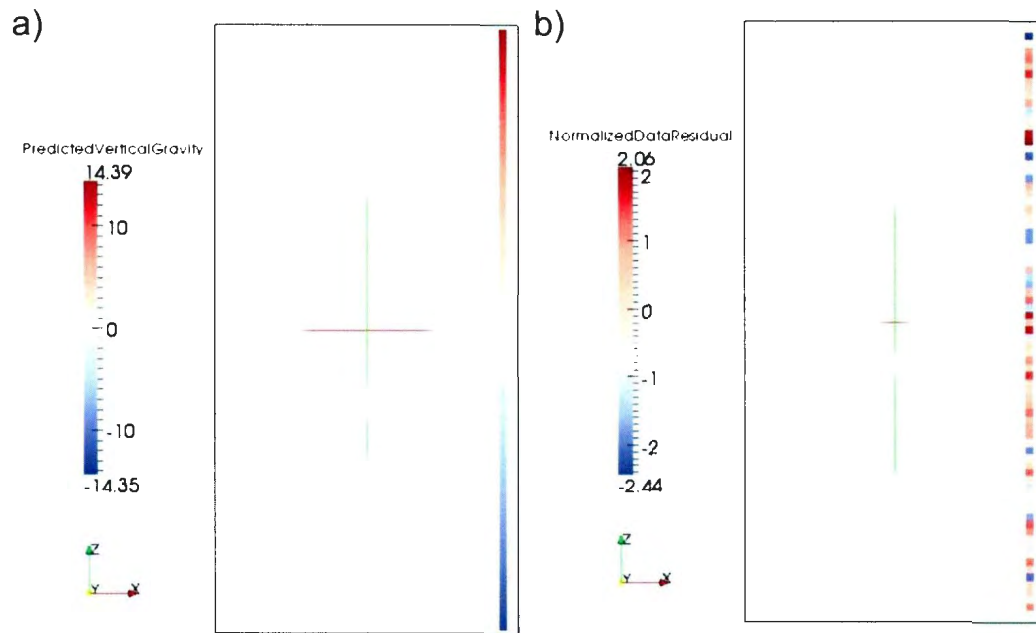


Fig. 4. 60: Predicted gravity data (a) and associated normalized data residuals (b) for the joint inversion of Mixed model synthetic data.

The density model produced by this inversion has located the sulphide body (Fig. 4. 61); however, it has not determined the size or shape of the body correctly. There is no indication that the main troctolite body has been imaged. However, the halo around the troctolite body is greater than that seen in the same sulphide-gneiss model inversion (Fig. 4. 27). This suggests that the inversion may be attempting to model the feeder pipe.

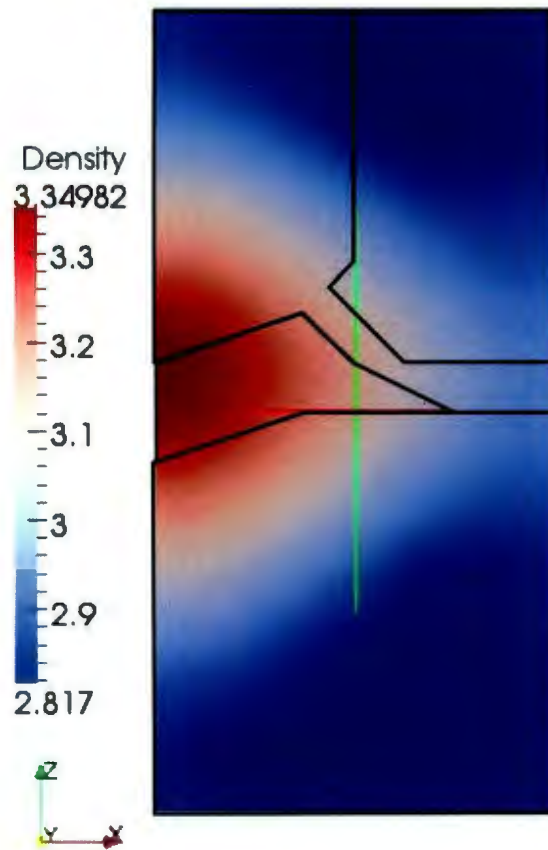


Fig. 4. 61 Resultant density model from the gravity-only inversion of the Mixed model synthetic data. The model is 200m across and 400m in depth. The black line outlines the location of the sulphide and troctolite bodies in the synthetic models.

Example 40: Joint Inversion

Table 4. 41: Summary of important input values for example 40.

Weighting	Type		Sensitivity
	wbeta		1.0
	wnorm		2.0
Target Misfits	Gravity	chifact	1.0
		chitol	0.2
	Travel-Time	chifact	1.0
		chitol	0.2
	Joint Inversion	Alphaj	1.0
		jchitol	0.05
Bounds	Density	Upper	5.817 g/cm ³
		Lower	2.817 g/cm ³
	Slowness	Upper	1.1623 s/km
		Lower	0.1623 s/km
Similarity	Rhoe		1.0

The gravity response predicted by this inversion and the associated normalized data residuals are similar to those seen in Fig. 4. 60. The normalized data residuals for this example range from -2.5 to 1.78. The seismic travel times predicted by this inversion and the associated normalized data residuals are similar to those in Fig. 4. 56. The normalized data residuals for this example range from -5.4 to 5.82.

The gravity model produced by this inversion shows that the inversion was unable to locate the sulphide or troctolite bodies (Fig. 4. 62a). The location of the dense material does indicate that the inversion determined that dense material existed towards the centre of the model. The slowness model has located the sulphide body but has not been able to resolve it clearly (Fig. 4. 62b). There are a lot of artefacts in the background of the model.

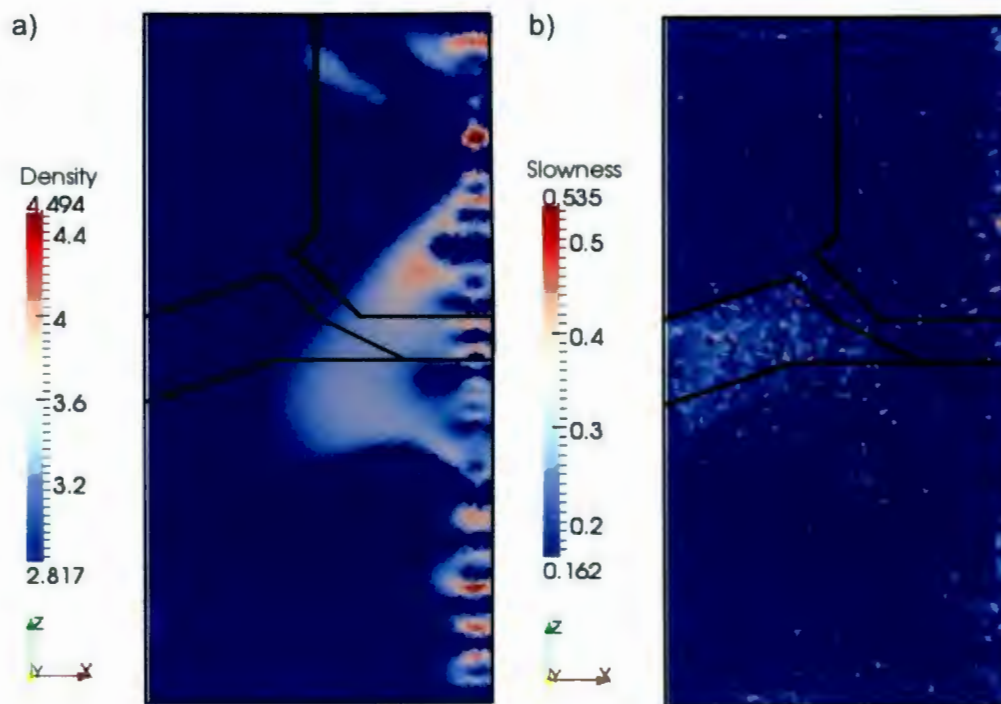


Fig. 4. 62: Resultant density (a) and slowness (b) model for the joint inversion of Mixed model synthetic data. The models are 200m across and 400m in depth. The black line outlines the location of the sulphide and troctolite bodies in the synthetic models.

4.2.5 Borehole A and B Gravity Stations

Example 41: Gravity-Only Inversions

Table 4. 42: Summary of important input values for example 41.

Weighting	Type	Sensitivity
	Wbeta	1.0
	Wnorm	2.0
Target Misfits	Chifact	1.0
	Chitol	0.2
Bounds	Upper	5.817 g/cm ³
	Lower	2.817 g/cm ³

The gravity response predicted by this inversion (fig. 4. 63a) is similar in range and topology to the clean synthetic data produced during forward modelling of the mixed model (fig 3.8). The normalized data residuals calculated from the predicted and moderate noise data are relatively small (fig. 4. 63b). The largest values occur near the sulphide-troctolite and sulphide-gneiss contacts.

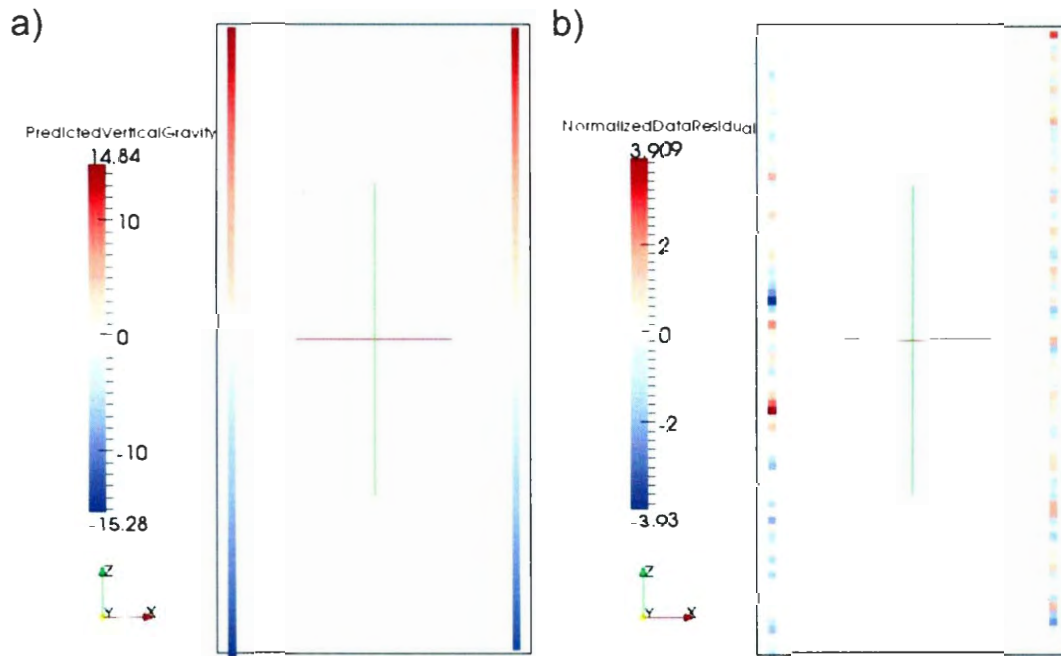


fig. 4. 63: Predicted gravity data (a) and associated normalized data residuals (b) for the joint inversion of Mixed model synthetic data.

The density model produced by this inversion has located and determined the approximate size of the sulphide body (Fig. 4. 64). The exact shape of the body has not been determined, and although the location of the upper contact has been well estimated the location of the lower contact has not been. There is some weakly anomalous material along the left edge of the model and along the troctolite feeder which suggests that the inversion was attempting to match the weak troctolite signal.

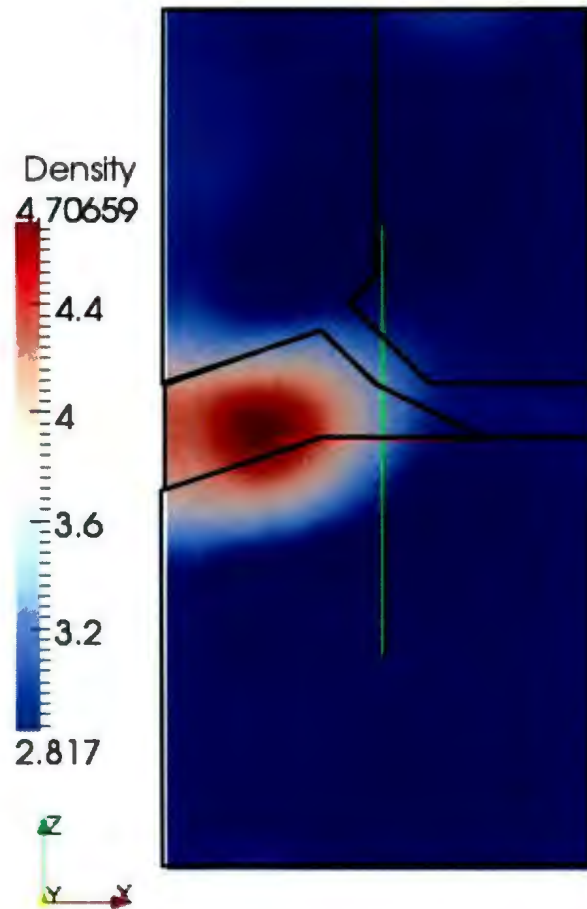


Fig. 4. 64 Resultant density model from the gravity-only inversion of the Mixed model synthetic data. The model is 200m across and 400m in depth. The black line outlines the location of the sulphide and troctolite bodies in the synthetic models.

Example 42: Joint Inversion

Table 4. 43: Summary of important input values for example 42.

Weighting	Type		Sensitivity
		wbeta	
	wnorm		2.0
Target Misfits	Gravity	chifact	1.0
		chitol	0.2
	Travel-Time	chifact	1.0
		chitol	0.2
	Joint Inversion	alphaj	1.0
		jchitol	0.05
Bounds	Density	Upper	5.817 g/cm ³
		Lower	2.817 g/cm ³
	Slowness	Upper	1.1623 s/km
		Lower	0.1623 s/km
Similarity	Rhoe		1.0

The gravity response predicted by this inversion and the associated normalized data residuals are similar to those seen in fig. 4. 63. The normalized data residuals for this example range from -5 to 4.93. The seismic travel times predicted by this inversion and the associated normalized data residuals are similar to those in Fig. 4. 56. The normalized data residuals for this example range from -4.4 to 5.15.

The density model produced by this inversion (Fig. 4. 65a) has determined the approximate size of the sulphide body. The location of the upper contact between the sulphide and the troctolite has been well defined; however, the lower contact between the sulphide and the gneiss has not. Weakly anomalous material along the left side of the model above the sulphide body indicates that the inversion may have been trying to match the weak troctolite signal.

The slowness model produced by this inversion (Fig. 4. 65b) has located and determined the approximate size and shape of the sulphide body; although, the lower contact is not as well determined as the upper. There is slightly moderate material along the left edge of the model and within the troctolite feeder pipe. This suggests that the inversion was attempting to match the weak troctolite signal.

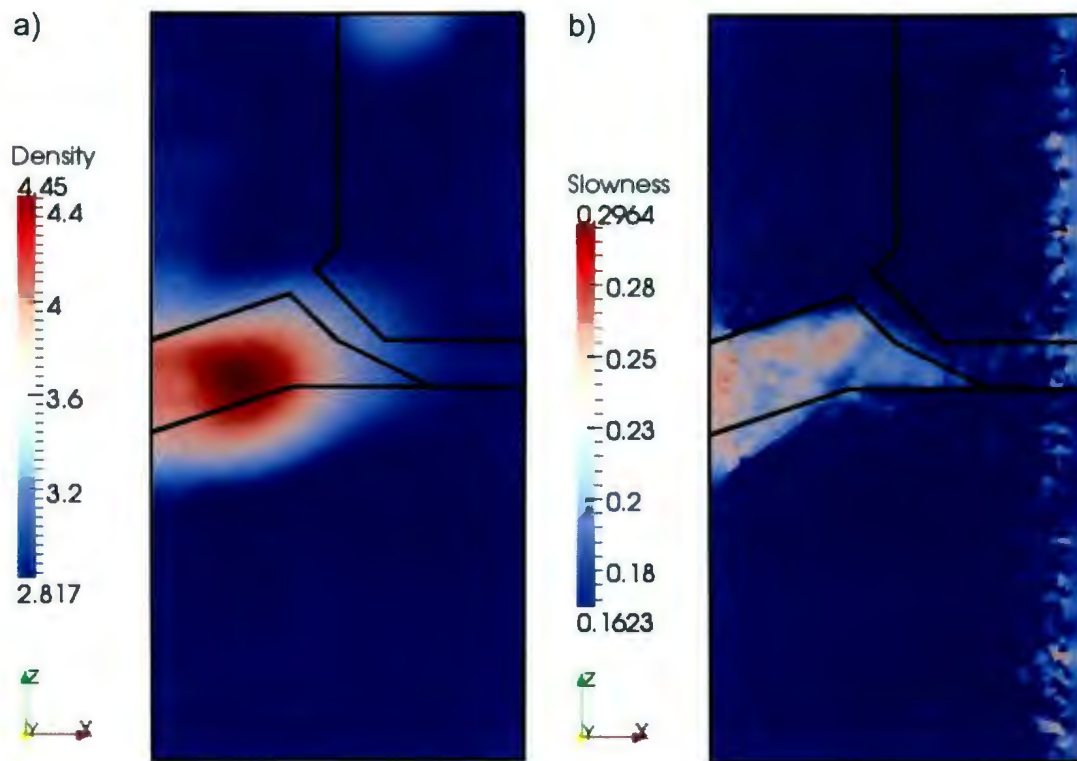


Fig. 4. 65: Resultant slowness (a) and density (b) model for the joint inversion of Mixed model synthetic data. The models are 200m across and 400m in depth. The black line outlines the location of the sulphide and troctolite bodies in the synthetic models.

4.2.6 All Station Results

Example 43: Gravity-Only Inversion

Table 4. 44: Summary of important input values for example 43.

Weighting	Type	Sensitivity
	Wbeta	1.0
	Wnorm	2.0
Target Misfits	Chifact	1.0
	Chitol	0.2
Bounds	Upper	5.817 g/cm ³
	Lower	2.817 g/cm ³

The density model produced by this inversion shows that the inversion has been able to locate the sulphide body and determined its approximate size (Fig. 4. 66). The upper sulphide-troctolite contact has been more accurately resolved than the lower contact. There is some weakly anomalous material along the left side of the model above the sulphide body as well as stretching from the sulphide body near the trace of the troctolite feeder.

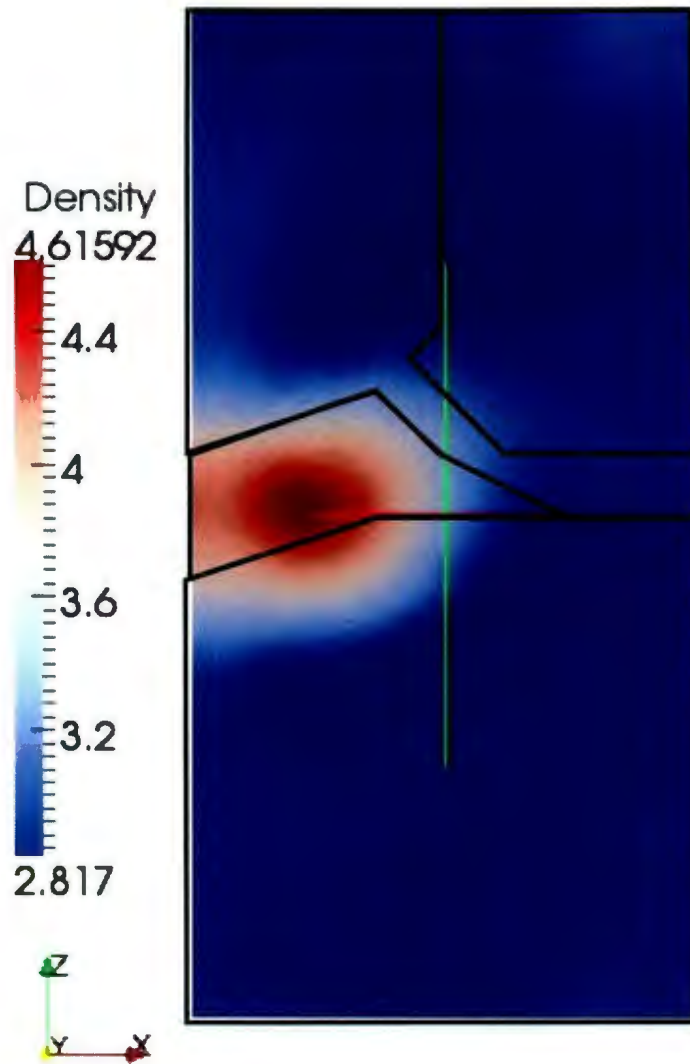


Fig. 4. 66: Resultant density model from the gravity-only inversion of the Mixed model synthetic data. The model is 200m across and 400m in depth. The black line outlines the location of the sulphide and troctolite bodies in the synthetic models.

Example 44: Joint Inversion

Table 4. 45: Summary of important input values for example 44.

Weighting	Type		Sensitivity
	wbeta		1.0
	wnorm		2.0
Target Misfits	Gravity	chifact	1.0
		chitol	0.2
	Travel-Time	chifact	1.0
		chitol	0.2
	Joint Inversion	alphaj	1.0
		jchitol	0.05
Bounds	Density	Upper	5.817 g/cm ³
		Lower	2.817 g/cm ³
	Slowness	Upper	1.1623 s/km
		Lower	0.1623 s/km
Similarity	Rhoe		10 ⁻⁴

The gravity response predicted by this inversion (Fig. 4. 67a) is similar in range and topology to the clean synthetic data produced during forward modelling of the mixed model (Fig. 4. 6). The normalized data residuals calculated from the predicted and moderate noise synthetic data are relatively low (Fig. 4. 67b). The higher normalized data residuals as associated closely with gravity stations close to the sulphide body in borehole A. The seismic travel times predicted by this inversion and the associated normalized data

residuals are similar to those in Fig. 4. 56. The normalized data residuals for this example range from -4.28 to 5.08.

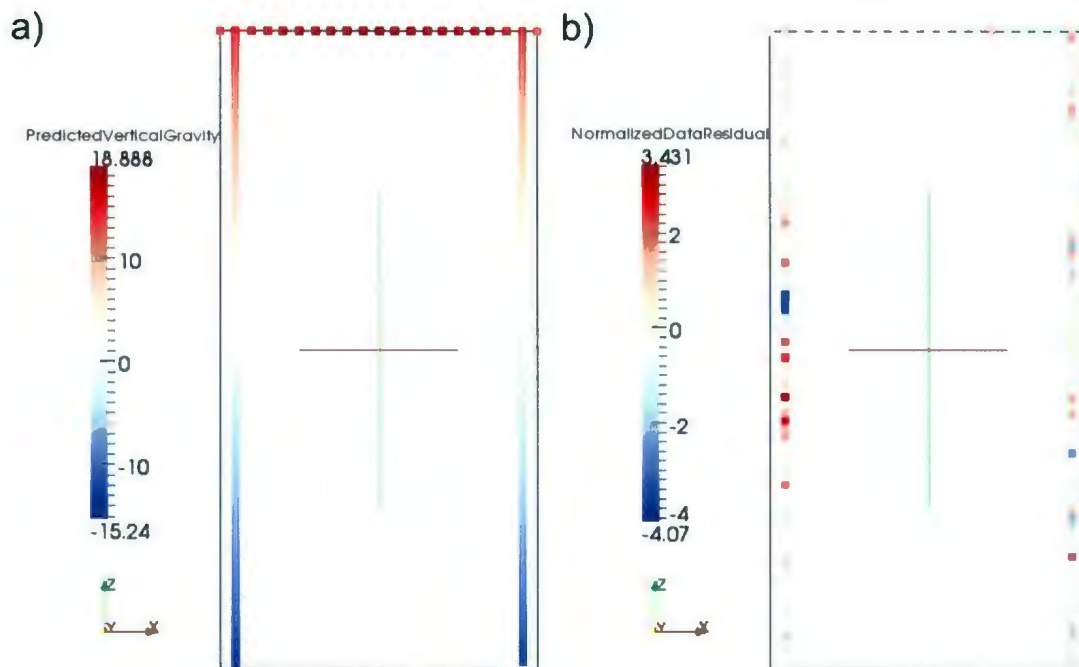


Fig. 4. 67: Predicted gravity data (a) and associated normalized data residuals (b) for the gravity-only inversion of Mixed model synthetic data.

The density model produced by this inversion shows that the inversion has been able to locate the sulphide body and determined its approximate size (Fig. 4. 68a). The upper sulphide-troctolite contact has been more accurately resolved than the lower contact. There is some weakly anomalous material along the left side of the model above the sulphide. The gravity response predicted by this inversion and the associated normalized

data residuals are similar to those seen in Fig. 4. 67. The normalized data residuals for this example range from -4.82 to 4.38.

The slowness model produced by this inversion (Fig. 4. 68b) has located and roughly determined the size and shape of the sulphide body. Although, the upper contact has been better resolved than the lower. There is some indication that the model is attempting to image the troctolite as there are some weakly anomalous cells both along the left edge of the model above the sulphide and in the vicinity of the feeder pipe.

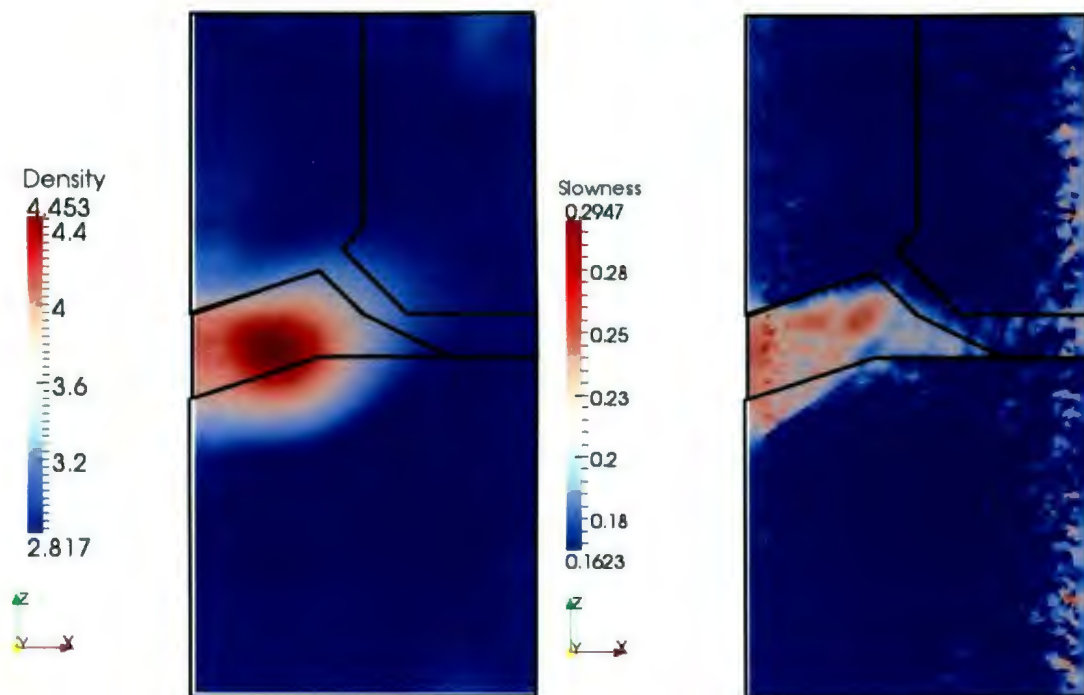


Fig. 4. 68: The resultant density (a) and slowness (b) models from the joint inversion of Mixed model synthetic data. The models are 200m across and 400m in depth. The black line outlines the location of the sulphide and troctolite bodies in the synthetic models.

4.3 Troctolite-Gneiss Model Inversion Results

The troctolite-gneiss model inversions were conducted using only the gravity station configuration involving all gravity stations. This was done to improve the data density and potentially improve the chances of seeing the troctolite body. Inversions were run with low and moderate amounts of noise.

4.3.1 Low Noise Inversion Results

Example 45: Gravity-Only Inversion

Table 4. 46: Summary of important input values for example 45.

Weighting	Type	Sensitivity
	Wbeta	1.0
	Wnorm	2.0
Target Misfits	Chifact	1.0
	Chitol	0.2
Bounds	Upper	5.817 g/cm ³
	Lower	2.817 g/cm ³

The gravity response predicted by this inversion (Fig. 4. 69a) is similar in range and topology to the synthetic data produced from forward modelling of troctolite. The normalized data residuals calculated from the predicted and low noise synthetic data are

relatively low (Fig. 4. 69b) indicating that the inversion was able to match the synthetic data well.

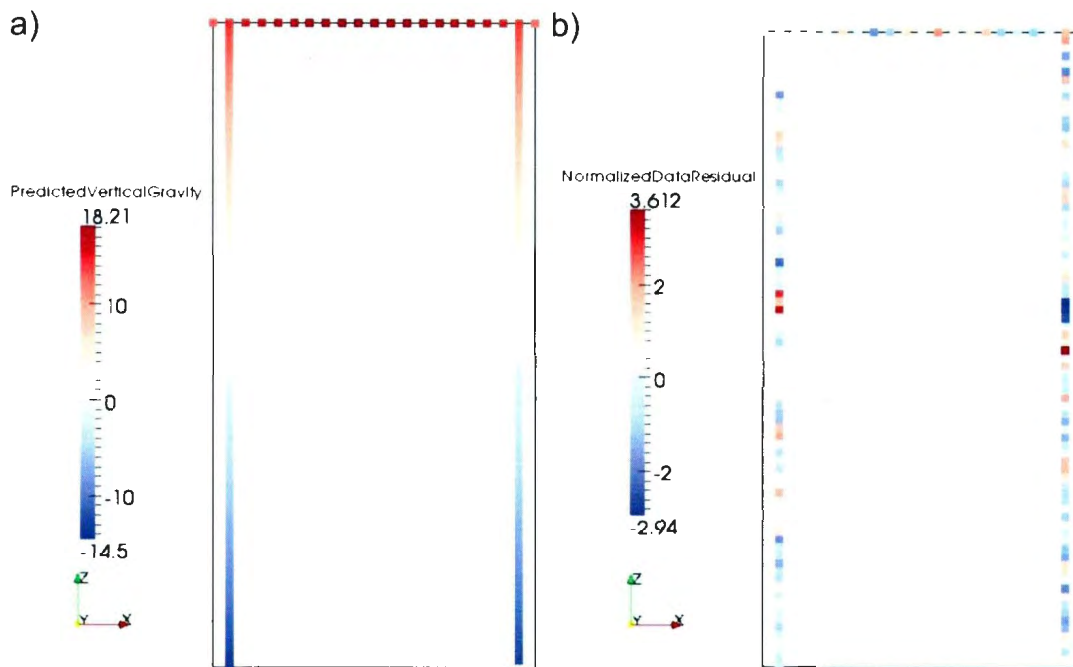


Fig. 4. 69: Predicted gravity data (a) and associated normalized data residuals (b) for the joint inversion of low noise sulphide-gneiss model synthetic data.

The gravity model produced by this inversion has located the main troctolite body well and determined its shape and size (Fig. 4. 70). A part of the feeder pipe has also been located; however, the angled portion of the feeder pipe has not been modelled. The inversion has estimated the density of the body well.

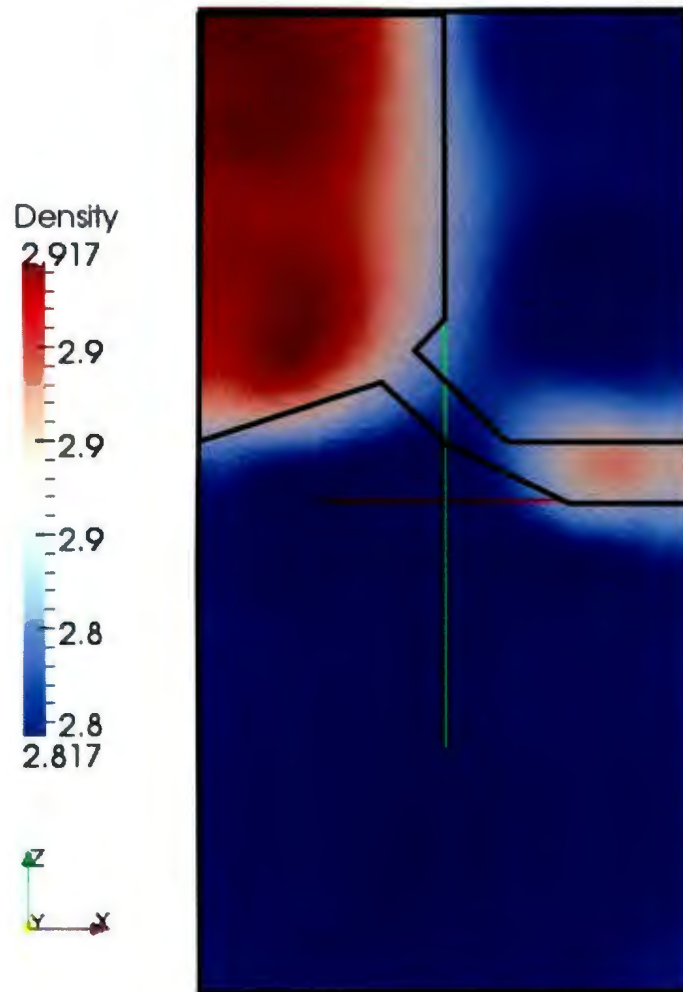


Fig. 4. 70: Resultant model from the gravity only version of low noise troctolite-gneiss model synthetic data. The model is 200m across and 400m in depth. The black line outlines the location of the troctolite body in the synthetic models.

Example 46: Seismic-Only Inversion

Table 4. 47: Summary of important input values for example 46.

Target Misfits	Chifact	1.0
	Chitol	0.2
Bounds	Upper	1.1623 s/km
	Lower	0.1623 s/km

The travel times predicted by this inversion resemble in topology and range of values the synthetic travel time data provided to the inversion (Fig. 4. 71a). The normalized data residuals calculated from the predicted and synthetic travel time data are moderately high (Fig. 4. 71b). This indicates that the inversion was having difficulty matching the synthetic data set. As the synthetic data contained very little noise the inversion will have increased difficulty matching the data.

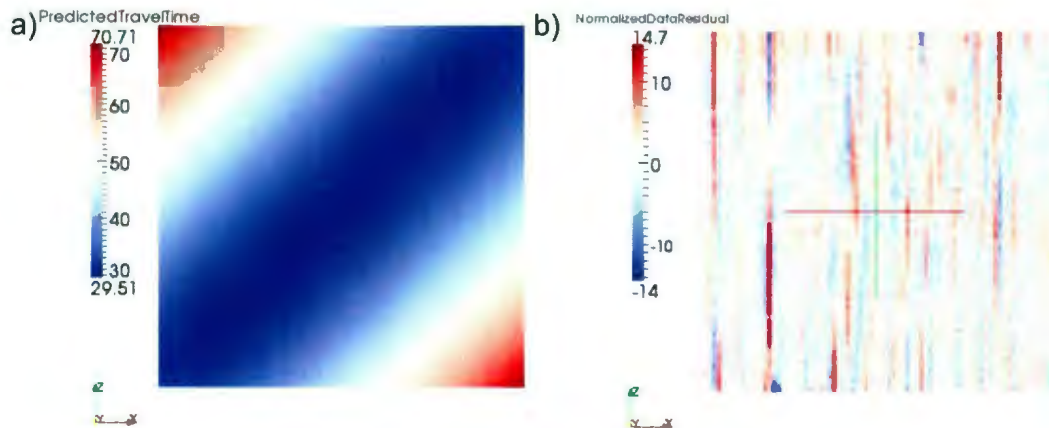


Fig. 4. 71: The travel time predicted by this model (a) and the associated normalized data residuals (b) from the seismic-only inversion of low noise troctolite-gneiss model synthetic data. The horizontal axis of both plots is the source number and the vertical axis is the receiver number (Fig 3.10).

The slowness model produced by the seismic-only inversion of low noise synthetic data has reproduced the troctolite body poorly. The troctolite appears as an area of slightly slower cells in the vicinity of the troctolite body; however, this slight increase is overshadowed by the high slowness noise around the locations of the seismic receivers (Fig. 4. 72). Had the synthetic model not been known it would have been very difficult to correctly interpret the results of this inversion.

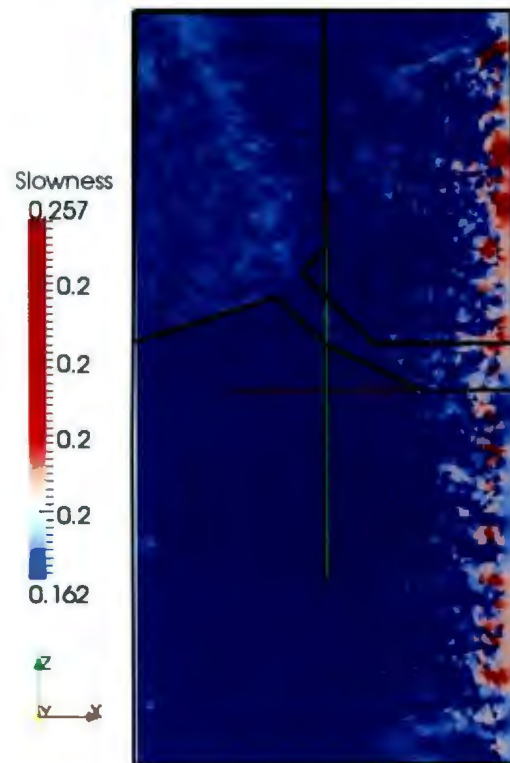


Fig. 4. 72: Resultant model from the seismic only inversion of low noise troctolite-gneiss model synthetic data. The model is 200m across and 400m in depth. The black line outlines the location of the troctolite body in the synthetic models.

Example 47: Joint Inversion

Table 4. 48: Summary of important input values for example 47.

Weighting	Type		Sensitivity
		wbeta	1.0
		wnorm	2.0
Target Misfits	Gravity	chifact	1.0
		chitol	0.2
	Travel-Time	chifact	1.0
		chitol	0.2
	Joint Inversion	Alphaj	1.0
		jchitol	0.05
Bounds	Density	Upper	5.817 g/cm ³
		Lower	2.817 g/cm ³
	Slowness	Upper	1.1623 s/km
		Lower	0.1623 s/km
Similarity	Rhoe		10 ⁻⁴

The seismic travel times predicted by this inversion and the associated normalized data residuals are similar to those seen in Fig. 4. 71. The normalized data residuals for this example range from -15.31 to 14.29. The gravity response predicted by this inversion and

the associated normalized data residuals are similar to those seen in Fig. 4. 69. The normalized data residuals for this example range from -2.38 to 3.08.

The slowness model produced by this inversion has located the troctolite body; however, due to the large abundance of seismic receiver artefacts (fig 4.74a). The slowness of the cells within the troctolite is estimated well. The slowness model has not located the feeder pipe. The density model produced by this inversion has located both the troctolite body and the horizontal portion of the feeder tube (Fig. 4. 73b). The density of the pluton and the horizontal portion of the feeder tube have been well estimated.

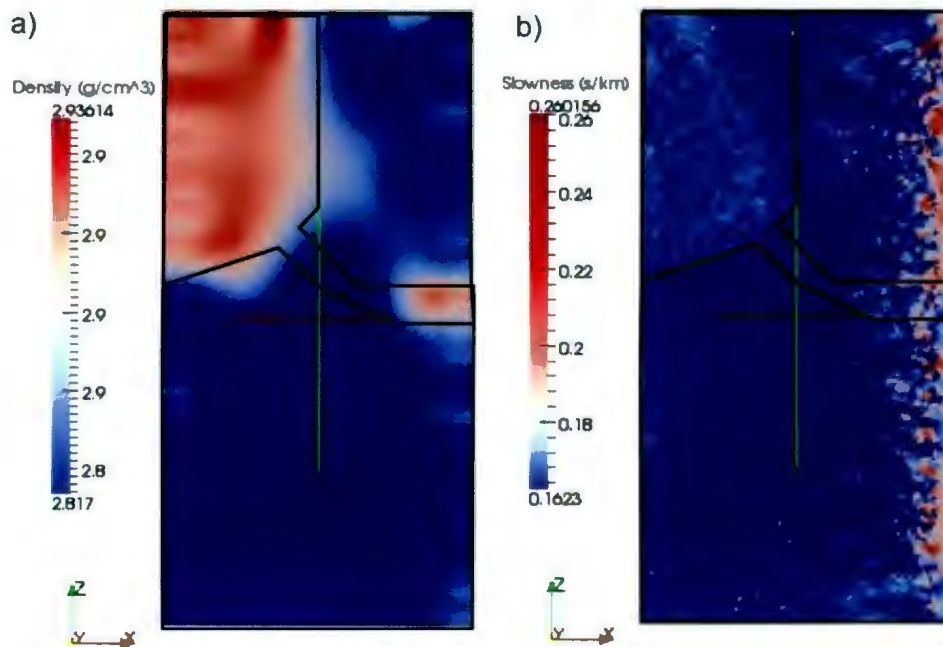


Fig. 4. 73: The resultant density (b) and slowness (b) models from the joint inversion of low noise troctolite-gneiss synthetic data. The models are 200m across and 400m in depth. The black line outlines the location of the troctolite body in the synthetic models.

4.3.2 Moderate Noise Inversion

Example 48: Gravity-Only Inversion

Table 4. 49: Summary of important input values for example 48.

Weighting	Type	Sensitivity
	Wbeta	1.0
	Wnorm	2.0
Target Misfits	Chifact	1.0
	Chitol	0.2
Bounds	Upper	5.817 g/cm ³
	Lower	2.817 g/cm ³

The gravity response predicted by this inversion and its associated normalized data residuals are similar to those seen in Fig. 4. 69. The normalized data residuals for this example range from -2.08 to 3.25.

The density model produced by this inversion of moderate noise synthetic data was able to locate the troctolite pluton vertically. However, the lateral extent of the pluton was not reproduced well (Fig. 4. 74). The density of the gneissic background has been estimated well, however, the density of the troctolite has been underestimated.

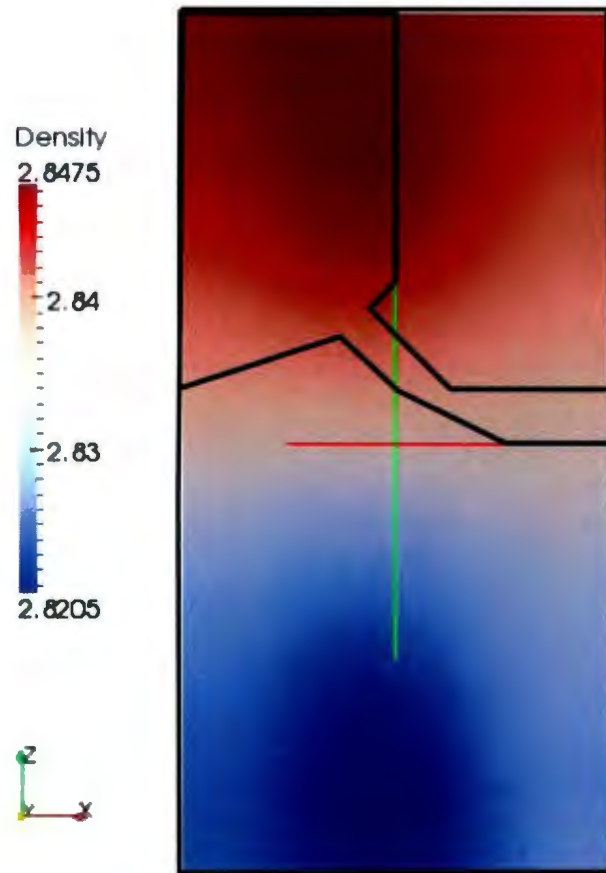


Fig. 4. 74: Resultant model from the gravity only inversion of moderately noise troctolite-gneiss model synthetic data. The model is 200m across and 400m in depth. The black line outlines the location of the troctolite body in the synthetic models.

Example 49: Seismic-Only Inversion

Table 4. 50: Summary of important input values for example 50.

Target Misfits	Chifact	1.0
	Chitol	0.2
Bounds	Upper	1.1623 s/km
	Lower	0.1623 s/km

The seismic travel times predicted by this inversion are similar to the clean synthetic data produced from forward modelling of the troctolite-gneiss model (Fig. 4. 75a). The normalized data residuals suggest that some of the sources were difficult to determine the travel times for many receivers and that the travel times were consistently over and underestimated for those sources.

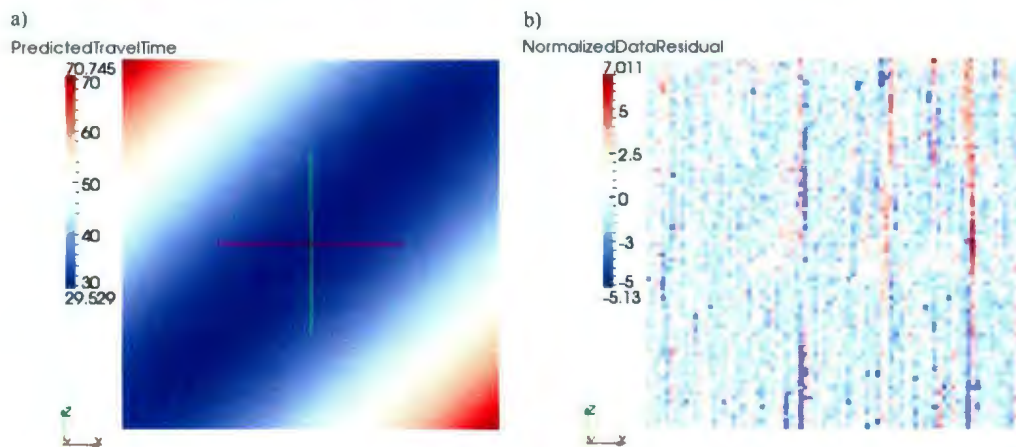


Fig. 4. 75: The travel time predicted by this model (a) and the associated normalized data residuals (b) from the seismic-only inversion of moderate noise troctolite-gneiss model synthetic data. The horizontal axis of both plots is the source number and the vertical axis is the receiver number (Fig 3.10).

The slowness model produced by this inversion has located the troctolite body. The area of the troctolite pluton shows as an increase in the slowness of the cells (Fig. 4. 76). However, the most variation in the slowness model is along the right side of the model where the seismic receivers are located. If the true model was not known correctly interpreting these results would be very difficult.

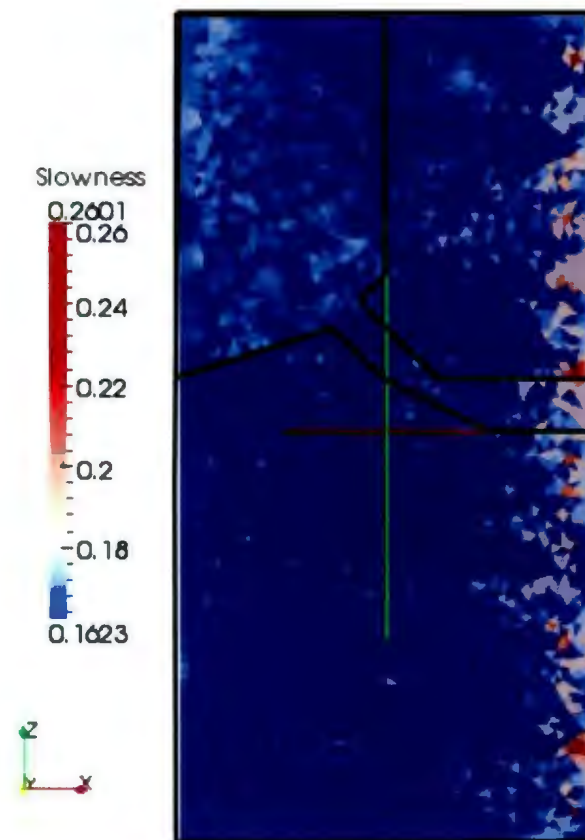


Fig. 4. 76: Resultant model from the seismic-only inversion of moderately noisy troctolite-gneiss model synthetic data. The model is 200m across and 400m in depth. The black line outlines the location of the troctolite body in the synthetic models.

Example 50: Joint Inversion

Table 4. 51: Summary of important input values for example 50.

Weighting	Type		Sensitivity
	wbeta		1.0
	wnorm		2.0
Target Misfits	Gravity	chifact	1.0
		chitol	0.2
	Travel-Time	chifact	1.0
		chitol	0.2
	Joint Inversion	Alphaj	1.0
		Jchitol	0.05
Bounds	Density	Upper	5.817 g/cm ³
		Lower	2.817 g/cm ³
	Slowness	Upper	1.1623 s/km
		Lower	0.1623 s/km
Similarity	Rhoe		1.0

The seismic travel times predicted by this inversion and the associated normalized data residuals are similar to those seen in Fig. 4. 75. The normalized data residuals from this example range from -5.19 to 6.94. The gravity response predicted by this inversion and

the associated normalized data residuals similar to Fig. 4. 69. The normalized data residuals range from -2.18 to 2.28.

The slowness and density models resultant from the joint inversion of moderate noise troctolite-gneiss model synthetic data has improved on the results of both the gravity-only and seismic-only inversions. The improvement in the lateral distribution in the density model is particularly notable (Fig. 4. 77b).

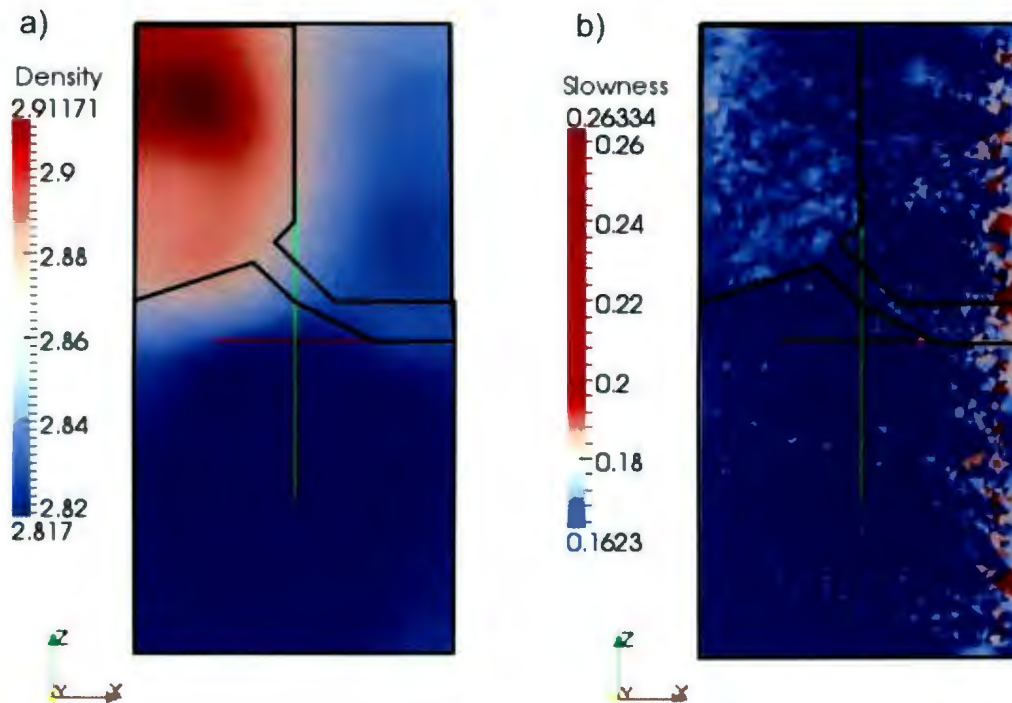


Fig. 4. 77: The resultant density (a) and slowness (b) models from the joint inversion of low noise troctolite-gneiss synthetic data. The models are 200m across and 400m in depth. The black line outlines the location of the troctolite body in the synthetic models.

4.3.3 High noise Inversions

Example 51: Gravity-Only Inversions

Table 4. 52: Summary of important input values for example 51.

Weighting	Type	Sensitivity
	Wbeta	1.0
	Wnorm	2.0
Target Misfits	Chifact	0.5
	Chitol	0.1
Bounds	Upper	5.817 g/cm ³
	Lower	2.817 g/cm ³

The gravity response predicted by this inversion exceeds the range of the clean synthetic troctolite-gneiss data (Fig. 4. 78a). The normalized data residuals are reasonably low and the majority are greater response was being overestimated.

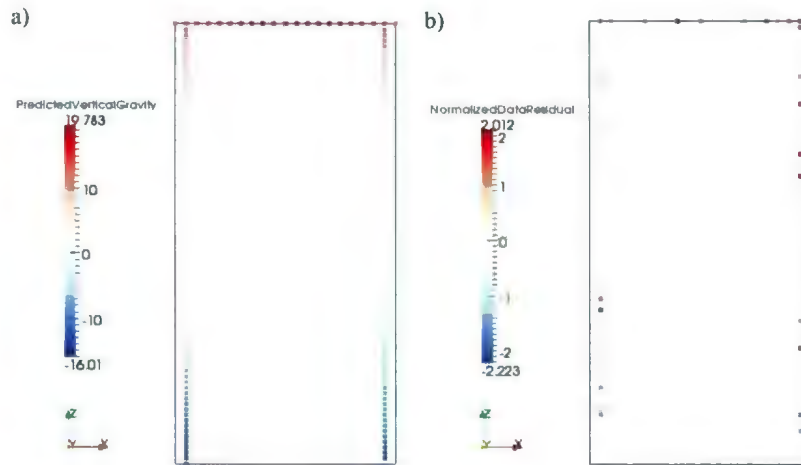


Fig. 4. 78: Predicted gravity data (a) and associated normalized data residuals (b) for the joint inversion of high noise sulphide-gneiss model synthetic data.

The density model produced by this inversion has been unable to locate the troctolite body in any way (Fig. 4. 79). High density material is collected near the gravity stations.

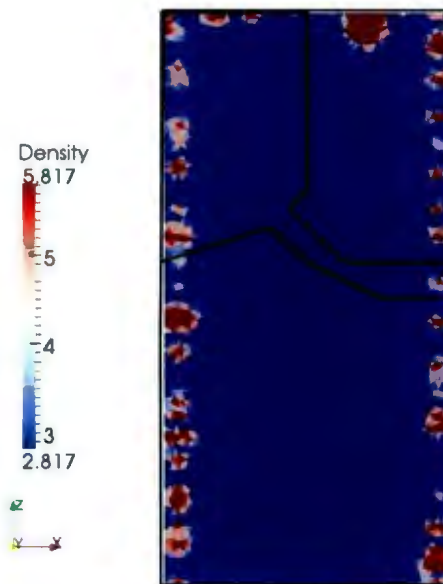


Fig. 4. 79: Resultant density model from the gravity-only inversion of the high noise Mixed model synthetic data. The model is 200m across and 400m in depth. The black line outlines the location of the troctolite body in the synthetic models.

Example 52: Seismic Only Inversion

Table 4. 53: Summary of important input values for example 52.

chifact		1.0
chitol		0.2
Bounds	Upper	1.1623 s/km
	Lower	0.1623 s/km

The seismic travel times predicted by this inversion and the associated normalized data residuals are similar to those seen in Fig. 4. 75. The normalized data residuals for this example range from -3.81 to 4.37.

The slowness model produced by this inversion has located the troctolite body (Fig. 4. 80) with comparable fidelity to the low (Fig. 4. 72) and moderate noise (Fig. 4. 74) although the shape of the body is somewhat sharper for the inversion with lower noise.

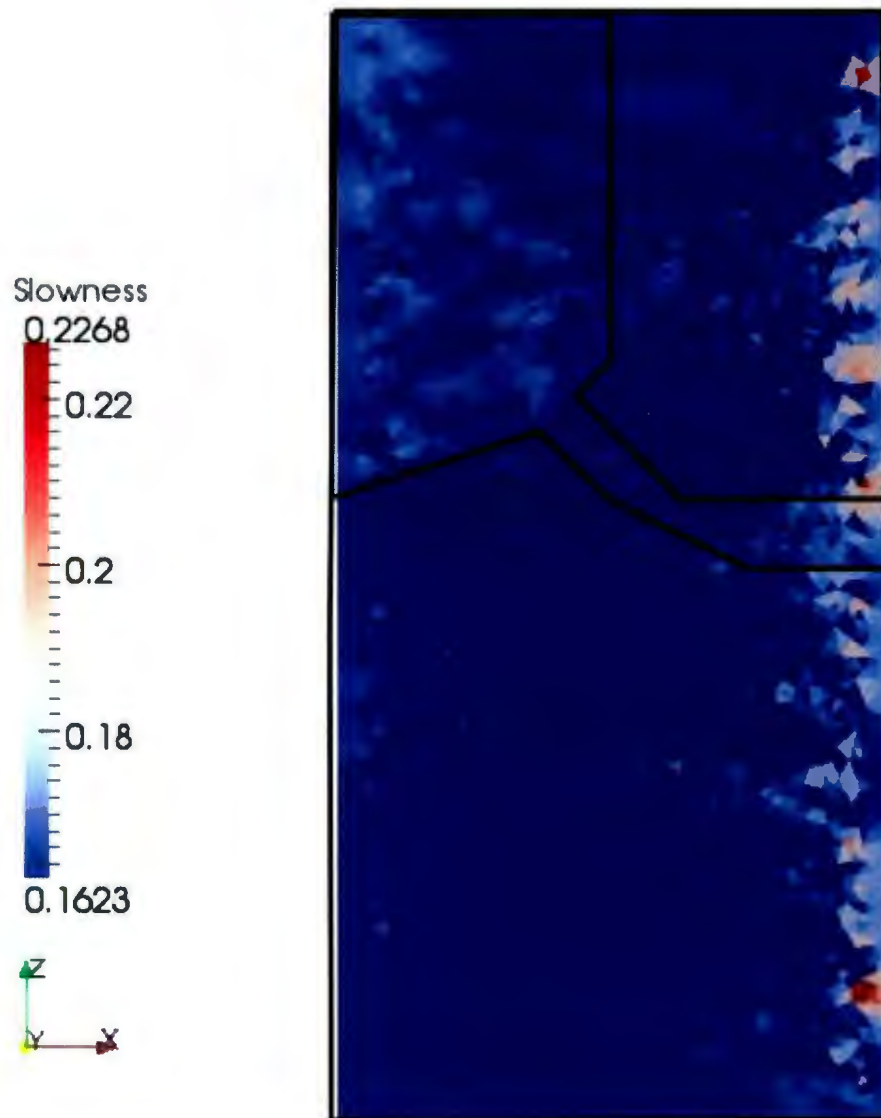


Fig. 4. 80: Resultant slowness model from the gravity-only inversion of the high noise Mixed model synthetic data. The model is 200m across and 400m in depth. The black line outlines the location of the troctolite body in the synthetic models.

Example 53: Joint Inversion

Table 4. 54: Summary of important input values for example 53.

Weighting	Type		Sensitivity
	wbeta		1.0
	wnorm		2.0
Target Misfits	Gravity	chifact	0.5
		chitol	0.1
	Travel-Time	chifact	1.0
		chitol	0.2
	Joint Inversion	alphaj	1.0
		jchitol	0.2
Bounds	Density	Upper	5.817 g/cm ³
		Lower	2.817 g/cm ³
	Slowness	Upper	1.1623 s/km
		Lower	0.1623 s/km
Similarity	Rhoe		10 ⁻¹⁰

The gravity response predicted by this inversion and the associated normalized data residuals are similar to those seen in Fig. 4. 69. The normalized data residuals for this example range from -2.32 to 2.41. The seismic travel times predicted by this inversion

and the associated normalized data residuals are similar to those seen in Fig. 4. 75. The normalized data residuals for this example range from -3.81 to 4.33.

The density model produced by this inversion (Fig. 4. 81a) is an improvement over the results of the gravity-only inversion (Fig. 4. 79), however, it still has not been able to locate the troctolite body. The slowness model produced by the inversion (Fig. 4. 81b) is nearly identical to the results of the seismic-only inversion of high noise data (Fig. 4. 80). The joint inversion in this instance yields little improvement.

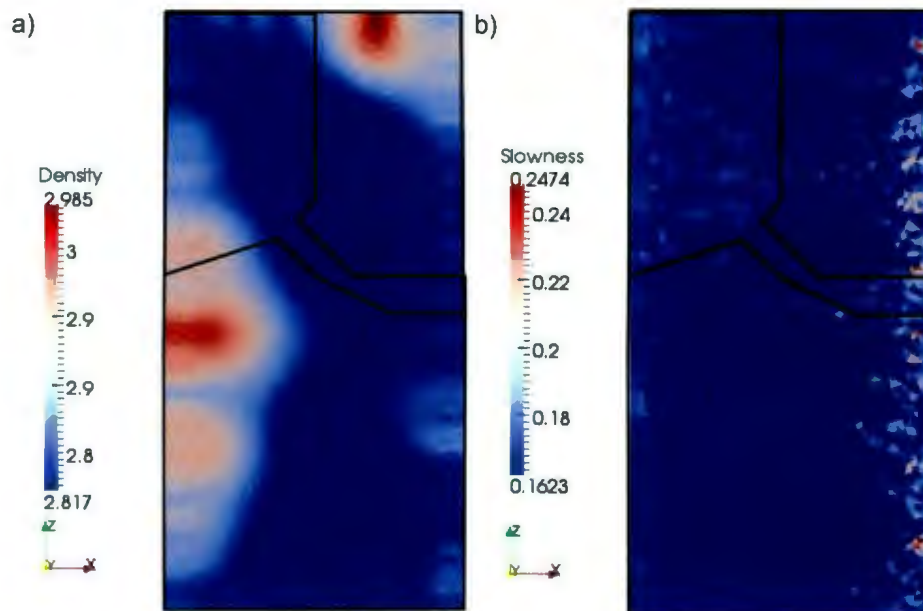


Fig. 4. 81: Resultant density (a) and slowness (b) model for the joint inversion of high noise sulphide-gneiss model synthetic data. The models are 200m across and 400m in depth. The black line outlines the location of the troctolite body in the synthetic models.

4.4 Discussion of 2D Inversion Results

4.4.1 Modelling High Contrast Buried Bodies

In this chapter insights gained from the 2D inversions are presented and conclusions about the effectiveness of the joint inversion methodology are drawn.

4.4.1.1 Discussion of Single Property Inversion Results

Seismic-Only Inversions

Seismic-only inversions were very successful in locating and determining the size, shape, and slowness of the small buried body (Fig. 4. 82). The general shape of the anomalous body was very well determined. Even the inversions of high noise data were able to model the high density body of the sulphide-gneiss model well (Fig. 4. 82c). The only indication that there is more noise in these data is the amount of chatter in the background compared to the result of the inversion of moderate noise data (Fig. 4. 82b). The presence of incorrectly assigned high slowness cells near the seismic receiver locations (right side of the model) are present to some degree in the slowness models from both joint and seismic-only inversions. These artefacts are common in this type of inversion (Lelievre, et al., 2011). The seismic-only inversions generally were able to determine the slowness of the sulphide body relatively well.

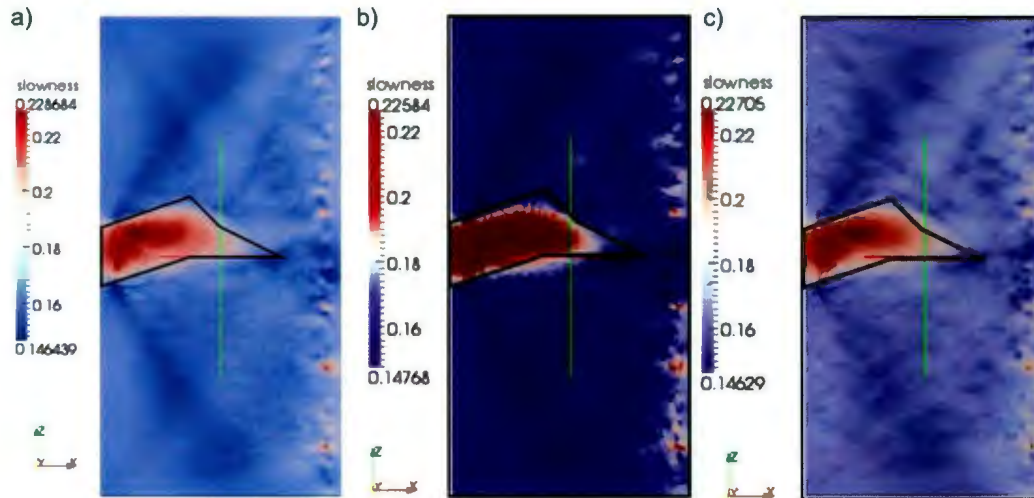


Fig. 4. 82: The slowness models resultant from the seismic-only inversion of low (a), moderate (b) and high noise (c) sulphide-gneiss model synthetic data. Slowness is given in s/km.

Gravity-Only Inversions

The success of gravity-only inversions to accurately locate and determine the size, shape, and density of the buried sulphide body is very dependent on the layout of the gravity stations. The proximity of the gravity stations to the sulphide body seemed to be a controlling factor affecting the inversion's ability to model the sulphide. As such, there were clear benefits to employing borehole gravity stations and it was evident that the closer the borehole to the sulphide body the better the results (Fig. 4. 83). The best gravity-only inversion results are seen for those inversions using all gravity stations, borehole A and B layout and the borehole A layout (Fig. 4. 83). These results clearly illustrated the benefits of having borehole gravity stations and the importance of the distance between the borehole and the sulphide body.

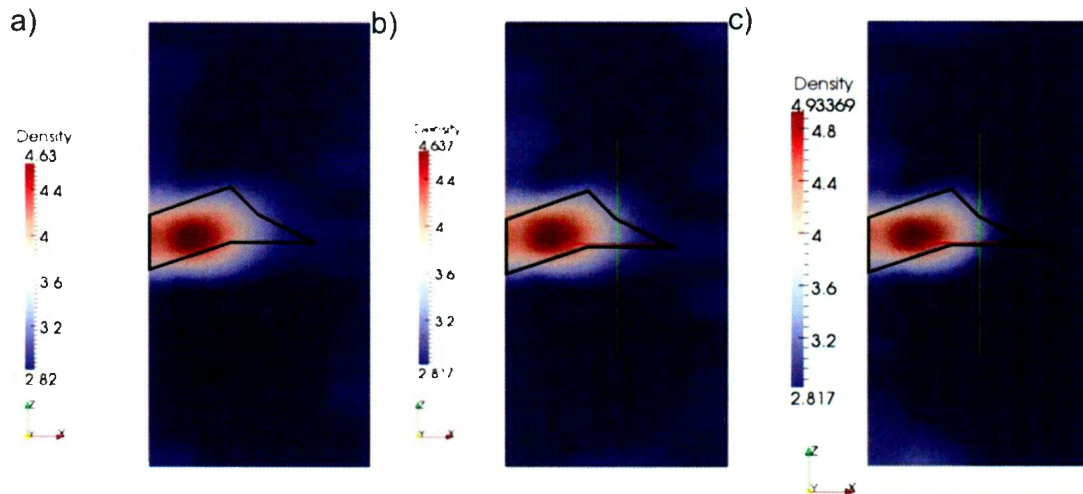


Fig. 4. 83: Typical results from moderate noise gravity-only inversions for a) all gravity stations, b) borehole A and B gravity stations, and c) borehole A gravity stations. Density values are given a g/cm^3 .

The gravity-only inversion using surface gravity stations and borehole B gravity stations were not as successful (Fig. 4. 84). The results showed that these inversions often had difficulty determining the size, shape and density of the sulphide body. Many of the surface inversions were unable to determine the location of the sulphide body accurately. Inversions using surface stations tended to determine the lateral positioning but were unable to determine the depth of the body. The inversion using borehole B stations could, generally, locate the body vertically but they had problems determining the lateral extent of the body (Fig. 4. 84).

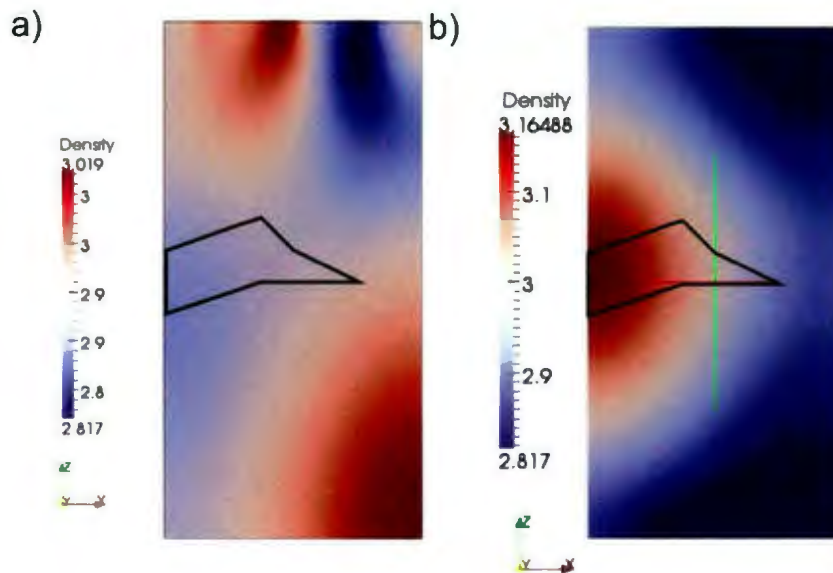


Fig. 4. 84: Gravity-only inversion for (a) surface stations data and (b) borehole B station data results showing the density in g/cm^3 .

The inversion experienced difficulty in matching the gravity response for observation location near the contacts between the sulphide body and surrounding gneiss. This is illustrated by the high normalized data residuals in Fig. 4. 85a. This feature is seen in the normalized data residuals for many of gravity and joint inversions in which gravity measurements in borehole A are used (fig. 4.43, 4.45, and 4.49). This difficulty in matching the gravity response near the boundaries between units is related to the smoothing regularization in the minimum structure inversion algorithm.

Another pattern occasionally seen in the normalized data residuals is depth dependence. The high positive normalized data residuals being associated with the shallow gravity stations and the high negative normalized data residuals being associated with the deep gravity stations (Fig. 4. 85b). This normalized data residual pattern is generally associated

with a good modelling of the size of the sulphide body, but an over estimation of the density of the body.

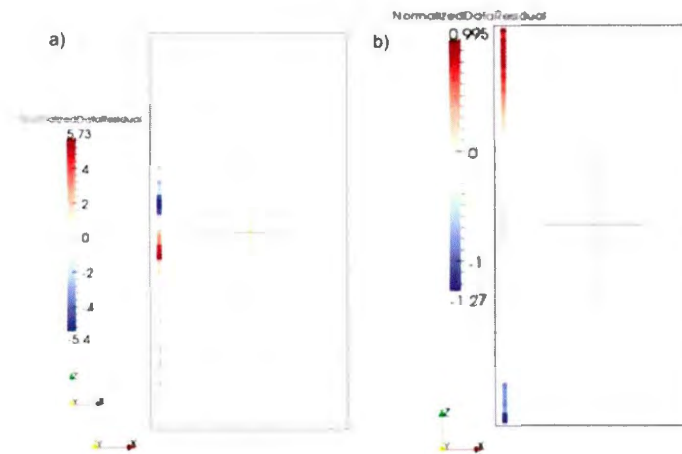


Fig. 4. 85: Example of various patterns seen in normalized data residuals from gravity inversions: a) contact affect; b) density estimation affect

Joint Inversion Results

Joint inversion using linear coupling (see Section 2.3.1) was shown to lead to consistent improvement over the results of the gravity-only inversions. The joint inversion was able to use the good results obtained through the seismic half of the inversion to lead the gravity half of the inversion to find a more accurate distribution of high density cells. The single property gravity inversion tended to overestimate the density of the cells; however, the joint inversion tended to underestimate the densities. There was not as much improvement of the slowness model of the sulphide body over the results of the seismic-only inversion; although occasionally the joint inversion would lead to a decrease in background noise.

The benefits of using a joint inversion are illustrated by the following example: the comparison of the gravity-only, seismic-only and joint inversion results for the high noise sulphide-gneiss model data with gravity data collected in borehole A and B stations (Fig. 4. 86). It can be seen that the joint inversion improved the resolution of the density distribution greatly. The joint inversion also reduced the amount of background noise seen in the slowness distribution compared to the seismic-only inversion.

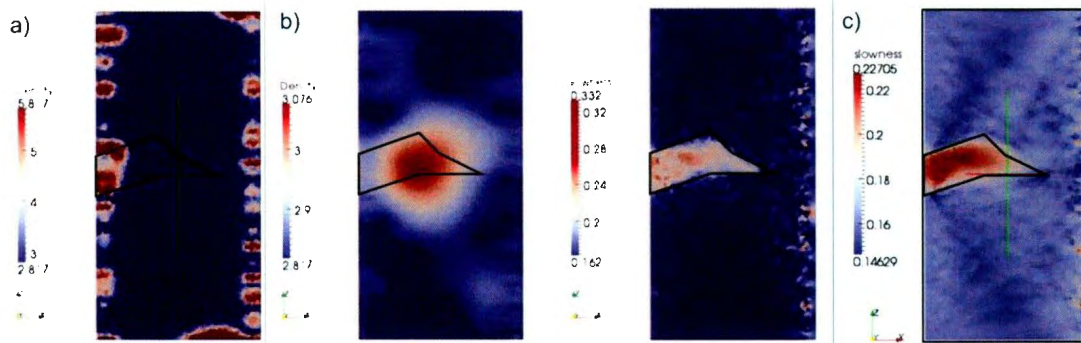


Fig. 4. 86: Comparison between the physical property models resultant from a) gravity-only inversion b) joint inversion c) seismic-only inversion of the same high noise data sets.

4.4.2 Modelling Low Contrast Bodies

The physical property contrasts between many common rock types are very small. These small contrasts make detecting geological contacts difficult. The troctolite-gneiss model was used in this project to test the inversion code's abilities to resolve the contact between two large geological units with a low contrast in properties. The code was quite successful in this regard; however, there is a strong relationship between the quality of the inversion results and the amount of noise in the data.

The best results were attained from single property (Fig. 4. 87a,b) and joint inversions (Fig. 4. 88a) for low noise data. At high noise the ability to discern the contact deteriorates; particularly for the determination of the density distribution (Fig. 4. 87e,f, Fig. 4. 88c). Further evidence that the quality of the inversion model is dependent on the amount of noise in the inverted data becomes clear when contrasting the results from the moderate noise inversions and the low noise inversions. The gravity-only moderate noise inversion (Fig. 4. 87d) has not resolved the troctolite body with the same success as is seen in the equivalent low noise inversion (Fig. 4. 87b). The moderate noise joint inversion has not been able to locate the feeder pipe; whereas, the low noise inversion has done so.

The inversions conducted with the low contrast show the best examples of the improvements possible through the use of joint inversion. By selecting a reasonable value for the similarity parameter the improvements seen can be quite striking. This is best illustrated by contrasting the results of the single property inversions (Fig. 4. 87c,d) and the joint inversion of moderately noisy data (Fig. 4. 88b). The gravity-only inversion has been able to determine that a body of slightly higher density exists near the surface of the model, however, it has not been able to determine the lateral extent of the body. The joint inversion clearly shows the extent of the troctolite body.

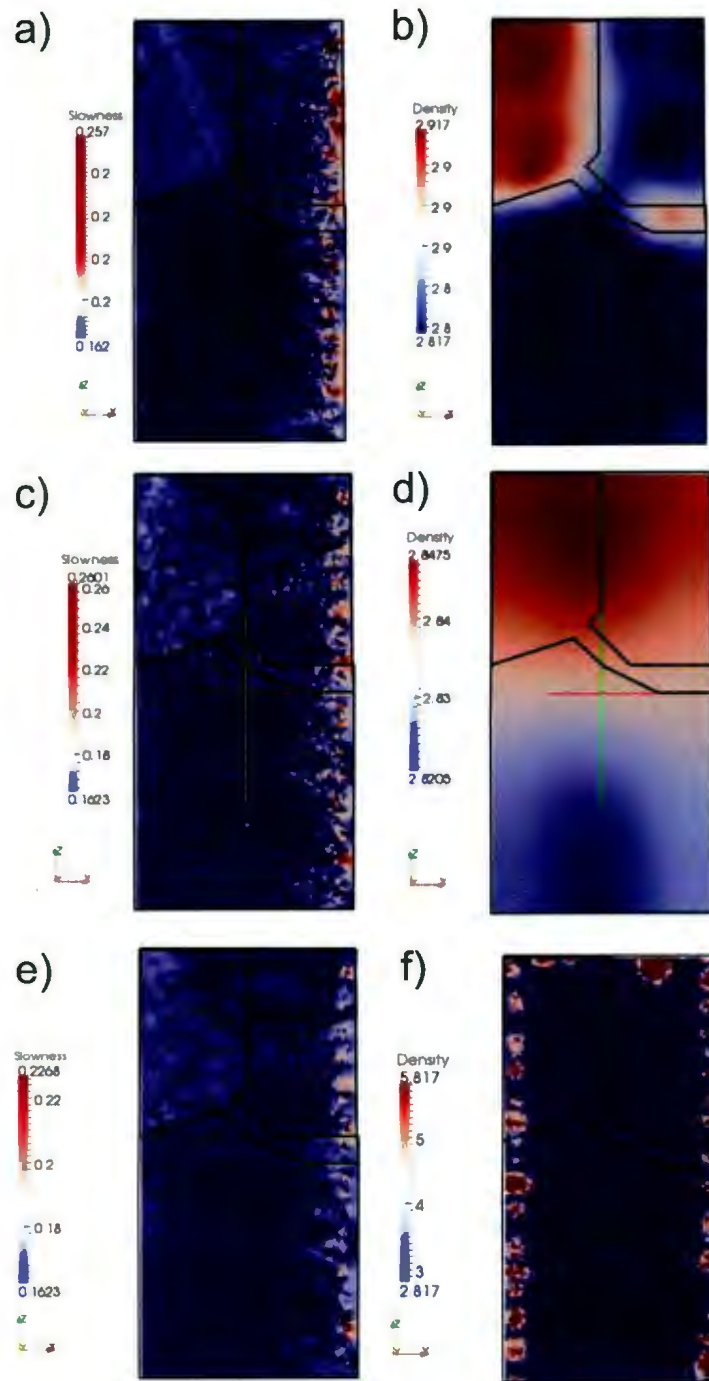


Fig. 4. 87: Single property inversion results for the troctolite-gneiss model: a) seismic-only low noise; b) gravity-only low noise; c) seismic-only moderate noise; d) gravity-only moderate noise; e) seismic-only high noise; f) gravity-only high noise.

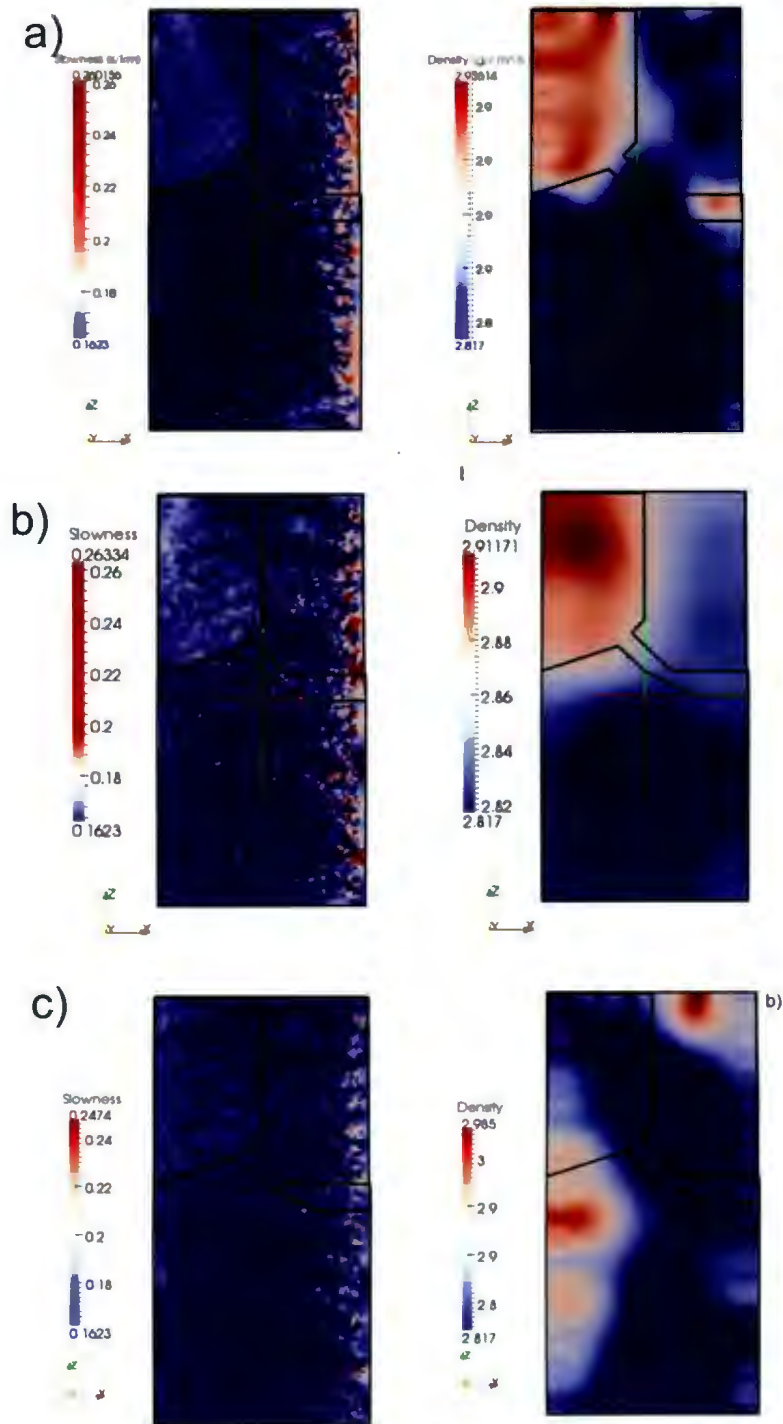


Fig. 4. 88: Joint inversion results from the troctolite-gneiss model tests: a) low noise results; b) moderate noise results; c) high noise results.

4.4.3 Modelling Mixed Models

It was clear from the mixed model tests that the dense sulphide body could be accurately modelled in a heterogeneous background (Fig. 4. 59, Fig. 4. 65, Fig. 4. 68). The ability of the code to model the sulphide body in a heterogeneous background is greatly improved through the employment of borehole gravity data. This is clearly demonstrated by the inability of the inversions using surface gravity stations only (Fig. 4. 54, Fig. 4. 56) to determine the location of the sulphide body. Although, using borehole A gravity stations (Fig. 4. 58, Fig. 4. 59) produced better results than borehole B gravity station inversions (Fig. 4. 61, Fig. 4. 62) both are significantly better than the surface-only station inversions.

The mixed model tests showed that the presence of a high contrast body decreased the codes ability to image a small contrast body. This is clearly illustrated by contrasting the moderate noise joint inversion of seismic and all-station gravity data from the troctolite-gneiss and mixed models (Fig. 4. 89). It can clearly be seen that the troctolite-gneiss model results have been able to clearly reproduced the main troctolite body (Fig. 4. 89a). In the mixed model results there is evidence of the presence of the troctolite body, however, the inversion has not resolved it clearly (Fig. 4. 89b).

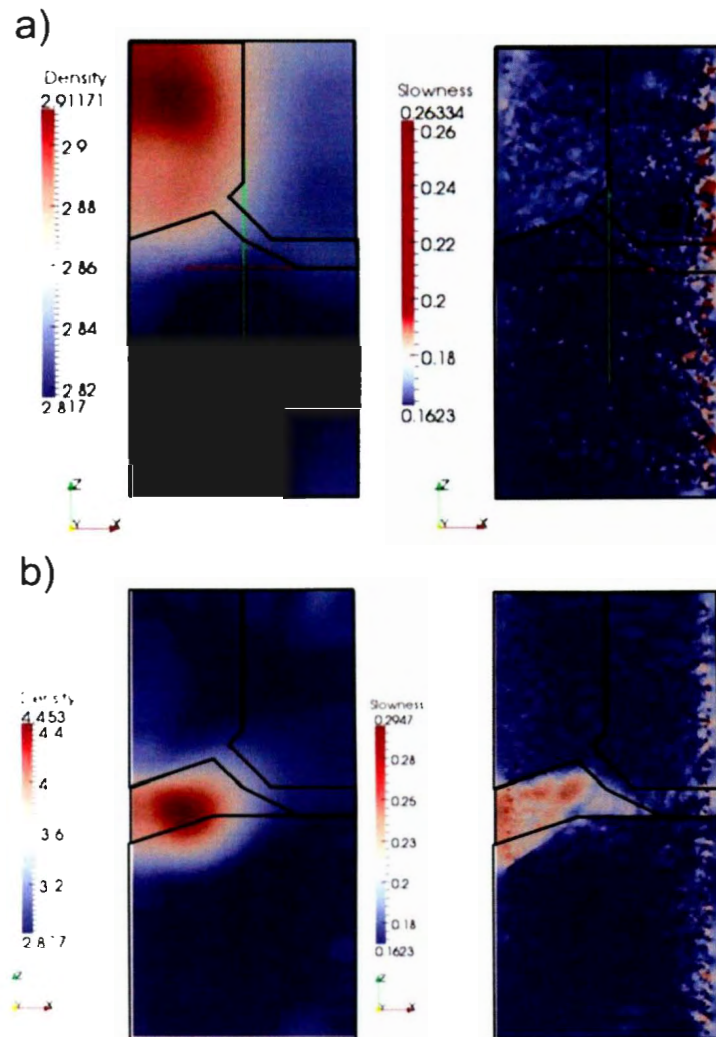


Fig. 4. 89: Contrasting the resultant density and slowness model from the moderate noise joint inversion of seismic and all station gravity data for the troctolite-gneiss model (a) and mixed model (b).

There is evidence of the presence of the troctolite model in most of the inversion results. This evidence can be more clearly seen if a black and white scale is used to represent the range of slowness and density values. In Fig. 4. 90 such a scale is used. The red circles indicate areas where parts of the troctolite body and feeder pipe have been modelled. Similar results were seen for many of the mixed model inversion.

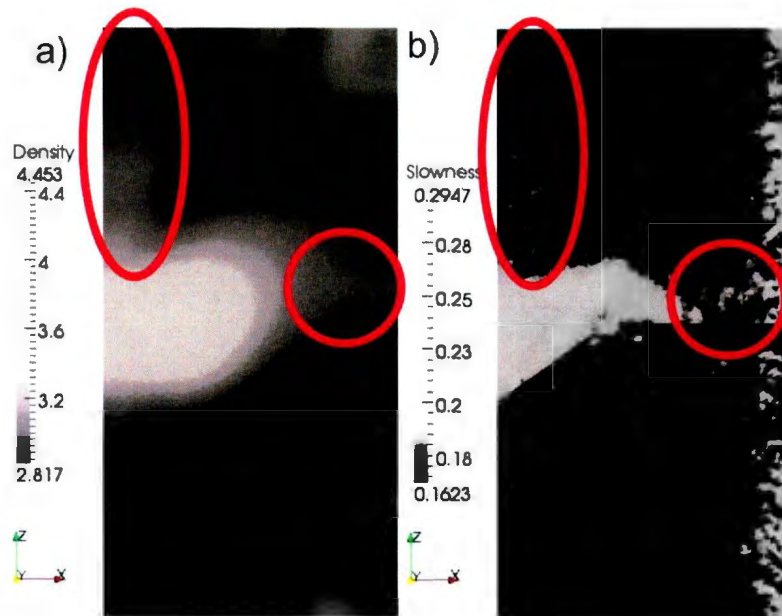


Fig. 4. 90: Black and white scaled version of the resultant density(a) and slowness(b) models from the joint inversion of moderate noise mixed model seismic and all station gravity data. The areas enclosed the red ovals indicate areas

4.4.4 Discussion of Key Inversion Parameters

4.4.4.1 RHOE Parameter

The similarity parameter, RHOE (discussed in sections 2.3.1 and 2.3.2). In the examples presented in this chapter the relationship outlined in eq. 2.10 was used. The effect of the RHOE parameter was crucial to attaining the best results from the inversions. The effect of the RHOE parameter is clearly illustrated through the results of inversions of high noise sulphide-gneiss model data. If RHOE is set too low there won't be enough similarity imposed between the two models. The seismic has been well modelled, however, the gravity is very poorly reproduced (Fig. 4. 91a). By increasing the RHOE

value and imposing a greater degree of similarity the model begins to improve. At some point the best result is attained (Fig. 4. 91b). If the RHOE factor is increased too far the seismic results begins to mimic the poorly modelled gravity and moves towards a homogenous half space by increasing the slowness of a small number of cells.

Initial estimates of the similarity parameter for a particular inversion can be informed by the results of the single property inversions. In a case where the models produced by the single property inversions are quite good the similarity parameter does not need to be particularly high as very little information needs to be shared to produce a good joint inversion. This is the case with most inversions run using many borehole gravity stations. If the single property inversion results are good for either gravity or seismic but not for both a higher similarity parameter should be used. This allows the good half of the inversion to inform the poor half thereby improving the poor inversion. If both single property inversions are poor it is difficult to attain a good joint inversion result.

There are issues with using a high similarity parameter. The similarity parameter can lead to one half of the inversion developing inversion artefacts seen in the other half of the inversion. Commonly this was seen as “patchy” appearance to a density model much like the patchy appearance seen in many slowness models. Another example is the appearance of seismic receiver artefacts in the density models. This is seen in Fig. 4. 91 where there are nearly identical artefacts along the right edge of both the slowness and gravity models.

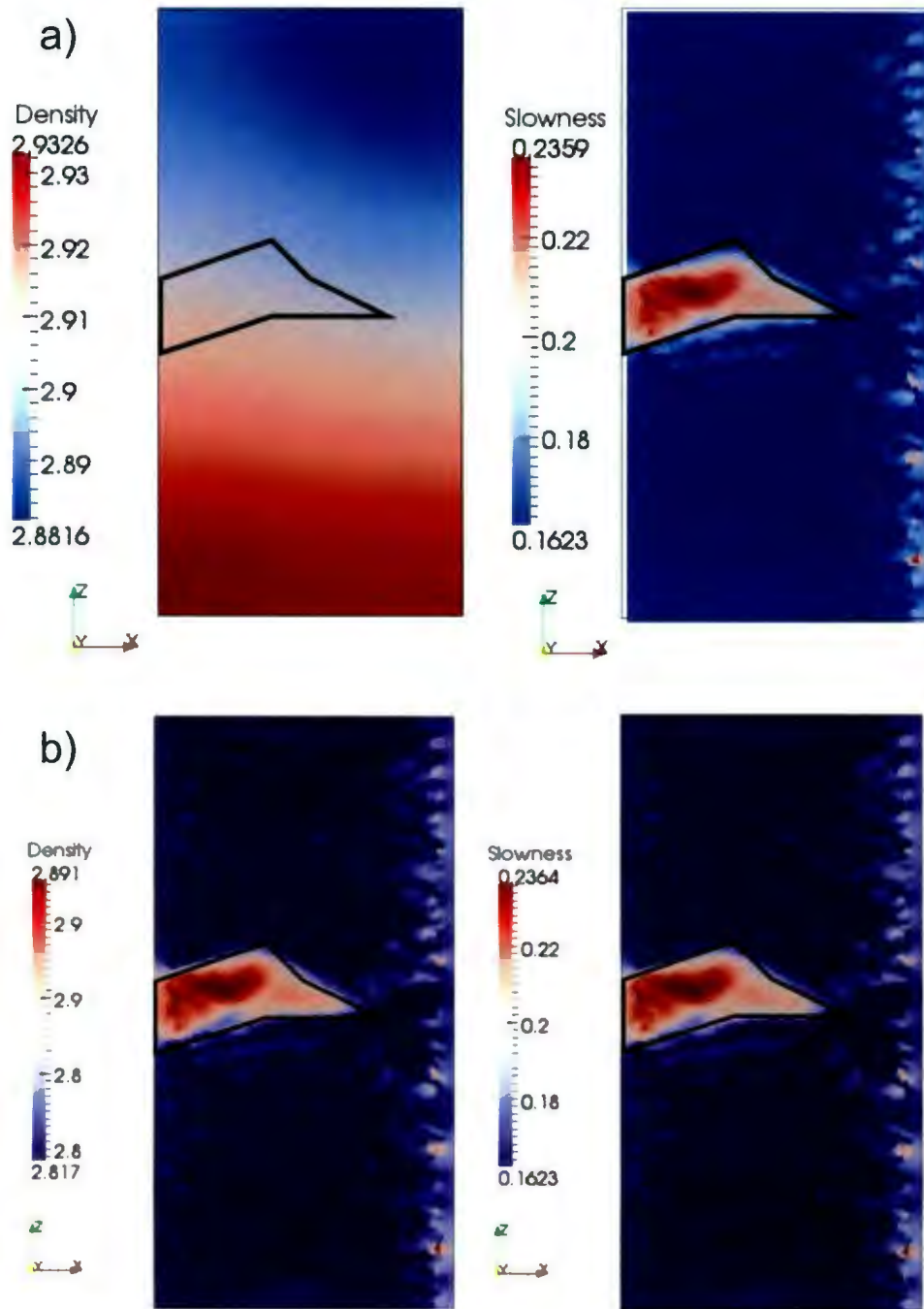


Fig. 4.91: Comparison between two joint inversions of high noise sulphide-gneiss model data with gravity from surface stations only: a) a low similarity parameter used ($\rho_e=0.01$) b) high similarity parameter ($\rho_e=1.0$)

4.4.4.2 Effect of Noise on Convergence

Issues with Low Noise Levels

The resultant slowness models from the seismic-only inversion of sulphide-gneiss model have accurately modelled the high contrast body at all noise levels (Fig. 4. 82). However, a striking difference between the three inversions can be seen when looking at the normalized data residuals calculated for these inversions (Fig. 4. 92). The low noise inversion has high normalized residuals (Fig. 4. 92a) in contrast to those calculated from the inversions of moderate (Fig. 4. 92b) and high noise (Fig. 4. 92c) data. This suggests that the inversions of low noise data were unable to match the synthetic data well. However, as these data residuals are normalized to the uncertainties on the data. The data points with high normalized residual values were often associated with the very small uncertainties on the low noise data. As such, these high normalized data residuals are more likely to be a reflection of the small uncertainties than a true measure of the codes ability to match a given data set. This leads to low noise inversions having more difficulty reaching target misfits even if they produce good inversion results. These high normalized data residual can cause an inversion to run longer than necessary; as such, increasing the target misfits for low noise inversion can lower the computation time while not compromising the quality of the resultant physical property models.

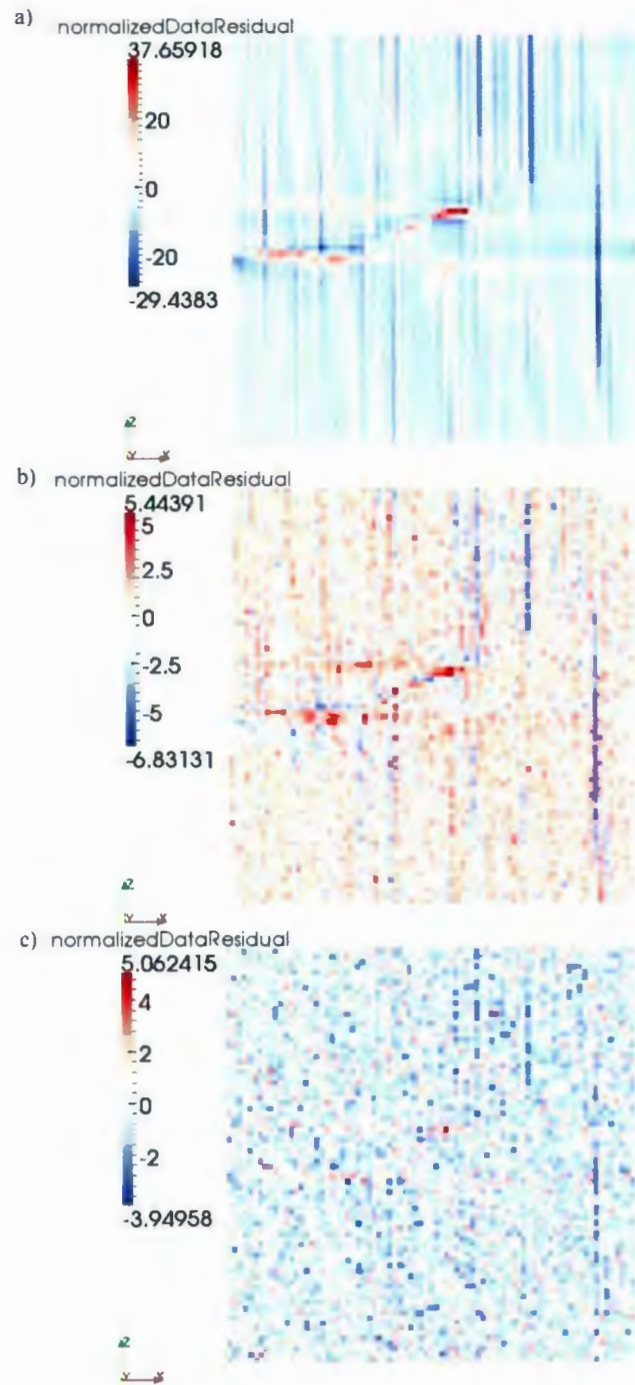


Fig. 4. 92: Normalized data residual for seismic only inversion of low noise sulphide-gneiss model data (a), moderate noise sulphide-gneiss model data (b), and high noise sulphide-gneiss model data (c).

Issues with High Noise Levels

From the results of gravity-only inversions of sulphide-gneiss model synthetic data another effect of noise levels can be seen. Good inversion results were produced by the inversion of low and moderate noise data (Fig. 4. 93a,b), however, the results of inversions of high noise data are very poor (Fig. 4. 82c).

This significant deterioration from the moderate to high noise in an inversion occurred for many models. These inversions often converged to the target misfits within 20 iterations and occasionally lowering the target misfits improved the resultant density model. This was a particular issue for gravity and was not seen as much for seismic inversions which tended to maintain their integrity better with increasing noise.

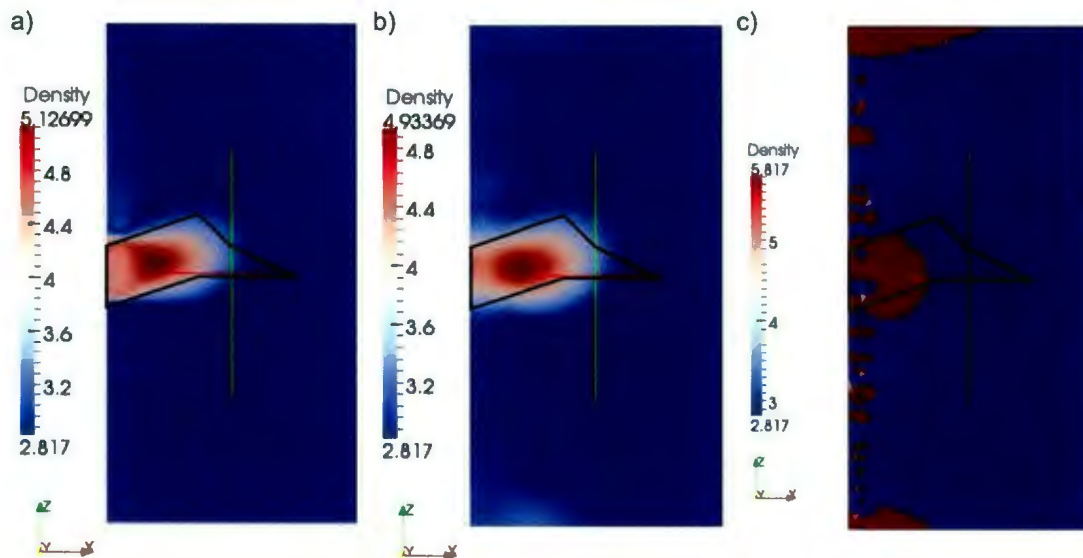


Fig. 4. 93: Density models from gravity-only borehole A inversion results: a) low noise; b) moderate noise; c) high noise.

4.4.4.3 Sensitivity Weighting

The effect of the sensitivity weighting on the results of the inversions is particularly important in cases where gravity data was collected down boreholes. In Fig. 4. 82 the density models for four inversions of the borehole A and B sulphide-gneiss model data are displayed. The parameters for these inversions were identical other than altering the *sens_norm* parameter (see Section 2.3.2). The higher the *sens_norm* the larger the effect of the sensitivity weighting on the inversion result. The first inversion (Fig. 4. 94a) the *sens_norm* was set to 2.0, in the second inversion (Fig. 4. 94b) the *sens_norm* was set to 1.0, in the third inversion (Fig. 4. 94c) the *sens_norm* was set to 0.5 and in the last inversion (Fig. 4. 94d) the *sens_norm* was set to 0. In such cases a high sensitivity coefficient will push the anomalous density material away from the borehole even if the borehole actually passes through that material (Fig. 4. 94a). By decreasing the sensitivity coefficient it allows the dense material to move closer to the correct location (Fig. 4. 94b,c). When the sensitivity weighting is decreased too far the anomalous material collects around the borehole (Fig. 4. 94d).

The improvement of the gravity inversions where data were collected only in the two boreholes was particularly good. With a high sensitivity weighting the dense material was collected directly between the two boreholes with excellent depth estimation. As the sensitivity was lowered the dense body shifts to the left and has fairly good correspondence to the sulphide body. Lowering the sensitivity too far, however, doesn't create the best result either as the inversion will move all of the dense material to the borehole.

If the true model is not known the sensitivity value could be varied based on the drill cuttings from drilling the borehole in which the gravity measurements are taken. Should the mineralogy show that there is an increase in the density in the borehole cuttings the sensitivity weighting would likely have to be lowered to allow the dense material. However, if there was no increase in density seen in the borehole the sensitivity weighting should be set such that none of the anomalous material occurs near the borehole gravity stations.

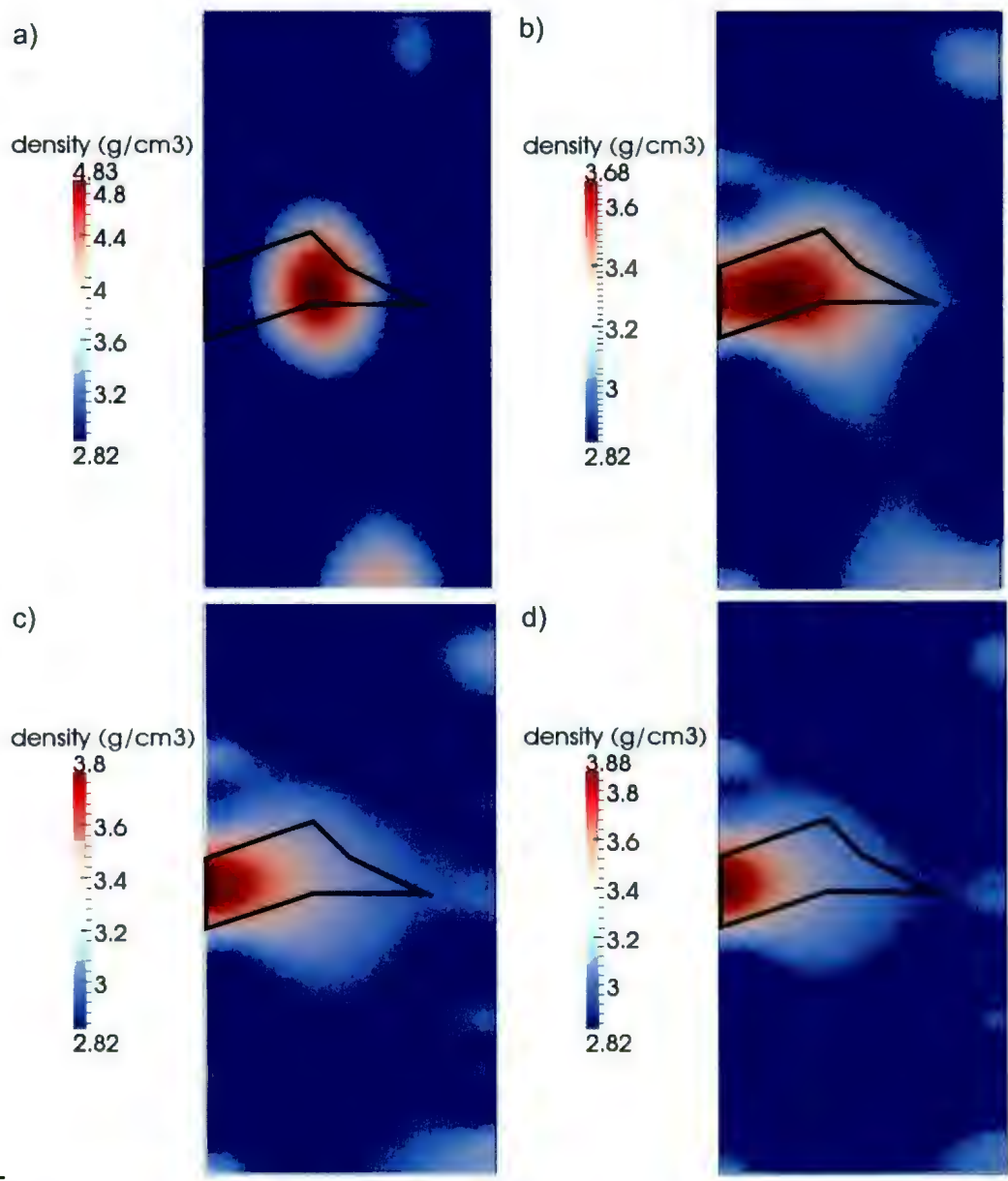


Fig. 4. 94: A demonstration of the effect of sensitivity weighting on gravity inversion result when borehole only data was employed. a) 2.0, b) 1.0, c) 0.5, d)0.0

4.5 Conclusions

Ability to model high contrast bodies was well demonstrated through the test conducted with the sulphide-gneiss model. The sulphide body could be modelled through both single property and joint inversions. Gravity inversion was greatly improved by using gravity stations in a borehole that penetrated the sulphide body. Joint inversion was able to improve the inversion results particularly when only surface gravity stations were used or when borehole B stations only were used.

The inversion code was able to model a body with low physical property contrasts; however, the quality of the results depended on the level of noise in the synthetic data. The slowness models, produced by the seismic-only inversion, show that seismic inversions are better able to incorporate increased noise levels than the gravity inversions.

This code was able to locate a small buried high physical property contrast body in the presence of a larger, low contrast body. It was not able to reproduce the low contrast body as well as the sulphide. This should be taken into consideration with the understanding that if a high contrast body is present determining the surrounding geology through this method is unrealistic. Conversely, it is probable that this technique can be used to locate high contrast bodies even in areas with multiple units that have low physical property contrasts. As such, although the technique has limited utility for geological mapping it shows promise for defining exploration targets.

Sensitivity and similarity weighting had strong effects on the results attained for inversions. These two weightings had to be chosen correctly in order to attain good inversion results. The results from the single property inversion can be used to inform the investigators as they are a good starting estimate for the similarity parameter. Based on the results presented in this chapter it is apparent that under favourable circumstances joint inversion produces individual physical property models which are better than those produced by the single property inversion.

Chapter 5: 3D Tetrahedral Earth Models

In this chapter the creation of the 3D tetrahedral models that will be used for the forward modelling are presented. As the triangular meshes are used to define the Earth models for 2D forward modelling (see Section 3.1) the 3D tetrahedral meshes are used to define the Earth models for 3D forward modelling. In section 5.1 the development of tetrahedral mesh Earth models from geological wireframes will be described. In section 5.2 the development of simplifications based on the model developed in section 5.1 is discussed. In section 5.3 the development of a piece of software to simplify the production of tetrahedral Earth models is presented.

5.1 Development of Tetrahedral Meshes

The three dimensional tetrahedral models used in this project were based on Datamine (CAE, 2010) wireframe models of the Eastern Deeps zone of the Voisey's Bay deposit. The Datamine models were developed by Vale Inco from borehole data (Fig. 5. 1). Unfortunately these wireframes as they are exported from Datamine are not appropriate for the meshing and modelling done in this project. They contain too much very fine scale detail increasing the complexity of the final mesh. However, the geophysical techniques being applied are not able to resolve this fine detail and as such it is an unnecessary complication. As each surface of the wireframe has been constructed separately there are intersections between the surfaces. In order to create the tetrahedral meshes all bodies must be surrounded by enclosed surfaces; however, the wireframe meshes aren't always closed surfaces. As such, the Datamine

wireframes were used to create a higher quality model to be used in the modelling process.

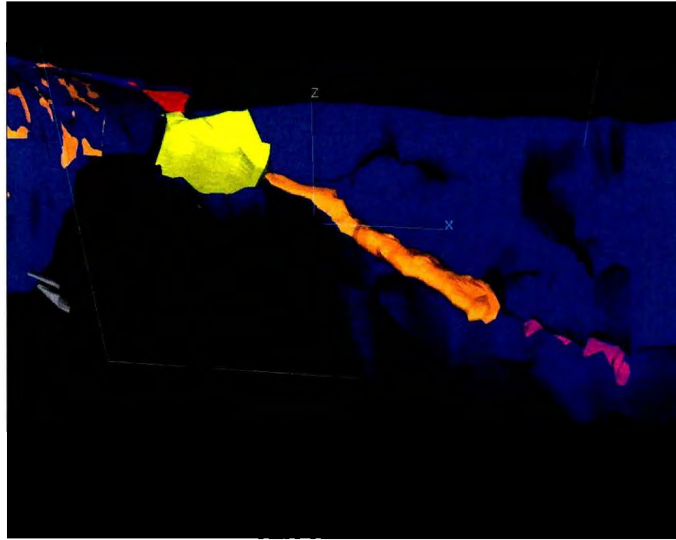


Fig. 5. 1: Datamine model of the eastern portion of the Voisey's Bay deposit looking towards the north. The orange body is the Eastern Deep's zone. The portion of the Voisey's Bay deposit model used is centred around 57000m East, 47500m North. It has an east-west extent of 2600m, and north-south extent of 1200m and a depth of 1210m.

Cross-sections through the Eastern Deeps zone were extracted every 10m along a north trending line as .jpeg images. Two variations of these cross-sections were used during model building; one at a large scale focusing on the sulphide ore body (Fig. 5. 2) and the other at a smaller scale showing as much of the troctolite pluton as possible (Fig. 5. 3). A selection was made from the extracted sections of those to be used in model building. If there was little change in the model between cross-sections 10m apart one was discarded and the section 10m past it was used. This was done to reduce the amount of work that was done. The selected cross-sections were printed and the digitization of the section was started.

5.1.1 Developing a Tetrahedral Model from a Surface Wireframe

The process of converting the, at times intricate, Datamine wireframe surfaces into a tetrahedral mesh was a tedious, time consuming process accomplished mostly through hand drafting. The tetrahedral meshes were produced using Tetgen (Si and Gartner, 2004, Si and Gartner, 2005), as such the surfaces had to be first described in a .poly file. This file type consists of three parts: a list of nodes, a list of facets, and information about the regional attributes. Nodes are points defined by three unique spatial co-ordinates. A facet is a planar element consisting of at least one polygon. In Tetgen a polygon is defined as a closed two dimensional shape defined by line segments between at least three nodes. All of the polygons in a facet must be coplanar. The regional attributes assign identification numbers to the individual, in this case geological, units. These identification numbers were later used to assign physical property values to the rock units.



Fig. 5. 2: A Data mine cross-section at large scale showing as much possible detail of the ore body (orange/red) as possible.

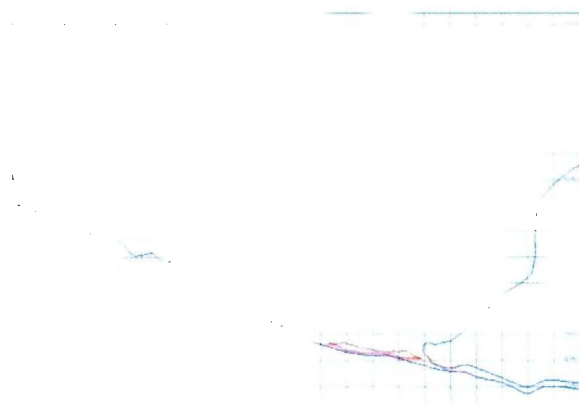


Fig. 5. 3: A small scale Datamine cross-section showing the full troctolite pluton.

5.1.1.1 Modelling the First Cross-Section

Model building was started by modelling the sulphide body in the Eastern Deeps zone. The writing of the .poly files was started with the southern-most Datamine cross-section. Nodes were selected on the boundary between the sulphide ore body and the troctolite. The selection of nodes should be done carefully to ensure that there are an adequate number of nodes to define the shape of the boundary but that excessive detail is avoided to minimize the complexity of the mesh. Generally the number of nodes selected on a cross-section does not greatly exceed the number on the preceding cross-section. The locations of the nodes were recorded into the nodes section of the .poly file. The following is an excerpt from the nodes list of a .poly file where the first row indicates the number of nodes in the poly file, the number of dimensions and two place holders. The list of nodes gives the node identification number, and the x, y, and z co-ordinates of the node.

```

# Part-1: Node List
#Node Count, dim, attrib., bound
765 3 0 0
#id, x, y, z
1 56080 42100 5210
2 56140 42100 4950
3 56400 42100 4850
4 56820 42100 4750

```

The first facet was defined by all of the nodes on the first cross-section and limits the southern-most extent of the ore body (Fig. 5. 4). This facet was then recorded in the facet list of the .poly file. An example of a facet list is shown below. The first line of the list indicates the total number of facets in the list and a place holder. Each facet is defined by three lines. The first is a comment line indicating the facet number. The second line indicates the number of polygons in the face; in this project this was always 1. The third line defines the nodes that make up the polygon. The first number on this line indicates the number of nodes in the polygon. The following numbers are the node indices of the nodes in the polygon in the order they are seen in the polygon.

```

#Facets
1040 0
#1
1
7 1 2 3 4 5 6 7
#2
1
3 8 9 1
#3
1
3 1 2 9
#4
1
3 2 9 10

```

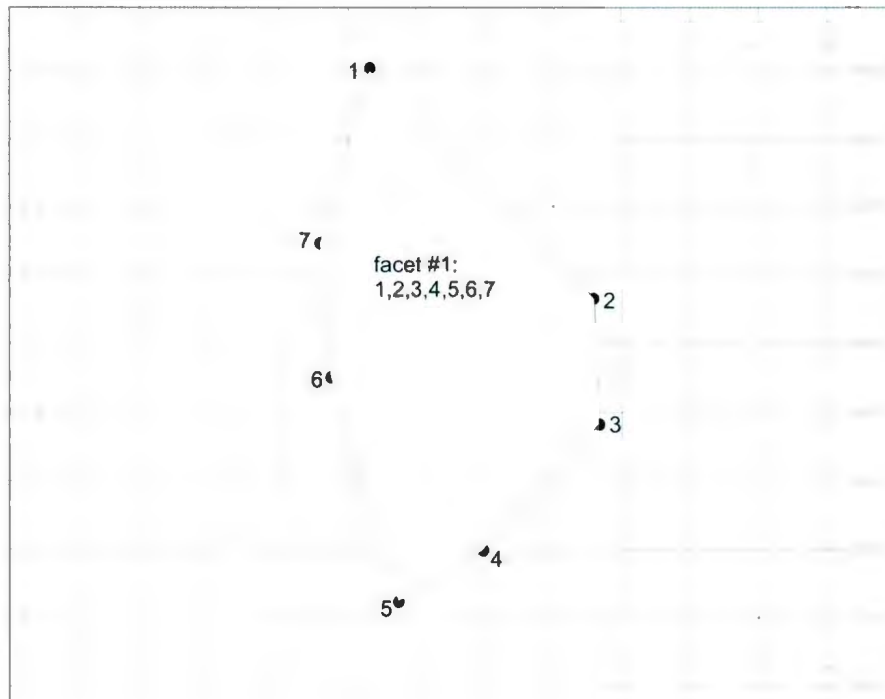


Fig. 5. 4: Node selections and facet selection on the southern-most Datamine cross-section. The yellow line is the actual intersection between the ore and troctolite and black numbered dots represent the nodes selected along this contact.

5.1.1.2 Modelling the Second Cross-Sections

The nodes selected on the first cross-section were then transcribed by hand onto the next cross-section, which was extracted 10m to the north. Nodes were chosen for the second cross-section, and were recorded in the .poly file. Facets were defined connecting the nodes of the second cross-section to those of the first forming a collection of triangles stitching the sulphide-troctolite contact in the first cross-section of the contact in the second cross-section (Fig. 5. 5). It is crucial that this stitching is done with care to avoid the creations of triangles with a high aspect ratio as well as holes and intersections in the mesh. In cases where very high aspect ratio triangles

appear necessary occasionally the insertion of nodes to split up the elongate triangle can be used to remedy the situation.

To facilitate the determination of the stitching facets projections of the nodes in the northing-elevation plane where the x-axis is the northing and the z-axis is the elevation were drawn to either side of the cross-section (Fig. 5. 5). The sketch to the right of the cross-sections is a projection looking from the east and only those nodes on the east side of the two cross-sections are included. The sketch to the left of the cross-sections is a projection looking from the west and only includes the nodes on the west side of the two cross-sections. The nodes with the highest and lowest elevations from both cross-sections are included in both projections ensuring that there are no gaps in the stitching facets. A temporary facet was created using all of the nodes assigned to the second cross-section in order to create an enclosed volume which could be tested for errors.

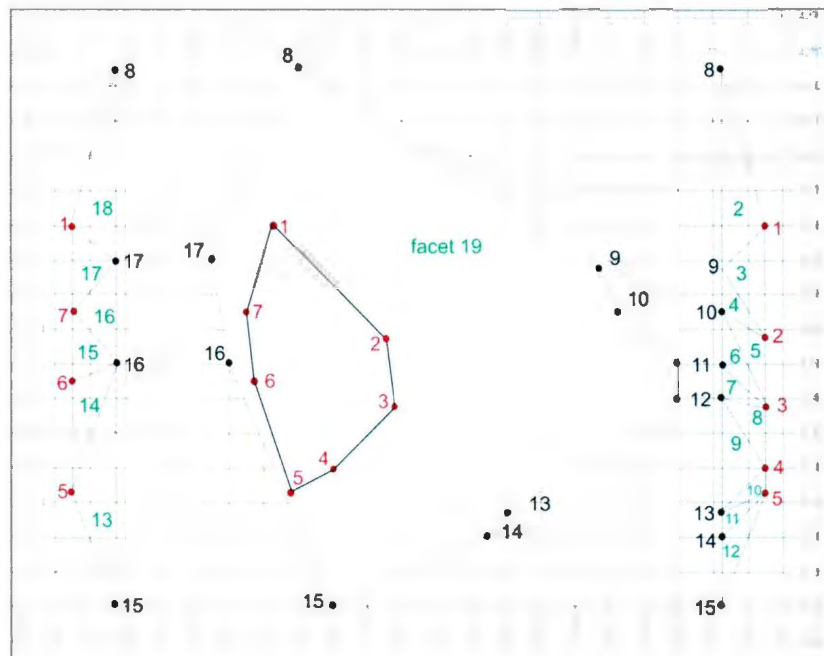


Fig. 5. 5: Node selection and facet formations for the second cross-section. The x-axis of the project is the easting and the z-axis is the elevation the red nodes are those transcribed from the first cross-section. The black nodes are those chosen for the second cross-section. The green numbers with in the enclosed shapes are the facets defined for this cross-section. Facet 19 is the temporary facet which is removed after the completion of the testing of this model.

5.1.1.3 Testing For Errors

Due to the nature of hand drafting and transcription of all the node and facet information the process of creating the tetrahedral meshes was fraught with human error. As such, it was necessary to test the .poly file rigorously after each cross-section. The first step in the error checking process is to create a .vtu file from the .poly file by running the utility *poly2vtu* which was written by Dr. Lelièvre. These .vtu files can be read by the 3D viewer *Paraview*. A close visual examination of the .vtu files often revealed any major flaws the .poly file.

Findholes, written by Dr. Lelièvre, is a utility which checks the edges of each facet to ensure that there is an adjacent facet. For example; in Fig. 5. 6 there is no facet defined for the node combination 4, 2, 5. *Findholes* would indicate the presence of the hole by providing the three line segment bounding the hole: 4, 2; 2, 5; 5,4. If *findholes* indicates that there are holes in the surface described in the .poly file then the outputs from *findholes* in conjunction with the .vtu file produced above can be used to determine which facets were incorrectly formed or missing and facilitate the corrections. Further testing of the .poly file can't be continued until all the holes have been fixed. If there are no holes found in the .poly file testing can continue without changes.

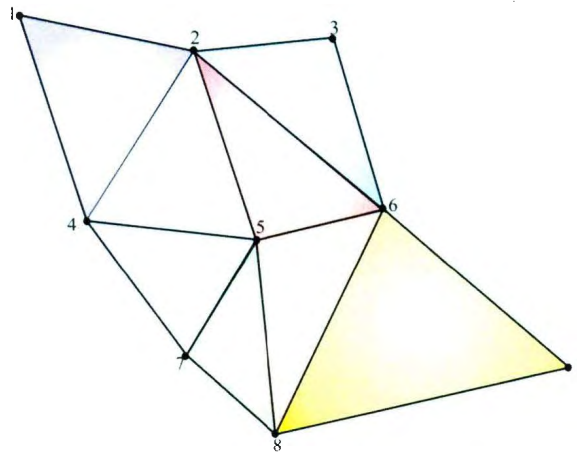


Fig. 5. 6: An example of a hole in a poly file.

The next steps involve the production of tetrahedral meshes of increasing complexity using *Tetgen*. The initial test is to run *Tetgen* without any flags. This creates the simplest possible tetrahedral mesh from the .poly file. As this mesh contains no limit

on the size of cells or their aspect ratio it is not appropriate for modelling. However, its simplicity makes it a good test of the quality of the .poly file. If running *Tetgen* in this way produces any errors it is likely that there is a major formatting error in the .poly file, such as an incorrect number of facets or nodes having been defined.

Once a simple mesh has been produced from the .poly file a series of tests increasing the complexity of the resulting mesh are performed. *Tetgen* was run a second time with the *-d* flag. This will test for intersecting facets in the .poly file. If intersecting facets are found in the poly file the outputs of *tetgen -d* in conjunction with the .vtu file produced above were used to correct the .poly file. Outputs from the *-d* flag identify which facets are intersecting by the facet identification numbers of the two facets. For this reason the .poly file was created with comment lines indicating the facet identification number. This is not necessary for formatting of a .poly file; however, it makes the correction of intersecting facets much easier. The *-d* flag can only be used in isolation; once the .poly file is proven to be free of intersecting facets the *-d* flag was not included in the command line.

Further complexity is added using the *-pq* flag, which imposes restrictions to the internal angles of the tetrahedrons imposing a quality mesh; volume restriction flag, *-a#*, where # was a maximum volume of the tetrahedrons; and the *-A* flag was used to assign the attributes defined in the .poly file to the tetrahedrons. After each mesh was constructed the utility *mesh2vtu*, written by Dr. Lelièvre, was used to create .vtu files of the meshes which could be inspected in *Paraview*.

5.1.1.4 Modelling Subsequent Cross-Sections

Once a .poly file passed through testing without errors a new cross-section can be added. The first step was to remove the temporary facet which created the enclosed volume for testing. Then the nodes from the most recent cross-section were transcribed to the new cross-section and the same process given for the first two cross-sections was used to add the new cross-section into the model. After the addition of each new cross section, the testing of the .poly file should be carried out again. The correction of errors after several cross-sections have been added is much more difficult.

The distance separating the cross-sections varied and which sections were chosen was based on the amount of change in the shape and position of the boundaries between the geological units. When there was a great deal of change a separation of 10m between sections was chosen, however, in areas of little change separations between sections were as large as 40m. This flexibility decreased the time it took to construct the models. In total 39 sections were used to construct the sulphide-troctolite boundary and 37 were used to construct the troctolite-gneiss boundary.

As the troctolite-gneiss boundary and the sulphide-troctolite boundary were constructed separately it was necessary to combine the two .poly files. This was accomplished using the utility written by Dr. Lelièvre called *combinepoly*. Tests after the combination of the two models revealed a great number of intersecting facets. Intersections between these two surfaces are to be expected as footwall incursion of sulphide as veins hosted in the footwall gneiss are not uncommon. For simplicity, it

was decided that the sulphide-troctolite boundary in this model should be within the troctolite-boundary. As such, the .vtu files created using *poly2vtu* and the outputs obtained from running *tetgen* with the *-d* flag were used to adjust the location of nodes along the edges of the troctolite-gneiss boundary and the sulphide-troctolite boundary until the sulphide-troctolite boundary was entirely enclosed within the troctolite-gneiss boundary.

5.1.1.5 Creating a Bounding Block

The model needed to be enclosed within a block which would enclose all gravity stations and seismic tomography source and receiver locations. This was accomplished by creating five walls of the block which were larger than the extent of the troctolite-gneiss boundary. The top of the block was created by stitching the top surface of the troctolite body into the top surface of the bounding block. This was done by plotting the nodes that lie along the top edge of the troctolite body onto the northing-easting plane (Fig. 5. 7) and forming multi-node facets from them and the nodes defining the outer edge of the bounding block. The outer edges of these facets are the outer edges of the bounding block (Fig. 5. 8).

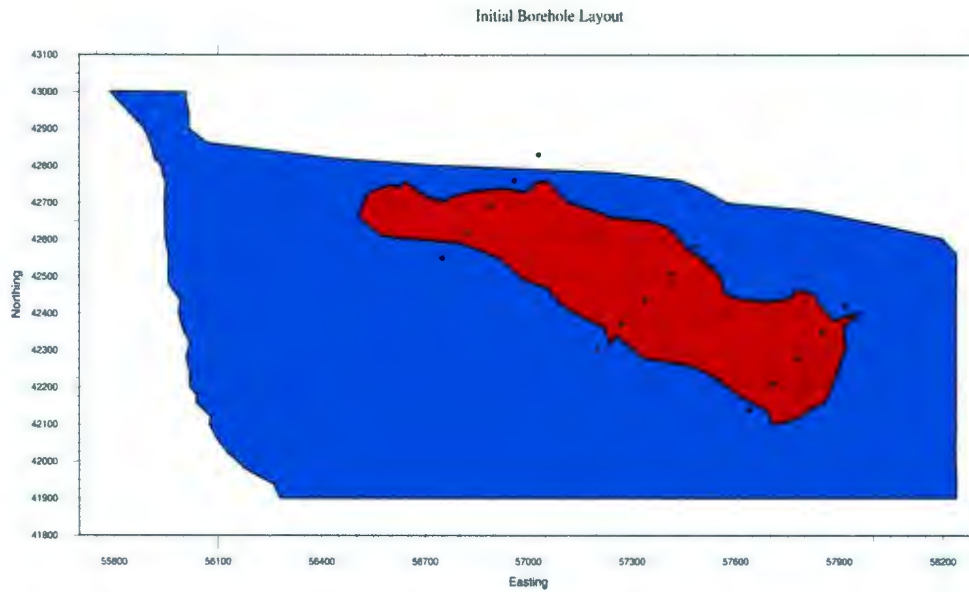


Fig. 5. 7: A “geological” map showing the surface exposure of the troctolite pluton within the footwall gneiss. The blue area indicates the surface exposure of the troctolite body, the red area is a projection to surface of the sulphide body, and the red dots are nodes on the edge of the upper surface of the troctolite (the black dots show the location of a hypothetical set of the boreholes).

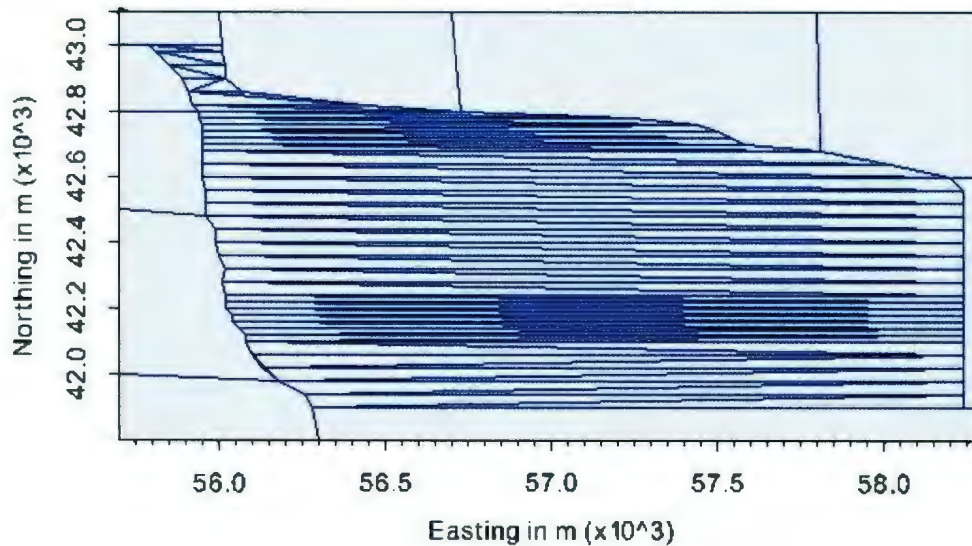


Fig. 5. 8: The upper surface of the 3D earth model showing out lines of the facets in blue.

5.1.1.6 Meshing the Final Model

The final model created consisted of a sulphide-troctolite boundary contained within a troctolite-gneiss boundary, all of which is enclosed in a block. The volume inside the sulphide-troctolite boundary was assigned the physical properties of massive sulphide. The volume outside of the sulphide-troctolite boundary but inside the troctolite-gneiss boundary was assigned the physical property values of the troctolite. The volume outside of the troctolite-gneiss boundary but within the block was assigned the attributes of the felsic footwall gneiss (Fig. 5. 9). The quality of the mesh was enforced using a combination of the internal tetrahedral angle restriction flag -q and the maximum cell value restriction flag -a. The maximum cell size set for a mesh depended on the use to which the mesh was being put. The maximum cell sizes are tabulated in Table 5.1. The necessity of the different maximum cell size meshes is discussed in more detail later.

Table 5. 1: Tabulation of the maximum cell sizes used in mesh generation.

Mesh Name	Maximum Cell Volume
Very Fine Mesh	1000 m ³
Fine Mesh	10 000 m ³
Moderate Mesh	50 000 m ³
Coarse Mesh	100 000 m ³
Very Coarse Mesh	250 000 m ³

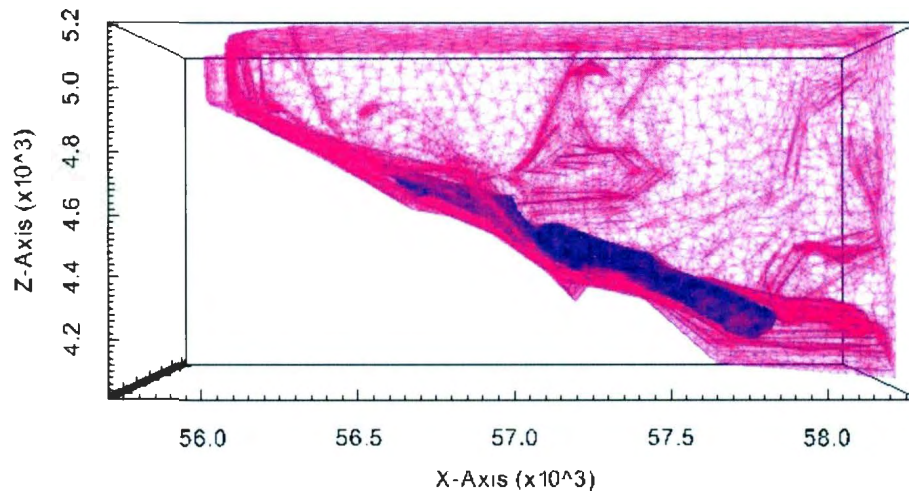


Fig. 5. 9: Figure showing a version of the final model where meshing has been done using a maximum cell size of $100\ 000\text{m}^3$. The outer block indicates the maximum extent of the model, the pink mesh is the troctolite body depicted by the facets on the contact surface between the troctolite and the gneiss, and the blue mesh is the sulphide body depicted by the facets on the contact surface between the sulphide and troctolite.

5.2 Developing Simpler Models for 3D Inversion Tests

One of the key findings of the 2D inversion tests was the understanding that different parameters could seriously affect the quality of an inversion. The problem with completing a comprehensive battery of test inversions using the 3D model of the Eastern Deeps zone is that the model is very large and the computer time and memory required to run an inversion can become prohibitive. As such, simplified models were created to be used for testing different factors affecting inversion such as parameters, gravity station location, and seismic source and receiver layouts.

5.2.1 The Block Model

The first simplified model consists of a rectangular prism in a homogenous half space.

The size of the prism and its orientation were closely based on the sulphide-gneiss boundary. The enclosed volume around the sulphide was designed to be as small as possible in order to minimize the size of the inversion problem while accommodating sufficient space to contain all data collection stations (Fig. 5. 10). This model was created using a utility called *blocks2poly* which was developed by Dr. Lelièvre.

Blocks2poly allows the user to design a .poly file by describing the dimensions and orientations of the blocks.

5.2.2 The Sulphide Model

The Sulphide Model consists for the sulphide body produced during the creation of the full Eastern Deeps model in a homogenous half space (Fig. 5. 10). By eliminating the troctolite body the whole model could be made significantly smaller and the entire model size more comparable to that of the block model. This model was used after tests were completed with the block modelled in order to add increased complexity and making the scenario more realistic while maintaining a relatively small model.

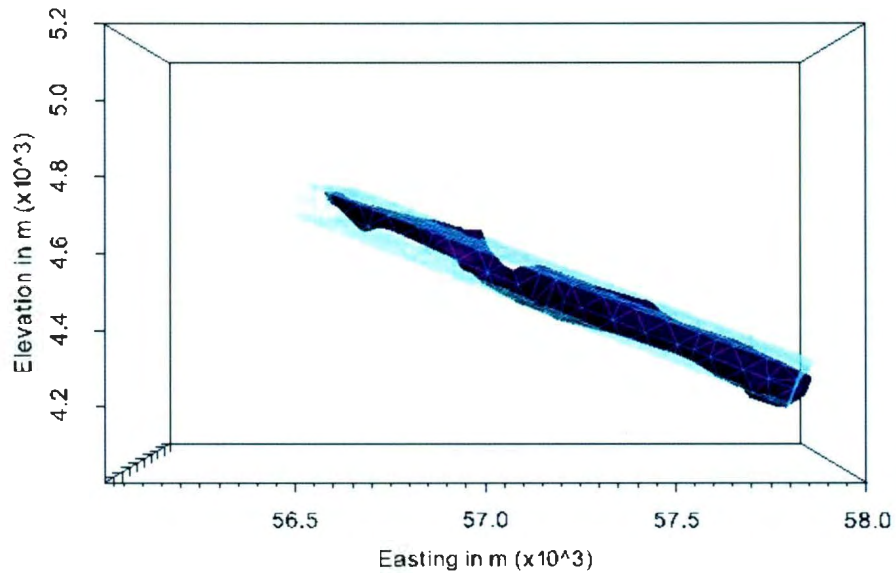


Fig. 5. 10: A combination of the block model and the sulphide model; showing a rectangular prism (in light blue) approximating the sulphide body (in purple) from Fig. 5. 9. The grey enclosing block shows the limits of the models which are smaller than the full model of the Eastern Deeps zone (Fig. 5. 9).

5.3 Developing Facet Modeller

The hand development of meshes as described in Section 5.1 is a very time consuming process. The necessity to type in all data introduces in a huge amount of human error into the process, which in turn requires significant time error checking and debugging the meshes after each layer is added. In order to decrease the amount of time required to produce mesh surfaces of good enough quality to use in numerical modelling codes a user interface software package was developed by G. Blades and named FacetModeller.

This program allows for simultaneous visualization of the model in both 2D and 3D (Fig. 5. 11). It also allowed for viewing only specific layers or facet groups at any one

time. Error check tools have been built into the program such as the detection and removal of duplicate nodes, duplication facets, and incorrectly defined facets. It also allows for the user to quickly find particular nodes or facets and in this way enables the user to more quickly locate and fix problems with the mesh.

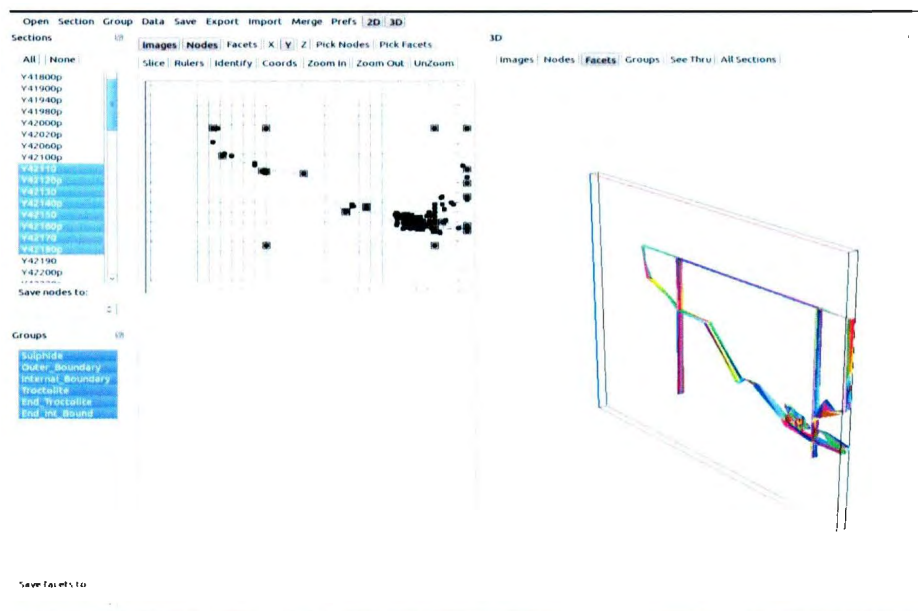


Fig. 5. 11: Screenshot showing both 2D and 3D visualization panels for Facet_Modeller.

Facet_Modeller has, subsequently, been used by others to develop complicated and realistic Earth models in both 2D and 3D (Fig. 5. 12). As it was developed to construct models where cross-sections were available this led to some limitations. In order to be applied to different approaches to constructing these models Facet_Modeller continues to undergo development by Dr. Lelièvre.

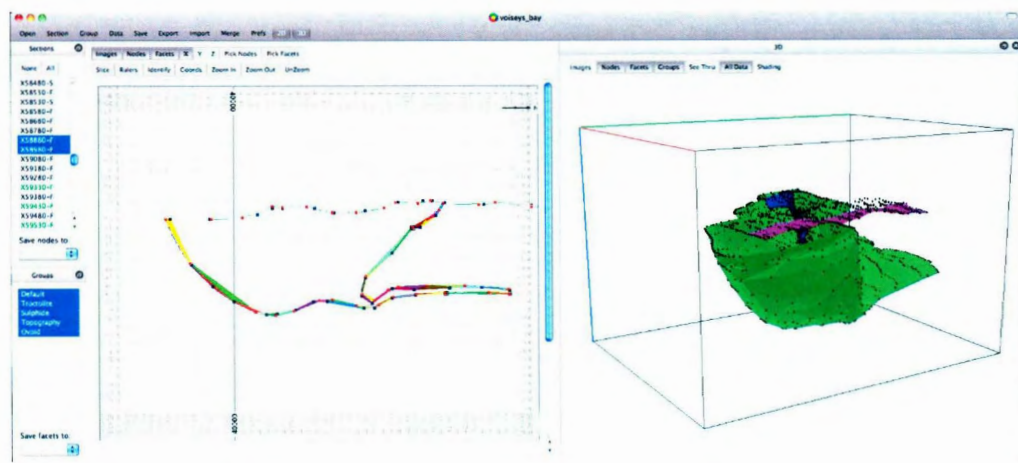


Fig. 5. 12: Screenshot of FacetModeller in use to create of complete model of the Voisey's Bay deposit with a correct topographic surface (picture courtesy of Cassandra Tycholiz).

Chapter 6: 3D Forward Modelling

In this chapter the forward modelling of the 3D models is presented. The choices made in forward modelling in terms of number and location of gravity measurements as well as the seismic arrays is much more important than it was for 2D. The size of the inversion problems for 3D is so much bigger than in the 2D case that the choices made for the datasets can affect the success or failure of the inversion. As such, this chapter consists of a discussion of the placement of gravity measurement locations and the results of gravity forward modelling as well as a discussion of the source-receiver arrays and seismic forward modelling results. All of the forward modelling for gravity (Jahandari, 2011) was completed using the *gravity_fwd* software discussed in Section 2.3.1 and all the seismic forward modelling (Lelievre, et al., 2011) was completed using the *seismics_fwd* software discussed in Section 2.3.2.

6.1 Seismic Source and Receiver Layout

The arrangement of the boreholes for seismic inversion was crucial as any increase in the number of sources and receivers can drastically increase the size of the inversion problem and thus the computation time and amount of memory necessary. Several different borehole patterns for seismic tomography were tested to find a good balance between the computational demands of the source-receiver array and a sufficient amount of data coverage to acquire good inversion results.

6.1.1 Panel Arrangement

The first borehole arrangement consisted of three panels of five boreholes (Fig. 6. 1) across the strike of the sulphide body with borehole separations of no more than 100m. This arrangement of sources and receivers was based on advice from Dr. C. Hurich, advice influenced by his experience working in the field. The distance between boreholes is a very important consideration. As seismic waves move through the ground they are attenuated and as such if the distance between the sources and receivers becomes too large the seismic waves will have attenuated so much that the receivers would not be able to differentiate between the arriving waves and background seismic noise. Hence, 100m is a typical maximum separation one would want. In this arrangement there are 144 receiver locations and 144 sources with a total of 1728 source-receiver pairs. No data is collected between the three panels.

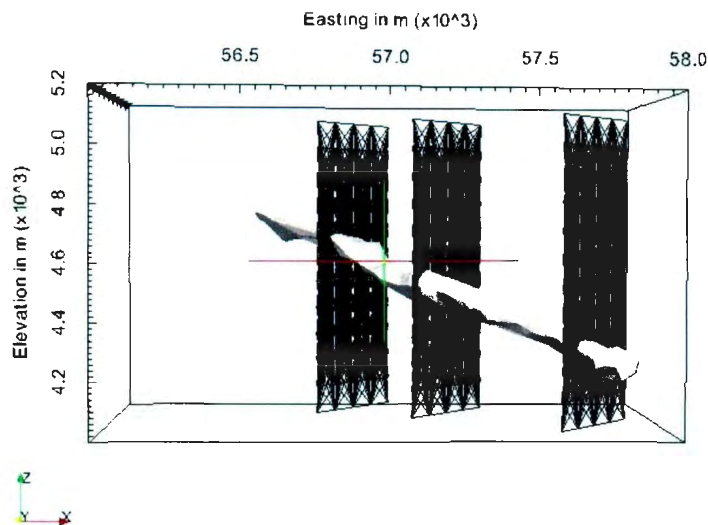


Fig. 6. 1: Visualization of the three borehole panels. The model extends 1300m along the axis into the page.

6.1.2 Grid-Like Borehole Layout

The second seismic source-receiver array considered allows for data collection in multiple directions, rather than simply across strike. The borehole locations are laid out in a pattern reminiscent of a grid (Fig. 6. 2). In this array there are 144 unique seismic sources and 1140 unique seismic receiver locations. In total this results in 30240 source-receiver combinations.

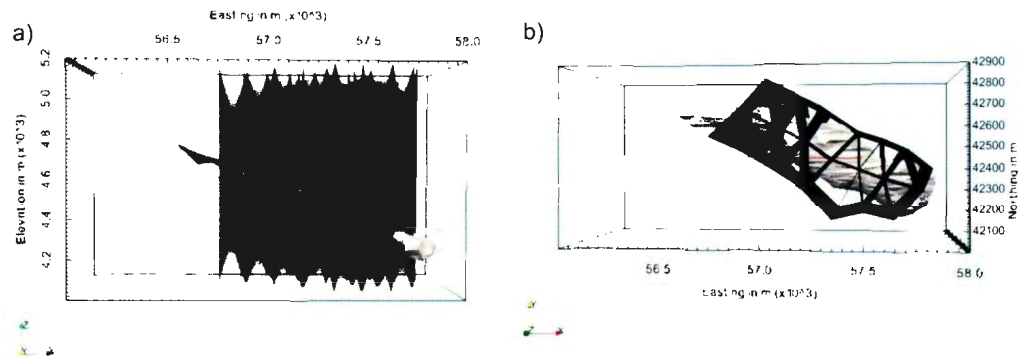


Fig. 6. 2: Side (a) and top (b) views of the straight paths from sources to receivers from the grid-like borehole layout. The surrounding block is the same as is seen in Fig. 6. 1.

The third source/receiver arrangement consisted of a reworking of the grid-like array. The principle of reciprocity states that there should be no difference between the travel-time for seismic waves travelling from A to B than from B to A. However, the method which is used for calculating the optimization equation in the inversion code makes it much more efficient if there are fewer sources and a larger number of receivers. As such an inversion for data shot A to B and B to C will have exactly the same forward modelling result as if the data was collected shooting from B to A and C however the inversion problem would take far longer for the A to B, B to C

situation as there are double the number of sources. So the second example was reworked to preserve the number of source receiver pairs but decrease the overall number of sources.

6.1.3 Starburst Layout

Two different “Starburst” layouts of sources and receivers were tested. These arrangements used the minimum number of source and receiver combinations to provide adequate data coverage without taking into consideration the attenuation of the seismic waves. As such the boreholes for the seismic array were placed much further apart than those in the previous layouts described above. This is done to reduce the computational demands of the inversion problem.

6.1.3.1 Starburst I

The first Starburst layout consisted of 12 sources in a single borehole located roughly at the centre of the model. The seismic waves propagated out from the sources to 96 receivers located in 8 boreholes arranged around the edges of the anomalous block (Fig. 6. 3). This layout of sources and receivers has a total of 1152 source-receiver pairs.

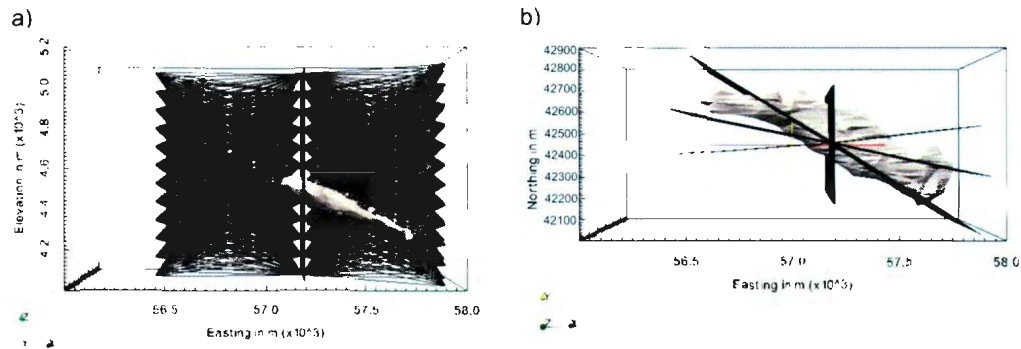


Fig. 6. 3: Straight ray paths for the Starburst I layout of sources and receivers a) side view b) top view.

6.1.3.2 Starburst II

The second Starburst layout consists of an additional 48 receivers, 12 in each of 4 additional boreholes. This is done to improve the coverage of the model and to determine how much extra computational time and memory is required to invert the data (Fig. 6. 4). The results from inversions using the Starburst II layout determine if the improvements in the model quality outweighs the increase in computational time and memory usage caused by the increase in the number of receivers. This layout consists of 1728 source-receiver pairs.

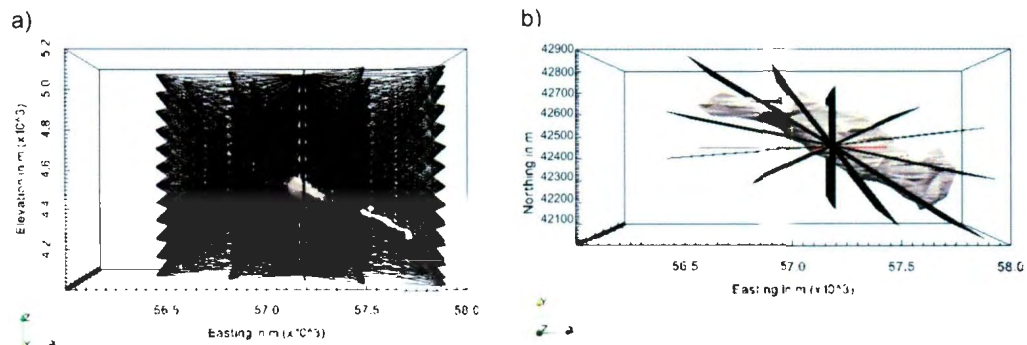


Fig. 6. 4: Straight ray paths for the Starburst II layout of sources and receivers. a) Viewed from the side and b) viewed from above.

6.2 Seismic Forward Modelling Results

In this section forward modelling results are presented. The seismic forward modelling in 3D was carried out using the fast marching method (Lelievre, et al., 2011) as was used in 2D (Section 2.3.2). Due to the similarity between the results for the different models the results presented below are the results of forward modelling the block model. The version of the block model used in forward modelling had a maximum cell size of 1000m^3 and contains 4 084 686 cells. This version was chosen to avoid any issues with high aspect ratio cells and to ensure that the plane wave approximation made in the fast marching method is preserved (Lelievre, et al., 2011).

6.2.1 Panel Layout

The travel times calculated during the seismic forward modelling of the block model using the grid-like source and receiver layout range from 16.69ms to 188.03ms (Fig. 6. 5). Similarly to the results from forward modelling seen in 2D (Fig. 3.11) the data is dominated by the effect of the distance between the source and receiver for which

the travel time value is being displayed. In Fig. 6. 5 each square represents the travel times for a set of sources and the sources at which travel times are measured for that set of receivers. In the case of this example all the sources are located in a single borehole and the receivers in a neighbouring borehole.

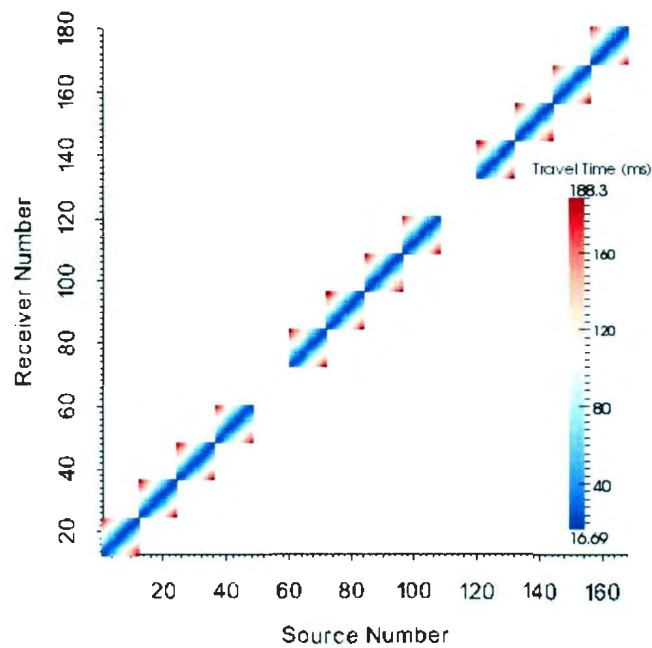


Fig. 6. 5: Resultant travel time data from the forward modelling of the block model using the panel source-receiver layout.

Anomalous travel times are the difference between the travel times calculated during forward modelling and what the travel time would be for the same path length if all cells were assigned the background slowness (see Section 3.3). In Fig. 6. 6 it can be seen that the anomalous travel times occur most often in the upper left and lower right quadrants of each panel. This can be seen more clearly in an enlargement of the four central panels shown in Fig. 6. 7. This is an effect of the location of the anomalously slow material in relation of the source and receiver locations in the boreholes. When

the sulphide body lies between the source and receiver locations a higher anomalous travel time is produced. In Fig. 6. 8 it shown that non-zero anomalous travel times only exist if the source and receiver are on opposite sides of the sulphide body; as only in that case would the wavefront pass through the sulphide body. As such, sources near surface (which have lower source numbers for any given borehole) will have higher anomalous travel times when paired with receivers that are positioned deeper in borehole (thus having higher receiver numbers). The exact distribution of the anomalous travel times depends greatly on the position, shape and slowness of cells between the source and receiver pairs.

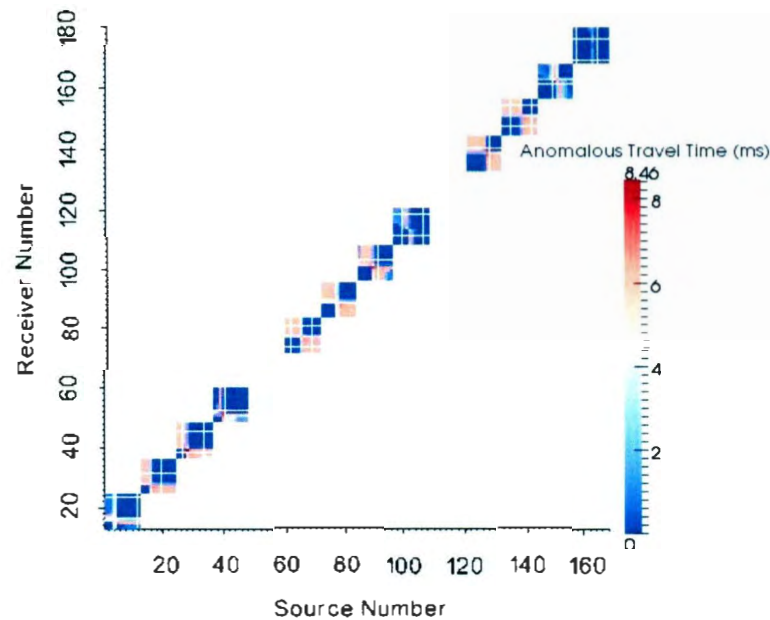


Fig. 6. 6: Anomalous travel-times from the forward modelling of the block model using the panel source-receiver layout.

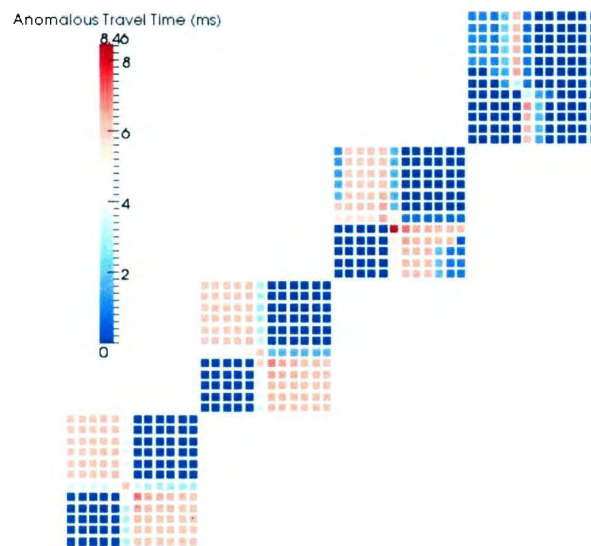


Fig. 6. 7: A zoom into the four central panels in Fig. 6. 6.

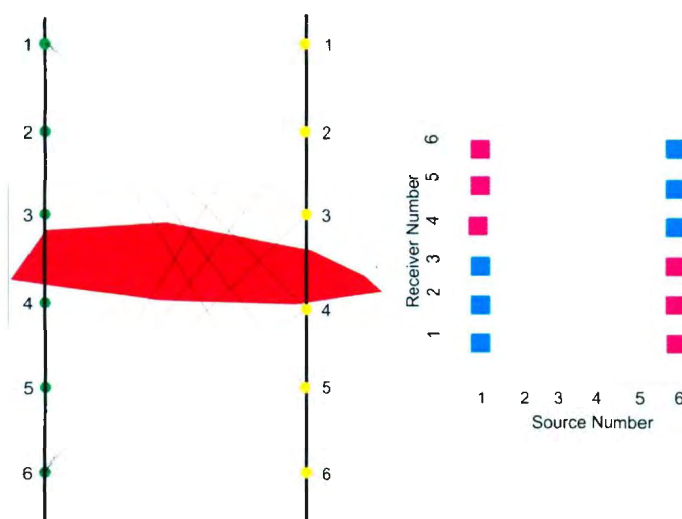


Fig. 6. 8: This figure illustrates the effect of the position of the area of anomalous slowness (red body to left) on the pattern seen in a plot (right side of figure). The thick black lines on the diagram (left) represent two boreholes with the green dots representing source locations and the yellow dots representing receiver locations. The thin black lines represent the wavefront path between sources and receivers. The pink squares on the plot (right) represent anomalous travel times and the blue squares on the same plot represent travel times consistent with the background slowness value.

6.2.2 Grid-Like Layout

The travel times calculated during the seismic forward modelling of the block model using the grid-like source and receiver layout range from 19.86ms to 205.5ms (Fig. 6.9). The anomalous travel times range from 0ms to 15.47ms. As in the panel layout, the location of the anomalous material is strongly influenced by the location of the slow sulphide body. This can be seen more clearly in Fig. 6.11 where the panels indicated in Fig. 6.10 are seen in more detail. This leads to a pattern of shallow sources paired with deep receivers and deep sources paired with shallow receivers tending to have the highest anomalous travel times.

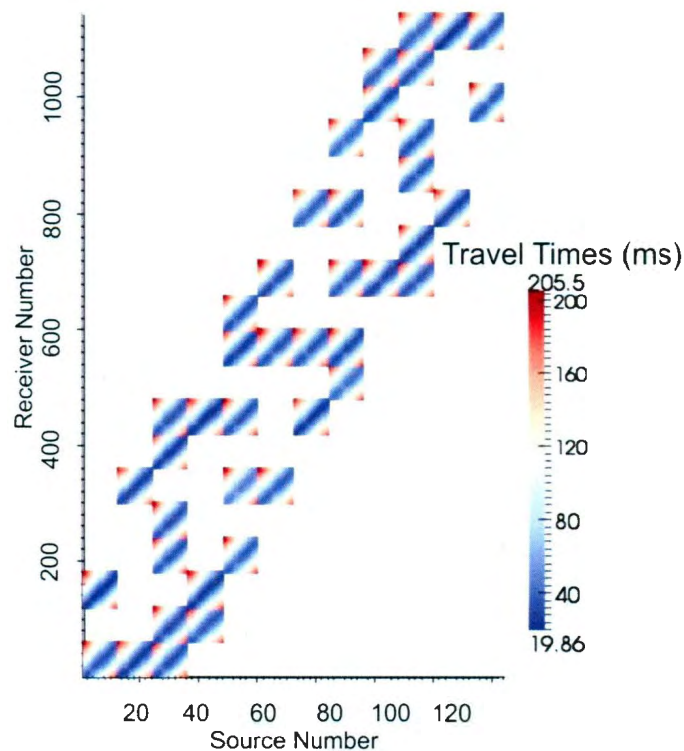


Fig. 6. 9: Resultant travel time data from the forward modelling of the block model using the grid-like array.

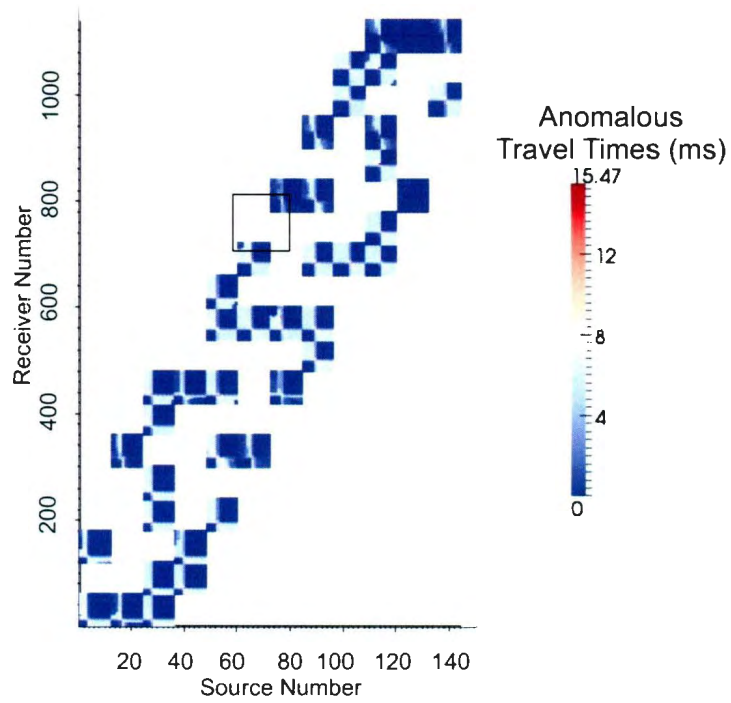


Fig. 6. 10: Resultant anomalous travel times from the forward modelling of the block model using the grid-like array. The area in the black box is shown in more detail below.

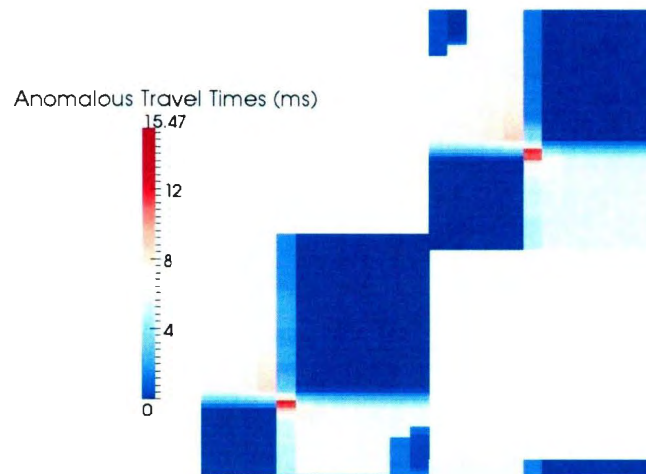


Fig. 6. 11: Zoom into the area surrounded by the black box in Fig. 6. 10.

6.2.3 Starburst I Layout

The travel times calculated during the seismic forward modelling of the block model using the Starburst source and receiver layout range from 46.95ms to 233.32ms (Fig. 6. 12). The anomalous travel times range from 0ms to 12.61ms. The pattern seen in the anomalous travel times for this example is similar to that described for the panel layout in Section 6.2.1. In this example it is seen even more strongly as all the sources are in the centre of the sulphide block and the absence of a troctolite body means that each source will have this case (Fig. 6. 13).

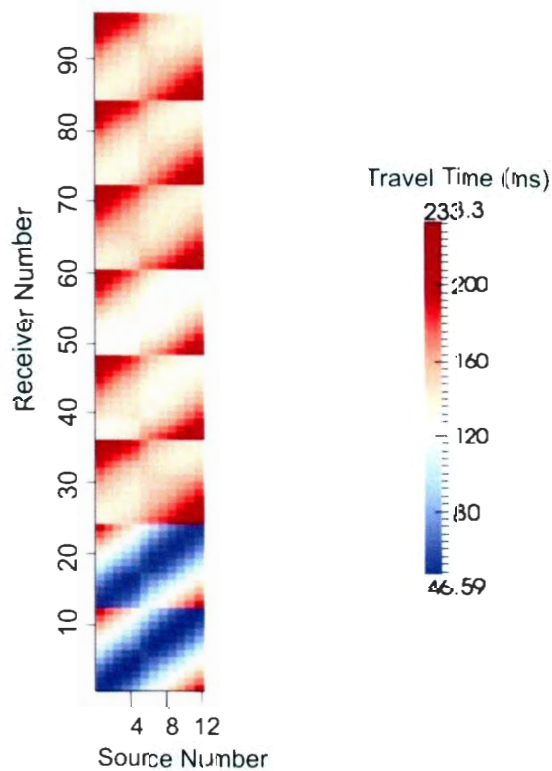


Fig. 6. 12: Resultant travel time data from the forward modelling of the block model.

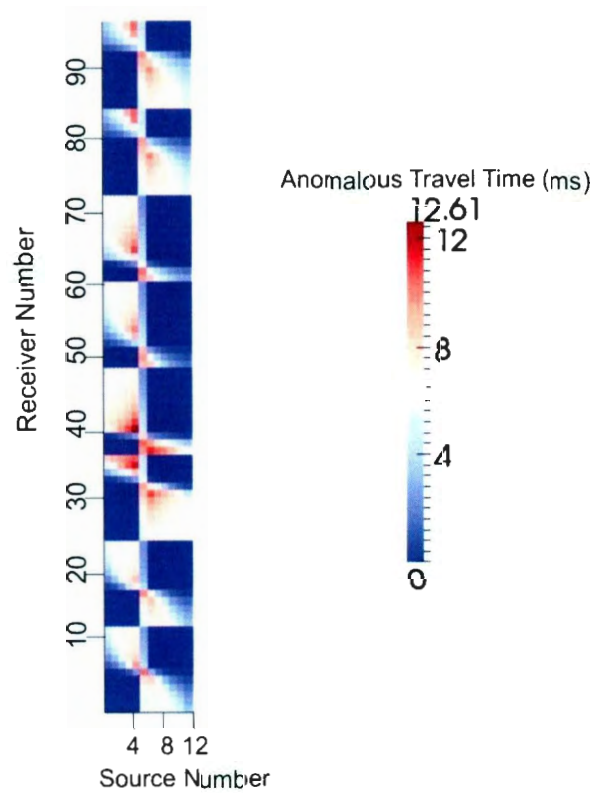


Fig. 6. 13: Resultant anomalous travel time data from the forward modelling of the block model.

6.2.4 Starburst II Layout

The travel times calculated during the seismic forward modelling of the block model using the Starburst II source and receiver layout range from 46.59ms to 233.32ms (Fig. 6. 14a). The anomalous travel times range from 0ms to 13.24ms. The pattern seen in the anomalous travel times for this example (Fig. 6. 15) is very similar to that seen for the Starburst I example (Section 6.2.3) and the reasoning behind it is the same as that explained in Section 6.2.1 .

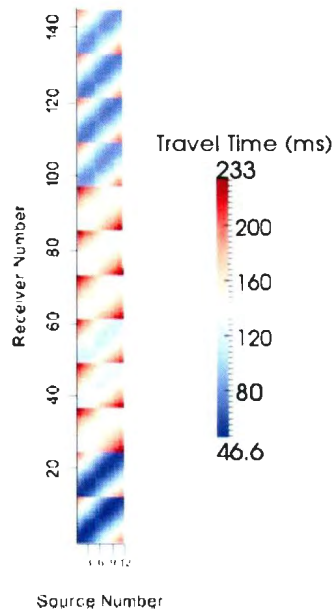


Fig. 6. 14: Resultant travel time data from the forward modelling of the block model.

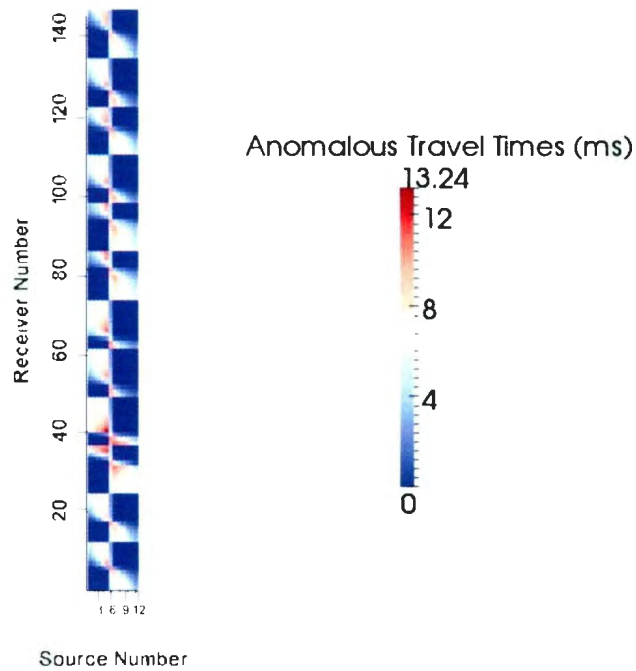


Fig. 6. 15: Resultant anomalous travel time data from the forward modelling of the block model.

6.2.5 Effect of Mesh Coarseness on Seismic Forward Modelling Results

The results from the initial seismic-only inversion showed poor results (this is discussed in more detail in Chapter 7). It was suggested an inappropriate low amount of noise was being added to the data; which, particularly in light of the fact that the inversion mesh was significantly coarser than the forward modelling mesh, could be contributing to these poor inversion results.

Initially the same parameters determined to have worked well in the 2D inversion models of adding a moderate amount (~1%) of noise to the data was used in the 3D case. In order to determine if this amount of noise was indeed too low in light of the coarseness of the mesh and what appropriate noise levels would be a series of tests were run on a simplified block model. The block test model was meshed in Tetgen to produce meshes with five different maximum cell sizes (Fig. 6. 16).

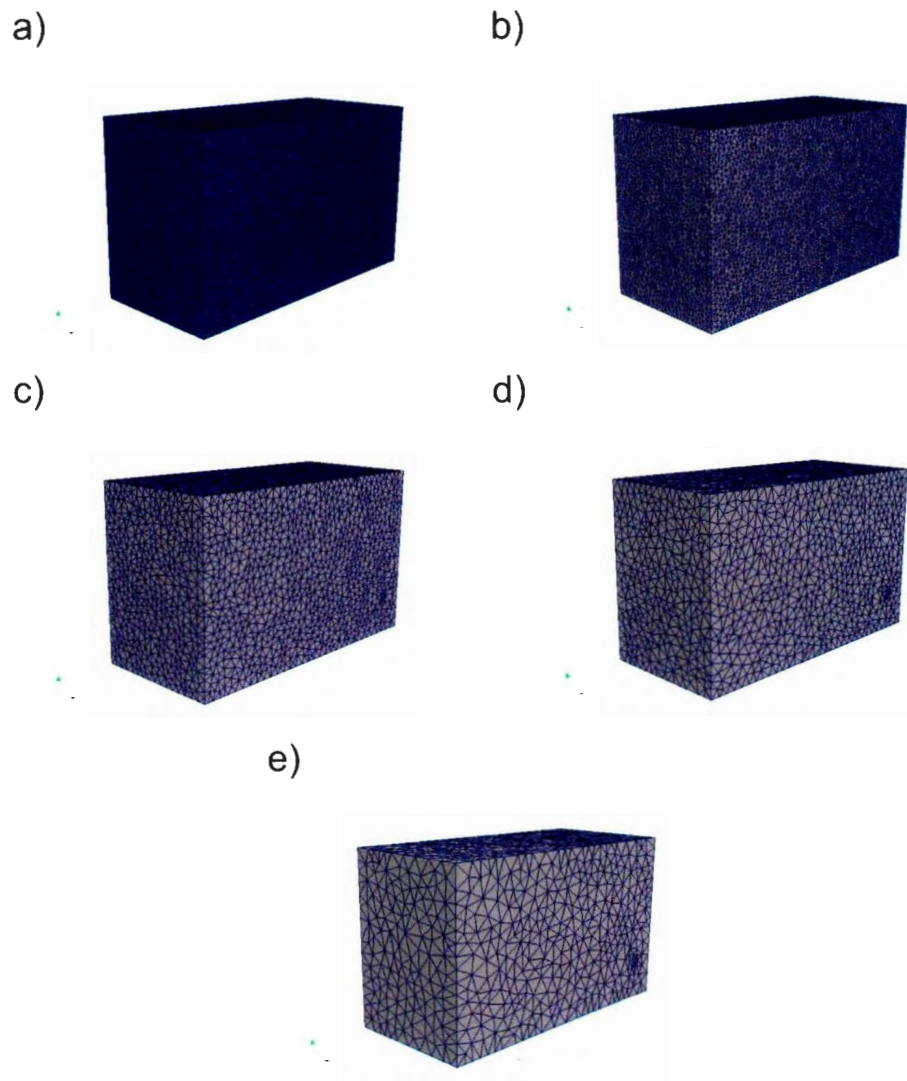


Fig. 6. 16: The block model (see Section 5. 2. 1) meshed with different maximum cell sizes: a) 1000m^3 maximum cell size and 4 084 686 cells, b) $10\ 000\text{m}^3$ maximum cell size and 411 300 cells, c) $50\ 000\text{m}^3$ maximum cell size and 82 369 cells, d) $100\ 000\text{m}^3$ maximum cell size ad 41 792 cells, e) $250\ 000\text{m}^3$ maximum cell size and 17 076 cells.

An approximation made by the fast marching method is that the seismic wavefront moves through a cell as a plane wave (Lelievre, et al., 2011). As such, the results from seismic forward modelling become more accurate as the mesh is made finer as the plane wave approximation will be the most accurate. In these tests the ‘grid-like’

source-receiver array is being used (see Section 6.2.2). In light of the plane wave approximation the travel times calculated from the 1000m³ mesh are considered to be the true seismic travel times for the model.

The results from the other four meshes were compared to those from the 1000m³ mesh by finding the difference between the travel times for each of the source-receiver pairs as follows:

$$difference = |t_{ij}^{1000} - t_{ij}^x| \quad 8.1$$

where t_{ij}^{1000} is the travel time for the i th source and the j th receiver for the 1000m³ mesh and t_{ij}^x is the travel time for the i th source and the j th receiver for x m³ mesh.

The largest difference between the travel times for the 1000m³ mesh and those of the coarser meshes are recorded in Table 6. 1.

Table 6. 1: Summary of the largest travel time differences between the finest mesh and other meshes.

Maximum Cell Size of Mesh	Highest Travel Time Difference (ms)
10 000m ³	4.54
50 000m ³	7.81
100 000m ³	10.13
250 000m ³	15.13

Using the utility *add_noise* various amounts of noise were added to the travel time data from the 1000m³ mesh. The largest absolute amount of noise added to the data for 1%, 2.5% and 5% gaussian noise are recorded in Table 6. 2.

Table 6. 2: Summary of the maximum change to the finest mesh travel time data with different levels of noise.

Amount of Noise Added	Largest Absolute Change to Data
1.0%	5.16ms
2.5%	15.02ms
5%	24.16ms

In order to compare the variations in the travel time data caused by the coarseness of the mesh (Table 6. 1) being used and the variations caused by adding noise to the clean very fine mesh data (Table 6. 2) the maximum absolute difference between the clean 1000m³ data and the noisy/coarse mesh data were plotted graphically. In Fig. 6. 1 the largest absolute difference for each of the meshes was plotted against the maximum cell size for the mesh. The straight lines indicate the maximum absolute difference due to adding 1% and 2.5% noise. It can be seen that only the 10 000m³ mesh adds less error to the inversion than 1% noise. As such, if inversions are being carried out using meshes of greater than 10 000m³, convergence would not be possible unless a greater amount of noise was added to the data being inverted. In the case of the 250 000m³ mesh more than 2.5% noise would have to be added to the data in order to allow for convergence of the inversion problem. In light of these findings it was concluded that increasing the amount of noise added to the data to 2.5% would allow for flexibility in the size of the mesh used for inversion and that whenever possible a 10 000m³ should be used for inversion.

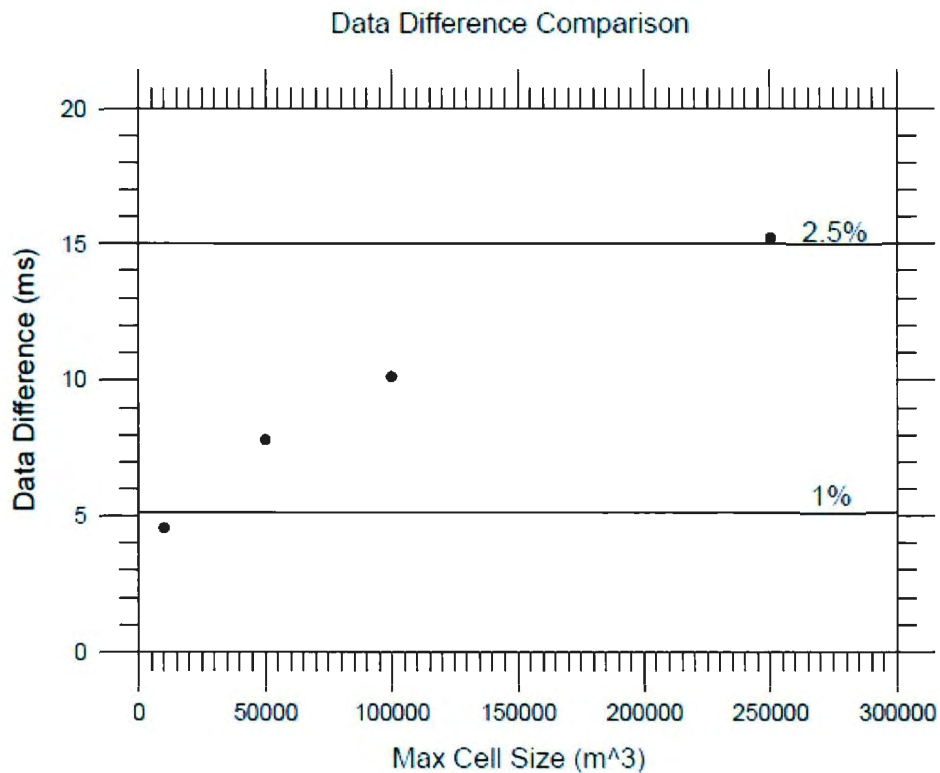


Fig. 6. 1: Comparison between the travel time deviations of various mesh sizes and the deviations caused by noise added to 1000m³ mesh data.

6.3 Gravity Forward Modelling

Similarly to the results from seismic forward modelling, the exact array to be used in gravity forward modelling greatly influenced the results attained during inversion modelling. The inversion results will be discussed in further detail in Chapter 7.

Below is a discussion of the evolution of the gravity measurement arrays used in this project and the synthetic data produced using these arrays in forward modelling.

6.3.1 Gravity Station Layouts and Forward Modelling Results

The process used to determine the arrangement of gravity measurement locations for successful and useful inversion results was a process of trial and error. This process was informed by the findings from the 2D inversion tests and an understanding of the computational challenges presented by 3D inversion.

Surface gravity stations presented a challenge. An array that covers an area adequately, by necessity, consists of many gravity stations. And increases to this number lead to increased computational demands (in the case of the code used in this project the computation time and memory usage generally increase proportionally to the number of gravity observations in the case of the single property gravity inversions). As such, the spacing between the stations for the attempted scenarios varied depending on the dimensions of the array. The larger the dimensions of the surface array the larger the spacing between stations.

The 2D inversion tests showed that using borehole gravity stations greatly improved the code's ability to locate a buried high physical property contrast body. As such, borehole stations are used in 3D as well. In Chapter 7 the effectiveness of using borehole gravity will be discussed in more detail in the light of 3D inversion test results. The number and locations of the boreholes used varied and, in joint inversion, borehole gravity stations always corresponded to the location of seismic source and receiver boreholes.

Gravity forward modelling of the sulphide model (see Section 5.2.2) was conducted for both borehole and surface gravity stations. The results from seismic inversions which are discussed in further detail in Chapter 7 showed that the full Eastern Deeps model was not practical. The gravity inversions and joint inversions were conducted using synthetic data from the sulphide-gneiss model. This preserves some of the geologically realistic nature of the full Eastern Deeps model while reducing its size and complexity.

The forward modelling results for four different gravity measurement location arrays presented in Section 6.3.1 are presented here.

6.3.1.1 Small Surface Array

The first is the anomalous gravity data for surface locations immediately over the sulphide-gneiss model. The surface gravity had a 25m spacing and over the entire top of the inversion block (Fig. 6. 17). The synthetic data shows a small gravity anomaly striking parallel to the sulphide body (Fig. 6. 18).

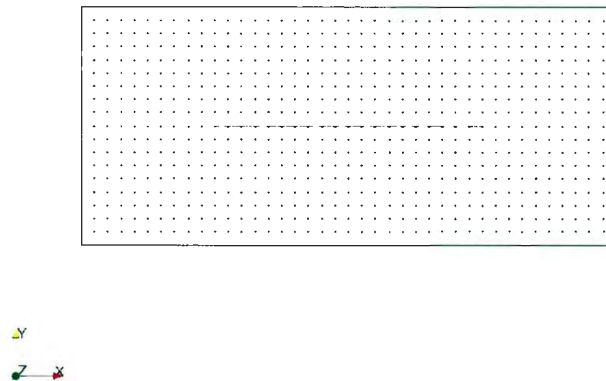


Fig. 6. 17: Small surface array.

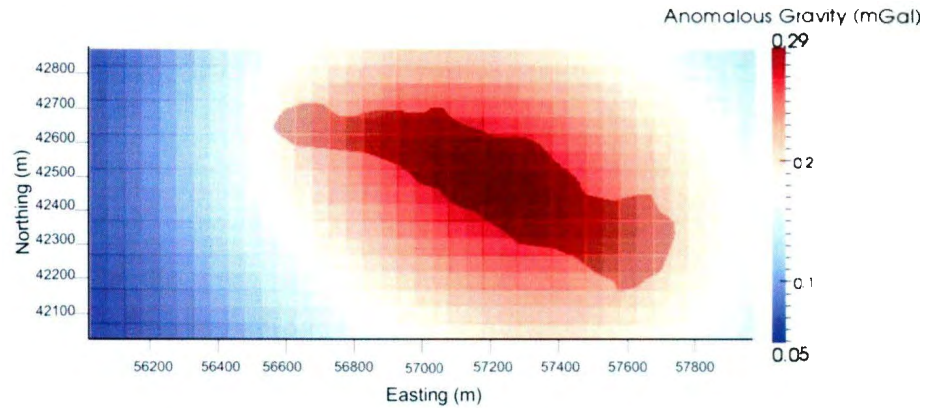


Fig. 6. 18: The anomalous gravity data shown with a surface projection of the sulphide body in the sulphide-gneiss model.

6.3.1.2 Large Surface Array

It is clear that the anomaly shown in Fig. 6. 18 is not the full anomaly. As such a second synthetic dataset was created using only surface stations over the sulphide-gneiss model. The array of gravity stations extends outside of the block sulphide-gneiss model allowing it to see the entire anomaly with gravity measurement locations spaced every 50m (Fig. 6. 19). The orientation of the anomaly is identical to that seen for the smaller array (Fig. 6. 18). However, now the entire anomaly can be seen (Fig. 6. 20).

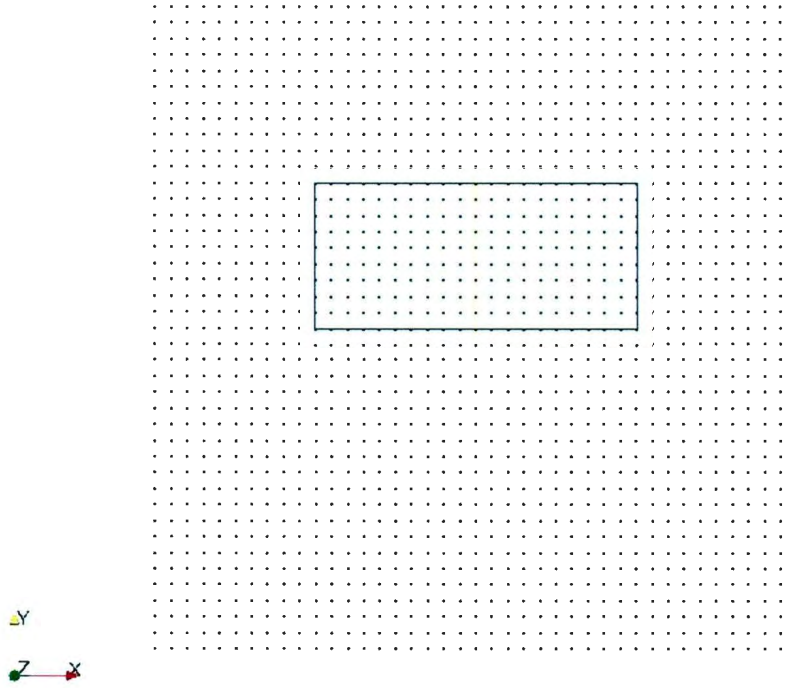


Fig. 6. 19: Birds-eye view of the extended array.

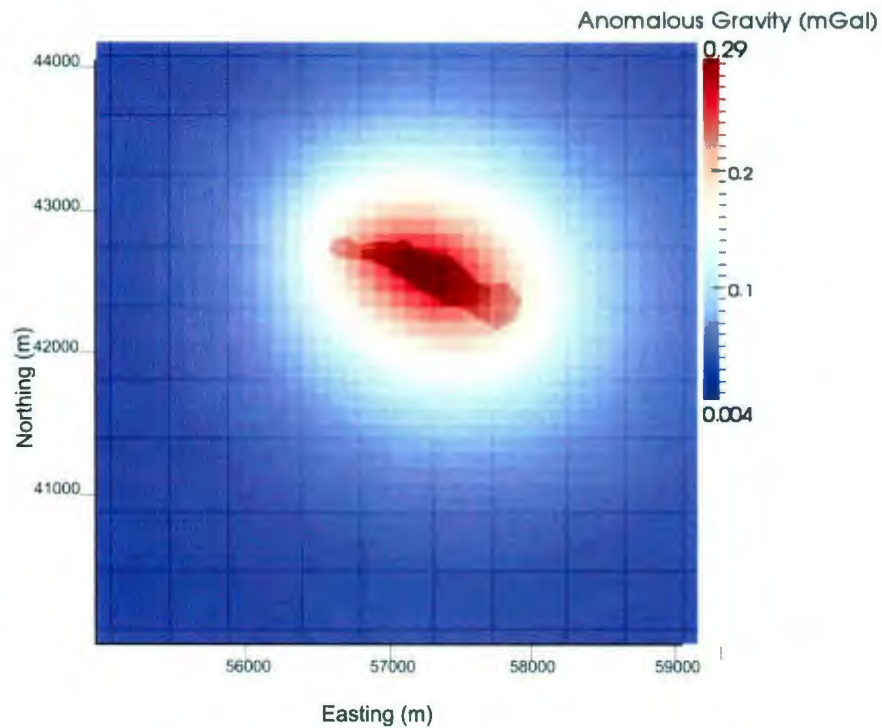


Fig. 6. 20: Results from gravity forward modelling of the sulphide model at surface stations for an extended surface grid.

6.3.1.3 Mixed Surface and Borehole Array

The results from inversions using the two surface gravity measurement location arrays (to be discussed in further detail in Chapter 7) in conjunction with the results seen in the 2D inversions (see Chapter 4) suggested that the use of borehole gravity measurements could improve the inversion results significantly. As such, the third array of gravity measurement locations which is a combination of the large surface array seen in Section 6.3.1.2 and a single borehole of gravity measurements located in the same location as the source borehole from the Starburst I seismic source-receiver array (see Section 6.1.3.1).

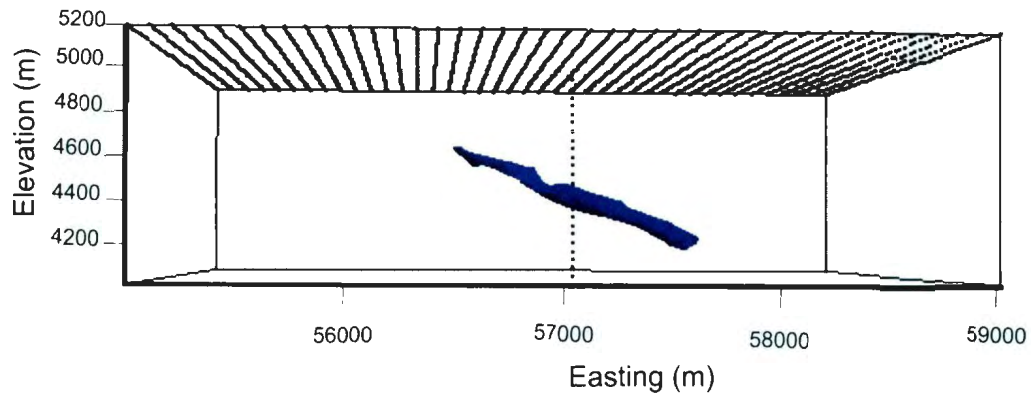


Fig. 6. 21: Mixed gravity measurement location array shown with the sulphide body from the Eastern Deeps model shown in blue. The axis going into the page is the northing and ranges from 40 000m north to 44 000m north

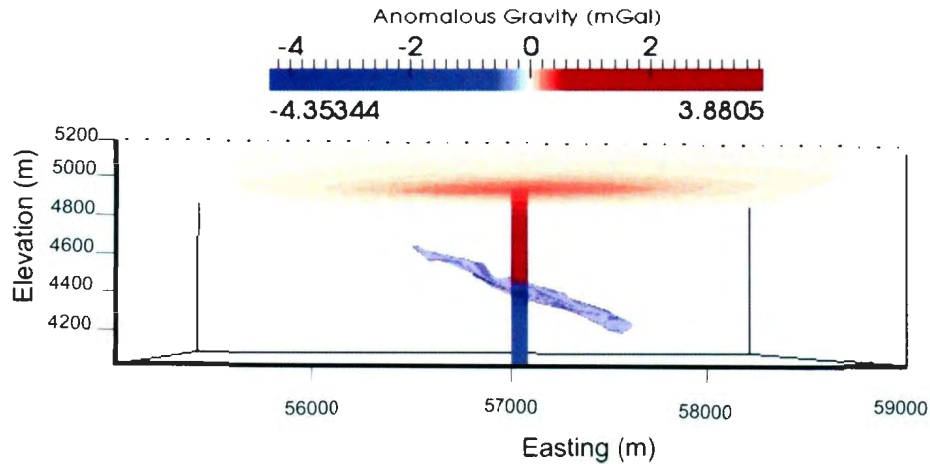


Fig. 6. 22: Gravity data for the mixed array shown in Fig. 6. 21. The axis going into the page is the northing and it ranges from 40 000m north to 44 000m north

6.3.1.4 Borehole-Only Array

Inversion results using the array seen in Fig. 6. 21 suggested that the surface data might not be contributing significantly to the inversion results (to be discussed in further detail in Chapter 7). As such an array was developed using only borehole gravity measurement locations. The location of the boreholes corresponds to the location of the source and receiver boreholes in the Starburst I array (see section

6.1.3.1). The forward modelling results from this array shows a positive to negative crossover in all boreholes with the largest anomaly seen in the borehole which pierces the sulphide body. As the sulphide body dips to the east it is not surprising that the positive cross over is deeper in the boreholes to the east of the model than those in the centre or west side of the model.

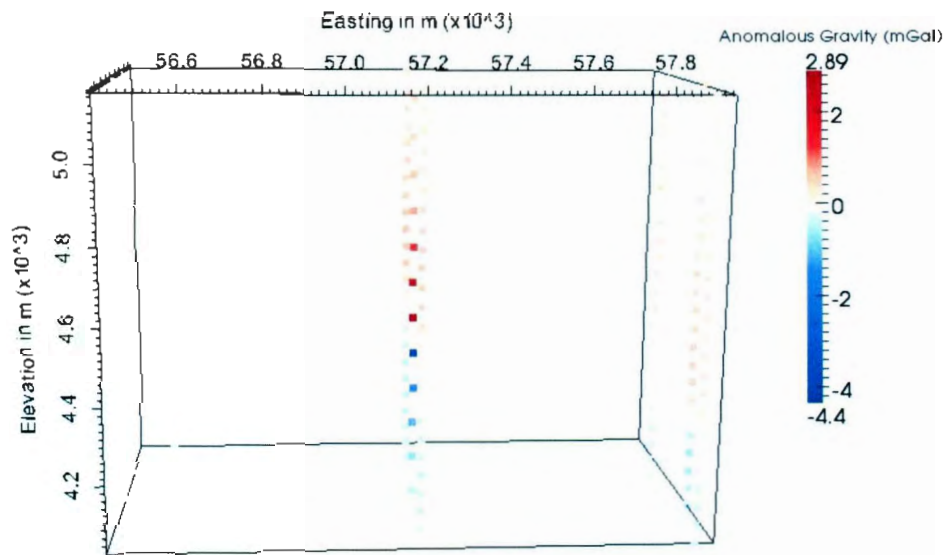


Fig. 6. 23: Results from gravity forward modelling of the sulphide model at borehole stations.

Chapter 7: 3D Inversion Results and Discussion

In this chapter the results for single and joint 3D inversions are presented and discussed. One of the major considerations when working with 3D inversions is the size of the inversion problem. If the size of the inversion problem is too large the time it will take to invert and the memory required to complete the inversion will be prohibitive.

When the memory demands of an inversion become too large the inversion will either stall or crash. Memory demands are associated with the number of sources and cells in the mesh. The examples shown in this chapter were run on a computer with 24 Gb of RAM and an example of an inversion where memory demands exceeded this memory capacity is the Double Starburst array example discussed below. This problem can be solved by decreasing the number of sources or the number of cells in the mesh.

In the case of inversions that are very large but don't require too much memory the processing time can stretch out to several weeks becoming prohibitive. The overall size of the inversion problem is a function of the number of data and the number of cells in the inversion mesh. In order to reduce the size of the problem either the number of data or the number of cells in the mesh has to be reduced.

Carrying out single property inversions were even more important in 3D inversions than it was for the 2D case. In many cases solving issues in the single property inversions greatly helped the quality of the joint inversion. As the single property

inversion also ran quicker than the joint inversion working through problems using the single property inversion saved a lot of time.

In section 7.1 a discussion of the single property seismic inversion results are presented and discussed. Section 7.1.1 presents a discussion of the results of inversions using the panel, grid and Starburst I arrays which were presented in Sections 6.2 and 6.3 of the previous chapter. In Section 7.1.2 a discussion of the effect of mesh coarseness on inversion results is presented. Sections 7.1.3 contains a discussion of the effectiveness of adding sources and receivers to the seismic array for improving inversion results through a presentation of the results of inversion using the Starburst II and Double Starburst arrays (as presented in Sections 6.2.3, 6.3.4 and 6.3.5). In Section 7.2 the results of single property gravity inversions are presented. This includes: a discussion of the need for restrictions on the physical property values (Section 7.2.1); the effect of using different layouts of gravity measurements; and the effects of a non-zero background when working with small model to target size. In Section 7.3 the results from the joint inversions are presented and discussed.

7.1 Single Property 3D Inversion Results

7.1.1 Effects of Borehole Layout on Seismic Inversion Results

When seismic data is collected in the field it often involves very dense data sampling with sources placed fairly close to receivers. The receivers are often positioned less than 10m apart and thus in boreholes that can be more than 500m long this can lead to huge amounts of data being collected (Enescu, et al., 2002, Perozzi, et al., in press).

When this work is used for 2D inversion the models often do not consist of enough cells for the inversion problem to become too large. The spacing, however, and the huge amount of data it leads to become an issue when looking into 3D inversion particularly on the scale of an ore deposit as the number of cells in the model increases and by extension the size of the inversion problem increases dramatically. In order to reduce the size of the inversion problem one must either reduce the number of data points or reduce the number of cells in the model. In this section the results from investigating different seismic source and receiver arrays will be presented.

7.1.1.1 Panel Array

The first array of sources and receivers used in this project was the panel array (see section 6.2.1). This array was used to forward model the full Eastern Deeps model (see Section 6.3.1) to which 1% Gaussian noise was added in the model shown in Section 2.3.3. This data was inverted using a blank inversion mesh containing 70 759 cells and with a maximum cell size of 250 000m³.

Target misfit for these inversions are set by assigning a value to the *chifact* inversion parameter (see Section 2.3.2). The *chifact* is

$$chifact = \frac{target\ misfit}{number\ of\ data} \tag{7.1}$$

For this inversion the *chifact* was set at 2.0 with a tolerance of 0.1. The inversion displays the misfit as the *omega* value which is given as

$$\omega = \frac{\text{misfit}}{\text{target misfit}}$$

7.2

Ideally the omega value at the end of the inversion process should be 1.0. In the case of this inversion the final omega reached by the inversion in 48 iterations was 18.07. This would suggest that the data has not been well matched.

There are two ways to measure the amount of time an inversion takes to run. The first is the computation time which regards the amount of time each CPU is in use. The second method is the wall clock time; which simply gives the amount of time from starting the inversion process to the end of the process with no consideration given to the activity or number of the cpus. In the case of this inversion the computation time was 1 day 1 hr 21.87min and the wall clock time was 1 day 1 hr and 22min.

In Fig. 7. 1 it is obvious that the slower cells were restricted to the plane of the panels. This was not a surprising result as the travel times from this array would not provide information about any other area of the model.

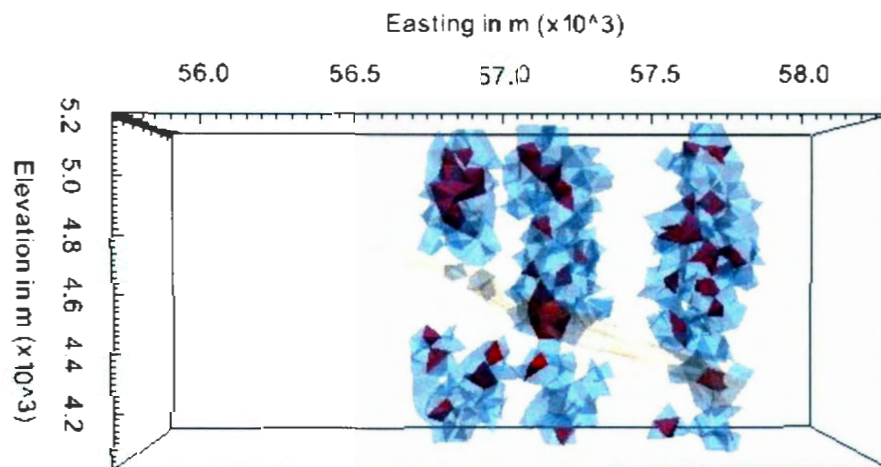


Fig. 7. 1: Result of a seismic only inversion of the Eastern Deeps model using the panel array of seismic sources and receivers. The red have slowness values between 0.164 s/km and 0.17 s/km, the blue cells have slowness values between 0.1625 s/km and 0.164 s/km, and the cells not shown have slowness values less than 0.1625 s/km. The transparent orange body is the sulphide body from the Eastern Deeps model. The axis going into the page is the northing and extends from 41900m to 43100m.

7.1.1.2 Grid Array

The development of the grid-like array was discussed in Section 6.2.2. This array was used to forward model the full Eastern Deeps model (see Section 6.3.2); to which 1% Gaussian noise was added in the model shown in Section 2.3.3. These data were inverted using a blank inversion mesh containing 46762 cells and with a maximum cell size of 250 000m³. This mesh is smaller in all dimensions than the mesh used in for panel array inversion presented in Section 7.1.1.1.

The chifact set for this inversion was 2.0 with a tolerance of 0.1. This inversion in 48 iterations reached an omega value of 8.47. This suggests that although the data fit was not good it was improved from the results of the panel array results. This inversion had a computation time of 1 day 19hrs 50min and had a wall clock time of 4 days 7hrs 6min.

The inversion results produced from the grid array data showed little true improvement over the results from the panel array data inversion (see Section 7.1.1.1). The inversions produced a greater number of high slowness cells; however, they did not convincingly model the sulphide body (Fig. 7. 2).

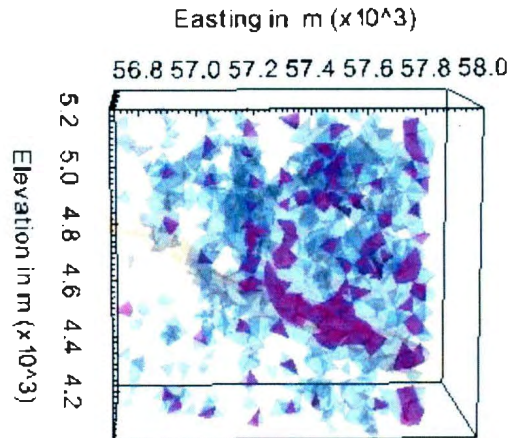


Fig. 7. 2: Results of a seismic only inversion using the grid-like source and receiver array. The purple cells have slownesses between 0.166 s/km and 0.174 s/km, the blue cells have between 0.164 s/km and 0.166 s/km, and all cells not shown have slownesses of less than 0.164 s/km. The axis going into the page is the northing and it extends from 42100m to 42900m.

The poor data fit exhibited by this inversion and the panel array inversion (see Section 7.1.1.1) was concerning. It was suggested that this could be due to the coarseness of the inversion mesh in comparison to the size of the mesh used to create the synthetic data. If the difference between the synthetic data created using a fine mesh and that created using a coarse mesh could not be accommodated by the noise added to the fine mesh synthetic data the inversion would always have trouble reaching the target misfit. In light of this the forward modelling tests discussed in Section 6.3.6 were conducted. From these tests it was concluded that to remove the necessity of using a fine mesh with a maximum cell size of 10 000m³ or less at least 2.5% Gaussian noise needed to be added to the synthetic dataset.

7.1.2 Effects of Grid Coarseness on Seismic Tomography Modelling

Increasing the amount of noise added to the data allowed for the use of a coarser inversion mesh; however, further problems with the use of a coarse inversion mesh were still possible:

1. When using a coarse inversion mesh there were a limited number of cells between the source and receiver locations. This limited the potential number of effective changes the inversion could make to the model. As such, it may have begun changing the slowness of cells that weren't between the sources and receivers. This could account for some of the scatter in slow cells seen in Fig. 7. 1 and Fig. 7. 2.
2. The large cells of the coarse mesh were often close to or larger than the thickness of the sulphide body in the Eastern Deeps model. This limited the number of cells that could be combined to approximate the sulphide body.

The first potential issue could be solved by increasing the distance between the sources and receivers in the array being used or by using a finer inversion mesh. The second issue could only be resolved by using a finer inversion mesh. To deal with these issues the Starburst I array was developed (see Section 6.2.3.1). The Starburst I array allows for the use of a coarse mesh by having widely set source-receiver pairs and the reduced number of source-receiver pairs also allows for the use of a finer inversion mesh as it reduces the size of the inversion problem significantly.

It was decided to run a set of test inversions using the synthetic data produced using the Block model (see Section 5.2.1 and 6.3.3) as a proxy for the sulphide body in the Eastern Deeps model. This model did not include the troctolite and as such the synthetic model is smaller and allowed an inversion mesh of the same dimensions to be used for inversion. The synthetic Block model data had 2.5% Gaussian noise added to it. Four inversions were run varying only in the maximum cell size of inversion mesh used. The inversion meshes are detailed in Table 7.1. The inversions were all run with a chifact of 1.0 with a tolerance of 0.1.

Table 7. 1: Mesh specification for the inversion meshes used during the coarseness tests.

Mesh	Maximum Cell Size	Number of Cells
Very Coarse Mesh	250 000 m ³	17 076
Coarse Mesh	100 000 m ³	41 792
Medium Mesh	50 000 m ³	82 369
Fine Mesh	10 000 m ³	411 300

7.1.1.3 Very Coarse Mesh Inversion

The first test was run using the very coarse mesh (Table 7. 1). The inversion reached an omega value of 1.947 in 48 iterations. This inversion had a computation time of 3 hrs 37min and a wall clock time of 3 hrs 40min. Although this inversion was not able to reach the target misfit it was able to match the synthetic data set significantly better than the results from the panel and grid array inversions. The inversion also took significantly less time than the panel and grid array inversions.

The slowness model produced by this inversion shows that the slow material is being concentrated into the block (Fig. 7. 3). Although the slowness model produced by this inversion is an improvement over those produced by the panel and grid array inversions it still lacks the smoothness that would be expected from a minimum structure inversion. It can also be seen that the cells are nearly the width of the block. As such, it was decided that a test should be performed to determine the ideal maximum cell size required to achieve acceptable inversion results.

The travel times predicted by this inversion (Fig. 7. 4a) are similar to those from forward modelling (Fig. 6.17) in topology although they are slightly different in range with the shortest travel time in Fig. 7. 4a being about 5ms longer and the longest travel time Fig. 7. 4a being about 2ms shorter than those seen in the forward modelled data. The normalized data residuals calculated for this inversion range from -4 to 4.5 and show no distinctly spatial distribution (Fig. 7. 4b). The relatively low normalized data residuals suggest that the inversion was able to match the seismic data provided to the inversion fairly well.

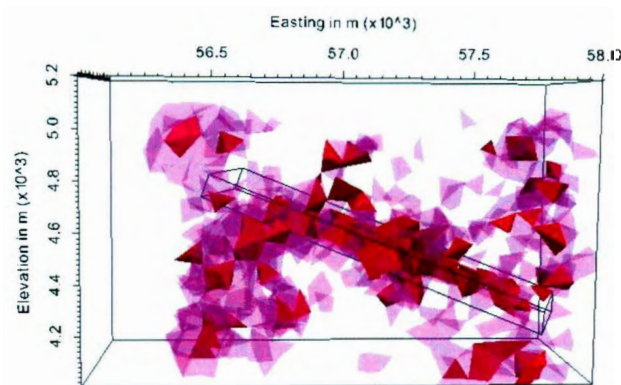


Fig. 7. 3: The slowness model for the seismic-only inversion of starburst array block model synthetic data inverted on a very coarse mesh. The dipping block

shown by an outline is the sulphide block from the block model (see Section 5.2.1). The red cells have slowness values between 0.185 s/km and 0.237 s/km. The purple cells have slowness values between 0.167 s/km and 0.185 s/km. All cells not shown have slowness values less than 0.167 s/km. Those cells not shown have slowness values less than 0.165ms. The axis going in to the page is the northing and extends from 42000m to 42900m.

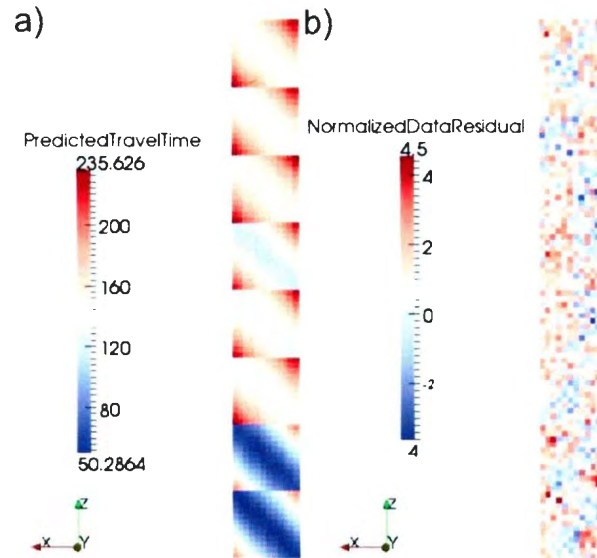


Fig. 7. 4: a) The predicted travel times and b) normalized data residuals in ms calculated for the slowness distribution seen in Fig. 7. 3.

7.1.2.2 Coarse Mesh Inversion

The next inversion was completed using a coarse mesh (Table 7. 1). This inversion reached a misfit of 1.44 in 48 iterations. This inversion had a computation time of 8 hrs and 38min and a wall clock time of 9hrs and 59min. The results of this inversion (Fig. 7. 5) are less scattered than those seen for the very coarse mesh (Fig. 7. 3). The highest slowness cells are entirely within the sulphide block; however, the amount of scatter still indicates that this was a poorly performing minimum structure inversion. The predicted travel times for this inversion (Fig. 7. 6a) are similar to the forward modelled data (Fig. 6.17) provided to the inversion. The range of predicted travel

times is closer to the range from the forward modelled data set than those from the very coarse mesh inversion (Fig. 7. 4a) with the shortest travel time being under 1ms longer and the longest travel time being about 1.5ms shorter than in the forward modelled date. The normalized data residuals (Fig. 7. 6b) calculated for this inversion range from -3 to 4.3. As with the normalized data residuals in Fig. 7. 4, there is no particular spatial distribution to the values. The decreased range of the normalized data residuals in comparison to the very coarse mesh example (Fig. 7. 4b) indicates that this inversion was able to fit the data more accurately.

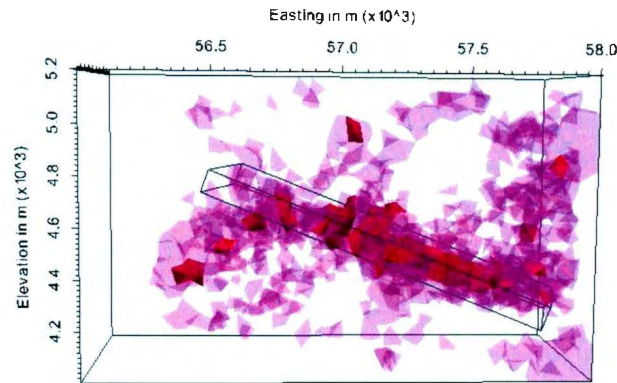


Fig. 7. 5: The slowness model for the seismic-only inversion of starburst array block model synthetic data inverted on a coarse mesh. The dipping block shown by an outline is the sulphide block from the block model (see Section 5.2.1). The red cells have slowness values between 0.19 s/km and 0.226 s/km. The purple cells have slowness values of 0.168 s/km and 0.19 s/km. All of the cells not shown have slowness values of less than 0.168 s/km. Those cells not shown have slowness values less than 0.165ms. The axis going in to the page is the northing and extends from 42000m to 42900m

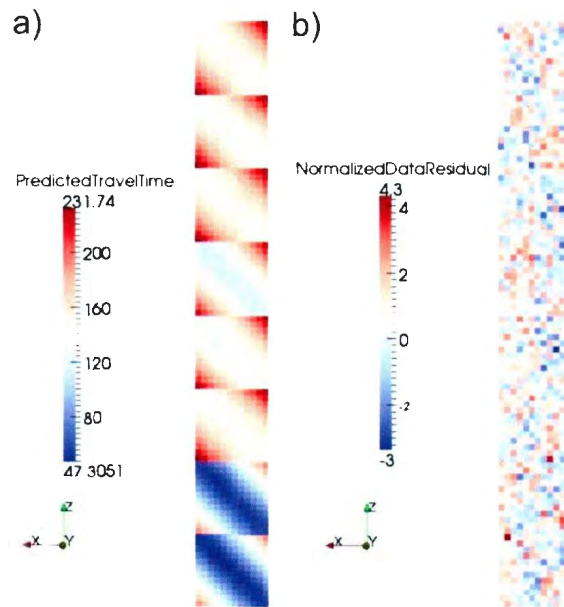


Fig. 7. 6: a) The predicted travel times and b) normalized data residuals in ms calculated from the slowness model in Fig. 7. 5.

7.1.2.3 Medium Mesh Inversion

The third inversion was run using a medium mesh (Table 7. 1). This inversion reached an omega value of 1.275 in 48 iterations. The inversion took a computation time of 22hrs 48mins and a wall clock time of 25hrs and 42mins. The results of the starburst inversion on this mesh are much closer to the type of result expected for a minimum structure inversion. There is a significant decrease in the amount of scatter and is restricted to the lowest of high slowness cell cut-offs (Fig. 7. 7). The normalized data residuals calculated for this inversion range from -3 to 4.3 with no particular spatial distribution (Fig. 7. 8).

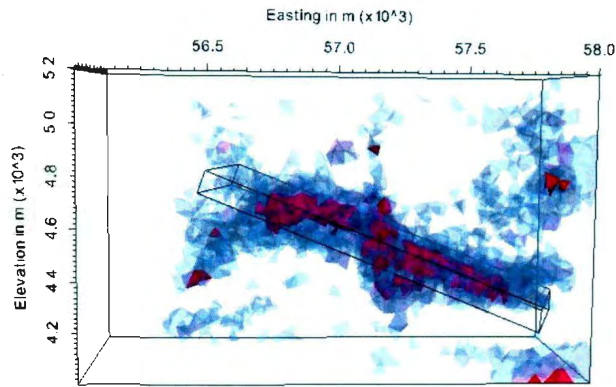


Fig. 7. 7: The slowness model from the seismic-only inversion of starburst array block model synthetic data inverted on a medium mesh. The dipping block shown by an outline is the sulphide block from the block model (see Section 5.2.1). The red cells have slowness values of 0.173 s/km to 0.1911 s/km. The purple cells have slowness values from 0.168 s/km to 0.173 s/km. The blue cells have slowness values between 0.164s/km and 0.167s/km. Those cells not shown have slowness values below 0.164 s/km. Those cells not shown have slowness values less than 0.165ms. The axis going in to the page is the northing and extends from 42000m to 42900m

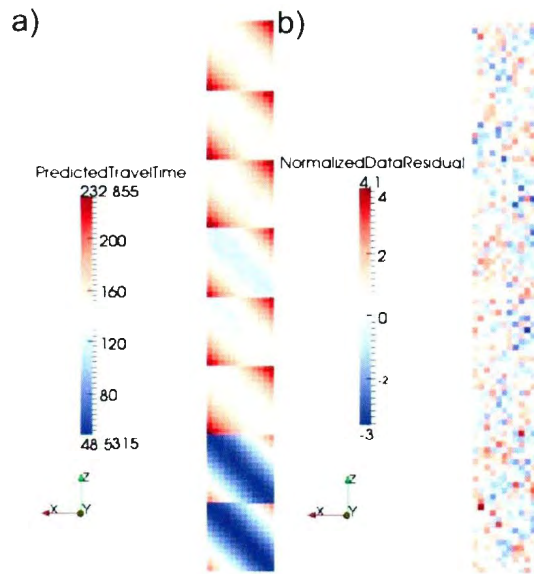


Fig. 7. 8: a)The predicted travel times and b) normalized data residuals in ms calculated from the slowness model in Fig. 7. 7.

7.1.2.4 Fine Mesh Inversion

The fourth inversion was run on a fine mesh (Table 7. 1). The inversion reached an omega value of 1.194 in 39 iterations making this the only grid coarseness test inversion to converge to the target misfit. The inversion took a computation time of 5 days 9hrs 38min and a wall clock time of 5 days 9hr 55min. The result of the starburst inversion is what one would expect from a minimum structure inversion. The high slowness cut-offs from a set of shells with the slowest cells completely within the sulphide block (Fig. 7. 9). There is very little scatter of the high slowness cells and all scattered cells belong to the least slow of the shells. The predicted travel times and normalized data residuals calculated for this inversion result range from -4 to 3. 4 with no particular spatial distribution (Fig. 7. 10b).

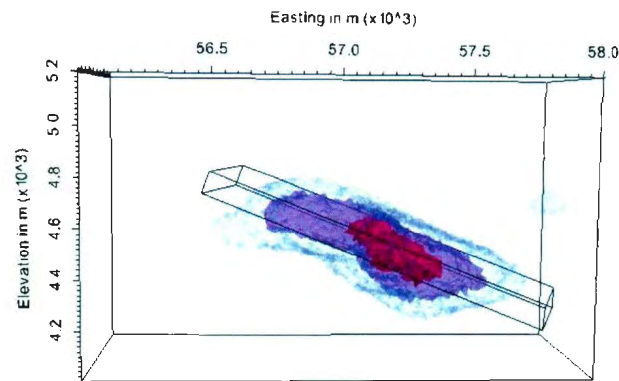


Fig. 7. 9: The slowness model for the seismic-only inversion of starburst array block model synthetic data inverted on a fine mesh. The dipping block shown by an outline is the sulphide block from the block model (see Section 5.2.1). Red cells have slowness values between 0.17s/km and 0.1745s/km. The purple cells have slowness values between 0.1675s/km to 0.17s/km. The blue cells have slowness values between 0.165s/km to 0.1675s/km. Those cells not shown have slowness values less than 0.165ms. The axis going in to the page is the northing and extends from 42000m to 42900m

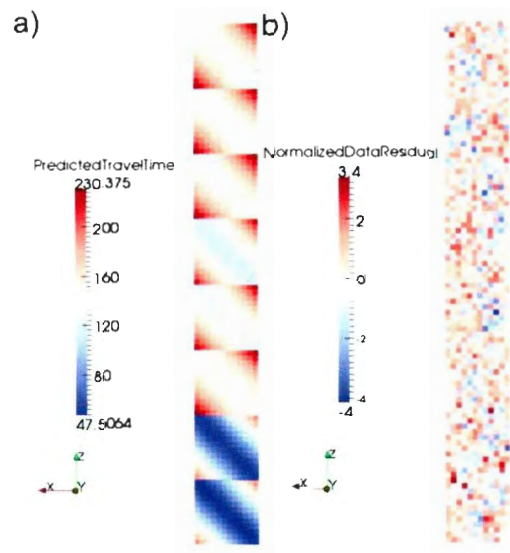


Fig. 7. 10: The predicted travel times (a) and normalized data residuals (b) calculated from the density distribution seen in Fig. 7. 9.

7.1.2.5 Insights from Mesh Coarseness Test Inversions

The results of these four test inversions clearly show that a fine mesh is necessary to attain acceptable inversion results. Only the inversion using the fine mesh (Fig. 7. 9) was able to model the block in a smooth manner expected of a well behaved minimum structure inversion.

With progressively finer meshes the inversions became closer to reaching the target misfit and the fine mesh inversion converged in less than 48 iterations. This suggests that using a sufficiently fine inversion mesh is necessary in order to accurately match the seismic data.

As expected the finer the inversion mesh the longer it took for the inversion to run.

This relationship is shown to be linear in nature as is shown in Fig. 7. 11. In this graph the computation times from the four test inversions presented above are plotted against the number of cells in the inversion mesh. However, in light of the greatly improved inversion results from the finer mesh the increased computation time must be accepted.

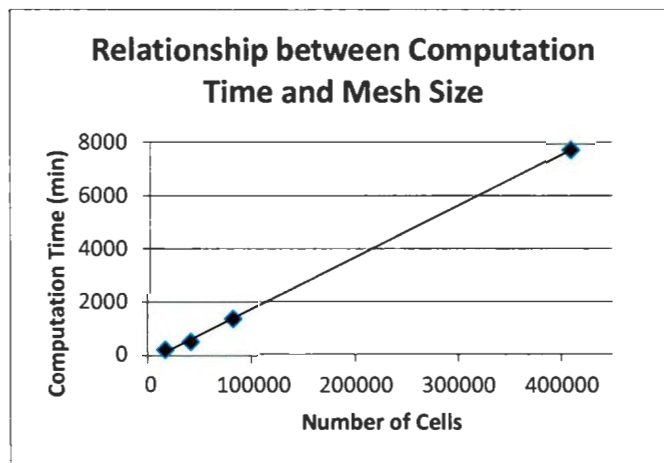


Fig. 7. 11: Graph showing the linear relationship between the number of cells in an inversion mesh and the computation time for the seismic inversion run using that mesh and the Starburst I array.

7.1.3 Adding Receivers: The Starburst II Array

The addition of 4 receiver boreholes to the seismic acquisition array leads to a fuller set of seismic data. The inversion reached an omega value of 1.439 in 48 iterations and took a computational time of 4 days 12 hr 55min and a wall clock time of 4 days 10hrs 48min. The seismic-only inversion tests using this array required, as was expected, a higher computational time of than was required by inversions using the starburst I array. However, the inversions took less computation time than those for the double starburst lay out. The results produced by this inversion (Fig. 7. 12)

indicate that the increased computation expense was rewarded by improvements to the slowness model. The slowness model is improved over that produced by the starburst I array. The body is less diffuse (Fig. 7. 12a) and has determined the dimensions of the block more accurately (Fig. 7. 12b).

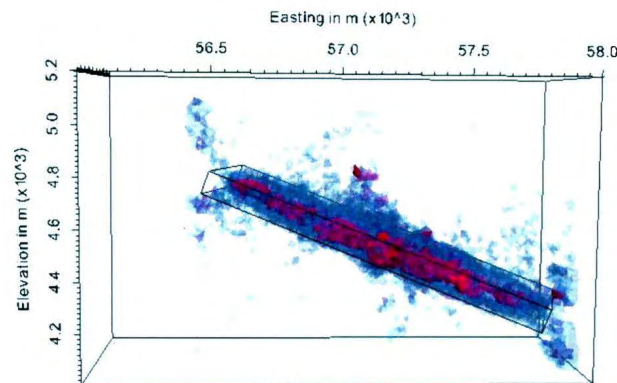


Fig. 7. 12: Resultant slowness model from the seismic-only inversion of block model synthetic data. . The dipping block shown by an outline is the sulphide block from the block model (see Section 5.2.1). The red cells have slowness values between 0.2 s/km and 0.24 s/km, the purple cells have slowness values between 0.18 s/km and 0.2 s/km, the blue cells have slowness values between 0.17 s/km to 0.18 s/km, and cells that are not shown have slowness values less than 0.17 s/km.

7.2 Gravity Inversion Results

Gravity-only inversions were run to investigate the effects of different measurement arrays and to investigate the effect of different inversion parameters prior to undertaking the joint inversions. The datasets used for these inversions were discussed in Section 6.3. Due to the low magnitude of the gravity response the amount of noise

added to these datasets was lower than that added to the seismic travel time data in Section 6.2.

7.2.1 Small Surface Array Inversion Results

The small surface array dataset is discussed in Section 6.3.1.1. The noise added to this data included 1% Gaussian noise and a noise floor of 0.001mGal. The inversion for this test was run using the fine inversion mesh. The inversion converged to an omega of 1.162 in 11 iterations with a computation time of 43hr 20min and a wall clock time of 12hr 11min. The gravity data predicted by this inversion (Fig. 7. 13a) is very close in range and topology to the synthetic dataset provided to the inversion (Fig. 6.21).

The normalized data residuals (Fig. 7. 13b) calculated from the predicted and synthetic datasets are relatively low and show no particular pattern. The normalized data residuals, in conjunction with the convergence of the inversion to the target misfit, suggest that inversion was able to match the small surface array datasets.

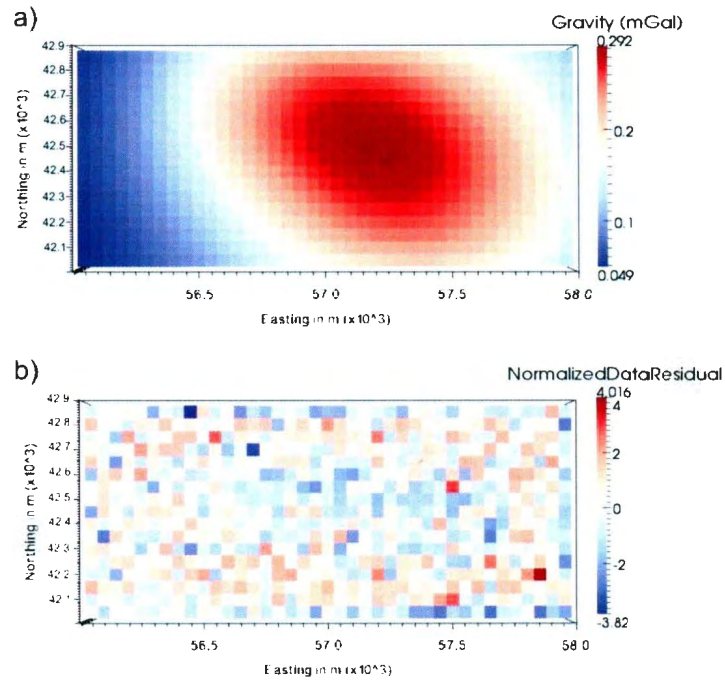


Fig. 7. 13: a) Predicted gravity anomaly and b) associated normalized data residuals for the small surface array data inversion on the fine inversion mesh.

The density model produced by this inversion (Fig. 7. 14) has significantly underestimated the density of the sulphide body. This is seen to lesser degree in the 2D density inversions (see Section 4.1.2). This is a common phenomenon in minimum structure gravity inversion where the logic of the inversion has poor depth resolution abilities. The distribution of anomalously dense cells indicates that the inversion has determined the orientation of the sulphide body. However, it has not resolved the shape or size of the body. The model has maintained the smooth nature expected of a minimum-structure inversion which indicates that the inversion is behaving well.

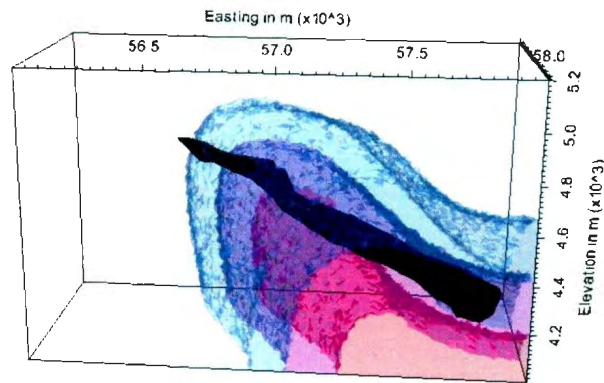


Fig. 7. 14: Resultant density distributions from the small surface array gravity inversion on the fine inversion mesh. The red cells had relative densities between 0.035 g/cm^3 to 0.0433 g/cm^3 , the purple cells have relative densities between 0.035 g/cm^3 and 0.035 g/cm^3 , the blue cells have densities between 0.015 g/cm^3 and 0.025 g/cm^3 and all other cells have densities less than 0.015 g/cm^3 . The sulphide body is shown in black and has a relative density of 1.652 g/cm^3 and the axis going in to the page is the northing and extends from 42000m to 42900m.

7.2.2 Large Surface Array Inversion Results

The anomaly seen in the small surface mesh data in Section 6.3.1.1 obviously extends beyond the edges of the array of measurements locations. As such, it was suggested that the resolution attained by an inversion may be improved by using a larger array of surface measurements; ensuring that the array covers the full extent of the gravity anomaly. The forward modelling of the sulphide model done using this large surface array is discussed in Section 6.3.1.2. The noise added to this data included 1% Gaussian noise and a noise floor of 0.001ms.

7.2.2.1 Investigation of the Effects of Sensitivity Weighting

The lack of depth resolution observed in the inversion results from the small surface array (Fig. 7. 14) suggests that the sensitivity weighting (see Section 2.3.1.2) may have been inappropriately chosen. If the sensitivity weighting has been set too high

this may lead to all the anomalous material being pushed too far from the measurement locations. In order to investigate this possibility a number of inversions were run to determine the most appropriate amount of sensitivity weighting to be used.

In light of the long cpu time for the gravity inversion presented in Section 7.2.1 a second mesh was designed to be used for quick test inversions for both gravity and joint inversions. It consists of three rectangular prisms the largest enclosing the second largest which encloses the smallest (Fig. 7. 15). This mesh consists of a total of 101 533 cells. A different maximum cell volume was set for each of the prisms. The smallest prism contains cells of no more than $10\,000\text{m}^3$. The medium prism contains cells of no more than $50\,000\text{m}^3$. And the largest prism contains cells of $150\,000\text{m}^3$. In a joint inversion using the Starburst I array the smallest prism would be centred around the borehole containing the seismic source locations. This preserves the validity of the plane wave approximation of the fast marching method (Lelievre, et al., 2011).

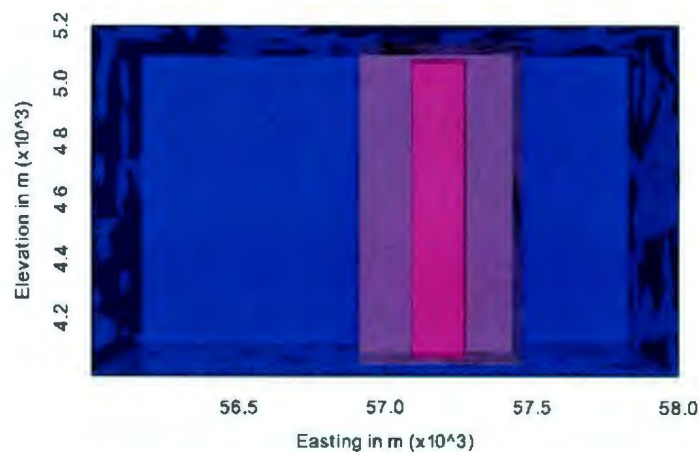


Fig. 7. 15: A depiction of the graduated block model showing the three prisms.

Default Sensitivity Inversion

The first inversion run used the default `sens_norm` (see Section 2.3.2) value of 2.0. The inversion was given target `chifact` of 1.0 with a tolerance of 0.2. The inversion was able to converge to an `omega` of 1.137 in 4 iterations with a computation time of 6hr 58min and a wall clock time of 43.09min. The gravity response predicted by this inversion (Fig. 7. 16a) is similar in topology and range to the synthetic data (Fig. 6.23). The normalized data residuals from this inversion are fairly small and have no particular pattern. This, in conjunction with the similarity between the predicted and synthetic data as well as the convergence of the inversion to the target misfit, suggests that it was able to fit the synthetic data well.

The relative density model (Fig. 7. 17) produced by this inversion is similar to the result of the small surface measurement array (Fig. 7. 14). However, this inversion has not determined the orientation of the sulphide body as well as small array inversion. This may be a consequence of using a coarser nature of the graduated inversion mesh. The relative density estimated by the inversion is still significantly underestimated, although it is a marginally better estimated than was seen in Fig. 7. 14. This result will be the basis to which the rest of the sensitivity test inversions will be compared.

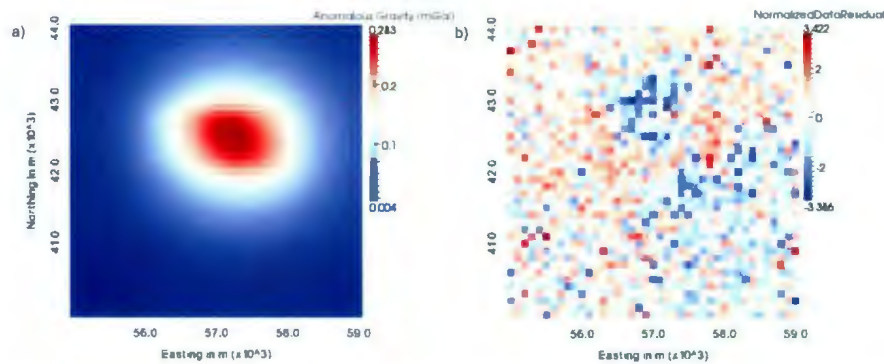


Fig. 7. 16: a) Predicted gravity anomaly and b) associated normalized data residuals for the default sens_norm inversion on the large surface gravity array.

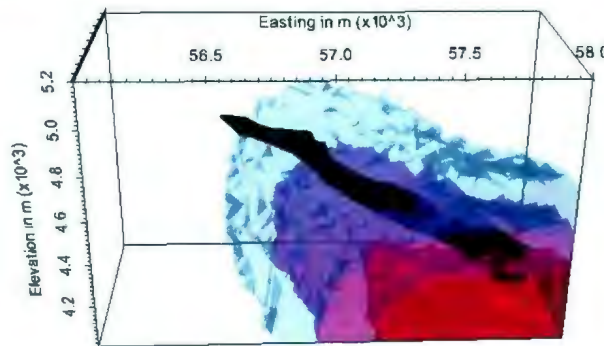


Fig. 7. 17: Resultant density distributions from the default sensitivity large surface array gravity inversion. The red cells had relative densities between 0.045 g/cm^3 to 0.0625 g/cm^3 , the purple cells have relative densities between 0.03 g/cm^3 and 0.045 g/cm^3 , the blue cells have densities between 0.015 g/cm^3 and 0.03 g/cm^3 and all other cells have densities less than 0.015 g/cm^3 . The sulphide body is shown in black and has a relative density of 1.652 g/cm^3 and the axis going in to the page is the northing and extends from 42000m to 42900m.

Moderate Sensitivity Inversion

The second large array inversion attempts to improve the inversion results by lowering the sensitivity weighting. This was done by lowering the sens_norm parameter from 2.0 to 1.0. In all other ways this inversion is identical to the inversion with the default sens_norm value seen above. The inversion converged to an omega of 1.155 in 11 iterations with a computation time of 12hr 10min and a wall clock time of 52.25min. The gravity data predicted by this inversion is similar to those in Fig. 7. 16a and range

from 0.004mGal to 0.293mGal. The normalized data residuals calculated from the predicted and synthetic data for this inversion are very similar to those seen in Fig. 7. 16 and range from 3.408 to -3.446. The relative density model for the inversion (Fig. 7. 18) shows that the orientation of the sulphide body has not been as well determined as it was in the default sensitivity inversion (Fig. 7. 17).

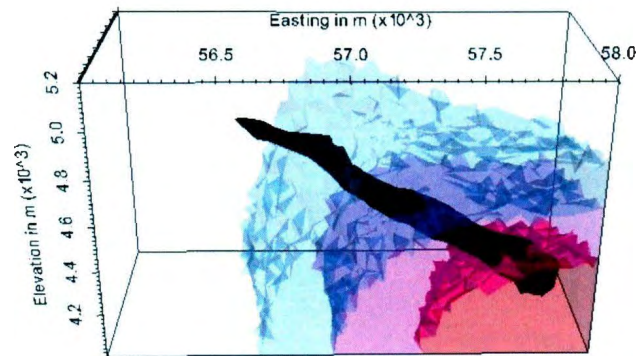


Fig. 7. 18: Resultant density distributions from the moderate sensitivity large surface array gravity inversion. The red cells had relative densities between 0.035 g/cm^3 to 0.0444 g/cm^3 , the purple cells have relative densities between 0.025 g/cm^3 and 0.035 g/cm^3 , the blue cells have densities between 0.015 g/cm^3 and 0.025 g/cm^3 and all other cells have densities less than 0.015 g/cm^3 . The sulphide body is shown in black and has a relative density of 1.652 g/cm^3 and the axis going in to the page is the northing and extends from 42000m to 42900m.

Low Sensitivity Inversion

The third large surface array inversion was attempted to see the effect of further decreasing the sensitivity weighting. This was accomplished by lowering the `sens_norm` from 1.0 to 0.5. The inversion converged to an omega of 1.173 in 15 iterations with a computation time of 20hr 39min and a wall clock time of 6hr 11min. The predicted gravity anomaly is similar to that seen in Fig. 7. 16a with a range of gravity data from 0.004 mGal to 0.300 mGal. The normalized data residuals for this inversion range from -3.52 to 3.39 and have a similar distribution to those seen in Fig.

7. 16b. The relative density model produced by this inversion (Fig. 7. 19) continues the same trend seen between the results of the default (Fig. 7. 17) and moderate (Fig. 7. 18) sensitivity results. The model's predicted orientation of the sulphide body has deteriorated compared to the previous two inversion and there has been little change in the estimation relative density of the sulphide body.

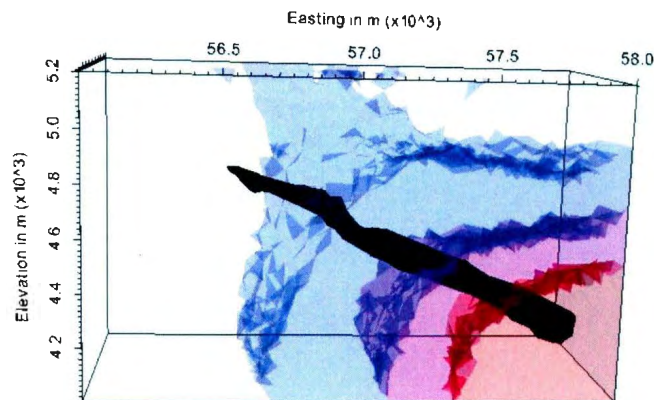


Fig. 7. 19: Resultant density distributions from the low sensitivity large surface array gravity inversion. The red cells had relative densities between 0.03 g/cm^3 to 0.036 g/cm^3 , the purple cells have relative densities between 0.025 g/cm^3 and 0.035 g/cm^3 , the blue cells have densities between 0.015 g/cm^3 and 0.025 g/cm^3 and all other cells have densities less than 0.015 g/cm^3 . The sulphide body is shown in black and has a relative density of 1.652 g/cm^3 and the axis going in to the page is the northing and extends from 42000m to 42900m.

No Sensitivity Weighting

The final large surface array inversion run using the graduated model investigated the effect of having no sensitivity weighting at all. In all other ways this inversion was run with the same settings as the three preceding inversions. The inversion converged to an omega of 1.157 in 16 iterations with a computation time of 13hr 35min and a wall clock time of 3hr 32min. The predicted gravity anomaly is similar to that seen in Fig.

7. 16a with a range of gravity data from 0.004 mGal to 0.293 mGal. The normalized data residuals for this inversion range from -3.405 to 3.405 and have a similar distribution to those seen in Fig. 7. 16b. The relative gravity model produced by this inversion (Fig. 7. 20) has continued the trend seen in the previous tests. The estimation of the orientation of the sulphide body continued to deteriorate as did the estimation of the density of the sulphide body.

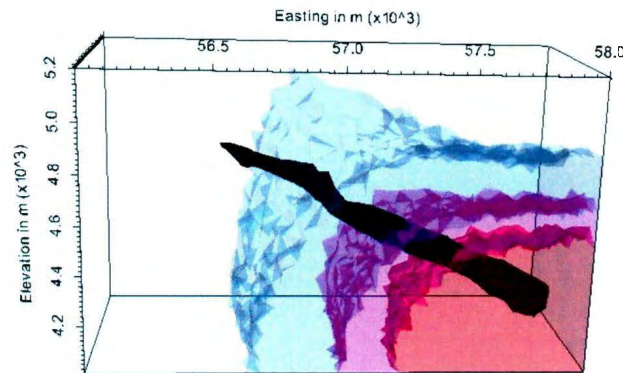


Fig. 7. 20: Resultant density distributions from the large surface array gravity inversion with no sensitivity weighting. The red cells had relative densities between 0.03 g/cm^3 to 0.039 g/cm^3 , the purple cells have relative densities between 0.025 g/cm^3 and 0.035 g/cm^3 , the blue cells have densities between 0.015 g/cm^3 and 0.025 g/cm^3 and all other cells have densities less than 0.015 g/cm^3 . The sulphide body is shown in black and has a relative density of 1.652 g/cm^3 and the axis going in to the page is the northing and extends from 42000m to 42900m.

The results of the four inversions with different sensitivity weighting showed that the best results were attained using the default surface weighting. All four inversions have similar density distributions and all have greatly underestimated the density of the sulphide body. However, the inversion run with the default sensitivity weighting has the highest density values and as such is the most accurate of the four tests.

7.2.2.2 Fine Mesh Inversion

The large surface array data set was inverted using the fine inversion mesh using the results of the inversions discussed in Section 7.2.2.1 which determined that using the default `sens_norm` value of 2.0 is the best. The inversion converged to an ω of 1.187 in 16 iterations with a computation time of 60hr 22min and a wall clock time of 20hr 39min. As with previous inversions using the large surface array the predicted gravity anomaly is similar to that seen in Fig. 7. 16a and the gravity values range from 0.004mGal to 0.283mGal. The normalized data residuals for this inversion range from -3.37 to 3.42 and have a similar distribution to those seen in Fig. 7. 16b.

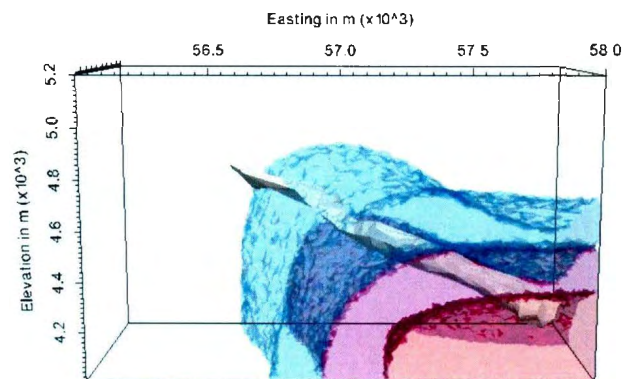


Fig. 7. 21: Resultant density distributions from the large surface array gravity inversion on the fine inversion mesh. The red cells had relative densities between 0.045 g/cm^3 to 0.06273 g/cm^3 , the purple cells have relative densities between 0.03 g/cm^3 and 0.045 g/cm^3 , the blue cells have relative densities between 0.015 g/cm^3 and 0.03 g/cm^3 and all other cells have densities less than 0.015 g/cm^3 . The sulphide body is shown in grey and has a relative density of 1.652 g/cm^3 and the axis going in to the page is the northing and extends from 42000m to

42900m.

7.2.3 Mixed Array Inversion Results

The use of borehole gravity measurements in 2D was shown to effectively improve the results of gravity inversions (see Section 4.1.1.1). As the results from both the small (Section 7.2.1) and large (Section 7.2.2) surface arrays did not satisfactorily model the sulphide body it was decided that borehole stations should be added to the large surface array. The development of this mixed array and the data produced for the array during forward modelling is presented in Section 6.3.1.3. The noise added to this data consisted of 1% Gaussian noise and a noise floor of 0.001mGal. Inversions were run for the mixed array dataset using both the graduate block mesh and the fine mesh.

7.2.3.1 Graduated Mesh Inversion

The inversion converged to an omega of 1.155 in 17 iterations with a computation time of 7hr 6min and a wall clock time of 2hr 0min. The gravity response (Fig. 7. 22) is more restricted in range than the synthetic data (Fig. 6.25) provided to the inversion. However, the topology of the gravity response is consistent with the synthetic data. The normalized data residuals calculated from the predicted and synthetic data associated with this inversion (Fig. 7. 23a) for the borehole measurement location has high normalized data residual values which are concerning. However, there are only two very high values and these are near the edges of the sulphide body and, as such, the large values are not a concern. The surface measurement location normalized data residuals (Fig. 7. 23b) show that the data point inside the inversion mesh was fit better than those outside the inversion mesh.

The relative density model (Fig. 7. 24) produced by this inversion is clearly an improvement over the models produced from inversion of only surface data (see Sections 7.2.1 and 7.2.2). Although, the inversion has not determined the size and shape of the sulphide body well it has determined the orientation of the sulphide body moderately well and the relative density of the sulphide is only slightly underestimated. The inversion has modelled the sulphide body best near the borehole gravity stations further indicating the importance of borehole gravity stations to attaining good gravity inversion results.

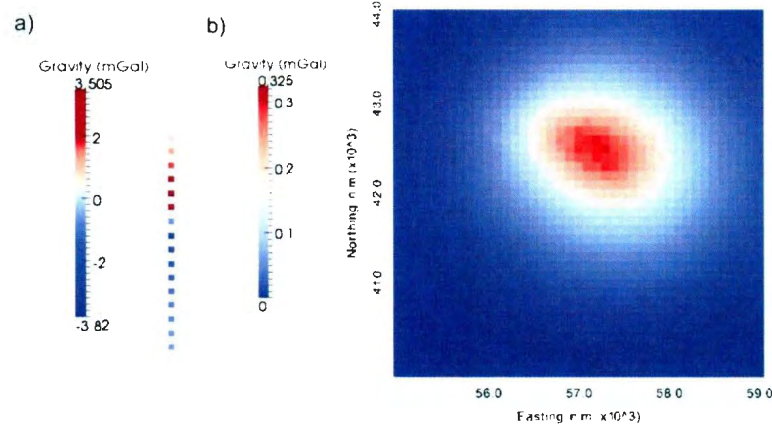


Fig. 7. 22: Predicted relative gravity measurements predicted by the inversion of mixed gravity array data for a) borehole measurements and b) surface measurements on the graduated inversion mesh.

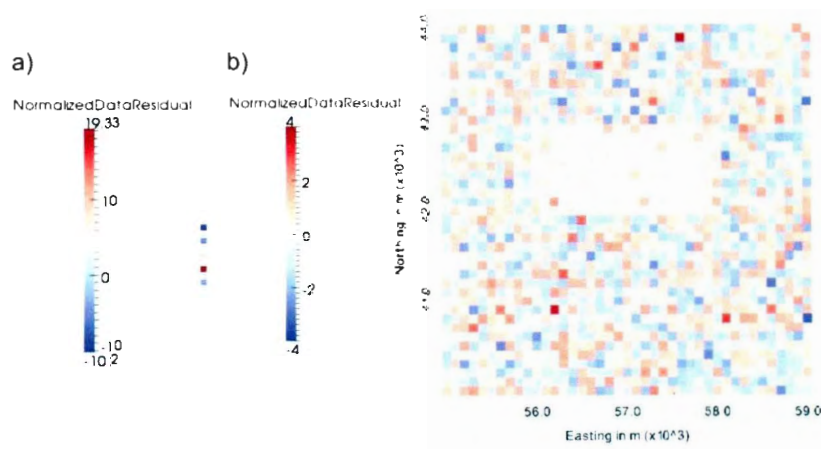
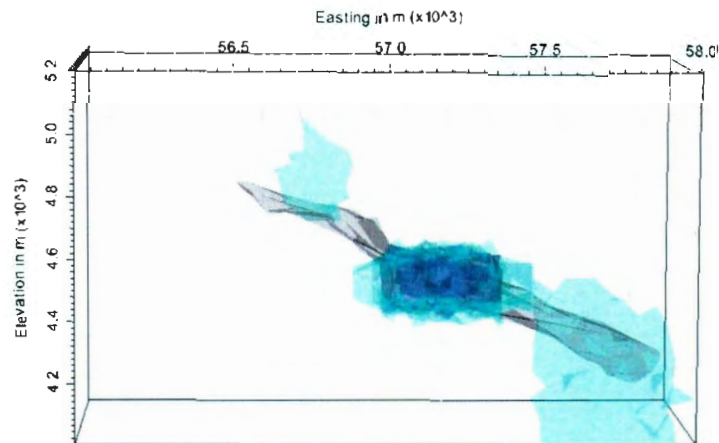


Fig. 7. 23: Normalized data residuals calculated for the results of the inversion of the mixed array a) for borehole measurements and b) surface locations on the graduated inversion mesh.



+

Fig. 7. 24: Resultant density distributions from the inversion of mixed array data on the graduated inversion mesh. The pink cells in the centre of the model have relative densities between 0.8 g/cm^3 to 1.451 g/cm^3 , the turquoise cells have relative densities between 0.25 g/cm^3 and 0.8 g/cm^3 , the light blue cells have densities between 0.10 g/cm^3 and 0.25 g/cm^3 and all other cells have densities less than 0.010 g/cm^3 . The sulphide body is shown in black and has a relative density of 1.652 g/cm^3 and the axis going in to the page is the northing and extends from 42000m to 42900m. The grey dots are gravity measurement locations.

7.2.3.2 Fine Mesh Inversion

The inversion converged to an omega of 1.155 in 17 iterations with a computation time of 7hr 6 min and a wall clock time of 2hr 0min. The gravity response predicted by this inversion is similar to that seen in Fig. 7. 22 with a range in values from -3.35mGal to 3.58mGal. Likewise the normalized data residuals calculated from the predicted and synthetic data for this example are similar to those in Fig. 7. 23 with a range from -8.26 to 20.5. The highest values are near the edges of the sulphide body with the rest of the values falling roughly between -3 and 4. Also, the surface measurements had lower normalized data residual values within the limits of the inversion mesh than those outside.

The relative gravity model produced by this inversion has located the sulphide body and gives some indication of its orientation. However, it has not determined the size or shape of the sulphide body. The inversion has predicted the relative density of the sulphide body more accurately than any of the previous inversions. Like in the equivalent graduated mesh inversion (Fig. 7. 24) the sulphide is modelled best in the vicinity of the borehole measurement locations reinforcing the importance of those measurements.

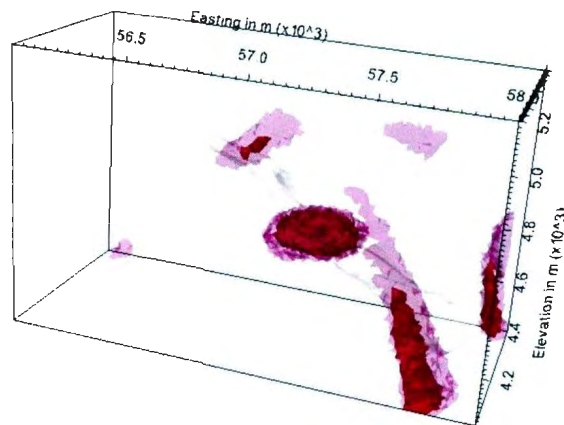


Fig. 7. 25: Resultant density distributions from the large surface array gravity inversion on the fine inversion mesh. The red cells had relative densities between 0.9 g/cm^3 to 2.1833 g/cm^3 , the purple cells have relative densities between 0.3 g/cm^3 and 0.9 g/cm^3 and all other cells have densities less than 0.015 g/cm^3 . The sulphide body is shown in grey and has a relative density of 1.652 g/cm^3 and the axis going in to the page is the northing and extends from 42000m to 429000m.

7.2.4 Borehole Array Inversion Results

In Section 7.2.3 improvements were achieved by using a single borehole in the array of gravity measurements and the surface measurements only seemed have a minimal contribution to the model. As such, the borehole array (see Section 6.3.1.4) was developed and synthetic data sets were developed. There are several advantages to using only borehole measurement locations. This includes having a smaller dataset which leads to lower computation times and taking advantage of the depth resolution possible from the borehole measurements.

7.2.4.1 Graduate Mesh Inversion

The inversion converged to an omega of 1.138 in 27 iterations with a computation time of 26hr 45min and a wall clock time of 7hr 39min. The gravity response predicted by this inversion (Fig. 7. 26) is more restricted in range than the data

provided to the inversion (Fig. 6.26) though the pattern is very similar. Although the normalized data residuals calculated for this inversion (Fig. 7. 27) have a moderately high range except those measurements very close to the edges of the sulphide body most are reasonably low suggesting that as a whole the inversion has fit the data reasonably well.

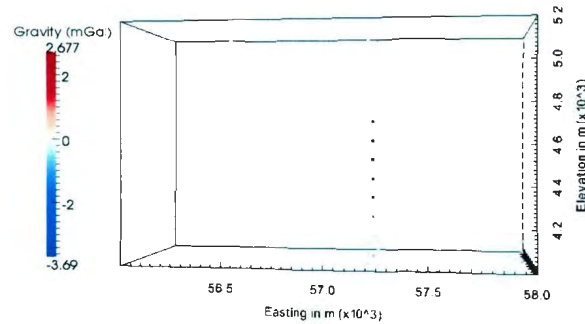


Fig. 7. 26: Predicted relative gravity measurements predicted by the inversion of borehole-only gravity array data on the graduated inversion mesh.

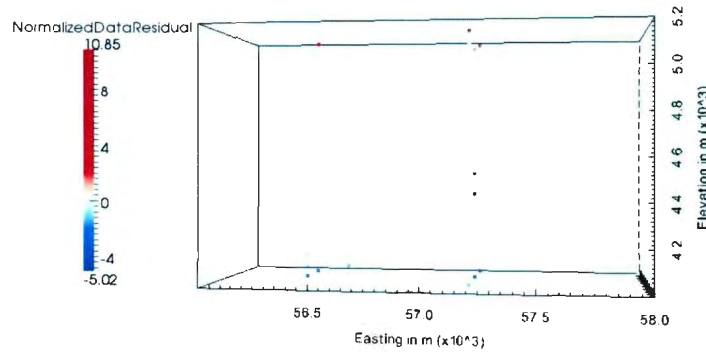


Fig. 7. 27: Normalized data residuals calculated for the results of the inversion of borehole-only gravity array data on the graduated inversion mesh.

The relative density model (Fig. 7. 28) produced by this inversion has located the sulphide body and estimated its relative density reasonably well. However, it has not determined the shape or size of the sulphide body. The presence of a few anomalously

dense cells in the deeper parts of the sulphide body indicates that the borehole array still provides some information on the lateral density distribution within the model.

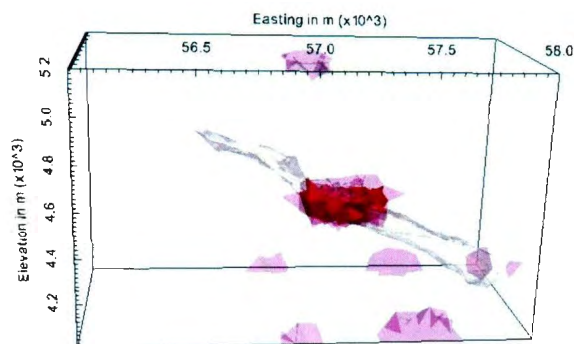


Fig. 7. 28: Resultant density distributions from the inversion on the graduated inversion mesh. The red cells had relative densities between 0.9 g/cm^3 to 2.0 g/cm^3 , the purple cells have relative densities between 0.3 g/cm^3 and 0.9 g/cm^3 and all other cells have densities less than 0.3 g/cm^3 . The sulphide body is shown in grey and has a relative density of 1.652 g/cm^3 and the axis going in to the page is the northing and extends from 42000m to 42900m.

7.2.4.2 Fine Mesh Inversion

The inversion converged to an omega of 1.144 in 21 iterations with a computation time of 5hr 3min and a wall clock time of 3hr 0min. The predicted gravity data from this inversion are very similar in distribution to those from the graduated mesh inversion (Fig. 7. 26) and ranged from -3.82 mGal to 2.73 mGal. The normalized data residuals from this inversion were also very similar to those seen in Fig. 7. 27 and range between -3.79 to 8.4.

The relative density model (Fig. 7. 29) produced by this inversion is improved over the equivalent inversion conducted using the graduated mesh (Fig. 7. 28). Like the graduated mesh inversion it has located and determined the relative density of the sulphide body well but has not been able to estimate the size or shape of the body

well. However, unlike the graduated mesh inversion this result has less extraneous artefacts and appears to have better lateral resolution.

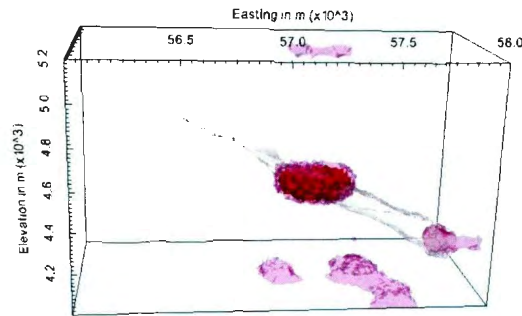


Fig. 7. 29: Resultant density distributions from the inversion on the fine inversion mesh. The red cells had relative densities between 0.9 g/cm^3 to 2.0 g/cm^3 , the purple cells have relative densities between 0.3 g/cm^3 and 0.9 g/cm^3 and all other cells have densities less than 0.3 g/cm^3 . The sulphide body is shown in grey and has a relative density of 1.652 g/cm^3 and the axis going in to the page is the northing and extends from 402000m to 429000m.

7.3 Joint Inversion Results

The set up for the joint inversions presented was developed based on the results seen in the single property gravity and seismic inversions. The slowness portion of the inversion used data forward modelled using the starburst I seismic array as this array was shown in Section 7.1 to be the most effective array for seismic inversion. The fine inversion mesh in section 7.1.2 was shown to allow the production of the best inversion results. Once the results from the graduated mesh inversion were shown to be acceptable the same inversion parameters were used to run an inversion with the fine inversion mesh. The gravity portion of the inversion was run using the borehole-only array of gravity measurement locations as this was shown in Section 7.2 to be the most effective. The same gravity specific inversion parameters as were used in the borehole-only inversions in Section 7.2.4 were used for the joint inversions as well.

7.3.1 Graduated Mesh Inversion

This inversion overshot the target misfits by more than the tolerance on the 19th iteration. All subsequent iterations involved the inversion simplifying the model in an effort to move within the misfit tolerance. The inversion ran for a total of 43 iterations and did not succeed in converging. The final omega values were 0.944 for the seismic half of the inversion 0.568 for the gravity half of the inversion. As this inversion was ended before it reached convergence computation and wall clock times are not available for this inversion.

The gravity response predicted by this inversion (Fig. 7. 30a) is similar in topology to the data provided to the inversion (Fig. 6.26) the pattern is very similar. However, the range of gravity data predicted by this inversion undershoots the largest negative gravity value and overshoots the largest positive value in the synthetic dataset.

Although the normalized data residuals calculated for this inversion (Fig. 7. 30b) has a moderately high range only those measurements very close to the edges of the sulphide body.

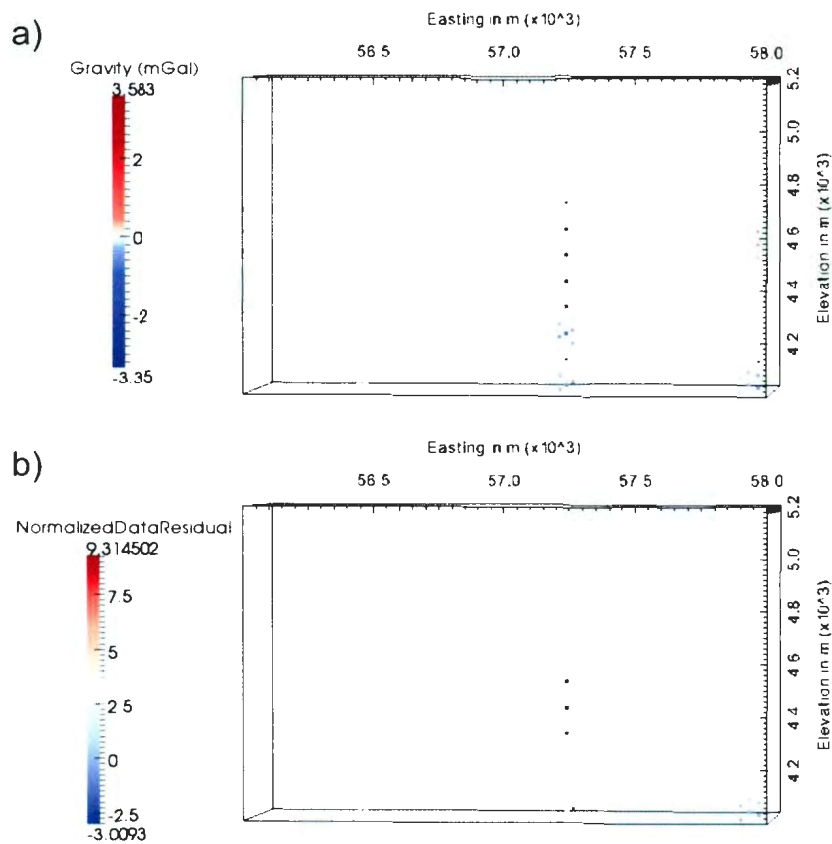


Fig. 7. 30: a) Gravity data and b) associated normalized data residuals for the gravity half of the joint inversion on the graduated inversion mesh.

The seismic travel-times predicted for this inversion (Fig. 7. 31a) are similar in topology and range of values to the synthetic data provided to the inversion (Fig. 6.13). The normalized data residuals (Fig. 7. 31b) associated with the seismic portion of this inversion are relatively low and show no particular spatial distribution.

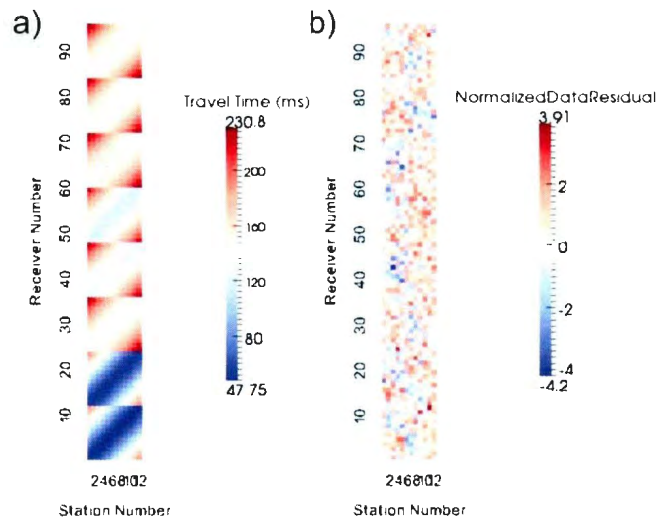


Fig. 7. 31: a) Travel time data and b) associated normalized data residuals for the gravity half of the joint inversion on the graduated inversion mesh.

The relative density distribution for this inversion (Fig. 7. 32) has located the sulphide body and determined its density with relatively good accuracy. However, it has not been able to determine the shape or size of the sulphide body nor does it show any sign of having determined the orientation of the body. The slowness model produced by this inversion (Fig. 7. 33) has located the sulphide body, determined its orientation. The model has overestimated the height and width of the body and has underestimated its length and significantly underestimates the slowness of the sulphide.

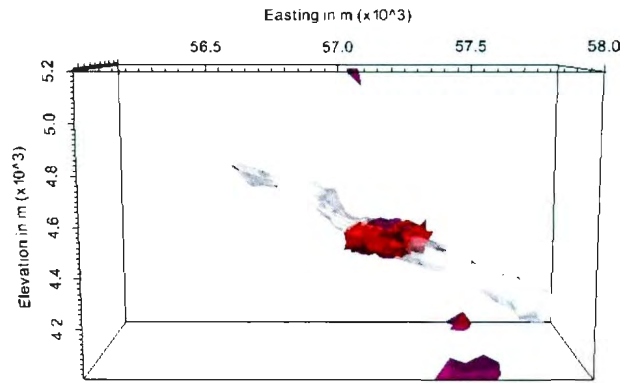


Fig. 7. 32: Resultant density distributions from the joint inversion on the graduated inversion mesh. The red cells had relative densities between 1 g/cm^3 to 2.0 g/cm^3 , the purple cells have relative densities between 0.3 g/cm^3 and 1.0 g/cm^3 and all other cells have densities less than 0.3 g/cm^3 . The sulphide body is shown in grey and has a relative density of 1.652 g/cm^3 and the axis going in to the page is the northing and extends from 42000m to 42900m.

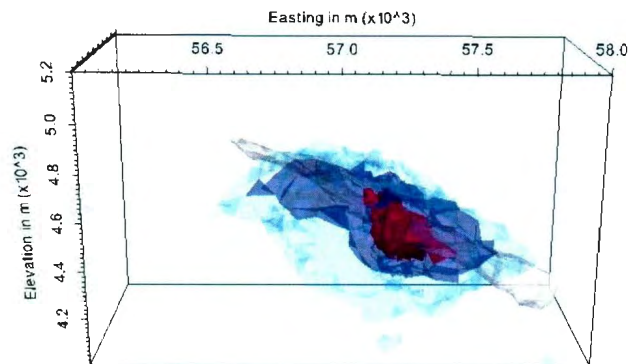


Fig. 7. 33: Slowness distributions from joint inversion on the graduated inversion mesh. The red cells had slowness values between 0.166 s/km to 0.169 s/km , the purple cells have slowness values between 0.164 s/km and 0.163 s/km and all other cells have slowness values less than 0.163 s/km . The sulphide body is shown in grey and has a slowness of 0.2218 s/km and the axis going in to the page is the northing and extends from 42000m to 42900m.

7.3.2 Fine Mesh Inversion

This inversion converged to a seismic omega value of 1.141 and a gravity omega value of 1.157 in 19 iterations with a computation time of 84hr 51min and a wall clock time of 73hr and 26min. This clearly shows that the use of parallel processing has far less benefit for joint inversion than for gravity-only due to the difficulty with parallel compatibility in the seismic portion of the inversion.

The gravity response predicted by this inversion (Fig. 7. 34a) is very similar in range and topology to the synthetic data provided to this inversion. Although this predicted gravity response is similar to that seen for the graduated mesh joint inversion (Fig. 7. 30a) in topology it has matched the synthetic dataset much better. The normalized data residuals (Fig. 7. 34b) calculated for this inversion are relatively low and certainly lower than those from the graduated mesh inversion (Fig. 7. 30b).

The seismic travel times predicted by this inversion are very similar in range and topology to those predicted by the graduated mesh joint inversion (Fig. 7. 31a). The travel times range from 47.94ms to 230.15ms. The normalized data residuals for this inversion also resemble those from the graduated mesh joint inversion (Fig. 7. 31b) quite closely. They have range from -3.89 to 3.5.

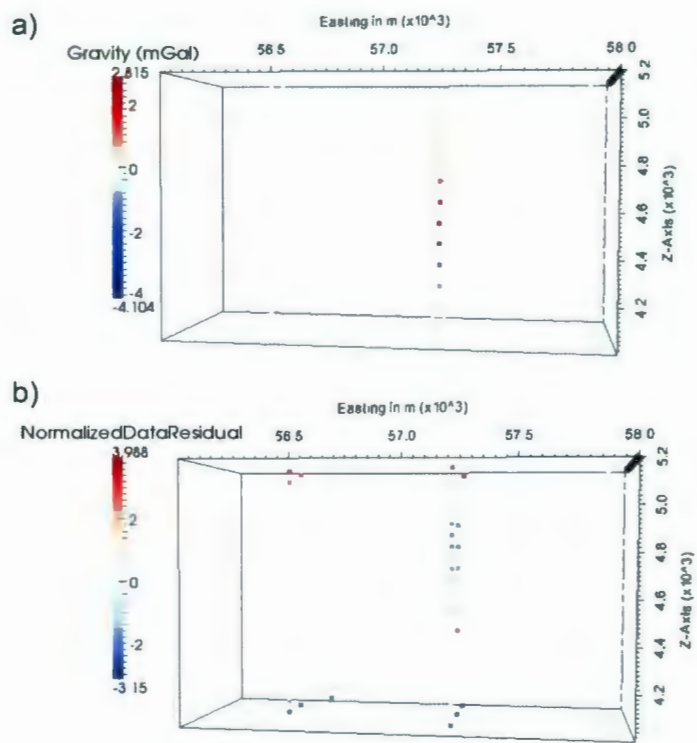


Fig. 7. 34: a) Gravity data and b) associated normalized data residuals for the gravity half of the joint inversion on the fine inversion mesh.

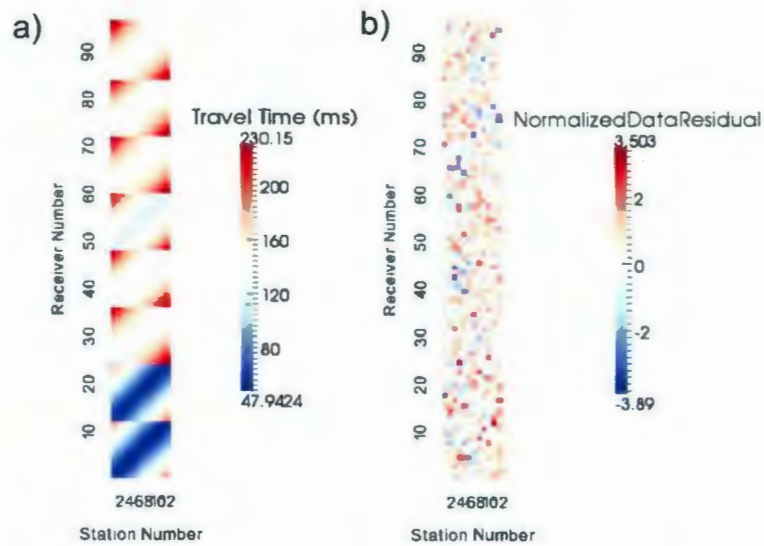


Fig. 7. 35: a) Travel time data and b) associated normalized data residuals for the gravity half of the joint inversion on the graduated inversion mesh.

The relative density model produced by this inversion (Fig. 7. 36a) has located the sulphide body and has estimated its relative slowness well. The inversion also shows some indication of having determined the orientation of the sulphide body as there are cells with relative densities of more than 0.3g/cm^3 in the deepest, most easterly end of the sulphide body. However, the model does have far more artefacts that are seen in the graduated mesh joint inversion result (Fig. 7. 32).

The slowness model produced by this inversion (Fig. 7. 36) has located the sulphide body and determined its orientation. However, the model has overestimated the height and width of the body and has underestimated its length. Although, the inversion has underestimated the slowness of the sulphide body it has estimated it better than the graduated mesh joint inversion (Fig. 7. 33).

It can be seen that the fine mesh joint inversion produced a number of improvements on the results from the graduated mesh joint inversion. The fine mesh was able to match the synthetic data for the gravity more closely and to more accurately estimate the slowness of the sulphide body. It was also able to reach the target misfit comfortably whereas the graduated mesh inversion began to match the synthetic data too closely, indicating that it may have started to match the noise as well as the data.

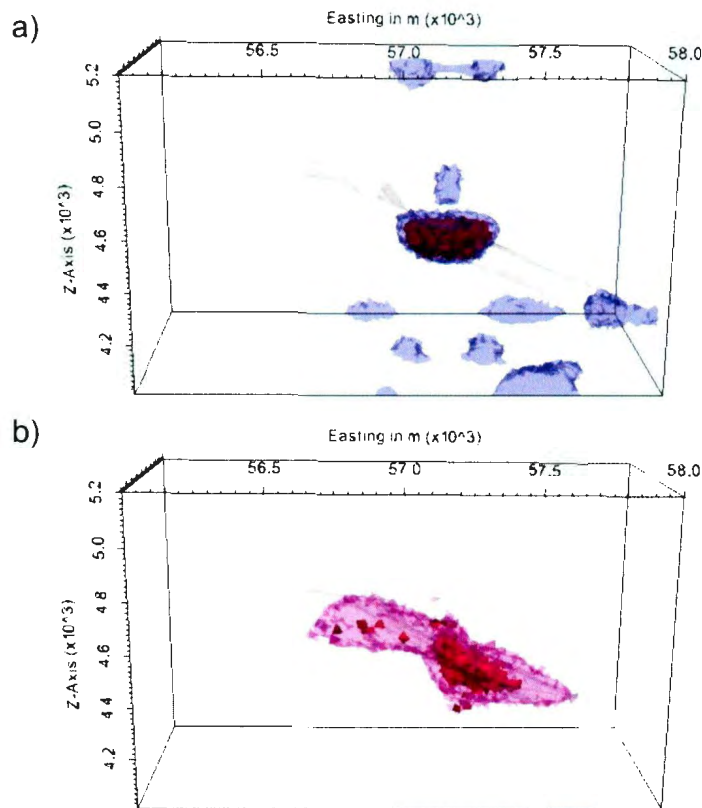


Fig. 7. 36: The sulphide body is shown in grey in both a) and b) has a relative density of 1.1652g/cm³ and a slowness 0.2218 s/km and the axis going in to the page is the northing and extends from 42000m to 42900m. a) Resultant density distributions from the joint inversion on the graduated inversion mesh. The red cells had relative densities between 1 g/cm³ to 2.0 g/cm³, the purple cells have relative densities between 0.3g/cm³ and 1.0 g/cm³ and all other cells have densities less than 0.3 g/cm³. b) Slowness distributions from joint inversion on the graduated inversion mesh. The red cells had slowness values between 0.175 s/km to 0.186 s/km, the purple cells have slowness values between 0.175 s/km and 0.170 s/km and all other cells have slowness values less than 0.170 s/km.

Chapter 8: Summary and Conclusions

The tests performed in 2D and 3D during this project show that joint inversion can be successfully used in the modelling of geological structures. It has been shown that using joint inversion rather than single-property inversion can lead to greater accuracy of modelling the physical property distribution. The use of seismic tomography can be shown to greatly improve the ability of the code to accurately reproduce a synthetic model. The addition to of gravity data to an inversion of seismic tomography data provides only a small amount of help, however this is worthwhile due to the relatively low cost of gravity acquisition.

The results of this project suggest that this technique may not be ideal for imaging deep targets in green field projects. Improvements in the quality of models were largely due to the necessity of having boreholes in nearly ideal locations. It has been shown that this is crucial both for seismic tomography and gravity.

There were a few factors that clearly improved the results from seismic tomography and gravity modelling for both 2D and 3D inversion. These included: choosing an appropriate similarity parameter; the use of borehole gravity data; and the use of a well-chosen sensitivity weighting. Other factors can affect the speed with which an inversion will converge. Including; correctly choosing a betainit value; and choosing appropriate target misfits in light of the noise in the data.

In light of the computationally expensive nature of 3D inversion there are a number of considerations that have to be made in order to attain good inversion results; both for single property and joint inversion:

- The cell size of the mesh was a critical factor during both seismic forward and seismic inversion modelling. In order to obtain successful models it is necessary to use a mesh that preserves the plane wave approximation of the fast marching method. Ideally the finest possible mesh should be used.
- Measurement locations for gravity data and seismic source and receiver arrays must be carefully chosen to ensure adequate data coverage but to avoid having data sets so large that the inversion problem becomes to computationally intensive.

In conclusion, the tests conducted through this project show that joint inversion is a potentially powerful tool for delimiting buried bodies and small physical property contrasts. The method presents some limitation due to the computational expense particularly in running 3D inversions. Results from single property and joint inversions in 2D and 3D showed that the use of borehole gravity data was crucial to getting good inversion results. As such, this approach would be more applicable to brownfields and mine development settings rather than purely greenfield exploration. Furthermore, the use of prior information about the surrounding geology and physical properties of the rocks in the areas makes this method more viable. A firm understanding of the challenges presented by this type of inversion and the scenario to

which it is being applied is necessary to develop compromises in terms of computational requirements.

Appendix A: Input Files for Modelling Code

The following is the documentation for the input files used to run three of Dr. Lelievre's programs: *gravity_fwd*, *seismics_fwd*, and *vinv*. This material is copied directly from the documentation provided with the code.

A.1 Gravity_fwd Input File

```
! Each line of the input file should be of the format
!   name value
! where name is the name of some modelling parameter and value is
! the value for that parameter.
! The possible parameters and default values are listed below.
! Note that some of the parameters
! are for use in inversion and are ignored for forward modelling
! purposes.
!   ismag      'f'           ! set to true if you want to
! perform magnetic modelling instead of gravity
!   istensor   'f'           ! specifies the type of gravity
data
!   zdir       1             ! specifies the coordinate system
!   gridtype   'unstructured' ! the type of grid (the other
! option is 'rectilinear')
!   meshfile   ''           ! file containing mesh information
!   modelfile  ''           ! file containing model information
!   split      0             ! how to convert from rectilinear
! to unstructured grid
!   obsfile    ''           ! file containing the observation
! locations
!   datafile   ''           ! file containing the data response
!   ai         1             ! attribute index to use as the
model
!   gmul       1.0          ! multiplicative scalar to convert
! model to density
!   gadd       0.0          ! additive scalar to convert
! model to density
!   approx     'f'         ! perform approximate modelling or
! not
!   move       'f'         ! allows you to copy the data to
! the x or z coordinate
!   incl       0.0          ! geomagnetic field inclination
! (only used if ismag=t)
```

```

!   decl      0.0           ! geomagnetic field declination
(only used if ismag=t)
!   str       1.0           ! geomagnetic field strength (only
used if ismag=t)
!   wmode     'none'       ! defines what type of weighting is
used in an inversion
!   wbeta     1.0           ! distance/sensitivity weighting
strength
!   wnorm     2.0           ! distance/sensitivity weighting
norm
!   wpower    0.0           ! depth/distance/sensitivity
weighting power
!   wzero     0.0           ! depth/distance weighting z0/r0
!   comps     tttttt       ! specify which tensor components
to use
!   mtxroot   ''           ! defines the file(s) containing
the sensitivity matrix/matrices
!   compmeth  'none'       ! compression method: none, noco,
wave, poly
!   compdir   'row'        ! compression mode: row, col
!   wavelet   'null'       ! type of wavelet compression:
daub[1-6], symm[4-6], null
!   tol       0.0           ! relative wavelet threshold OR
absolute tolerance used in polynomial compression
!   order     0             ! polynomial fitting order
!   window    0             ! polynomial fitting minimum window
size

```

A.2 Seismic_fwd Input File

```

! ---- INPUT FILE ----
!
! Each line of the input file should be of the format
!   name value
! where name is the name of some modelling parameter and value is
the value for that parameter.
! The possible parameters and default values are listed below.
Note that some of the parameters
! are for use in inversion and are ignored for forward modelling
purposes.
!
!   zdir      1             ! specifies the coordinate
system
!   gridtype  'unstructured' ! the type of grid (the other
option is 'rectilinear')
!   meshfile  ''           ! file containing mesh
information
!   modelfile ''           ! file containing model
information

```

```

!   neighfile      ''           ! another file containing mesh
information (unstructured grids only)
!   split          0           ! how to convert from
rectilinear to unstructured grid
!   sourcesfile    ''           ! node file specifying the
source locations
!   receiversfile  ''           ! node file specifying the
receiver locations
!   combosfile     'null'       ! ele file specifying the
source-receiver combinations
!   datafile       ''           ! file containing the data
response
!   ai             1           ! attribute index to use as the
model
!   tmul           1.0         ! multiplicative scalar to
convert model to slowness
!   tadd           0.0         ! additiative scalar to convert
model to slowness
!   trend          0.0         ! background slowness depth
trend
!   recip          'f'         ! set to true ('t') to perform
reciprocal modelling
!   nmarch         1           ! number of marches to perform
in the fast marching
!   radius         10.0        ! the initialization radius in
the fast marching
!   thresh         0.0         ! a threshold on the
sensitivity values
!   tracemode      'none'      ! specifies the type of tracing
to perform (if any)
!   gradflag       't'         ! how to interpolate
traveltimes at the receiver locations
!   senflag        'f'         ! set to true ('t') to
calculate the sensitivity matrix
!   senfullflag    'f'         ! set to true ('t') to use a
full sensitivity matrix instead of sparse
!   bruteflag      'f'         ! set to true ('t') to perform
a brute-force finite-difference sensitivity calculation
!   writettimes    't'         ! if true ('t') then the
traveltimes are written to the output unstructured grid files
!   writetypes     'f'         ! if true ('t') then the travel
types are written to the output unstructured grid files
!   writesen       'f'         ! if true ('t') then the
sensitivity matrix is written to the output unstructured grid
files
!   sloray         0.0         ! homogeneous slowness value to
remove when calculating traveltimes along ray paths

```

A.3 VINV Input File

```
! ---- INPUT FILE ----
!
! Each line of the input file should be of the format
!   name [index] value
! where name is the name of some modelling parameter and value is
! the value for that parameter.
! Some parameters required that an index is specified to link the
! parameter to a specific data set and associated physical property
! (currently, it is assumed that each data set is associated with
! a different physical property).
! The possible parameters and default values are listed below.
! Those that require the index specifier are indicated with [].
!
! MESH INFORMATION:
!   zdir          1                ! specifies the coordinate
! system
!   gridtype      'unstructured' ! the type of grid (the other
! option is 'rectilinear')
!   meshfile      ''              ! file containing mesh
! information
!   modelfile     ''              ! file containing model
! information
!   neighfile     ''              ! another file containing
! mesh information (unstructured grids only)
!   split         0                ! how to convert from
! rectilinear to unstructured grid
! DATA-RELATED OPTIONS:
!   ndatasets     1                ! number of data sets to
! invert
!   datatype      [] ''           ! type of data (for a
! particular data set)
!   datainp       [] ''           ! input file (for a
! particular data set)
!   gamma         [] 1.0          ! multiplier on the data
! misfit term (for a particular data set)
!   chifact       [] 1.0          ! normalized target misfit
!   chitol        [] 0.05        ! relative tolerance on the
! target misfit (for a particular data set)
!   jchitol       0.05           ! relative tolerance on the
! joint pareto misfit
! REGULARIZATION OPTIONS:
!   initfile      [] ''           ! file containing an initial
! model (for a particular physical property)
!   initindex     [] 0            ! attribute index to use in
! an initial model file (for a particular physical property)
!   initvalue     [] 0.0         ! initial model value (for a
! particular physical property)
```

```

!   reffile      [] ''          ! file containing a reference
model (for a particular physical property)
!   refindex    [] 0           ! attribute index to use in a
reference model file (for a particular physical property)
!   refvalue    [] 0.0        ! reference model value (for
a particular physical property)
!   wsfile      [] ''          ! file containing smallness
weights (for a particular physical property)
!   wsindex     []            ! attribute index to use in
the wsfile smallness weights file
!   rotate      'f'           ! set to true to rotate the
smoothness axes
!   wmfile      ''            ! file containing across-face
smoothness weights
!   wminindex   0             ! attribute index to use in
the wmfile across-face smoothness weights file
!   weightsfile ''            ! file containing cell-
centred smoothness weights and smoothness axes rotation
information
!   wzindex     0             ! attribute index to use in
the weightsfile for the z-direction cell-centred smoothness
!   strikeindex 0             ! attribute index to use in
the weightsfile for the strike rotation angle
!   dipindex    0             ! attribute index to use in
the weightsfile for the dip    rotation angle
!   tiltindex   0             ! attribute index to use in
the weightsfile for the tilt   rotation angle
!   strikevalue 0.0           ! strike rotation angle for
the entire mesh
!   dipvalue    90.0          ! dip    rotation angle for
the entire mesh
!   tiltvalue   0.0           ! tilt   rotation angle for
the entire mesh
!   gradtol     0.0           ! tolerance on minimum
vertex/dihedral angle when generating the gradient operators
!   alphas      [] 0.0        ! multiplier on the smallness
regularization (for a particular physical property)
!   alpham      1.0           ! across-face smoothness
regularization multiplier
!   alphax      1.0           ! x-directional smoothness
regularization multiplier
!   alphay      1.0           ! y-directional smoothness
regularization multiplier
!   alphaz      1.0           ! z-directional smoothness
regularization multiplier
!   alphab     [] 1.0        ! multiplier on the
regularization term (for a particular data set)
!   measure0    'ell2'       ! specifies the type of
measure to use in the smallness regularization term

```

```

!   measure1      'ell2'          ! specifies the type of
measure to use in the smoothness regularization term
!   ekblomp       2.0             ! the p-value for the Ekblom
measure or total-variation measure
!   ekblome       0.0             ! the epsilon value for the
Ekblom measure or or total-variation measure
!   cauchys       1.0             ! the sigma value for the
Cauchy measure
!   compacte     1.0E-6           ! the epsilon value for the
compact-model measure
! CONSTRAINT OPTIONS:
!   usebounds     'f'             ! set to true ('t') to
perform a bound-constrained inversion
!   boundsfile   [] ''           ! file containing model
bounds
!   lowerindex   [] 1             ! attribute index to use for
the lower bound in a bounds file
!   upperindex   [] 2             ! attribute index to use for
the upper bound in a bounds file
!   lowervalue   [] 0.0           ! lower bound value for the
entire mesh
!   uppervalue   [] 1.0           ! upper bound value for the
entire mesh
! JOINT INVERSION OPTIONS:
!   alphaj       0.0             ! multiplier on the sum of
joint measures
!   issqr        't'             ! set to false ('f') if you
want to specify a positive or negative correlation
!   pn           0               ! the sign specifies a
positive or negative correlation (only used if issqr is false)
!   fcmf         2.0             ! an exponential power used
in the fuzzy c-means joint measure
!   nclusters    0               ! number of clusters for the
fuzzy c-means or Gaussian PDF joint measure
!   clusters     [] ''           ! cluster centre
specification for the fuzzy c-means or Gaussian PDF joint
measures
!   spreads      [] ''           ! cluster spread
specificaiton for the Gaussian PDF joint measure
!   rotations    ''             ! cluster rotation
specification for the Gaussian PDF joint measure
!   nstepse      0               ! number of beta steps over
which to heat the rhoe value
!   nstepsc      0               ! number of beta steps over
which to heat the rhoc value
!   nstepsx      0               ! number of beta steps over
which to heat the rhox value
!   nstepsf      0               ! number of beta steps over
which to heat the rhof value

```

```

!   nstepsp      0           ! number of beta steps over
which to heat the rhop value
!   rhoe         0.0        ! final multiplier value for
the equal joint measure
!   rhoc         0.0        ! final multiplier value for
the correlation joint measure
!   rhox         0.0        ! final multiplier value for
the cross-gradient joint measure
!   rhof         0.0        ! final multiplier value for
the fuzzy c-means joint measure
!   rhop         0.0        ! final multiplier value for
the Gaussian PDF joint measure
!   stageinit    0          ! the joint inversion will
start at this stage
!   searchr      't'        ! set to false ('f') to avoid
ratio search for beta
! OPTIMIZATION OPTIONS:
!   maxsteps0    2          ! maximum number of model
perturbations for each beta value for beta-search stage
!   maxstepsj    4          ! maximum number of model
perturbations for each beta value for joint inversion stage
!   cgtol        1.0E-3     ! tolerance for the CG
algorithm when solving for the search direction
!   cgmaxit      2000       ! maximum iterations for the
CG algorithm when solving for the search direction
!   betainit     0.0        ! initial beta value
!   minbetasteps 4          ! minimum number of steps in
beta-search
!   maxbetasteps 48         ! maximum number of steps in
beta-search
!   betafactmin  1.05       ! minimum multiplication
factor when adjusting beta
!   betafactmax  2.0        ! maximum multiplication
factor when adjusting beta
!   betamult     1.0        ! increasing this factor will
lead to larger adjustments when close to the target
!   ratiomult    1.5        ! increasing this factor will
lead to larger adjustments when close to the target
! OUTPUT OPTIONS:
!   writeinter   't'        ! set false to not output
inversion results (models and data) at intermediate iterations
!   totitprefix  'f'        ! set true to adjust prefix
of intermediate output files to indicate total iteration number

```

Appendix B:

Data Files for 2D Models, Forward Modelling, and Inversion

- Sulphide-Gneiss Model
 - Model
 - Contains the .poly file defining the sulphide-gneiss model and the files created
 - Forward Modelling
 - All Gravity Stations
 - Borehole A and B Stations
 - Borehole A Stations
 - Borehole B Stations
 - Travel Time Data
 - Surface-only Stations
 - Inversions
 - i1t2r1_dense
 - contains data for Example 32 in Chapter 4
 - i1t2r2_joint
 - contains data for Example 33 in Chapter 4
 - i1t1r2_slow
 - contains data for Example 2 in Chapter 4
 - i2t2r1_dense
 - contains data for Example 26 in Chapter 4
 - i2t2r2_joint

- i2t2r3_joint
 - contains data for Example 27 in Chapter 4
- i3t2r1_dense
 - contains data for Example 14 in Chapter 4
- i3t2r2_joint
- i3t2r3_joint
 - contains data for Example 15 in Chapter 4
- i4t2r1_dense
 - contains data for Example 20 in Chapter 4
- i4t2r2_joint
 - contains data for Example 21 in Chapter 4
- i5r6_joint
- i5r7_joint
- i5r8_joint
- i5r9_joint
 - contains data for Example 7 in Chapter 4
- i5r10_dense
- i5r11_dense
- i5r12_dense
- i5r13_dense
 - contains data for Example 6 in Chapter 4
- i5r14_dense

- i5r15_dense
- i5r17_joint
- i6t2r1_dense
 - contains data for Example 28 in Chapter 4
- i6t2r2_joint
 - contains data for Example 29 in Chapter 4
- i6t2r3_slow
 - contains data for Example 1 in Chapter 4
- i7t2r1_dense
 - contains data for Example 22 in Chapter 4
- i7t2r2_joint
 - contains data for Example 23 in Chapter 4
- i8t2r1_dense
- i8t2r2_dense
 - contains data for Example 10 in Chapter 4
- i8t2r3_joint
 - contains data for Example 11 in Chapter 4
- i9t2r1_dense
- i9t2r2_dense
 - contains data for Example 16 in Chapter 4
- i9t2r3_joint
- i9t2r4_joint

- i9t2r5_joint
 - contains data for Example 17 in Chapter 4
- i9t2r6
- i9t2r7
- i10t2r1_dense
- i10t2r2_joint
- i10t2r3_dense
- i10t2r4_dense
- i10t2r5_dense
- i10t2r6_dense
- i10t2r7_dense
- i10t2r8_dense
 - contains data for Example 4 in Chapter 4
- i10t2r9_joint
 - contains data for Example 5 in Chapter 4
- i11r2_seismic
 - contains data for Example 3 in Chapter 4
- i11r16_joint
 - contains data for Example 31 in Chapter 4
- i11t2_r3_dense
 - contains data for Example 30 in Chapter 4
- i11r16_joint

- i12t2r1_dense
 - contains data for Example 24 in Chapter 4
- i12t2r2_joint
 - contains data for Example 25 in Chapter 4
- i13t2r1_dense
 - contains data for Example 18 in Chapter 4
- i13t2r2_joint
 - contains data for Example 19 in Chapter 4
- i14t2r1_dense
 - contains data for Example 12 in Chapter 4
- i14t2r2_joint
- i14t2r3_joint
 - contains data for Example 13 in Chapter 4
- i15r15_dense
- i15r16_dense
- i15r17_joint
- i15r18_joint
 - contains data for Example 9 in Chapter 4
- i15r19_joint
- i15r20_joint
- i15r21_dense
- i15r22_dense

- contains data for Example 8 in Chapter 4
- Troctolite-Gneiss Model
 - Model
 - Forward Modelling
 - All Gravity Stations
 -
 - Borehole A and B Stations
 - Borehole A Stations
 - Borehole B Stations
 - Travel Time Data
 - Surface-only Stations
 - Inversions
 - i16r5_dense
 - files from a gravity-only inversion of low noise troctolite-gneiss model synthetic data
 - contains the data for Example 45 in Chapter 4
 - i16r5_joint
 - files from a joint inversion of low noise troctolite-gneiss model synthetic data
 - contains data for Example 47 in Chapter 4
 - i16r6_seismic
 - contains data for Example 46 in Chapter 4

- i21t2r1_dense
 - contains data for Example 48 in Chapter 4
 - i21t2r2_slow
 - contains data for Example 49 in Chapter 4
 - i21t2r3_joint
 - contains data for Example 50 in Chapter 4
 - i21t2r4_dense
 - i21t2r5_joint
 - i26r1_dense
 - contains data for Example 51 in Chapter 4
 - i26r2_joint
 - files from a joint inversion of high noise troctolite-gneiss model synthetic data
 - contains data for Example 53 in Chapter 4
 - i26r3_slow
 - contains data for Example 52 in Chapter 4
- Mixed Model
 - Model
 - Forward Modelling
 - All Gravity Stations
 -
 - Borehole A and B Stations

- Borehole A Stations
- Borehole B Stations
- Travel Time Data
- Surface-only Stations
- Inversions
 - i31t2r1_dense
 - contains data for Example 43 in Chapter 4
 - i31t2r2_joint
 - contains data for Example 44 in Chapter 4
 - i31t2r2_joint
 - i31t2r4_joint
 - i32t2r1_dense
 - contains data for Example 41 in Chapter 4
 - i32t2r2_joint
 - contains data for Example 42 in Chapter 4
 - i33t2r1_dense
 - contains data from Example 37 in Chapter 4
 - i33t2r2_joint
 - contains data form Example 38 in Chapter 4
 - i34t2r1_dense
 - contains data from Example 39 in Chapter 4
 - i34t2r2_joint

- contains data from Example 40 in Chapter 4
- i35t2r1_dense
 - contains data for Example 35 in Chapter 4
- i35t2r2_dense
- i35t2r3_dense
- i35t2r4_joint
 - contains data from Example 36 in Chapter 4
- i35r2_seismic
 - contains data from Example 34 in Chapter 4

Appendix C: 3D Models, Forward Modelling, and Inversions

- Models
 - Block Model
 - Datamine Cross-Sections
 - Full model
 - Sulphide
- Forward Modelling
 - Gravity Forward Modelling
 - 1bh_surf
 - Lg_surface
 - Starburst
 - Surface
 - Seismic Forward Modelling
 - Grid
 - Panel
 - Starburst
 - Starburst II
 - Seismic Forward Modelling Tests
 - Coarse Mesh
 - Fine Mesh
 - Moderate Mesh

- Very Coarse Mesh
 - Very Fine Mesh
- Inversion
 - Gravity
 - Inv2_gonly_bho_0gbg
 - Contains data for the example shown in Section 7.2.4.1
 - Inv2_gsurf_0gbg
 - Contains data for Fig. 7.16
 - Inv2_smgsurf_0gbg
 - Inv3_smgsurf_0gbg
 - Contains data for example shown in Section 7.2.1
 - Inv2_g1bh_0gbg
 - Contains data for example in Section 7.2.3.2
 - Inv_gsurf_0gbg
 - Contains data for example in Fig. 7.14 and 7.15
 - Inv5_gsurf_0gbg
 - Contains data for the example in Fig. 7.17
 - Inv6_gsurf_0gbg
 - Contains data for the example in Fig. 7.18
 - Inv7_gsurf_0gbg
 - Contains data for the example in Section 7.2.2.2
 - Inv_g1bh_0gbg

- Contains data for the example in Section 7.2.3.1
 - Inv_gonly_bho_0gbg
 - Contains data for the example in Section 7.2.4.2
- Inversion meshes
 - Coarse Mesh
 - Fine mesh
 - Graduated mesh
 - Large Coarse Mesh
 - Moderate Mesh
 - Small Cube Coarse
 - Very Coarse mesh
- Joint
 - Inv1_gbho_0gbg
 - Contains data for the example in Section 7.3.1
 - Inv2_gbho_0gbg
 - Contains data for the example in Section 7.3.2
 - Inv3_gbho_0gbg
 - Inv3_j_gbho_0gbg
- Seismic
 - Cm_inv_starburst_ai3
 - Contains data for the example in Section 7.1.2.2
 - Fm_inv_starburst

- Contains data for the example in Section 7.1.2.4
- Fm_inv_starburst2
 - Contains data for the example in Section 7.1.3
- Mm_inv_starburst
 - Contains data for the example in 7.1.2.3
- Seismic_grid
 - Contains data for the example in 7.1.1.2
- Seismic_trial1_panel
 - Contains data for the example in 7.1.1.1
- Seismic_trial2_panel
- Vcm_inv_starburst_ai3
 - Contains data for the example in 7.1.2.1

